# POLITECNICO DI TORINO

**Master's Degree in Civil Engineering**

**Master's Degree Thesis**

# Analysis of the stability of a relict landslide in bimsoils by stochastic approach

**Supervisors**

**Prof. Monica BARBERO**

**Dr. Maria Lia NAPOLI**

**Candidate**

**Hidayat ULLAH**

**December 2020**

# Summary

Bimrocks are structurally complex heterogeneous materials that may cause problems during the design and construction of structures. They are defined as "a mixture of rocks, composed of geotechnically significant blocks within a bonded matrix of finer texture."(Medley, 1994). This type of material is found in more than sixty countries worldwide. A careful and correct characterization can reduce costly design errors and unwelcome surprises during construction or excavation.

This dissertation is an extension of the slope stability analysis of the relict landslide in bimrocks studied by Minuto and Morandi (2015). They analyzed the slope with the LEM code and used both the homogeneous and heterogeneous approaches for the analyses. Minuto and Morandi (2015), from borehole logs and the Medley's (1997) chart of uncertainty for VBP calculation, found the block content to be in the range of 15% to 30%. So, two VBPs of 15% and 30% were used for the analyses. They used rectangular shaped blocks analysis and tracked the failure surface around these blocks.

This thesis focused on the numerical analyses of this relict landslide using the RS2 code (Rocscience Inc). In the first phase, the results of Minuto and Morandi were validated with LEM, for both the fine matrix and coarse matrix. Due to the high spatial and dimensional variability of bimrocks, the use of a stochastic approach is proposed for the rock block distribution in the slope. The used rock blocks were elliptical, with eccentricity values between 0.4 and 0.9. For each VBP, ten different block configurations were used to statistically establish the results. The slope is also analysed with two different strength criteria of Lindquist (1994) and Kalender et al. (2014). Such criteria consider bimrocks to be homogenous and isotropic materials. These models were analysed with both the FEM and LEM approaches.

The numerical analysis of slope revealed that shallow failure surfaces have a higher probability of occurrence as compared to the deep failure surfaces considered by Minuto and Morandi (2015). The heterogeneous approach of analysis had the same results as that obtained by Minuto and Morandi (2015) for coarse matrix and 15% VBP. For 30% VBP, the heterogeneous approach had 10% lower SF value.

# Acknowledgements

I would like to express gratitude to my supervisor Prof. Monica Barbero for her dedicated support and guidance. I woe special gratitude to co-supervisor Dr. Maria Lia Napoli for her thoughtful comments and recommendations on the writing of this thesis. I would also like to acknowledge Dr. Diego Minuto and Dr. Luca Morandi. They provided the data and consistent guidance during the study. I cannot forget to thank my family and friends for all the unconditional support.

***To Jannat and Ibrahim, my mom and dad.***

# Table of Contents

# List of Tables

# List of Figures

# Introduction

Bimrocks are structurally complex heterogeneous materials that may cause problems during design and construction of structures. This type of material is found in many parts of the world and engineering works may deal with this challenging materials. A careful and correct characterization can reduce costly design errors and unwelcome surprises during construction or excavation.

The term bimrocks was introduced by Medley (1994) to indicate geological mixtures of geotechnically significant blocks of rock within a bonded rock matrix of finer texture. These materials present a sufficient mechanical contrast between the blocks and the matrix to force failure surfaces to develop around the blocks in tortuous fashion and a sufficient size and number of blocks to affect the overall mechanical properties. As part of this thesis will be used interchangeably the terms bimrocks, melange, heterogeneous formations or structurally complex rock mass.

In this dissertation, a study was carried out to analyse the stability of a relict landslide in bimrocks in the downtown of Genova, Italy. The slope stability analysis of the relict landslide studied by Minuto and Morandi (2015) was based on a real case study in the downtown of Genova, Italy. The authors analyzed the slope with the LEM code and used the homogenous approach for the analyses. Minuto and Morandi (2015), from borehole logs and the Medley's (1997) chart of uncertainty for VBP calculation, found the block content to be in the range of 15% to 30%. So, two VBPs of 15% and 30% were used for the analyses.

In this thesis, the same slope was analysed with both heterogeneous and homogenous approaches using LEM and FEM methods. First, two different types of matrices were analyzed named 'fine matrix' and 'coarse matrix' with LEM to validate the results of Minuto and Morandi (2015). The fine matrix, as its name implies, has the properties of the fine material only. However, since the slope had a high content of gravel a “coarse matrix”, with the properties of both the fine material and gravel, was also analyzed. In order to perform the FEM analyses, the FEM code RS2 was used. Since bimrocks have inherent spatial and dimensional variability in their nature a stochastic approach for the distribution of rock blocks in the slope was used. The rock blocks were randomly distributed in the slope using the stochastic approach of Napoli et al. (2018). To statistically validate the results, ten different analyses were done for each VBP considered (i.e. 15% and 30%) with different positions, dimensions and shapes of blocks. The equivalent homogenous approach of Lindquist (1994) and Kalender et al. (2014) were also used. These two models were analyzed with both FEM and LEM codes.

Chapter 1 contains a general introduction to bimrocks and their significance in geotechnical engineering. Some characteristics of bimrocks such as rock block distribution, scale independence, VBP estimation and their related uncertainties are also discussed. The chapter includes different studies from literature aiming at the mechanical properties and other aspects of bimrocks.

Chapter 2 deals with the slope stability analysis in bimrock materials. The main considered aspect was the effect of block proportion on slope stability. Limit equilibrium and numerical analyses carried out by different authors indicate that volumetric block proportion is an important factor in the variation of the factor of safety. The blocks also influence the tortuosity of failure surfaces. The use of a stochastic approach for rock block distribution is also discussed in the chapter.

Chapter 3 provides an introduction to the case study of Minuto and Morandi (2015). The model implementation and their characteristics are also illustrated in the chapter. The last part of the chapter discusses the procedure to obtain the material properties used for homogeneous approaches of Lindquist (1994) Kalender et al. (2014).

In chapter 4 the results of both heterogeneous and homogeneous approaches are discussed and are compared with that obtained by Minuto and Morandi (2015).

# Chapter 1

# Bimrocks

## 1.1 General introduction

Bimrocks are heterogeneous materials consisting of a weak soil matrix and geotechnically significant blocks. Medley (1994) defined bimrocks as *"a mixture of rocks, composed of geotechnically significant blocks within a bonded matrix of finer texture"*. The expression "geotechnically significant" means that the blocks have higher strength in contrast to the matrix. Bimrocks/bimsoils are widely found in mountain ranges over the world. They are found in around 60 countries including the USA, Italy, Turkey, and Iran (Medley 1994). According to Medley (2002), the minimum strength contrast between the rock blocks and the matrix should be of the order of two or greater i.e. $\tan\phi_{block}/\tan\phi_{matrix} \geq 2$ and $E_{block}/E_{matrix} \geq 2$

There are many different geological terms for such materials where we have a sheared matrix and strong blocks, such as olistostromes, argille scagliose (northern Italy), complex formations, friction carpet, wild flysch, mega-breccia, and polygenetic breccia. These are geologically rich terms and have geological connotations. So, the researchers in the geotechnical engineering field have tried to simplify the confusing genesis of rocks and provide a geotechnically relevant name.

Raymond (1984) named the mélange, opisthosomas, and other geologically complex formations as *Blocks In Matrix* rocks. The expression Blocks In Matrix was later abbreviated by Medley in 1994 as "bimrocks". The term bimrocks is free from any geological connotations and focuses more on the fundamental engineering problems related to such types of materials. Fig. 1.1 shows the worldwide occurrence of bimrocks and Fig. 1.2 shows some examples of bimrocks.

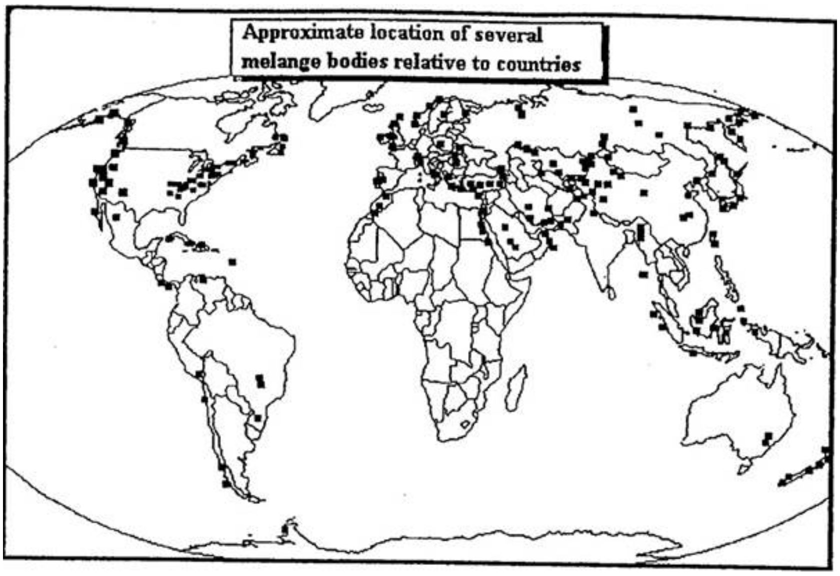


**Figure 1.1:** Map showing the worldwide occurrence of mélanges. (Medley 1994)

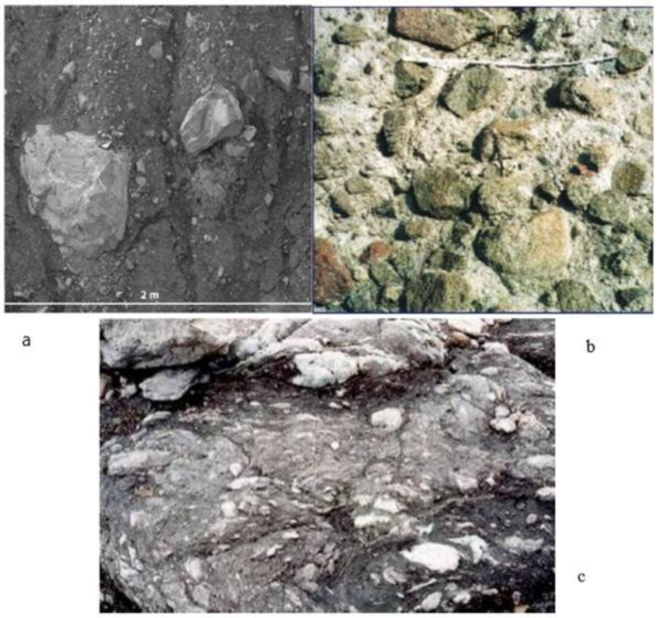


**Figure 1.2:** Example of typical bimrocks. (a)- Santa Barbara Italy (Coli 2011) (b) Ankara Agglomerate (Sonmez, 2004 ) (c) Franciscan melange (Medley 1994)

Similarly, the term bimsoils has been used for mixtures which include rock blocks surrounded by soil-like matrix material, such as colluvium and glacial tills (Medley 1994).

### 1.1.1 Significance of bimrocks

Bimrocks, when encountered in the field, pose some issues. The eminent being the difficulty in the characterization of such soils. It is very hard to get undisturbed samples from bimrocks because we come across the rock blocks while drilling which would need non-standard techniques for sampling. Even if a sample is managed to retrieve it would not be representative of the whole soil mass. In-field tests are a possibility, but they need larger equipment and more economical and physical resources.

The problem in the characterization of bimrocks is well defined in Fig. 1.3. In practice, the soil profiles are prepared from the borehole logs. During exploration, a driller does not know if the rock which is encountered is the bedrock or is a rock block. On the left side of figure 1-3 is the actual subsoil condition. On the right is the interpretation based on borehole logs of four borings. The mistake of confusing a large block with the bedrock will result in wrong subsoil characterization and will result in an incorrect assessment of the spatial variation of blocks in the matrix.

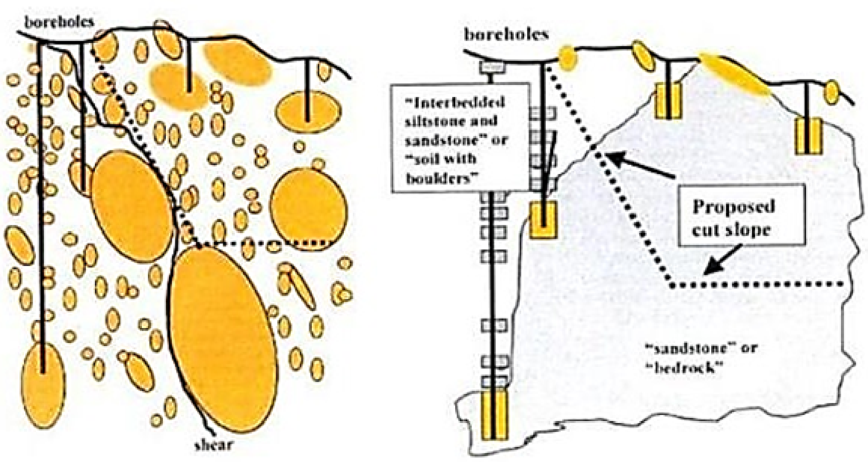


**Figure 1.3:** The left sketch shows rock mass in bimrocks and the right sketch is the soil profile based on the drilling of the area. If not checked thoroughly for the possibility of bimrocks this can result in disaster (Medley, 1999)

The significance of bimrocks also arises from the fact that they can be problematic during excavation and other earthworks. The hindrance during excavation might result in interruptions, as rock blocks are hard to excavate by conventional methods in comparison with soil.

In slope stability analyses, practitioners mostly design the slopes based on the strength of the matrix, ignoring the effect of blocks. The blocks strongly affect the mechanical properties of the matrix, as proven by studies on different physical models (Lindquist, 1994; Altinsoy, 2006; Afifipour et al., 2013 and Kalender et al., 2014), numerical models (Barbero et al., 2008; Pan et al., 2008; Xu et al., 2008; Yayong et al., 2014 and Xu et al., 2016), and on-filed large scale testing (Coli, 2011 and Xu et al.,2015). In the presence of geotechnically significant blocks, the failure surfaces are forced to negotiate around the blocks creating a zig-zagging phenomenon called 'tortuosity'. So, a slope designed considering only the mechanical properties of the matrix will generally produce a conservative design. Therefore, even in case of very low block content or great uncertainty, which is often the case, the characterization of bimrocks has fruitful results.

No guidelines for the characterization and analysis of bimrocks are available, which are internationally recognized among the rock mechanics societies. However, some efforts have been made to introduce some rules by researchers (Medley, 2007a; Kalender et al., 2014).

## 1.2 Characteristics of bimrocks

Different studies on different types of bimrocks have revealed that there are some common characteristics among them. Franciscan melanges, studied by Medley (1994), follow a specific block size distribution. Medley (1997) found that the melanges are self-similar suggesting that blocks are encountered at every scale of engineering interest. This means that the melanges are scale independent. These and other characteristics of bimrocks are discussed in what follows.

### 1.2.1 Block size distribution

Bimrocks express a large variability in the dimension and size of the blocks. The blocks vary from millimetre to kilometre in size (Medley 1994). Studies on the size of the outcrops of Franciscan mélanges showed that the block size distribution is fractal (Medley 1994; Medley & Lindquist, 1995; Riedmüller et al., 2001; Medley, 2002). This nature of bimrocks is seen in other areas too such as in Italy.

The negative power law of bimrocks implies that there is a fewer number of larger blocks and a higher number of small blocks. In some bimrocks, it might be due to weathering and erosion which occur naturally. So, we expect more small blocks and as a result, a negative exponential relationship between their frequencies.

The negative power law is of the following form:

$$N = n^{-D}$$

where N represents the relative frequency of elements in an interval of frequency class n. The exponent D is called the 'fractal dimension' (Mandelbrot, 1983;

Turcotte, 1997). The fractal dimension D is defined by (Peitgen et al. 1992), as follows:

$$D = \frac{logN(n)}{log(n)}$$

Analysing a three-dimensional bimrock body would require a fractal dimension in 3D. So, for the fractal dimension in three dimensions ($D_{3D}$) a unit is added to the two-dimensional fractal dimension. This is valid as long as it takes stereographically that the areal percentage of the blocks is equivalent to the volume percentage of the blocks (Mandelbrot, 1983; Sammis & Biegel, 1989). In the case of the Franciscan, given the average fractal dimension of two-dimensional D = 1.3 (Medley & Lindquist 1995), the three-dimensional fractal dimension is equal to $D_{3D} = 2.3$. This means that for n blocks in a particular class there are $n^{2.3}$ blocks inside of the previous class.

### 1.2.2 Self-similarity and scale independence

Studies conducted by Cowan (1985) demonstrated that the images of melanges at different scales appeared to be similar when compared. A more quantitative approach to the problem was subsequently addressed by Lindquist (1991) and further studies were carried out by Medley and Lindquist (1995).

Medley (1994a) extended the work of Lindquist and studied over 1900 blocks and showed that the block size distributions of a variety of Franciscan mélanges at many scales were self-similar. He measured the maximum observed dimension ($d_{mod}$) of blocks of different photographs and geological maps of different scales. The maximum observed dimension, as its name implies, is the maximum observable dimension of an outcropping rock block. Fig.1.4 shows the ($d_{mod}$) of one such photograph of Caspar Beach California.

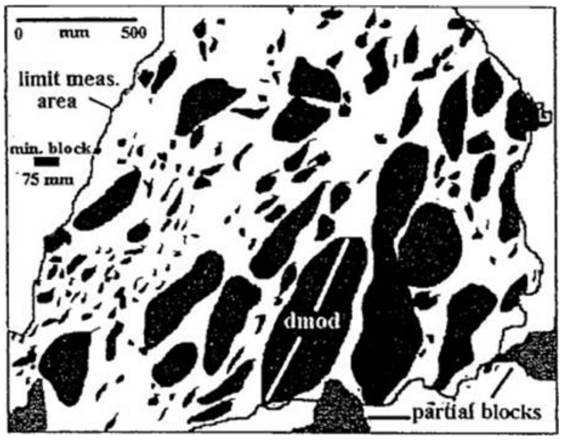


**Figure 1.4:** Outcropping rock blocks on Caspar Beach California. (Medley 1994a)

The measured block sizes ($d_{mod}$) were divided into different classes, where each successive class was double the range of the previous class i.e. 0.025-0.05, 0.05-0.1, 0.1-0.2 etc. The author prepared log histograms as shown in Fig.1.5 for two different areas. The top one has an area of 7.9 $m^2$ with $d_{max}$ of 1.98m and the bottom one has an area of 920 $km^2$ and $d_{max}$ of 18km, where $d_{max}$ is the size of the largest block observed in those areas. In Fig.1.5 'D' represent the fractal dimension (magnitude of the slope of best-fit line, which is also the absolute value of the exponent of the negative power law) which are 1.4 for the top and 1.61 for the bottom graph.

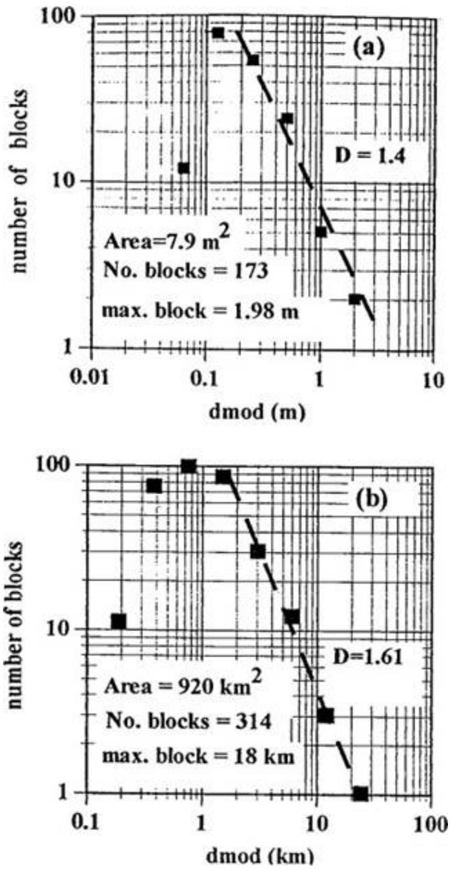


**Figure 1.5:** Log-log histograms of two different areas prepared by Medley. The difference in areas are very large but the self-similar nature is evident. (Medley 1994)

These histograms have three parts. An ascent part from left to right then a peak and lastly a descent part. These log histograms appear similar although the block size and the area studied differ largely. These histograms, also called "log-log linear", are very useful. Based on these histograms we can predict the size and number of blocks within a mélange.

In their study Medley (1994a) compared many such histograms by normalizing them as follows.

- The absolute frequencies of blocks were changed to relative frequencies by dividing the number of blocks in any size class by the total number of blocks in the measured area. Thus, making it area independent.
- Maximum observable dimension ($d_{mod}$) was made unit less by dividing it by $\sqrt{A}$, where 'A' is the area of sites under study.

After applying this procedure many log histograms of different areas were plotted. The result of such operation is shown in Fig.1.6. The plot is astonishing in many ways. The normalized plots are very similar in shape to each other, despite the great range in the areas of measurement. The similarity of shape thus translates into the fact that Franciscan mélanges are scale independent and are fractal.

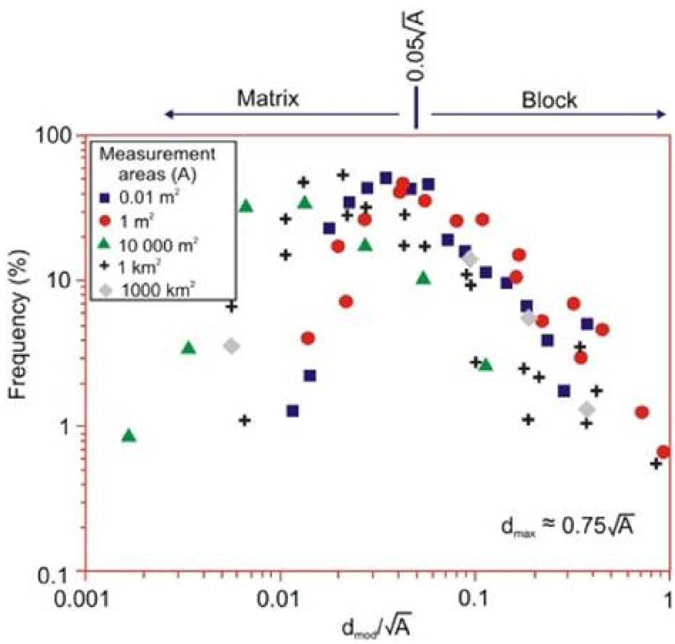


**Figure 1.6:** Compilation of log-histograms of block sizes of 1900 blocks in Franciscan mélanges ranging from millimetres to kilometres (Medley 1994)

In Fig.1.6 the peaks of all curves are almost at $0.05\sqrt{A}$. There are fewer relative frequencies at the left of peaks because blocks become too small to measure and classes become smaller. The largest block is of magnitude $\sqrt{A}$ for any scale of interest. Since 99% the blocks are smaller than 0.75A it is defined as the maximum size of the blocks ($d_{max}$). Also, the blocks up to the size of $0.75\sqrt{A}$ contribute largely to volumetric block proportion.

So, it is defined that material with the size smaller than $0.05\sqrt{A}$ is considered as a matrix and above it as a block. It is because material less than $0.05\sqrt{A}$ contribute negligibly towards the mechanical properties of bimrocks.

### 1.2.3 Characteristic engineering length

In the previous section, it was established that bimrocks are scale independent and that blocks can be found at any scale of engineering interest. The scale of engineering interest practically ranges from millimetres (laboratory sample) to meters (engineering work). Thus, a definition to distinguish between matrix and blocks was needed. Medley and Lindquist (1995) defined the threshold between matrix and blocks to be $0.05\sqrt{A}$. Since mélanges are scale independent, the threshold dividing the matrix form blocks can also be related to the engineering scale of interest named the “characteristic engineering length" (Lc). When scaled by ‘Lc’, the block matrix/threshold is thus 0.05Lc and the largest block, $d_{max}$, is 0.75Lc. It can be seen that there are many ways to describe the block/matrix threshold at any scale of interest: 0.05Lc, $0.05\sqrt{A}$, and 0.05 $d_{max}$. Similarly, the largest reasonable block can be defined as 0.75Lc, $0.75\sqrt{A}$ and $0.05d_{max}$.

The ‘Lc’ can be the diameter of laboratory specimen, tunnel diameter or width of footing. It can be the depth of the failure surface or the height of the slope. Lc can be the $\sqrt{A}$ for the excavation of area ‘A’ or the area of any project site under study or the size of the largest mapped or estimated largest block ($d_{max}$.) at the site.

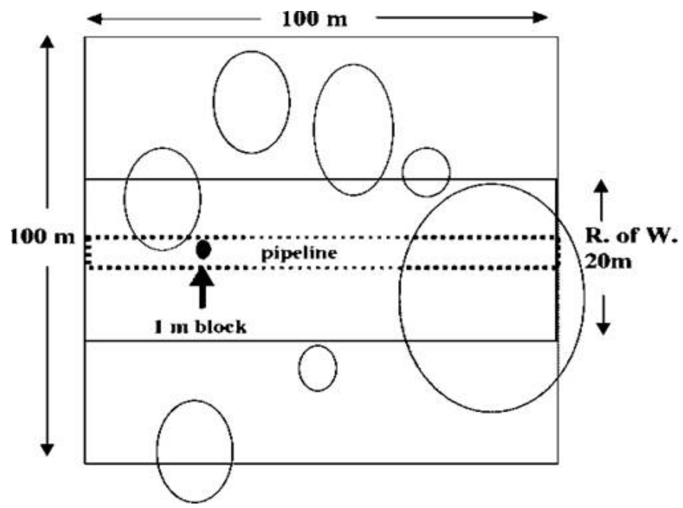


**Figure 1.7:** Sketch showing various scales of interest for an area and the concept of block/matrix threshold. The right side reads as “Road of Width 20m” (Medley 2001)

The sketch in Fig.1.7 shows some different scales of interests. The dotted lines show a pipeline. The arrows at the right show a 20m wide road. It is an arbitrary site of 100×100 m with area summing up to 10,000 $m^2$. When dealing with the whole site of interest the Characteristic Engineering Dimension (Lc) would be $\sqrt{A}$ = 100m. The block/matrix threshold at this scale is 5 m (0.05 Lc or 0.05 $\sqrt{A}$). Hence, the 1m block in the centre of the sketch is part of the matrix for the overall site scale. At the same scale, the large body at the right of the sketch is a block as it is less than 0.75Lc (75 m) in size.

Now changing the scale of interest to the level of the road, the Lc would be the width of the road, i.e. 20m. Thus, the threshold between block and matrix would be 1m. The 1m block in the middle of the road would no longer be a part of the matrix and the large body of rock on the right side is a massive rock now. It is larger than the geotechnically significant blocks i.e. 0.75Lc or 15m

At the scale of 2m wide pipeline, the Lc is the depth of the trench which is 2m. The matrix/block threshold is 0.1m and the largest geotechnically significant block is 1.5m. Now looking at these numbers it is evident that 1m block is a rock block to the scale of pipeline and the rock block at the right is massive rock body

### 1.2.4 Volumetric Block Proportion (VBP)

Volumetric Block Proportion, in simple words, is the ratio between the volume of the block inclusions and the total volume of the heterogeneous rock mass. In the literature, many studies are done on the influence of VBP in bimrocks. Many researchers, with laboratory, in-situ and numerical studies have found that the strength of bimrocks is directly related to the volumetric proportion of the blocks (Irfan & Tang, 1993; Lindquist, 1994; Lindquist & Goodman, 1994; Medley, 1994; Sonmez et al., 2006a; Barbero et al., 2008; Coli 2011). The strength of bimrocks increases with an increase in VBP. Other factors affecting the strength of bimrocks include the size, shape and eccentricity of the rock block inclusions.

#### Estimation of VBP

Since the VBP affects markedly the mechanical behaviour of complex formations with a block-in-matrix fabric, it is necessary to make an estimate as accurate as possible of their block content. It can be estimated from maps and scanlines or bore drillings. Scanlines and bore drillings are one-dimensional methods of estimating the VBP. Geological mapping and image analyses of photographs are two-dimensional methods. A three-dimensional method which involves the separation of the matrix and the blocks by a sieve analysis is more reliable and more accurate, although it can only be feasible in the laboratory whereas on-site the use of such methods is very cumbersome and would still not yield any positive results. Such large scale tests are economically not resourceful. Some researchers (Coli 2011) have performed large scale, on-site sieve analyses. Despite the large scale of such analyses, they do not elicit anything about the shape, orientation, direction and the variability of blocks in bimrocks.

Two-dimensional methods involve the study of photographs and maps. Many researchers (Medley, 1994; Gokceoglu, 2002; Sonmez et al., 2004a) have used digital image analysis methods for VBP estimation. The use of aerial photographs and maps with 2D analysis allows the collection of information on the geometric properties of the blocks such as maximum and minimum observable size, the exposed area of each block, aspect ratio, orientation, and spatial distribution. For instance, Medley and Goodman (1994) used the manual and computer-aided image analyses for VBP estimation. Authors used a hand tracing of a photograph of melange from Caspar headlands California as shown in Fig.1.8 and digitalized into an array of pixels in the greyscale.

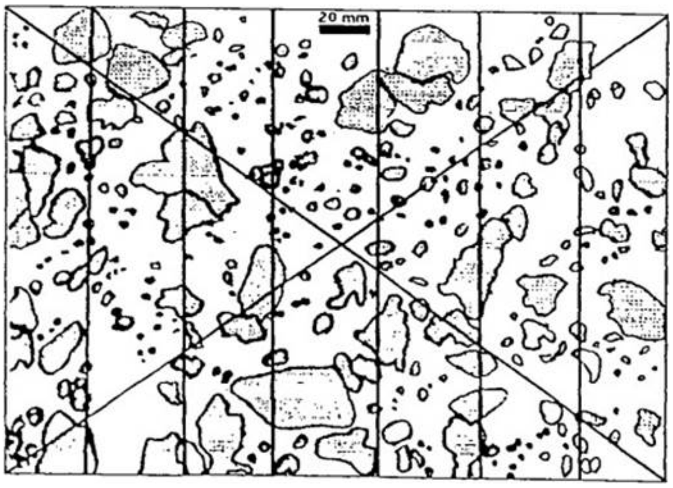


**Figure 1.8:** Hand traced photograph from Caspar beach California. Such images, after image analysis, can be used for the estimation of block inclusions in bimrocks. (Medley and Goodman 1994)

After digitalizing the image, a software of image analysis was used to measure the geometric parameters like area, axial dimensions and parameters of individual blocks. In this case, the individual block area summed to 35.6% of the total areal area. It was also possible to plot the frequency distribution of block sizes.

Still, in practice, we are seldomly lucky to have maximum blocks visually accessible. And also, such analyses are subjected to uncertainties. The uncertainties related to this type of analyses depend on the shape and exposure of the blocks relative to the exposed plan, from the availability of outcrops to the photographic surveys, as well as the colour contrast between the blocks and the matrix.

With one-dimensional (1D) methods, the VBP can be determined based on the assumption that it is stereologically equivalent to the linear cumulative proportion of the same lithology as measured in the stratigraphy. This assumption, however, is valid only in the presence of an adequate sampling length. 1D methods have great uncertainties as the blocks in the ground are not generally spherical in shape and are distributed randomly so it is difficult to estimate the VBP from few borehole logs. In the presence of a sufficient sampling length which, according to Medley (1997), is at least ten times the maximum dimension of the blocks, the linear proportion of lithology characteristic can be correlated with the VBP.

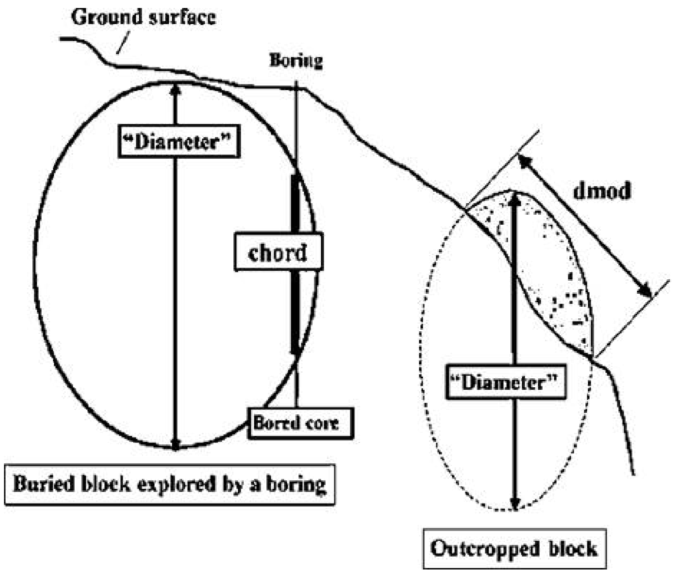


**Figure 1.9:** Sketch showing the concept of chord and diameter length. The boring necessarily might not pass the maximum side of the block thus resulting in the underestimation of the block size. The $d_{mod}$ is the maximum observed dimension on the outcrop of area. (Medley 2001)

From the analysis of cores, it is not possible to identify certainly the maximum dimension of the blocks. Fig.1.9 shows how the drilling can be misleading about the size of the buried block. The block is drilled through a chord length instead of the diameter which is the maximum length. In Fig.1.9 $d_{mod}$ is the maximum observed dimension. It is the maximum size of blocks which can be observed on the outcrop surface. In this case, $d_{mod}$ does not represent the maximum size of the block.

The effectiveness of the one-dimensional method depends on many factors. First, the orientation of blocks relative to the drilling direction. It means, during drilling, whether the block is encountered at its diameter or its chord as shown in Fig.1.9. When drilled in chord length, it results in a phenomenon called "tailing", which tends to underestimate the block size. Second, the volumetric block proportion. With higher VBP the probability to encounter a block during drilling increases resulting in fewer uncertainties. Last, the total length of drilling also influences the effectiveness of the one-dimensional method for estimation of VBP. Medley (1997) recommended using at least ten times the largest block size as drilling length.

Medley (2001) compared the 1D (chord) distribution with the 3D block size distribution. It was found that 1D distribution does not exactly replicate the 3D block size distribution. Due to the effect of tailing, 1D chord distribution overestimates the small size blocks. The comparison is shown in Fig.1.10.

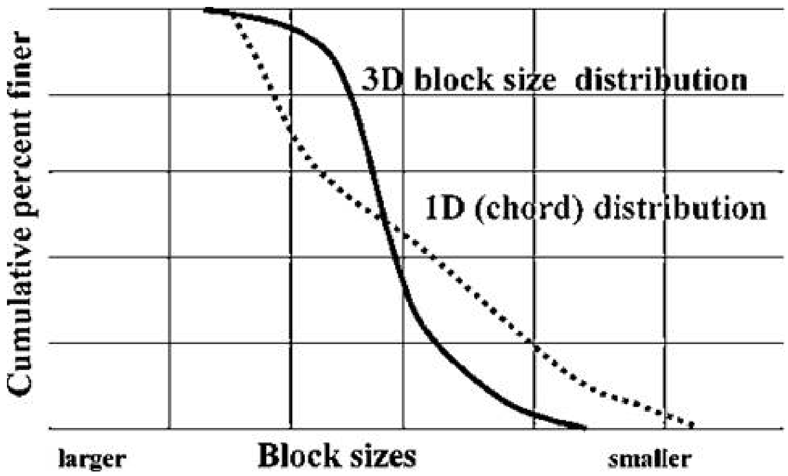


**Figure 1.10:** 1D chord distribution weakly replicates the 3D block size distribution. 1D chord underestimates the larger block sizes and overestimates the smaller sizes. (Medley 2001)

Recent studies have also highlighted how the 1D sampling methods, in the absence of other data, may significantly underestimate the average size of the blocks and the VBP, with errors that can reach 50% for medium sized and 90% for VBP (Haneberg, 2004).

### Uncertainties in estimating VBP

As discussed, the borehole might create chords of different lengths which vary between a maximum value equal to the diameter and minimum value equal to the smaller chord at one end of a block shown in Fig.1.9. So, there is always ample room for uncertainties when the estimation of VBP is done using the scanlines or borehole logs.

Medley (1997) studied the uncertainties in such estimation. The author constructed four physical models with different VBPs of 13%, 32%, 42% and 55%.

They were composed of the matrix of plaster of paris with ellipsoidal blocks of dried pottery clay and play-ash. The dimensions of the models were 150×100 mm with depths between 100-150mm and area was 170 $cm^2$. Blocks had a ratio between major, intermediate, and minor axes of 2:1:1. Blocks varied in five size classes of 3-6mm, 6-12mm, 12-24mm, 24-48mm and 48-96mm. These classes are divided with a threshold of $0.05d_{max}$ i.e. $0.1d_{max}$, $0.2d_{max}$, $0.4d_{max}$, $0.8d_{max}$. The length of the largest block ($d_{max}$) was 70-95mm

The block size distribution had the fractal distribution of $2n^{2.3}$, which is the typical block size distribution of Franciscan mélange (Medley and Lindquist, 1995). The samples were prepared and cured for 24 hours. Then the models were cut into 10 slices and photographed. In Fig.1.11, one such photograph of a slice can be seen. Ten scanlines were drawn on each photograph depicting the drillings in the ground. So, in total 100 model boreholes were defined for each sample.

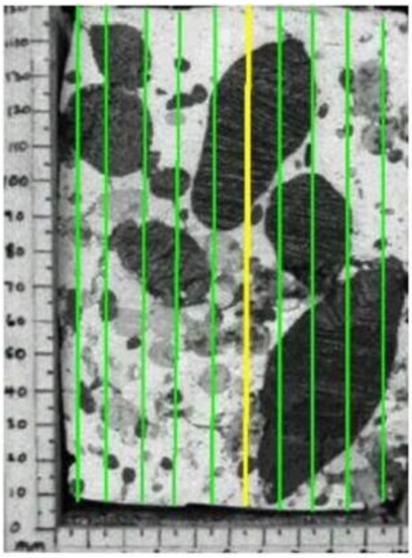

**Figure 1.11:** Scanlines on a cut of slice from the physical model sample. This particular sample has a VBP of 42%. Hundred such slices of the fabricated physical model were studied. (Medley 1997)

Shown in Fig.1.11 is a portion of a model characterized by VBP equal to 42%. Green scanlines represent the drilling of boreholes from which it is possible to get the information related to the linear fraction of the blocks. The yellow line indicates the centre of the sample.

Measuring the size of the blocks intersected by boreholes (scanlines) larger than $0.05\sqrt{A}$ i.e. 6 mm (this is the scale independent threshold length between block and matrix discussed earlier). The block linear proportion for each scanline was calculated. Block linear proportion is the sum of the block length intercepts divided by the total length of the scanline. These linear proportions varied a lot locally, but if cumulated they come closer to the actual block volumetric proportions. Indicating that extensive sampling would result in a good estimation of actual VBP. But such large-scale drilling is not feasible in the field. The researchers also measured the $1/3^{rd}$ of the scanline to depict a case of shallow boring.

Through a randomization process, subsets of slices were selected. The cumulative linear proportion for these subsets was calculated and plotted against N*$d_{max}$, where N*$d_{max}$ is the total length of sampling used for each point expressed as a multiple of the length of the largest block ($d_{max}$) used in the model. It was observed that as the sampling size increases the scatter in the data decreases, and it gets near to actual VBP. For the higher VBPs, the scatter decreases at even less sampling length.

To determine the uncertainty, a plot between SD/Vv (considered as a measure of uncertainty) and N*$d_{max}$ was constructed as shown in Fig.1.12. Here SD is the standard deviation of linear proportion and Vv is the actual volumetric proportion. The plot, shown in Fig.1.12, indicates that as volumetric proportion increases the uncertainty decreases and it also decreases with an increase in sampling length.

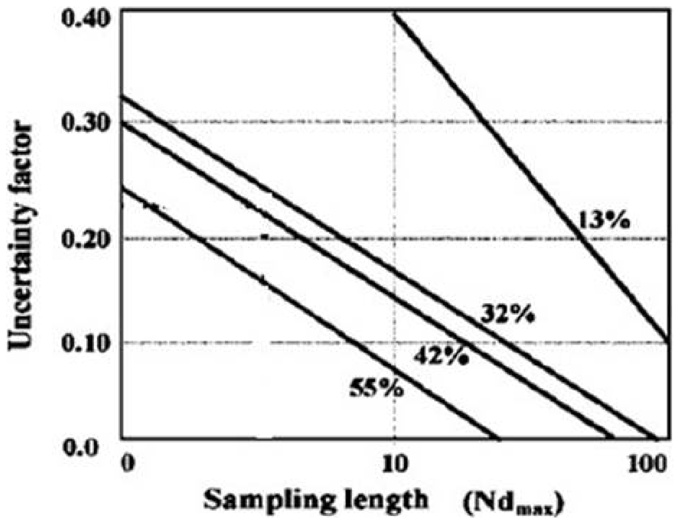


**Figure 1.12:** Plot between SD/Vv (uncertainty factor) on the vertical axis and N*dmax on the horizontal axis. Such plots, in practice, are used to count for the uncertainties in using linear block proportion as volumetric block proportion. (Medley 1997)

In 2002 Medley revisited this data and compared it with the 3D Block Size distribution (3D BSD). The comparison shows very less agreement between the 3D BSD and 1D Chord Length Distributions (1D CLDs). The Fig.1.13 shows the result of the comparison. The effect of “tailing” due to boring is elucidated. A higher number of smaller sized blocks were created than the actual 3D BSD.

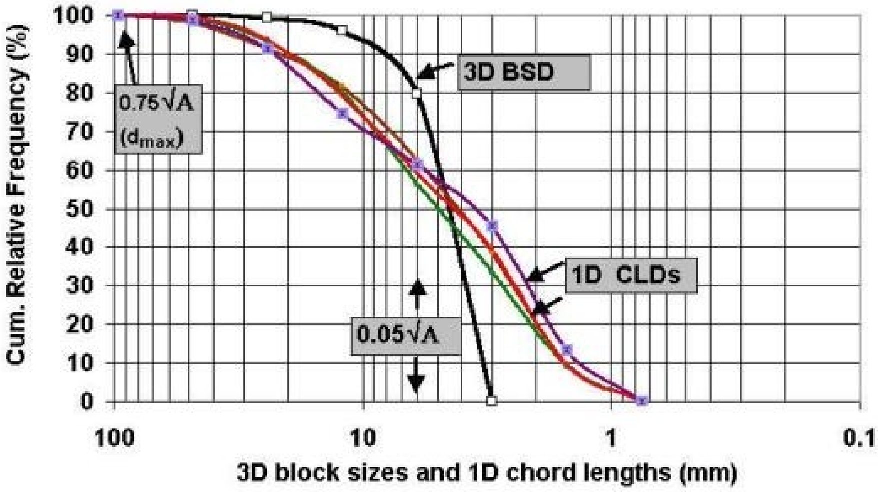


**Figure 1.13:** Comparison between 3D block size distribution (3D BSD) and 1D chord length distributions (3D CLD). (Medley 2002)

### VBP estimation based on chords: the physical model of Lindquist 1994

Mentioned above, was Medley's model which he prepared to calculate uncertainty in the process of estimating VBP from scanlines or drilling.

Earlier Lindquist (1994), also prepared physical models for testing the mechanical properties of bimrocks. The author used bentonite-Portland cement mixture for matrix material and sand-Portland cement fly ash mixture for blocks. He used three different block proportions and four different orientations of blocks, relative to the vertical direction of the load axis. The significance of the orientation of blocks is discussed later in the section on the mechanical properties of bimrocks. Cylindrical samples with a diameter of 150 mm and a height of 300 mm were used. Three different VBPs of 30%, 50%, and 70% were used in modelling. The block sizes ranged between 12-116.5 mm. The size classes were selected as 10-19mm, 19-38mm, 38-75mm, and 75-150 mm. Relative frequency of blocks in each class size was 75.3%, 18.9%, 4.7%, and 1.2% respectively.

Medley in 2002 used these specimens to trace the circumferential surfaces on trace paper. One such trace of block surface is shown in Fig.1.14. On the left is the tracing of vertical blocks with VBP equal to 34%. On the right is the horizontal block's tracing of block proportion equal to 72%.

These tracings were sampled with ten vertical scanlines (grey lines in Fig.1.14) and block intercepts were measured. Block linear proportions were calculated by summing the block intercepts and dividing by the total length of scanlines. These

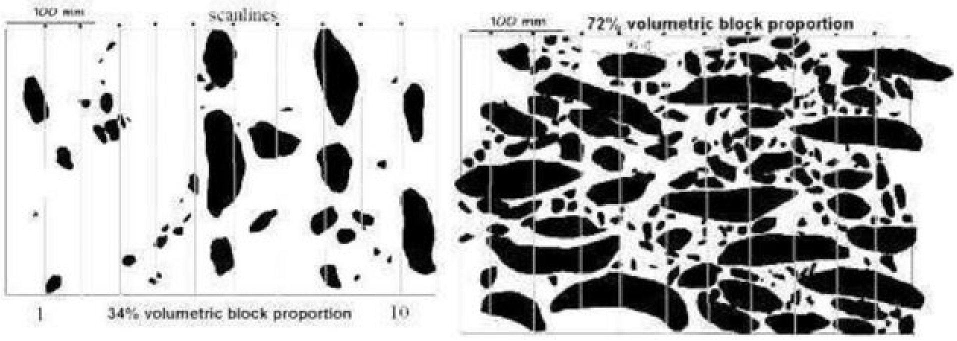


**Figure 1.14:** Tracings of blocks from circumferential surfaces of physical models of Lindquist 1994. (Medley 1997)

1D chord length distributions were compared with the known block volumetric proportions and 3D blocks size distribution (BSD). The results are shown in Fig.1.15.

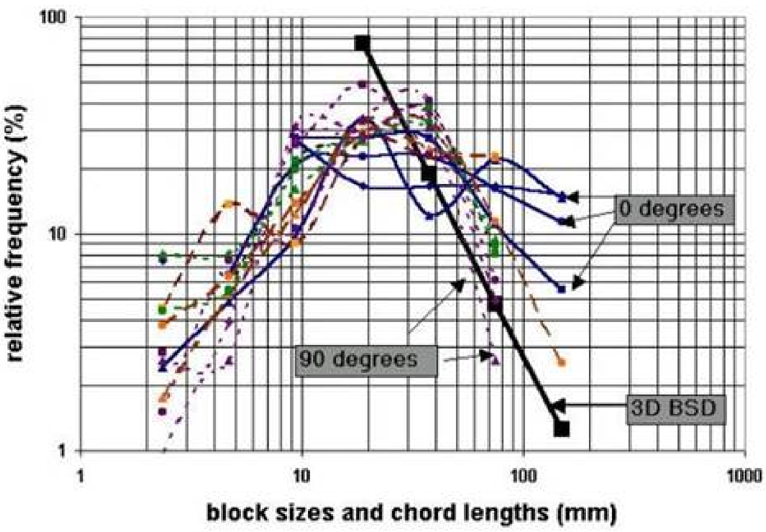


**Figure 1.15:** Comparison of 3D Block Size Distribution and 1D chord length distributions obtained from scanline on tracings of blocks as shown in Fig. 1-14. (Medley 2002)

It is evident from Fig.1.15 that scanline results are deficient in representing the real 3D block size distribution. However, there is a consistency in the peak of linear block proportion (LBP) and high frequency of smallest size blocks in 3D.

It can be concluded, after discussing these two physical models of Lindquist

(1994) and Medley (1997), that 1D chord length distribution hardly replicates the real 3D block size distribution. 1D chord length distributions can be converted to 3D block size distributions considering the statistical uncertainties. In practice, geo-practitioners have used the uncertainty chart of Medley (1997) (Fig.1.12) for estimating the VBP. Minuto and Morandi (2015), have used this approach for converting 1D drilling lengths to VBP.

## 1.3 Mechanical properties of bimrocks

The vast structural heterogeneity in bimrocks makes their mechanical characterization a challenging job. Even the modern techniques of analysis, used in rock mechanics are not enough. A laboratory sample obtained from drilling does not represent the overall bimrocks mass. So, a large scale in-situ test and a full-scale site investigation, wide enough to study the position, location, volumetric proportion of blocks would give confidence to designers. But such large-scale tests are often not feasible, neither economically nor physically.

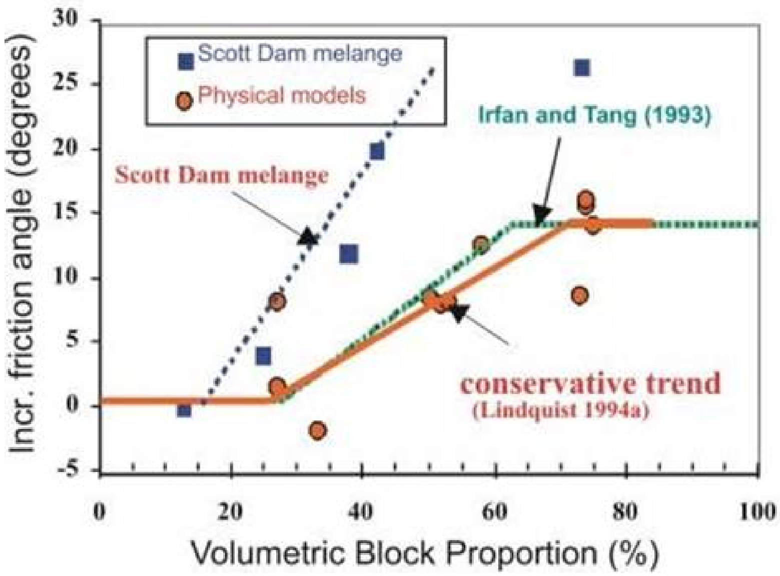


**Figure 1.16:** Mechanical properties of bimrocks increase with an increase in VBP. Irfan and Tang 1993 studied the Colluvium of Hong Kong and Lindquist fabricated physical models of bimrocks. There is an increasing trend in the friction angle in all three studies (Lindquist 1994)

In literature, some simplified approaches have been developed that can be used to predict the strength of bimrocks by a weighted average of relative strengths of the blocks and weaker matrix based on their VBPs. Researchers have shown in laboratory and by means of large in-situ tests that the strength of matrix increase with the increase of block inclusions (Fig.1.16). Not only VBP but also the position, shape, size, and orientation of blocks in the weak matrix influence the mechanical properties of bimrocks. The scale of study or interest is another aspect of importance because the matrix-block threshold changes with the scale of interest. According to Medley (1994, 2001, 2002) and Medley & Lindquist (1995), the blocks with a size greater than 0.05Lc and lower than 0.75Lc have an impact on the mechanical properties of bimrocks. The Lc, here is the "characteristic engineering dimension" discussed in section 1.2.3.

In what follows, are the different studies that were carried out for the determination of mechanical characteristics of bimrocks. These studies are divided into three categories. First, the studies which were carried out on laboratory, small scale, artificially fabricated physical models. Second, the studies which deal with large-scale tests are discussed. Such tests were carried out in the field. Lastly, numerical studies are discussed which were carried out on virtual laboratory samples using numerical codes.

### 1.3.1 Artificially fabricated physical samples

As established earlier bimrocks are large bodies of heterogeneous material. Therefore bimrocks are difficult to study at a small scale. So, researchers fabricated small scale samples to imitate the bimrocks. In such studies, samples were fabricated consisting of a weaker matrix and specific content of blocks. These samples were then tested in the laboratory. The effect of block content and orientation of blocks on mechanical properties of bimrocks were analysed. In literature, some of these studies include Lindquist (1994), Altinsoy (2006), Afifipour et al.( 2013), Kalender et al. (2014).

The strength parameters of bimrocks are closely related to the properties of the block inclusions. Generally, it was found that VBP less than 25% does not affect the strength properties. From 25% to 75%, there is a gradual increase in the friction angle and a decrease in cohesion (Lindquist 1994). After 75% of the VBP, the strength characteristics do not change drastically. Afifipour et al. (2013) studied the effect of VBP greater than 70% on the mechanical properties of bimrocks. It is one of the few studies which considers VBP higher than 75%.

Lindquist (1994) conducted a series of triaxial compression tests on the artificially fabricated physical bimrocks samples in the laboratory. The samples consisted of the matrix of bentonite-Portland and blocks, with elliptical shapes, were made of sand-Portland cement-fly ash mixture. The blocks had a major to minor axis ratio of 2:1.

The samples had different block proportions varying between 25% to 75%. The author also studied the effect of the orientation of the block inclusions, relative to the vertical direction of the load application, on the mechanical properties of bimrocks. Four blocks orientations of 0°, 30°, 60°, and 90° were studied. Fig.1.17 shows the four different orientation angles of rock blocks relative to load application.

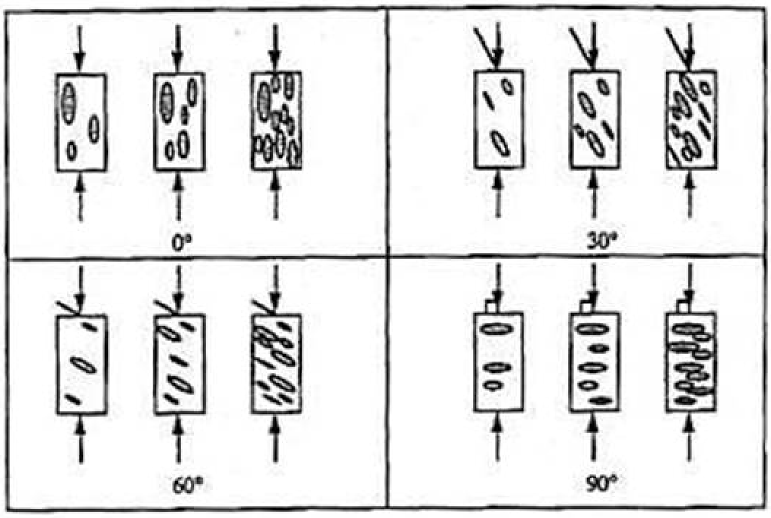


**Figure 1.17:** Fabricated physical models of bimrocks. Four different orientation angles relative to the load application axis can also be seen. (Lindquist 1994)

The tests results showed an increase in the friction angle of bimrocks up to 15°-20° with an increase in VBP from 25-75%. Cohesion, instead showed a decreasing trend with the increase in VBP. The result of the friction angle increase and cohesion angle decrease is shown in Fig.1.18 (a) and (b) respectively. The failure plane was found to make its way through the block-matrix contacts due to the fact that blocks are stiffer than the matrix. The decrease in cohesion is due to the poor mechanical properties of the matrix in the interface around the edges of the blocks, where the deformations tend to develop. So, higher proportion of blocks means more diffused weak areas, resulting in low cohesion. The friction angle increases due to the tortuosity phenomenon. This occurs due to the fact that blocks and matrix are mechanically high contrasted i.e. blocks are geotechnically more significant.

The specimen with 30° orientations had the lowest cohesion as compared to other orientations for the same VBP. At low VBP, the cohesion and friction angle, for the 0° and 60° specimen had similar values to that of the matrix material.

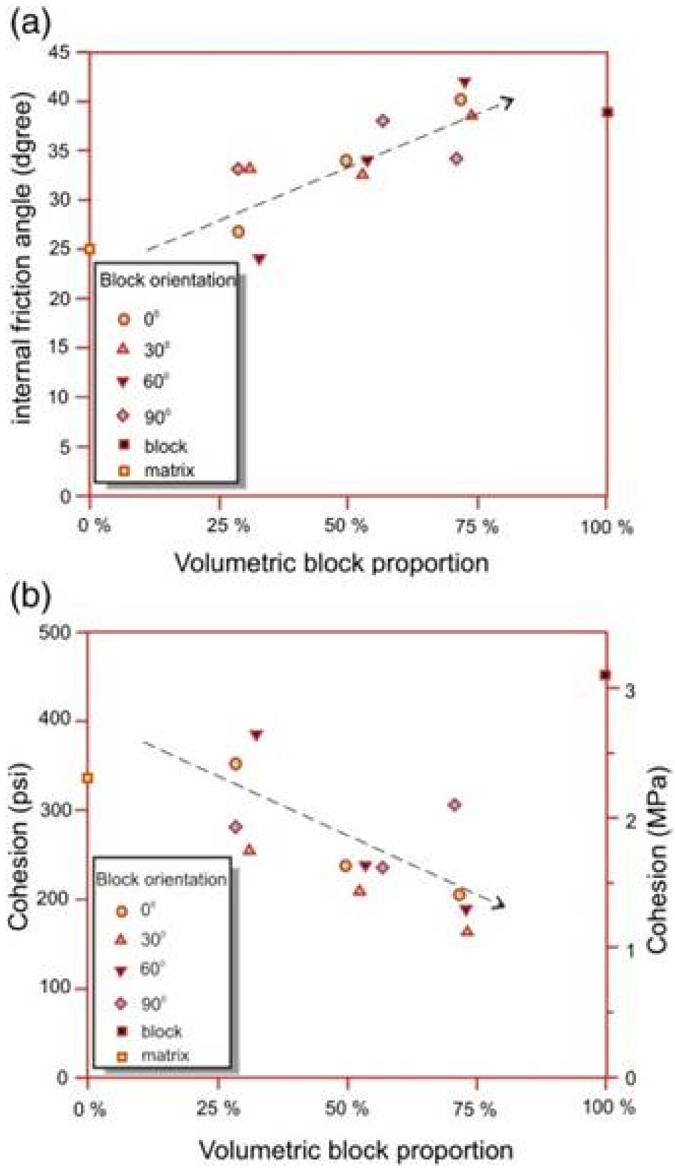


**Figure 1.18:** (a) Friction angle showed an increase of 15-20° with the increase in VBP up to 75% VBP. (b) Cohesion shows a downward trend with the increase in VBP. (Lindquist 1994)

In recent research studies, more attention has been paid to develop empirical approaches which can predict the strength parameters (c and $\phi$) or Unconfined Compressive Strength (UCS) of bimrocks. They include the works of Lindquist (1994), Gokceoglu (2002), Sonmez et al., (2006), Sonmez et al., (2009) and Kalender et al., (2014) etc. The Lindquist (1994) approach provides the cohesion and friction angle values for different VBP as discussed. Currently, no such empirical approach is internationally recognized in rock mechanics societies.

In another study for the development of empirical approach, Sonmez et al. (2006) performed uniaxial compression tests on artificially prepared samples. The samples had the matrix of Plaster of Paris, bentonite, cement and rock blocks of natural rock pieces prepared from tuff and andesite blocks. Four block contents of 0% (matrix only), 10%, 30%, and 50% by weight were used.

The UCS, Mohr-Coulomb (MC) parameters i.e. cohesion (c) and friction angle ($\phi$), and Hoek-Brown (HB) parameters were calculated for each VBP. These parameters were then normalized by dividing them for the values of the matrix-only and plotted against VBP. The following empirical equations were obtained which can be used to predict these parameters.

Mohar-Coloumb parameters:

$$c_{bimrock} = c_N c_{matrix}; \quad \text{where} \quad c_N = 1.25 - exp\,(\frac{VBP - 100}{75})$$

$$\phi_{bimrock} = \phi_N \phi_{matrix}; \quad \text{where} \qquad \phi_N = exp\,(\frac{8\,VBP}{1000})$$

$$UCS_{bimrock} = UCS_N \times UCS_{matrix}; \quad \text{where} \qquad UCS_N = 1 - exp\,(\frac{VBP - 100}{75})$$

Hoek-Brown parameters:

$$UCS_{bimrock} = \frac{2c\cos\phi_{bimrock}}{1 - \sin\phi_{bimrock}} \qquad\qquad \sigma_1 = UCS_{bimrock} + (\frac{1 + \sin\phi}{1 - \sin\phi})\sigma_3$$

$$m_{i\_N} = exp \quad (0.015\,VBP) \qquad\qquad m_{i\_bimrock} = m_{i\_N} \times m_{i\_matrix}$$

$$\sigma_1 = \sigma_3 + UCS_{bimrock}\sqrt{m_{bimrock}\,\frac{\sigma_3}{UCS_{bimrock}} + 1}$$

The values of these MC and HB parameters were evaluated by the re-calculated values of major principal stress ($\sigma_1$). The measured values were evaluated to obtain the error ratio and the graph in Fig. 1.19 shows that more than 60% of data have an error ratio of less than 3%.

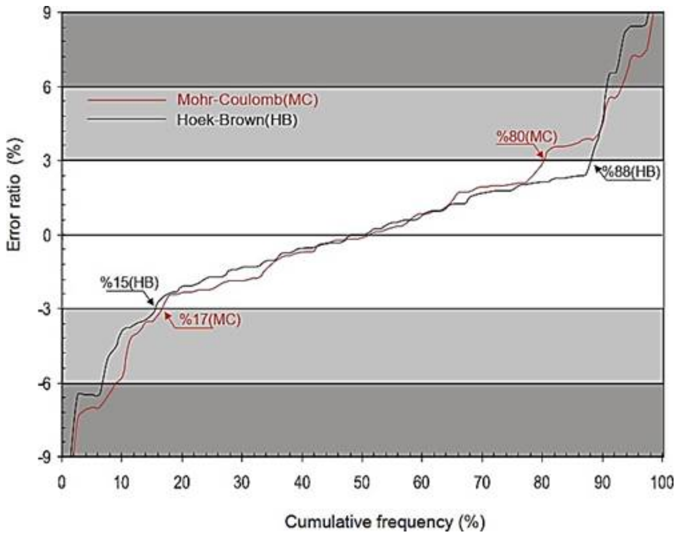


**Figure 1.19:** The cumulative frequency distribution of error ratio obtained by using major principal stress ($\sigma_1$) values predicted by the proposed empirical equations for both Mohar-Coulomb and Hoek-Brown criterion (Sonmez et al. 2006)

Despite having a lower error ratio, this empirical approach cannot be anonymously used because it is based on a limited number of artificially made samples and may not replicate the actual ground situations.

Sonmez et al. (2009) presented another conceptual approach for predicting the overall strength of bimrocks with some defined set of boundary conditions. The boundary conditions being:

- the internal friction angle of bimrocks increases with low increment up to 25% VBP and at a higher rate from 25-75% VBP.
- It does not increase after 75% and at this VBP the friction angle is equal to the angle of repose ($\alpha$), which is the maximum possible.
- The Unconfined Compressive Strength (UCS) of bimrocks decreases to zero with the increase in VBP.

Using these boundary conditions the following equations were obtained. These equations are shown in the form of curves in Fig. 1.20.

$$\phi_{bimrocks} = \phi_{matrix}\left[1 + \frac{1000[\frac{\tan\alpha}{\tan\phi_{matrix}} - 1]}{100 + 5(\frac{100-VBP}{15})}\left(\frac{VBP}{VBP+1}\right)\right] \tag{1.1}$$

$$UCS_{bimrock} = \left[\frac{A - A^{\frac{VBP}{100}}}{A-1}\right]UCS_{matrix} \qquad 0.1 \leq A \leq 500 \tag{1.2}$$

$$c_{bimrock} = \frac{UCS_{bimrock}[1 - \sin\phi_{bimrock}]}{[2\ \cos\phi_{bimrock}]} \tag{1.3}$$

The authors used among the others, the data from artificially fabricated physical models of Lindquist (1994) and Altinsoy (2006) for comparison with the empirical approach. The data of these two studies can be seen in the graphical representation of empirical equations in Fig. 1.20 (b).

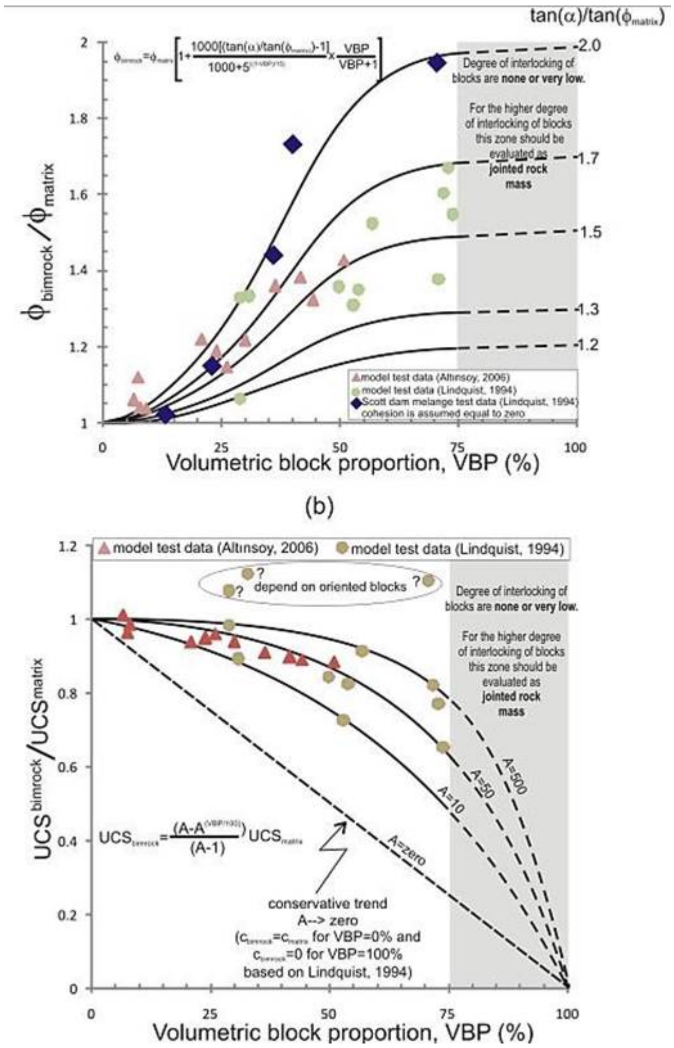


**Figure 1.20:** Graphical representation of empirical equations of Sönmez et al. 2009. The top graph is for the prediction of friction angle and the bottom is for the UCS prediction of bimrocks. (Sönmez et al. 2009)

There is a use of a constant "A" which depends on the adhesion between the blocks and matrix. For higher adhesions, the value of “A” approaches to 500 and for almost no adhesion its value is 0, which is a conservative trend. This empirical approach has the shortcoming of fewer data. The grey portion in Fig. 1.20 shows that there is no available data for VBP greater than 75%.

Most of the contemporary studies have focused on the VBP of less than 75%. Afifipour et al. (2013) tested the laboratory samples with block inclusions higher than 70%. The authors prepared two samples of 100×200mm and 150×300 with block proportion, by weight, of 70%, 80%, and 90% and tested under triaxial compression tests. For higher block inclusions, like this, the VBP can be assumed to be equal to weighted block proportion. The addition of the findings of this study in the empirical approach of Sonmez et al. (2009) is shown in Fig. 1.22

Kalender et al. (2014), created a database of studies consisting of Lindquist (1994), Altinsoy (2006), BimTests (Coli et al. 2011; discussed later in the sections of the large-scale test), Afifipour et al. (2013) and Calaveras dam data. These data were plotted on the graphical representation of the empirical equations of Sonmez et al 2009. The graphs are shown in Fig. 1.21 and Fig. 1.22.

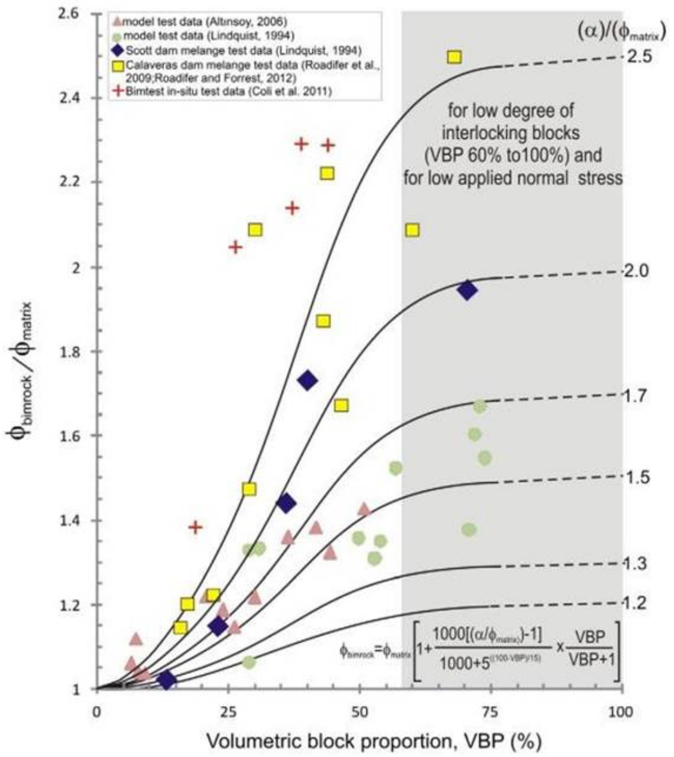


**Figure 1.21:** Graphical presentation of the empirical approach of Sonmez et al 2009 for predicting the friction angle of bimrocks. It also includes two more studies of Bimtest (Coli et al 2011) and Calaveras dam. (Kalender et al. 2014)

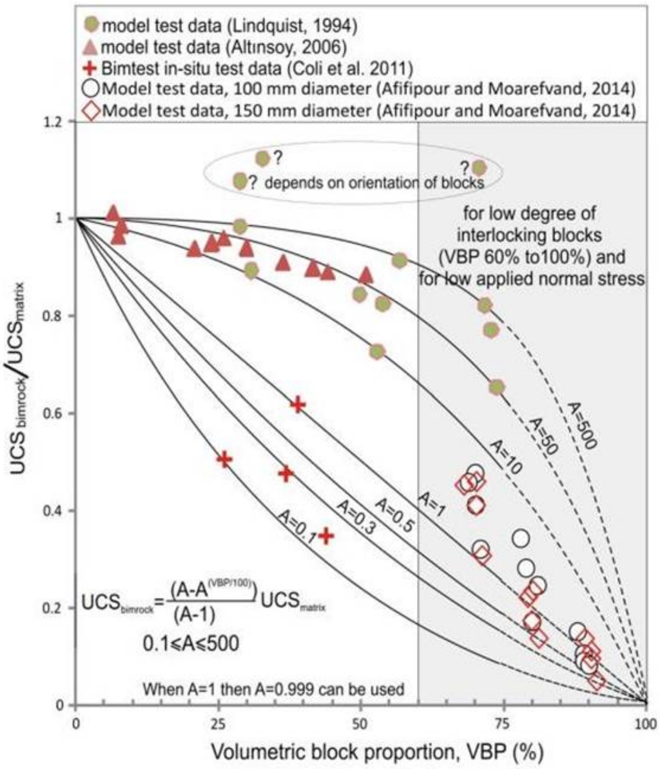


**Figure 1.22:** Graphical representation of the empirical approach for predicting the UCS of bimrocks. The data from BimTest (Coli 2011) and Afifipour et al. 2013 are also included. (Kalender et al 2014)

This approach comparatively has more data and complements some of the case studies carried out in the field. But the universality of the approach is yet to be tested and there is ample room for improvement. Napoli et al. (2018) have compared the result of this approach with the heterogeneous approach in their study of the stochastic approach for slope stability.

### 1.3.2 Large scale in-situ tests

Large scale tests are another source for determining the mechanical characteristics of bimrocks. Contradictory to the general, in-situ testing on bimrocks are economically and structurally not easy to conduct.

In Santa Barbara open-pit mines Italy, such large-scale tests were carried out. The area of Santa Barbara mine is abundant in Shale-Limestone Chaotic Complex (SLCC) bimrocks. Coli et al. (2011) carried out six non-conventional shear tests and labelled them as “BimTests”. These were called non-conventional tests because, unlike standardized shear tests, the slip surface is allowed freely to develop in the specimen.

The specimens were 80×80 cm in size and had a height of 50 cm with a volume of 0.3 $m^3$. The VBP for each specimen was determined by the in-situ large scale sieve analysis. The arrangements of BimTest are shown in Fig.1.23.

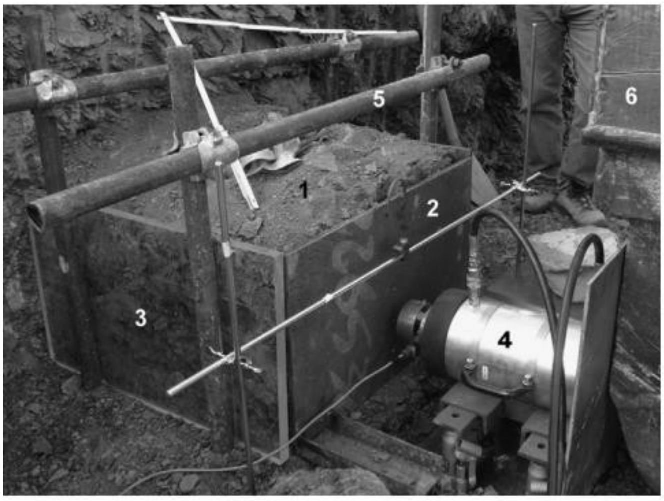


**Figure 1.23:** In-situ non-conventional shear test apparatus. (1) Specimen (2) Frontal steel plate (3) Lateral plexiglass plate (4) Hydraulic jack (5) Iron bars (6) Reacting Caterpillar Dozer (Coli 2011)

The results of the tests, when plotted on force-displacement curves, showed two yield levels unlike soils, which shows one yield level. One such plot is shown in Fig.1.24 for test specimen P3.

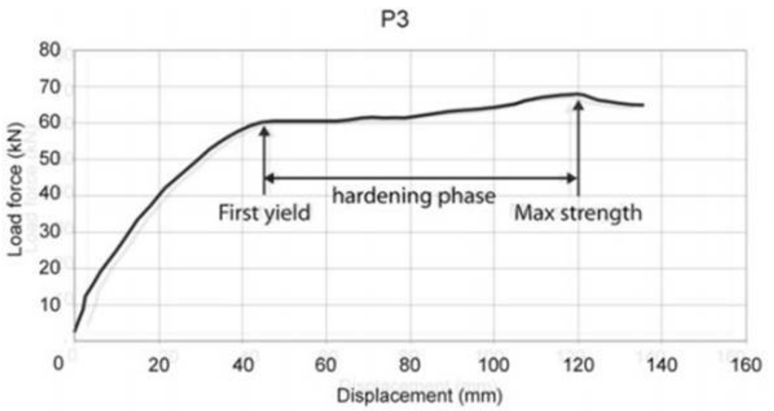


**Figure 1.24:** Load-displacement curve for specimen P3. Two yield behaviour and a hardening phase are evident. (Coli 2011)

Values of Mohr-Coulomb parameters i.e. c and $\phi$ were calculated using the simplified limit equilibrium criterion. The trend confirmed the result of earlier studies and showed an increase in friction angle with the increase of VBP and a decreasing trend in cohesion. The plots are shown in Fig.1.25.

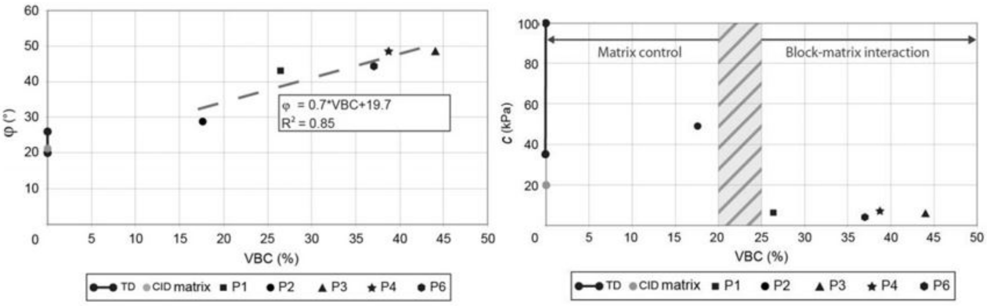


**Figure 1.25:** Result of BimTests. left) The friction angle increases with an increase in VBP right) a decrease in cohesion with an increase in VBP. (Coli 2011)

In Fig.1.25 right plot, there is a sudden drop in cohesion which might be a threshold between blocks and matrix. Above this VBP the blocks seem to be taking control of the mechanical behaviour of bimrocks. The matrix/block threshold is shown as a grey strip.

A similar in-situ large-scale direct shear test was carried out by Xu et al. (2015). They studied the effect of rock block inclusions in soil used for the core wall in a high embankment dam in China. They carried out four direct shear tests under different normal loads and compared the results with that of soil only.

The size of the test sample was 60×60 cm and had a height of 30 cm. Concrete material was used to provide enough bearing reaction from horizontal load jack. The normal load was applied through sandbags put over supporting columns. To control the normal loads, jacks were used. The arrangement of the test is shown in Fig.1.26.

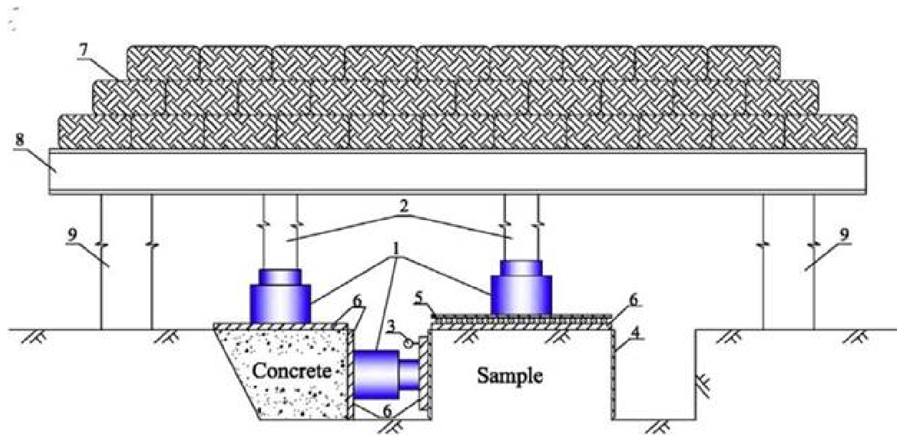


**Figure 1.26:** Test equipment of the large-scale direct shear test 1- Jacks 2- Force transfer column 3- Dial indicator 4- Shear box 5- Sliding steel plate 6- Steel plate 7- Back pressure system 8- Beam 9- Supporting column (Xu et al. 2015)

The block content in the sample was 35%. The stress-strain curve showed that there was a hardening phase before the peak strength. Generally, the peak strength was higher as compared to the soil only. An increase of 7° was observed in the friction angle and the cohesion decreased by 35 kPa. The relationship between shear strength and normal stress is shown Fig.1.27. SRM in the plot is “Soil Rock Mixture” an alternative term for bimrocks/bimsoils, more commonly used among the researchers of China.

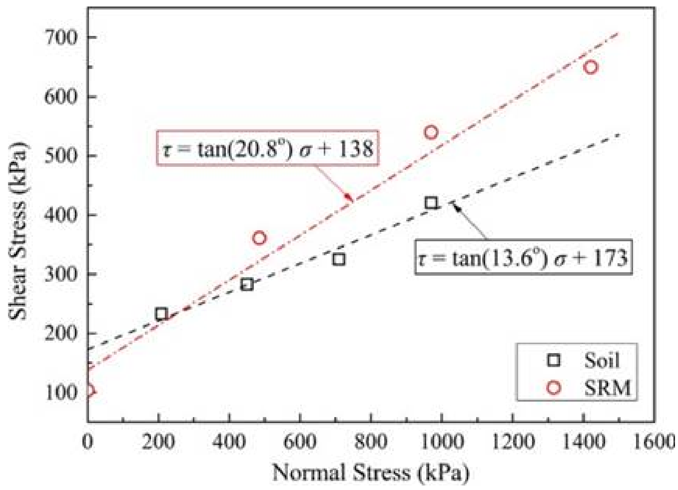


**Figure 1.27:** Relationship between shear strength and normal stress for both soil and bimrocks. (Xu et al. 2015)

These large-scale studies have some deficiencies. One being the non-uniformity of stresses and strains in the sample due to its large size. Another deficiency is that the side friction of the shearing box might affect the procedure. Even the large-scale test might not be effective in the case of bimrocks where rock blocks are more than tens of meters. But these tests have confirmed the trends of mechanical properties reported in the literature.

### 1.3.3 Numerical modelling of laboratory tests

Numerical studies have been used for simulating the tests in any numerical method environment such as the Finite Element Method (FEM), Finite Difference Method (FDM), or Discrete Element Method (DEM). In such studies different sample sizes, extending to meters can be tested. Some prominent numerical studies in the literature include Barbero et al. (2008), Pan et al. (2008), Xu et al. (2008), Yayong et al. (2014), and Xu et al. (2016). In their respective studies, they have also confirmed the trends of laboratory studies.

Barbero et al. (2008) simulated compressive tests on bimrocks using finite difference and finite element methods. With the use of the statistical distribution, it was possible to generate blocks of random size, orientation and position in the specimens. They performed both 2D and 3D simulation of confined and unconfined compressive tests with VBP ranging between 12-54% for 2D and 10-40% for 3D models. It was found that the unconfined compressive strength increases with the increase in VBP. The same trend was observed for the deformation modulus. The plot in Fig.1.28 shows these trends.

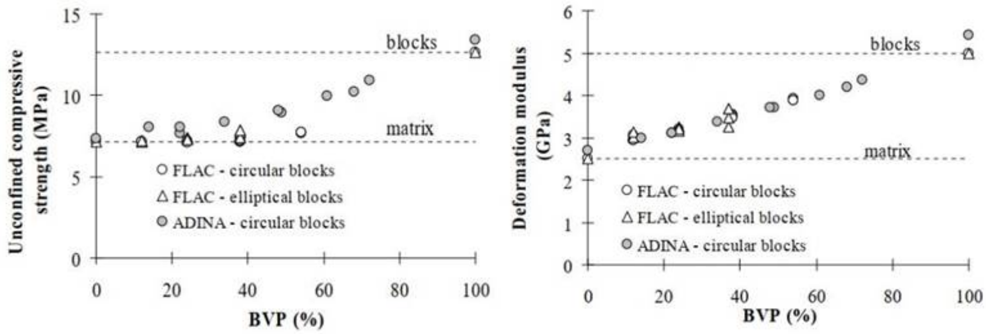


**Figure 1.28:** Relationship between VBP and UCS. (left) and VBP and deformation modulus (right) for 2D blocks. Different numerical codes results are compared. (Barbero et al. 2008)

Similar results were found for the 3D analyses. At 10% of VBP, there was no difference in the mechanical response in comparison with the matrix-only. There is an indication that the block-matrix threshold is at 20%, above which the effect of block inclusions is substantial. The compressive strength and deformability modulus increase with the increase in the VBP.

Pan et al. (2008) studied the effects of block content, orientation and aspect ratio of rock blocks in their numerical study of virtual samples. These simulated specimens were tested in the triaxial compression test. The effects of different shapes as triangular, quadrangle or pentagonal were studied. The VBP ranged between 30-75% and the block orientation, relative to the vertical axis ranged between 0-90°. Four aspect ratios (length: width) of 1:1 1.5:1, 2:1 and 3:1 were used as shown in Fig.1.29.

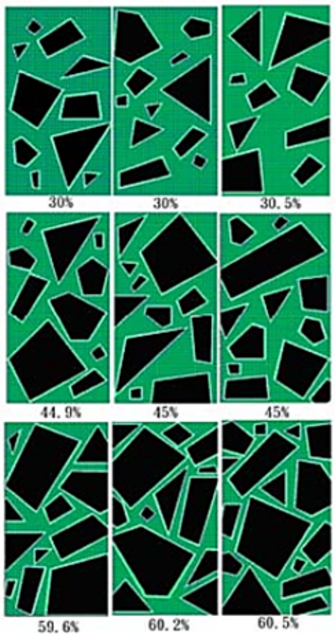


**Figure 1.29:** The specimens at the top have 30%, middle ones have 45% and the bottom ones have 60% VBP. The specimens have blocks of different shapes, orientation and aspect ratios. (Pan et al., 2008).

The tests were carried out with the Finite Difference method (FDM) code. The results were in agreement with that of Lindquist (1994). With the increase in the VBP the strength of bimrocks, the strength being the ultimate deviatoric stress on the stress-strain curve, increased. The increase was prominent as the VBP crossed 50%. The Young Modulus also increased, reinforcing earlier studies. The orientation of blocks influenced the mechanical properties. The lowest strength occurred at 45° of orientation for similar block proportion and aspect ratio. For Lindquist(1994), this lower value of strength occurred at 30°. Lindquist had block orientation of only 30º and 60º and no value in between. Young modulus decreased with an increase in orientation. The influence was significant between 15-45°.

Regarding the aspect ratio, the mechanical properties increased with the increase in the difference between length and width, but the influence was negligible. This might be because of the small size of the specimen.

Yayong et al. (2014) carried out triaxial compression tests on soil rock mixture (bimrocks) with a three-dimensional Finite Difference code. The authors used the stochastic approach for the size, position, and orientation of rock blocks. He found a three-staged yield in the stress-strain curve of bimsoils as shown in Fig.1.30. In the large scale in-situ 'BimTests', Coli (2011) found that bimrocks showed a two-staged yield.

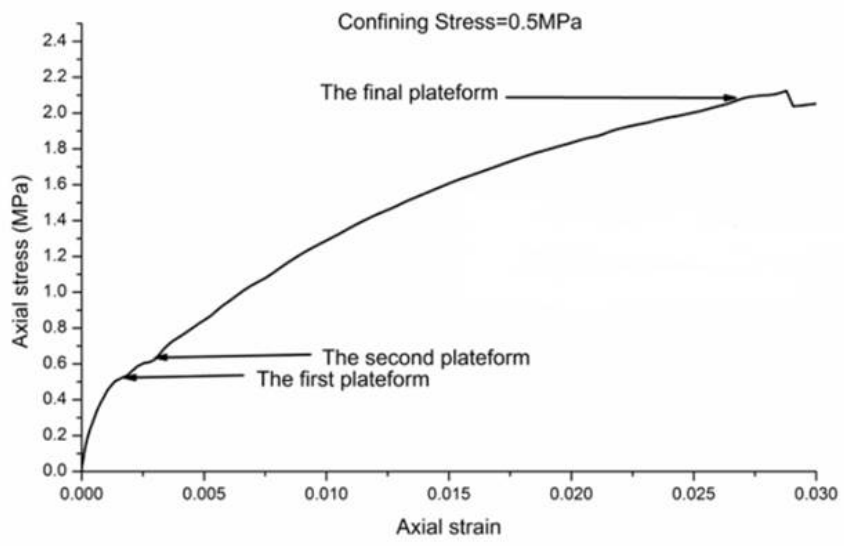


**Figure 1.30:** The stress-strain curve of the virtual model tested using the triaxial test. The three-staged yield of material is evident (Yayong, 2014)

# Chapter 2

# Slope stability in bimrocks

## 2.1 General introduction

This chapter aims at the aspects of the stability of slopes in bimrocks and how the inclusion of blocks affects the slope stability. As mentioned in the earlier chapter, the rock block inclusions in bimsoils force failure surfaces to navigate around the blocks. This creates the *"tortuosity"*. The phenomenon of tortuosity and failure mechanism in bimrocks are discussed in the first part of this chapter. Due to inherent dimensional and spatial variability of bimrocks, the use of a stochastic approach is reasonable and auspicious which is discussed at the end of this chapter.

When analyzing the slope, practitioners often consider whole soil mass as an equivalent homogenous material. This makes them unable to get the description of the heterogeneity of rock mass, since they assign the mechanical properties of the weaker matrix to whole rock mass. The presence of blocks results in an increase in the safety factor. There are many studies in literature focusing on the slope stability analysis in bimrocks. Irfan and tang (1993) studied the slopes in colluvium of Hong Kong. Medley & Sanz (2004) studied the slopes of Ankara conglomerates and Minuto & Morandi (2015) studied a relict landslide of bimrocks in Genova, Italy. Barbero et al. (2006), Guerra et al. (2016), Napoli et al. (2018) and many other researchers have studied theoretical slope models in bimrocks.

Although bimrocks are common worldwide, recently some indications have been surfaced for their characterization and design (Medley, 2001; Medley & Wakabayashi, 2004) but these are not yet recognized internationally among the societies of rock and soil mechanics.

## 2.2 Tortuosity of failure surfaces in slopes

In the previous chapter, we established that bimrocks consist of rock blocks and matrix. The block inclusions are geotechnically significant as compared to the soil matrix. According to Medley (1994), the expression "geotechnically significant" implies that $\tan\phi_{block}/\tan\phi_{matrix} \geq 2$ and $E_{block}/E_{matrix} \geq 2$ hold. The block-matrix contact is generally the weakest part of bimrocks, thus failure surfaces occur in this weak zone. The phenomenon of tortuosity can arise, depending on the VBP, size, shape, and orientation of the rock blocks. Thus, geotechnical motivation to understand the geometry and characteristics of failure surfaces in bimrocks emerges.

The distribution, position, and orientation of blocks in slopes change the path of failure surfaces. This is elucidated in Fig.2.1. In Fig.2.1 (a) the slope has a low VBP and it has no effect whatsoever on the path of the failure surface. In Fig.2.1 (b) the orientation of the blocks is along the slip surface and the slip surface has changed its path but is not tortuous enough. In the case of Fig.2.1 (c), the orientation of blocks is vertical and affects the failure surface position. Also, the blocks are almost uniformly distributed and there are no block-rich regions. So, in the case of Fig.2.1 (c) the tortuosity increases and has a higher factor of safety. Fig.2.1 (d) has a higher block content but due to the presence of block rich regions, the failure surface is not as much tortuous as that of Fig.2.1 (c). Large blocks or block-rich regions at the toe of slopes tend to bolster the slopes and add stability to the slope.

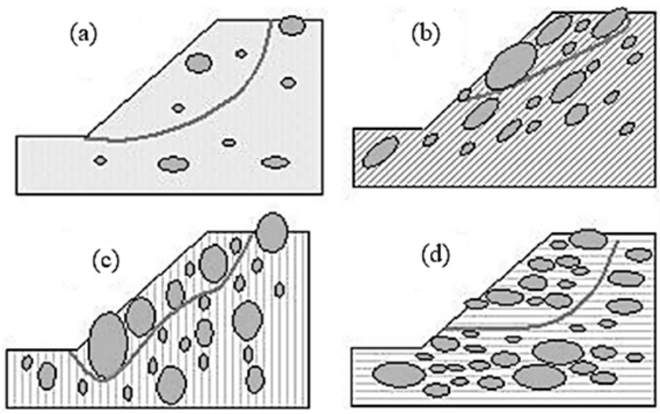


**Figure 2.1:** Four different scenarios for the path of the failure surface. (Medley 2004)

Lindquist (1994) fabricated more than 100 models and carried triaxial tests on them. The models and results are discussed in the previous chapter. These samples had a diameter of 150 mm and height of 300 mm. The VBP varied between 30-70%

and blocks had the orientations of 0°, 30°, 60° and 90°. Lindquist (1994) showed that failure surfaces passed around blocks and that the increase in the friction angle component of strength was due to the tortuosity of the failure surfaces. Medley & Sonmez (2004) observed that when the failure surfaces of Lindquist samples are closely inspected, it can be concluded that test specimens had approximately the same block size distributions, but different VBPs and block orientations. The sketch of Fig.2.2 shows the influence of varying block size distribution on the apparent zig-zag effect of the failure surface for two block configurations having roughly the same block volumetric proportion. The graded distribution forces a more tortuous failure path, despite the unrealistically smooth, rounded blocks. Medley (2004) found that block shape influences the tortuosity of the failure surfaces mainly when coupled with the orientation of the blocks.

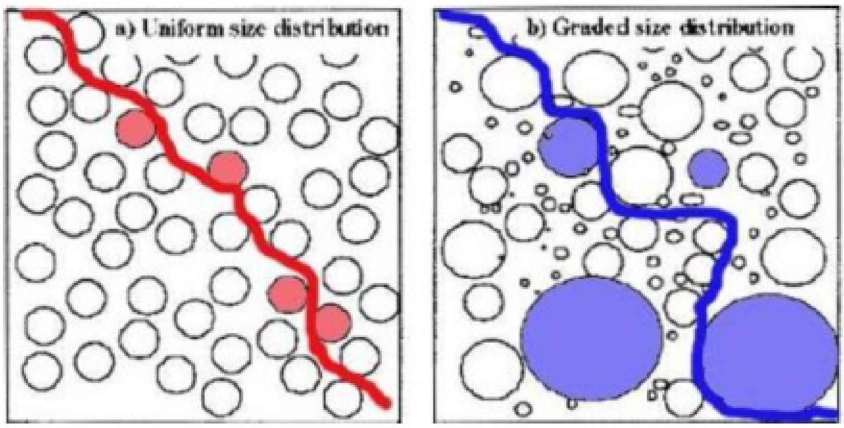


**Figure 2.2:** Failure surface in case of uniform block size distribution (left) and well-graded distribution (right) (Lindquist & Goodman, 1994)

Medley (2004) studied the failed physical models of Lindquist (1994) and presented different characteristics of tortuous failure surface and their dependence on VBP and block orientation. In Fig.2.3 three failed samples from the study of Lindquist (1994) are shown. At the top of figure orientation of block relative to the direction of load application and VBP can be seen.

Medley (2004) traced these failure surfaces on a plane tracing paper by wrapping the paper around the sample. The tracing of the failure surface of sample (C) in Fig.2.3 is shown in Fig.2.4. These tracings of failure surfaces were used to investigate their characteristics. The failure surfaces were expressed on the cylinder surface as irregular lines which tortuously negotiated around blocks (yellow line in Fig.2.4). The length of lines was measured using a flexible chain made of fine links that allowed it to be wrapped around tight bends and was called tortuous length

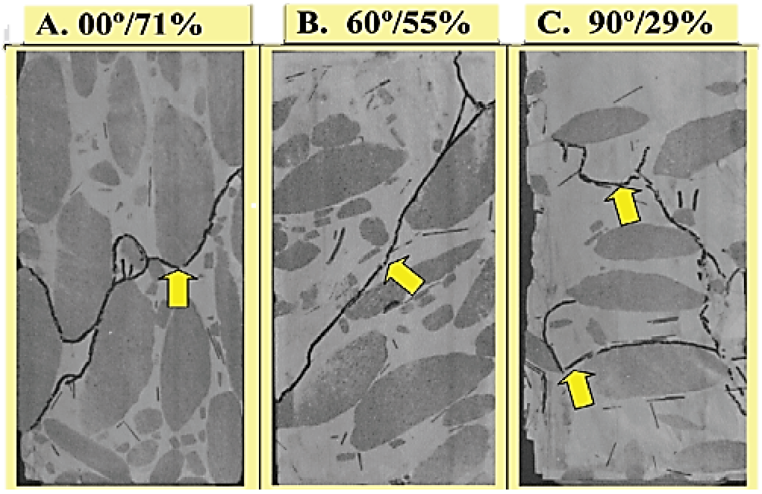


**Figure 2.3:** Cross-section of failed samples from fabricated physical models of Lindquist (1994). The arrows show the failure surface in samples after testing triaxially (Medley, 2004)

and indicated with L'. Another smooth line was also drawn which represented the failure surface if no blocks were present (red line in Fig.2.4). The individual lengths of block/failure surface contacts (blue line segments in Fig.2.4) were also measured, and these were summed up to produce a total block/failure contact length, identified as 't'.

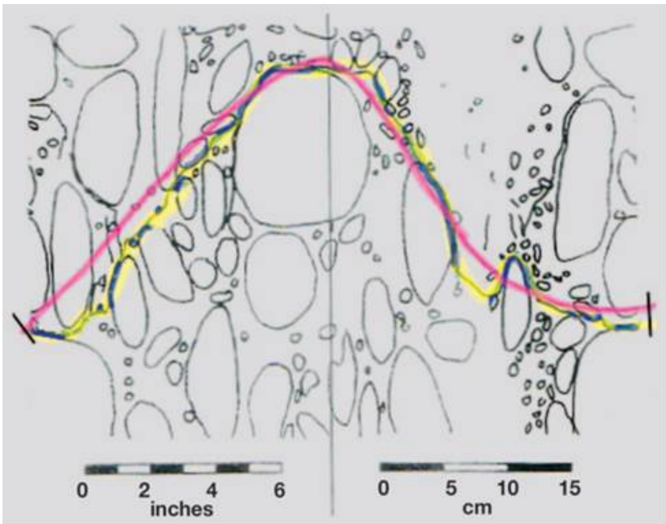


**Figure 2.4:** Tracing of failure surface of triaxially tested physical sample of Lindquist (Medley, 2004).

The smoothed line was first measured manually by the chain, then it was also re-measured digitally, and declared to be Lo. About 70 tortuous failure lines and smooth lines were measured.

Specimens with the same VBP and block orientation were grouped. Each tortuous line was drawn relative to its companion smooth line. The tortuous line was wandering around the smooth line. The specimens having more than one failure surfaces were also drawn. The final result of these tracing is shown in Fig.2.5 (for the samples shown in Fig.2.3). On comparing with Joint Roughness Coefficients (JRC) profiles, the JRC value turns out to be 10-20 (Barton & Choubey, 1977).

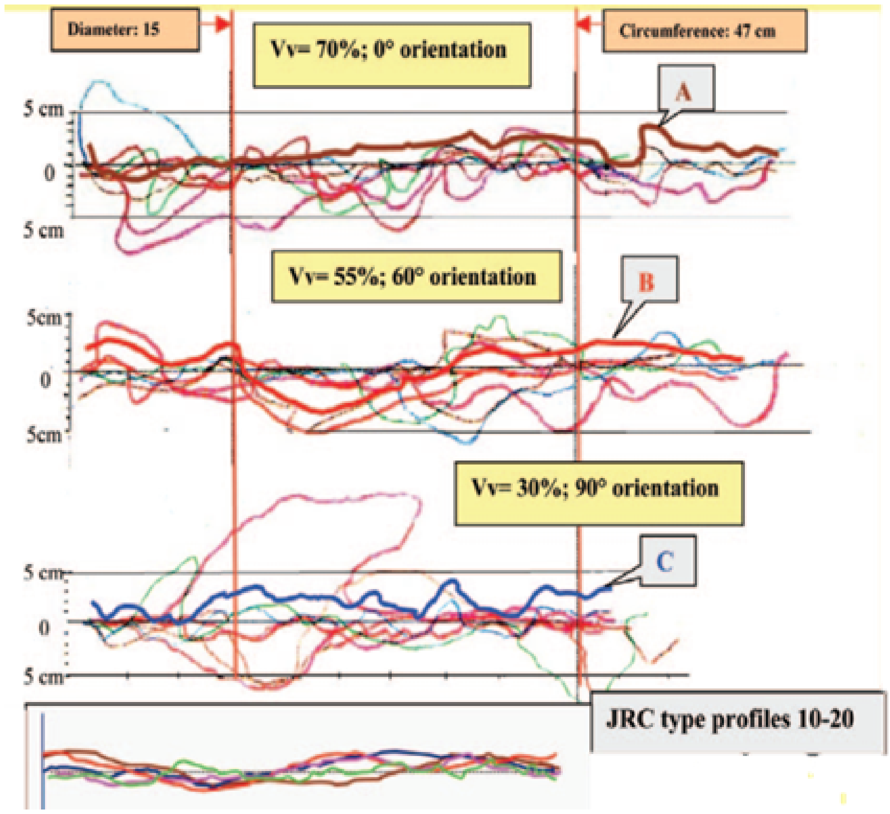


**Figure 2.5:** Scans of traced lines of failure surfaces and compared to type profiles for JRC 10 to 20. Highlighted tracings of failure surfaces are for specimens shown in Fig.2.3. (Medley, 2004)

Several intuitive parameters were generated from the measurements, as illustrated in Fig.2.6. One measure of tortuosity is the ratio of the length of the tortuous line connecting two points to the length of the shortest line between the same two points. This is referred to as the "tortuous length ratio" (L'/Lo) in this case.

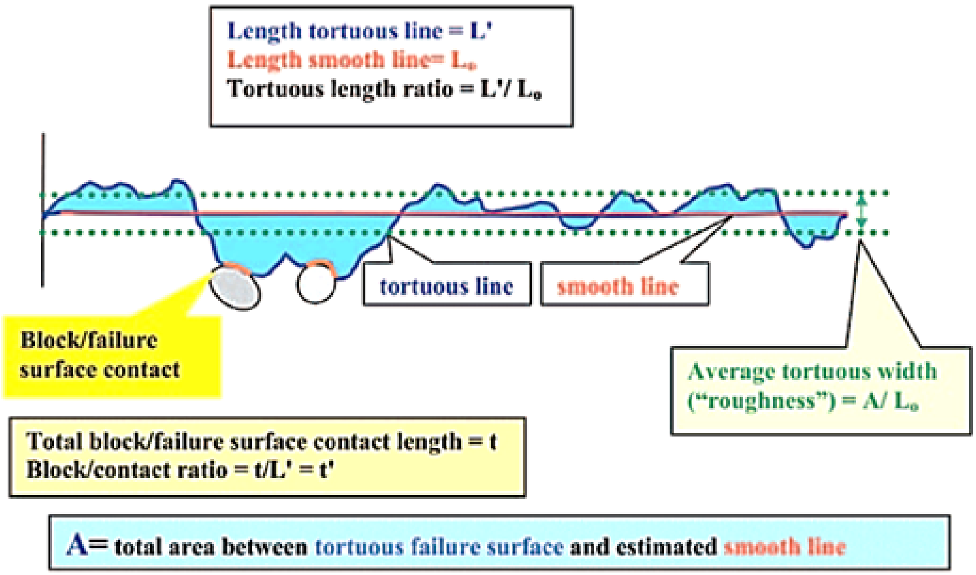


**Figure 2.6:** Parameters measured and calculated from traced lines of tortuous failure (Medley, 2004)

A summary of the results is presented in Fig.2.7 and Table.2.1. As shown in Fig.2.7(top plot), the author evidenced little dependence of the tortuous length ratio on VBP and block orientation. Tortuous length ratio varied more for lower block proportions (about 30%). The results summarized in the plots of Fig.2.7 suggest that, overall, there is little systematic variation between the geometry of failure surfaces with block proportions and block orientations. Medley (2004) however underlined that further work is needed to understand the reason for variation, and particularly why there is relatively little variation at about 50% VBP.

| Parameter | Unit | Symbol | Count | Mean | Standard deviation | Minimum | Maximum |
|---|---|---|---|---|---|---|---|
| Length Smooth Line* | cm | $L_o$ | 72 | 58.2 | 10.4 | 31.6 | 77.8 |
| Length Tortuous Line | cm | L' | 72 | 70.9 | 13.7 | 38.9 | 110.2 |
| **Tortuous Extension Ratio** | | L'/ $L_o$ | 72 | **1.22** | **0.046** | 1.03 | 1.6 |
| Total Length block Contacts | cm | t | 72 | 32.9 | 12.5 | 9.7 | 66.8 |
| **Block Contact Ratio** | | t/ L' | 72 | **0.46** | **0.18** | 0.12 | 0.79 |
| Tortuous Area | $cm^2$ | A | 73 | 84.2 | 37.7 | 24.9 | 225.4 |
| Length Smooth Line** | cm | $L_o$ | 73 | 59.4 | 9.5 | 41.7 | 81 |
| **Tortuous Width** | cm | A/$L_o$ | 73 | **1.44** | **0.68** | 0.5 | 4.45 |

* $L_o$ measured manually, ** $L_o$ measured digitally

**Table 2.1:** Summary of statistics (Medley, 2004)

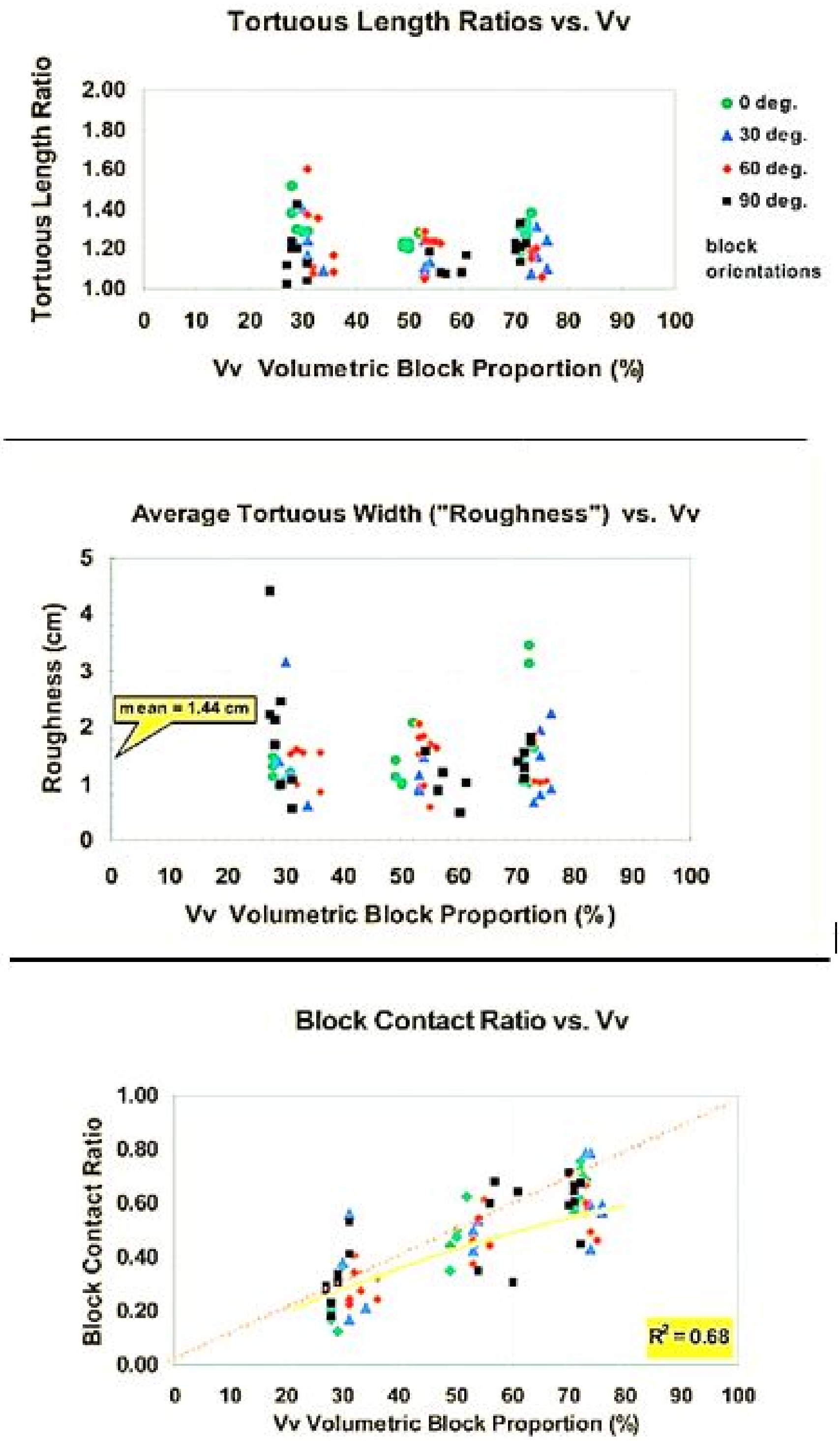


**Figure 2.7:** Plots of volumetric block proportions and: top) tortuous length ratios; middle) block/failure surface contact ratios and, bottom) average tortuous width (Medley, 2004).

The author also measured the surface roughness (or in this case "average tortuous width") defined as the average deviation of a surface above a mean line. The surface roughness was calculated by dividing the total of the areas between the irregular surface and the mean line (A), by the length of the mean line (Lo) as shown in Fig.2.6. The length Lo used was that measured digitally rather than the manual length measured using chains discussed above.

From Fig.2.7 (middle plot) it can be noticed that there is little sensitivity between the average tortuous width (roughness), VBP and block orientations, although there is more variation for the lowest block proportions. The mean tortuous width value for all 73 failure surfaces measured from Lindquist's triaxial specimens was 1.44 cm, with a standard deviation of 0.68 cm, shown in table.2.1. Accordingly, since the triaxial specimen diameter was 15 cm (Lc), the mean tortuous width was thus approximately 10% of the diameter plus or minus about 5% (for one standard deviation). Hence, an initial suggestion is that at any scale of engineering interest, once the characteristic engineering dimension has been selected (Medley, 2001), a first-order estimate of the thickness of a potential failure zone would be 5% to 15% of that width (Medley, 2004).

Fig.2.7 (bottom plot) summarizes the results for block/failure surface contact ratios (t/L'). There is some initial linear dependence between the proportion of failure surfaces that are tangent to blocks and the volumetric block proportions, but the linear dependence diminishes beyond about 50% volumetric block proportion. However, the author considers it would be conservative to assume that the linear dependence continues (as indicated by the red line on the plot).

Medley (2004) concluded that there is little value in defining potential failure surfaces for bimrocks. Instead, it is both prudent and appropriate to define failure zones with the thickness between 5% and 15% of the appropriate characteristic engineering dimension. It was also demonstrated that conventional rock engineering design approaches, which incorporate joint roughness coefficients selected according to specific type profiles, will be inappropriate. This is because the "roughness" of the failure surfaces in bimrocks far exceeds the roughness of the JRC type categories. Furthermore, the "joints" are not joints but are relatively thick zones of rock/soil mixtures that require analysis involving soil engineering approaches.

## 2.3 Failure mechanism in bimrocks

Generally, the shape and position of failure surfaces depend on the rock block proportion, mechanical contrast of the rock blocks to the matrix, and rock blocks' geometrical properties (Lindquist 1994; Medley 1994; Ke 1995; Sonmez et al. 2009; Coli et al. 2011; Afifipour et al. 2013). According to these effective factors, the schematic descriptions of three possible failure types in bimrocks specimens are depicted in Fig.2.8 (Xu et al. 2008).

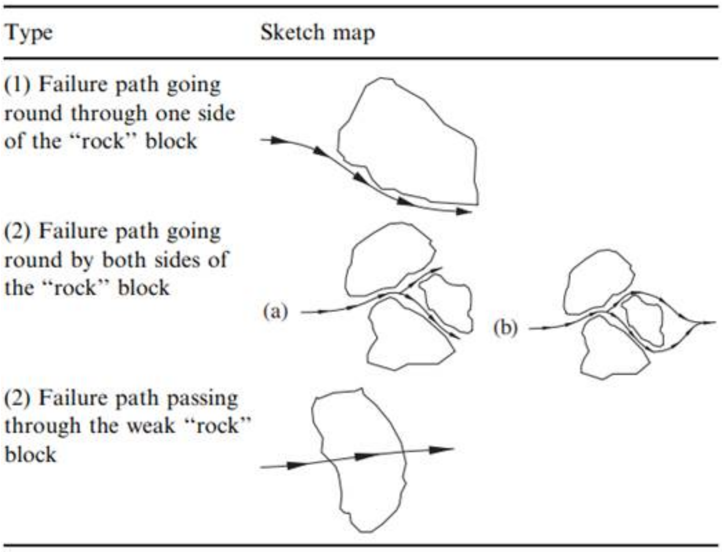


**Figure 2.8:** Three possible failure propagation models of bimrocks (Xu et al. 2008)

Type one is the deviation of failure path around rock blocks. This kind of failure occurs when the matrix is weaker and softer than interior rock blocks and when the blocks have enough relative space among them (i.e. floating condition). Typical examples of this type of failure are matrix-supported conglomerates, non-cemented coarse-grain alluviums and colluviums, mélanges (Medley, 1994; Lindquist, 1994), and andesite-tuff agglomerates (Sonmez et al., 2004b).

Type two is branching or widening the failure surface. This condition can be observed when the embedded rock blocks are stiffer than the matrix. A typical example of this condition are clast-supported conglomerates (conglomerates with a high proportion of rock blocks).

Type three is passing through rock blocks and matrix. This case corresponds to the conditions when mechanical contrast of the rock blocks to matrix is very low. Typical examples of this condition are calcite-cemented alluviums and colluviums, calcite cemented conglomerates, and fault breccias (Kahraman & Alber 2008).

## 2.4 Slope stability analysis in bimrocks

As discussed, the presence of blocks produces the phenomenon of "tortuosity". Due to this effect the factor of safety against failure increases. There have been some attempts to analyse the stability of slopes in bimrocks according to their VBP. Medley and Sanz (2004), Barbero et al. (2006), Minuto and Morandi (2015), Guerra et al. (2016), Napoli et al. (2018) are some prominent researchers who have analysed this topic. Medley and Sanz (2004) and Minuto and Morandi (2015) have used limit equilibrium methods (LEM) to analyse the slopes, while the other cited researchers have used numerical methods for stability analyses.

Lindquist and Goodman (1994) determined that bimrocks strength was generally lower when the inclination of blocks was about 30° degrees relative to the direction of the maximum principal stress. Pan et al. 2008 found the least strength at blocks orientation of 45° in their numerically tested model specimens. From the slope stability viewpoint, it is thus important to characterize the fabric of anisotropic bimrocks with sub-parallel blocks and shear. The blocks oriented at high angles to slopes increases stability due to an increase in the tortuosity. However, in melanges and fault rocks, the orientation of blocks and shear fabric can vary throughout the rock mass. So, the orientation of failure surfaces will vary throughout the slope (Medley and Sanz 2004).

### 2.4.1 Effects of block proportion on slope stability

The inclusion of blocks increases the slope stability as compared to the stability of the slope in matrix-only. To investigate the effect of the rock inclusions, Medley and Sanz (2003) prepared an idealized bimrock slope model, as shown in Fig.2.9. The slope had a height of 10 m, which would be the characteristic engineering length (Lc), and the face inclination of 35°. Rectangular blocks, having an aspect ratio of 2:1, and block distribution equal to that of Franciscan melanges were incorporated in the slope. Three different areal block proportions of 13%, 25% and 50% were used, assuming that the areal block proportion is the same as the volumetric block proportion.

The LEM analysis of the matrix-only model yielded a safety factor of 1.26. The failure surface is shown in Fig.2.9 as the dashed line. For the different block proportion models, potential slip surfaces were defined, and the factor of safety analysed. The values of these safety factors were normalized by dividing them by the value of the safety factor of the matrix only model and were plotted against the block proportion. The result is shown in Fig.2.10. All other variables being constant, the safety factor depends on an increase in the tortuous lengths of failure surfaces with increasing volumetric block proportion.

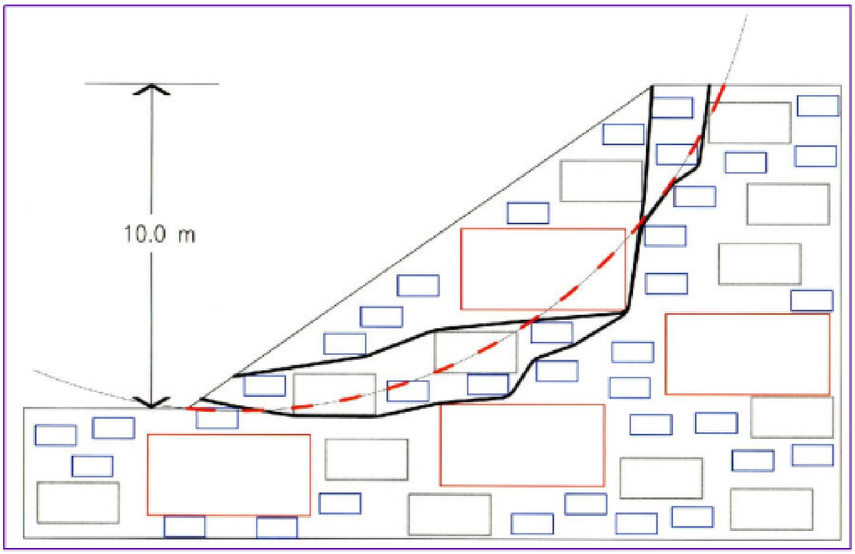


**Figure 2.9:** Example of a model bimrocks with 50% areal block proportion and randomly distributed blocks. (Medley  Sanz, 2004)

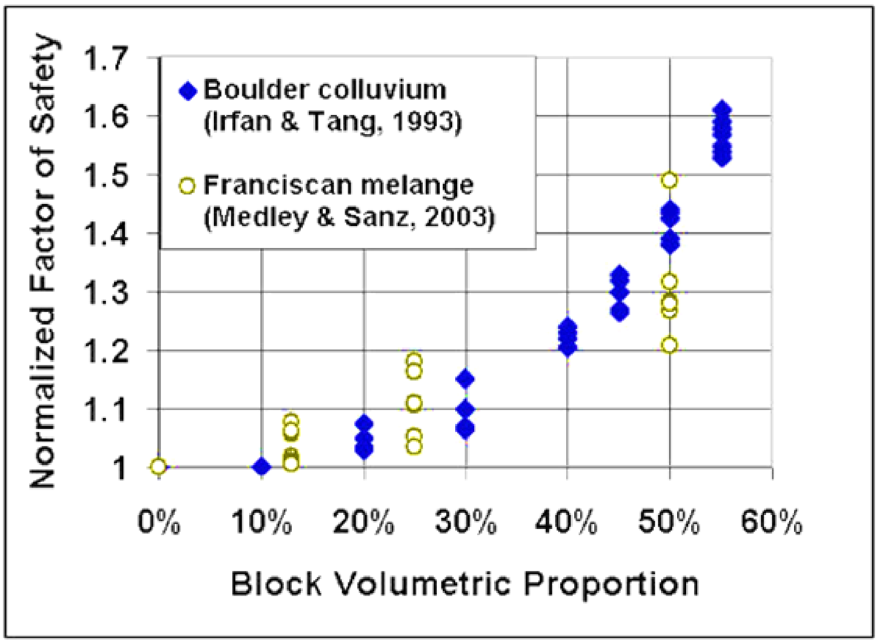


**Figure 2.10:** Comparison of results for Hong Kong colluvium (Irfan and Tang, 1993) and model slope of Medley and Sanz, 2004. The factor of safety increases with the increase in block proportion in slope. (Medley & Sanz, 2004)

A comparative study of the Medley & Sanz (2004) model with that of Irfan Tang (1993) was done. Irfan and Tang (1993) performed stability analyses of slopes in colluvium soil of Hong Kong. The model slopes were 10 m high and inclined about 60 degrees. A slope is shown in Fig.2.11.

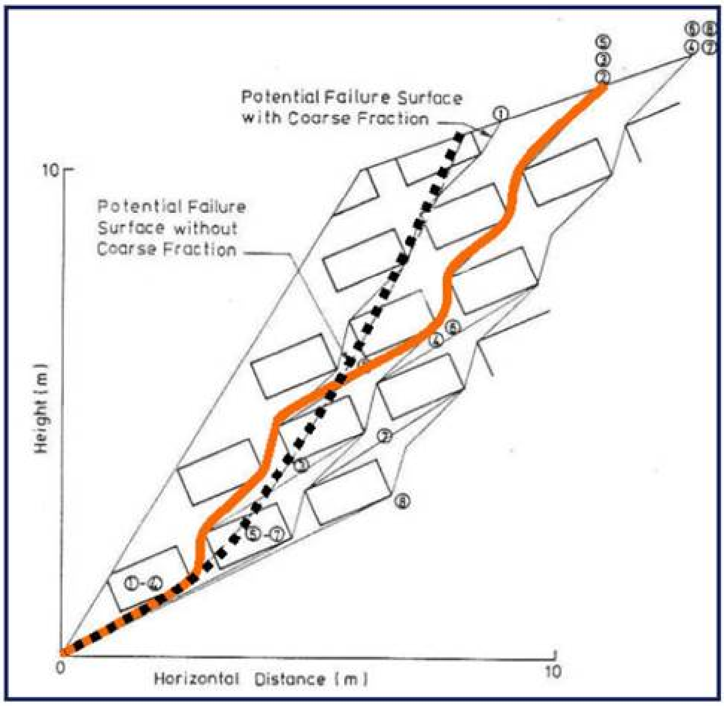


**Figure 2.11:** A 20% block proportion model of boulder colluvium. The dotted line is a critical failure surface for matrix only. The solid line is a tortuous trial failure surface (Irfan & Tang, 1992).

The Authors assumed uniform size and uniformly separated blocks layered out-of-slope. The block proportions varied between 10% and 55%. LEM was used for slope analysis. Irfan & Tang (1993) determined that the layering of blocks was as important as the volumetric proportion itself. Blocks with their long directions oriented parallel to sliding yielded lower normalized factors of safety as compared to blocks arrayed normal to the sliding direction. This is due to increases in the tortuosity of failure surfaces around the blocks. The comparison of the two studies can be seen in Fig.2.10. Despite the significant differences in the model geometries, the orientation of blocks, geology of the modelled materials, and analytical methods used for the analyses in both studies, there is a good relationship between the normalized factors of safety and the volumetric block proportions.

Medley & Sanz (2004) underlined that more analyses should be performed to define the statistical variations. Although it appears that up to about 25% to 30%

block proportion, the presence of blocks provides relatively little geo-mechanical advantage. From this lower limit to greater than 55%, there is a marked increase in slope stability.

Barbero et al. (2006) used the Finite Difference Method (FDM) for their theoretical slope stability analysis. They used a stochastic approach (discussed in the next section) to randomize the distribution, size and orientation of blocks in slope. The VBP varied between 20% and 50%. The shapes of blocks were circular and elliptical with different ratios between minor to the major axis (labelled as 'e') as shown in Fig.2.12 (b). With the use of a prepared code, based on the stochastic approach, indices of the blocks were generated as shown in Fig.2.12.

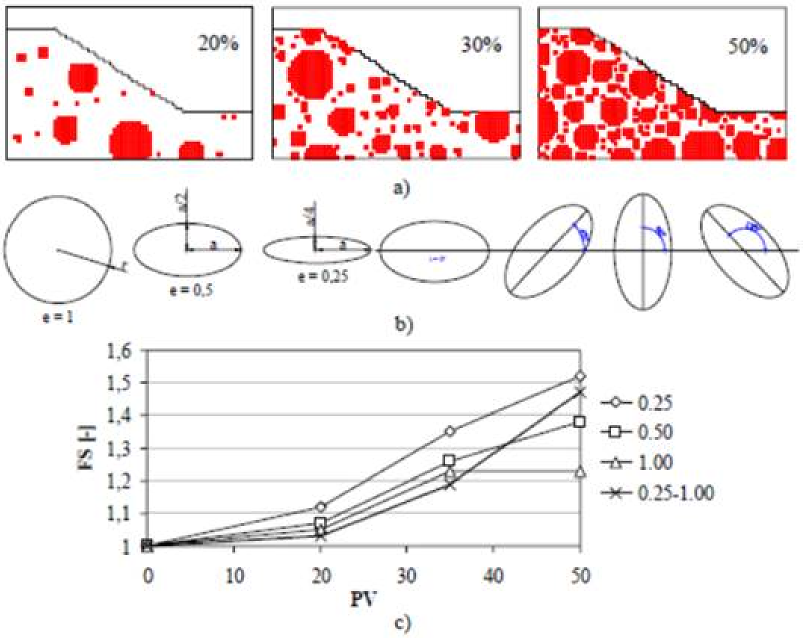


**Figure 2.12:** a) slope models for different VBP; b) shapes and orientations of blocks analysed; c) trend of safety factor with changing VBP (Barbero et al., 2006)

Barbero et al.(2006) found that the safety factor (FS) increases with increase in VBP. This increase is significant after 20% of VBP, indicating potentially a threshold below which the slope acts as if was matrix only (Fig.2.12 c). FS is higher for the blocks with a lower major to minor axis ratio (lower values of 'e').

Minuto and Morandi (2015) studied a relict landslide in the downtown of Genova Italy. After carrying out six boreholes on the site they estimated the VBP of the slope counting for uncertainties subjected to estimation of VBP from boreholes (Medley 1997). Rectangular blocks with two different block proportion of 15% and 30% were used. The slope was analysed using Slide, a LEM code, and found that the safety factor increases with the increase of VBP. This study is further extended in this thesis with the application of the stochastic approach and is analysed numerically.

### 2.4.2 Use of stochastic approach in slope stability

Bimrocks have inherent variabilities of spatial and dimensional kind. So, the analysis of slope is affected by variabilities, such as the VBP, shape, size distribution, position, and shape of blocks. Generally, researchers have used a deterministic approach for blocks size distribution, location and shapes of blocks which does not involve any statistical approach. Using a stochastic approach, the shape, size and positions of blocks are extracted from a code which is based on some statistical simulations. Napoli et al., (2018) adopted a stochastic approach for their analysis of model slope. To this aim, they prepared a code in Matlab® (MathWorks) which generated random sized blocks. The code needed as input some parameters including the VBP, the exponent of the negative power law for the frequency distribution of the size of blocks, the minimum and maximum dimensions of elliptical blocks used in the model, the ratio between the minor and the major axis of ellipses, the average direction and the standard deviation of the maximum diameter.

The Matlab code randomly generates the blocks from a population distributed according to following cumulative distribution function (Eqn. 2.1), so that the probability density function will be the truncated negative power law of Eqn. 2.2

$$F(d) = -\frac{a^{1+q} - d^{1+q}}{a^{1+q} - b^{1+q}} \tag{2.1}$$

$$f(d) = -\frac{1-q}{a^{1+q} - b^{1+q}}\, d^{\,q} \tag{2.2}$$

where q is the fractal dimension, a and b are the maximum and minimum block sizes, which will be 0.05Lc and 0.75Lc respectively.

In their study, Napoli et al., (2018) used both LEM and FEM analyses for the model slope of hight 10 m which would be the Engineering Characteristic Length (Lc). The 2D stability analyses were performed on several slope models of same geometry with VBP ranging between 0% (matrix only) to 70%. The Matlab code places the blocks correctly in the model slope following these requirements.

- Blocks cannot overlap each other, or it would not mean anything physically.
- To make the VBP same as that required, the blocks cannot be outside the external boundary. In such a case, it would underestimate the VBP.

So, a minimum distance of 10 cm among blocks and between blocks and boundary, was set to meet the two cases stated above. The output of this code is a text file with the diameters and coordinates of the block inclusions. These could be exported to AutoCAD, saved in .dxf format and then exported to LEM and FEM codes for the analysis. Fig.2.13 shows one such model in $Phase^2$ (FEM code by Rocscience Inc.) with blocks of different sizes. The model shown is meshed with triangular elements.

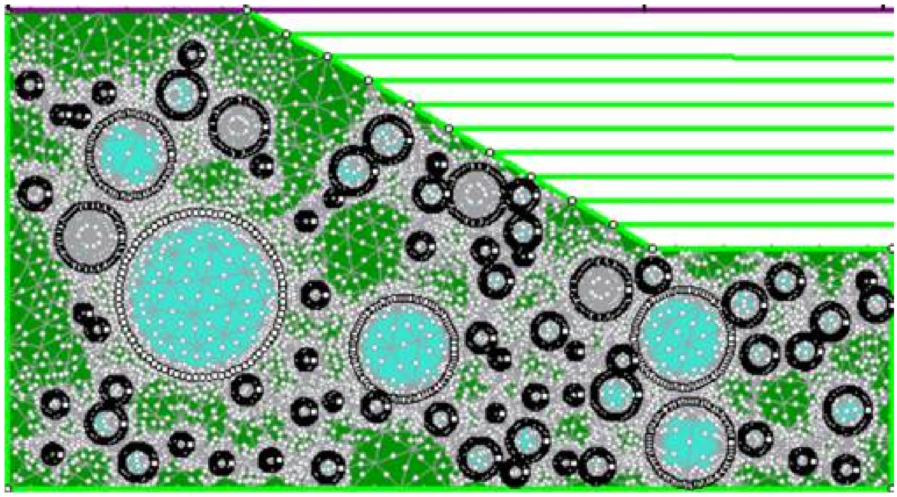

**Figure 2.13:** Model slope with rock inclusions in the FEM code RS2. The model is meshed. Different sizes of blocks are extracted from the code based on numerical Monte Carlo simulations. Ten such extractions, each one with different blocks positions and sizes were used for each VBP to validate the results statistically. (Napoli et al. 2018)

The novelty of Napoli et al. (2018) approach is that they performed ten extractions for each VBP to establish the validity of results statistically. They observed the increase in factor of safety with an increase in VBP complementing the previous studies. The increase in the safety factor was significant for VBP greater than 55

# Chapter 3

# Introduction to the case study and models implementation

This chapter is a recap of the study on the stability analysis of a relict landslide in the downtown of Genova, Italy by Minuto and Morandi (2015). The later part of the chapter explains the implementation of numerical and limit equilibrium models for the same study using the stochastic approach of Napoli et al. (2018).

For this thesis, the slope was analysed with two different types of approaches. One being the heterogeneous approach in which rock blocks are incorporated in the model and they have higher mechanical properties as compare to the matrix. Another being the equivalent homogenous approach in which only matrix material is used after increasing the mechanical properties of the matrix by taking into account the block content. In literature, two prominent empirical strength criteria, which assume the material to be homogenous and isotropic are the Lindquist (1994) and Kalender et al. (2014) criteria. This chapter also aims at describing the model implementation for such equivalent homogenous approaches.

## 3.1 Introduction to the case study

Minuto and Morandi (2015) studied the stability of a relict landslide in the downtown of Genova (Italy) with the Limit Equilibrium Method (LEM). The material of the slope is a mixture of colluvium with rock blocks so it was classified as bimrocks/bimsoils. The local bedrock consists of flysch sediments related to a turbidite sequence of limestones, marls and mudstone. The area of study is an adjoining slope at the toe of a large quaternary landslide located on the right bank of Fereggiano creek. Two retaining walls of concrete are also present to retain some expected failures in the slope. The maximum height of the slope is about 40m and the groundwater table was monitored through standpipe piezometers.

No earlier geotechnical or geological survey data was available. So, to define the depth of bedrock and estimate the Volumetric Block Proportion (VBP) in the slope body, six boreholes were carried out. Samples were also retrieved from boreholes for laboratory testing. The result of sieve analyses showed that there was gravel (30% to 63%) and sand (18% to 46%) with some fraction of finer material. The standard direct shear tests carried out on undisturbed samples of fine material revealed the effective strength parameters i.e. c' (cohesion) and $\phi'$ (friction angle) to be 10 kPa and 27° respectively.

The strength parameters obtained from the direct shear test are not representative of the whole slope due to the high percentage/quantity of inclusion of coarse material and rock blocks. From literature (Irfan & Tang, 1993; Lindquist 1994) it is evident that the friction angle of the matrix increases with increase in coarse fraction. So, the friction angle of fine material was increased by 4° for every 10% increase in coarse fraction after the total coarse content exceeds 25%. So, for an average gravel content of 50% the friction angle was increased by 8° and, therefore, the overall friction angle of the fine and coarse content (fine + coarse matrix in Table 3.1) would be 35°.

The estimation of VBP was done according to Medley (1994). The lower and upper limit of blocks are 0.05Lc and 0.75Lc, Lc being the characteristic engineering dimension. Minuto and Morandi (2015) assumed Lc to be the depth of the failure surface, which is not known beforehand. So, a value of 10m was used, obtained from the deepest failure surface of the matrix-only analysis with LEM, based on laboratory parameters. The linear blocks proportion, which is obtained by summing the lengths of the block intercepted by the boreholes and dividing this value by the total length of borings, turns out to be around 18%. The uncertainty factor obtained from Medley (1997) chart of uncertainty (Fig.1.12) was 0.3. So, the VBP ranged between 13-25% which, for practical reasons, was assumed to be 15% and 30%. From literature it is observed that an increase in VBP results in an increase in friction angle and decrease in cohesion. The change in parameters was taken into account only for 30% VBP because the effect on the shear strength is usually negligible for VBP less than 25% (Lindquist and Goodman 1994). Therefore the friction angle was increased by 2° and effective cohesion was reduced to 5kPa. The effective shear strength parameters implemented in the slope stability model are summarised in Table 3.1.

| | Geotechnial properties | |
|---|---|---|
| | c' (kPa) | $\phi'$ (°) |
| Fine matrix | 10 | 27 |
| Coarse Matrix | 10 | 35 |
| 15% blocks | 10 | 35 |
| 30% blocks | 5 | 37 |

**Table 3.1:** Geotechnical properties of different models used in the analyses (Minuto & Morandi 2015)

The authors used rectangular blocks based on their observations of the slope area. The blocks used in the analysis were selected based on a simple statistical analysis for the blocks intercepted by the boreholes. Three different blocks dimensions of 0.5×1 m, 1×1.5 m and 1.5×2.5m were used having percentage of 55%, 35% and 10% of the block content. The blocks were distributed deterministically in the slope model.

The slope was analysed with the Slide 5.0 code (Rocscience Inc), which is a limit equilibrium code. The Mohr-Coulomb failure criterion was adopted as the constitutive law for the material and the GLE/Morgenstern-Price (1965) method was used for the analysis. The authors neglected the shallow slip surfaces, as the commissioners/sponsors of the study were interested in potential deep failure which may occur in future. For fine matrix analysis, a safety factor of 0.99 was obtained while for the coarse matrix the safety factor was 1.28, which is 30% more than that of the fine matrix. These slipe surfaces obtained by Minuto and Morandi (2015) are shown in Fig.3.1

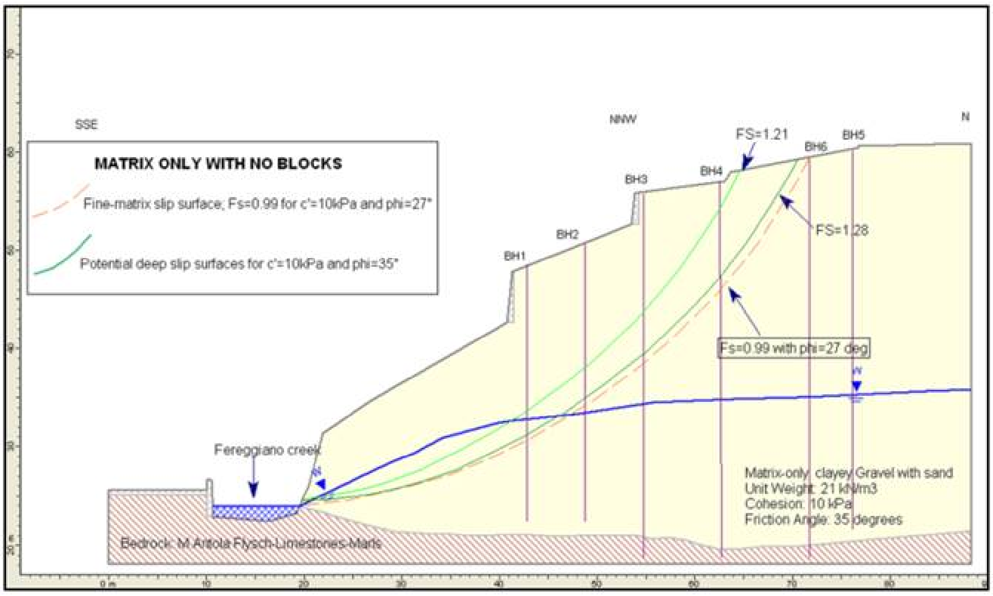


**Figure 3.1:** The failure surfaces of fine matrix and coarse matrix analyses. The blue line shows the piezometric line which shows the average height of groundwater measured during the rainy season. The location and depth of six boreholes (BH) are also shown. The hatched elements near BH1 and BH3 are two earth retaining walls. (Minuto & Morandi 2015)

The analyses of the slope with VBPs 15% and 30% had an increase of 12% and 23% respectively in the safety factor as compared to the coarse matrix model. The tortuous failure surfaces, obtained by tracking the failure surface around the blocks for these two different VBPs, are shown in Fig.3.2 and Fig.3.3 respectively.

The authors concluded that an upper and lower value of safety factor is probably more appropriate than a single value due to high uncertainty in content, size and position of blocks. They recommended a study with the finite element method would be more auspicious.

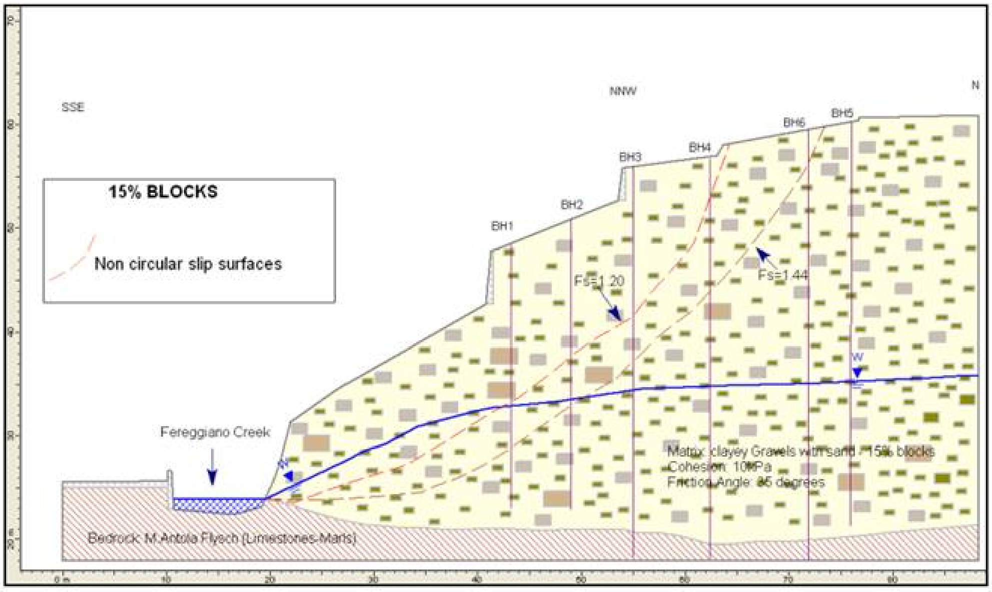


**Figure 3.2:** The failure surfaces for the 15% VBP analysed with LEM code Slide. (Minuto & Morandi, 2015)

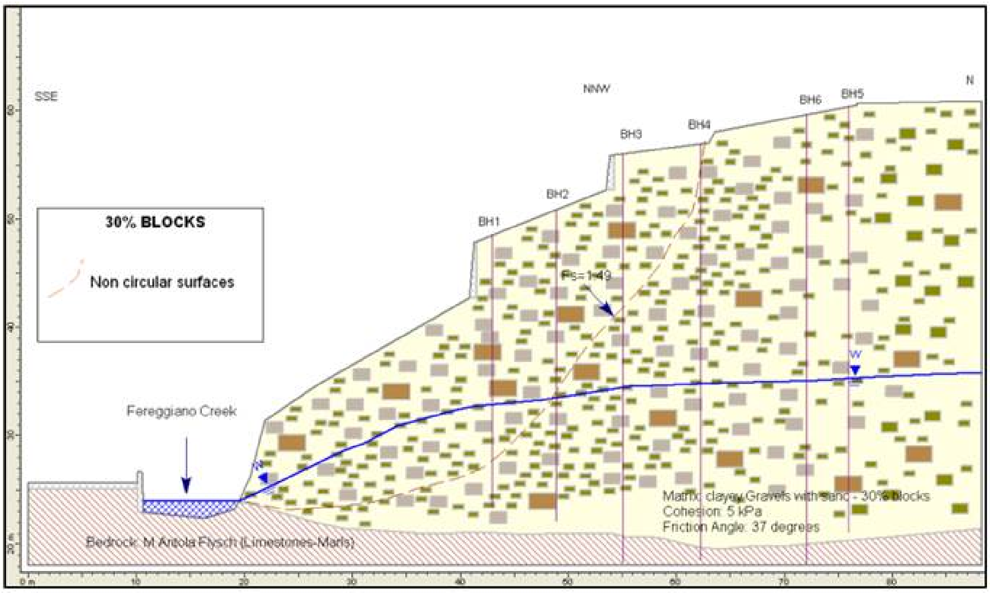


**Figure 3.3:** The slip surface for the 30% VBP model analysed with Slide. (Minuto & Morandi, 2015)

## 3.2 Extension of Minuto and Morandi (2015) study

As part of this thesis, a numerical finite element code was used to evaluate slope stability of the slope discussed. For the numerical analysis, the finite element code RS2 11.0 was used. The fine matrix and coarse matrix configurations were analysed also with the limit equilibrium code Slide2 9.0.

The stochastic approach proposed by Napoli et al. (2018) was used for a random rock block distribution in the slope. This approach takes into account the VBP, size, shape, position, orientation, and eccentricity of the rock blocks. Specifically, a Matlab code, based on Monte Carlo simulations, was written to generate rock blocks with different geometrical properties and given VBPs from a statistical distribution discussed in section 2.4.2 of chapter 2. In this study, the shape of blocks was elliptical unlike that of Minuto and Morandi (20015), who used rectangular blocks. The use of elliptical shape is more auspicious as the problem of stress concentration at the corners was feared if rectangular shaped rock blocks were incorporated. The slope was also analysed using the empirical strength criteria of Lindquist (1994) and Kalender et al. (2014). In such approaches slope consists of only the matrix material after its mechanical properties are modified by taking into account the block inclusions. Kalender et al. (2014) also take into account other factors such as the Unconfined Compressive Strength of the matrix ($UCS_{matrix}$), angle of repose of blocks and parameter "A" which depends on the $UCS_{matrix}$ and adhesion between the blocks and matrix.

## 3.3 Model implementation

Different 2D models were defined for fine matrix, coarse matrix, 15% VBP and 30% VBP. Two models were also defined for the Lindquist and Kalender's homogenous approaches. The models of the fine matrix, coarse matrix, Lindquist and Kalender were analysed with both FEM and LEM codes, while the heterogeneous models with 15% and 30% VBPs were analysed with the FEM code only. Ten different configurations of block inclusions were used to statistically validate the results. The rock blocks for 15% and 30% VBP models were extracted from the Matlab code of Napoli et al. (2018). The steps for the construction of the models are described below.

- Matlab

The Matlab code of Napoli et al. (2018) generates the coordinates and dimensions of ellipses as a .txt file.

- AutoCAD

The profile of the slope in AutoCAD is based on the in-field observations of Minuto and Morandi (2015). For the fine matrix and coarse matrix slope models, the profile was converted from .dwg to a .dxf file. For 15% and 30% VBPs models, the rock blocks were created by importing the .txt files of Napoli et al. (2018) Matlab code and then .dxf files were created.

- Slide2

The .dxf files were imported and the models were refined for analysis. To validate the results of Minuto  Morandi (2015) the fine matrix and the coarse matrix models were analysed with Slide2. The homogeneous models based on the criteria of Lindquist (1994) and Kalender et al. (2014) were also analysed with Slide2.

- RS2

The .dxf files of AutoCAD were imported and the models were refined for analysis.

### 3.3.1 Matlab code of Napoli et al. (2018)

The stochastic approach of Napoli et al. (2018) is based on the numerical Monte Carlo simulation. The stochastic approach was explained in section 2.4.2 of chapter 2. The code generates random rock blocks drawn from a population distributed according to a power-law whose probability density, and distribution functions are given by Equations 2.1 and 2.2 in chapter 2. The code was edited to be compatible with the elliptical shape. Each extraction had eccentricity values ranging between 0.4-0.9 with varying average eccentricity. The result of the code is a .txt file which contains the position and dimension of ellipses in the slope.

### 3.3.2 Models in AutoCAD

The .txt files were imported into AutoCAD by adding the word "ellipse" on the first line and copy-pasting these coordinates and dimensions of the ellipses in the 'command line' of AutoCAD. This operation generated the ellipses within the slope. Some of these ellipses were out of the geometry of slope because it does not have a regular shape. The ellipses which were out of boundary were deleted and the area of the remaining ellipses (rock blocks) was calculated. A tolerance of ±0.2% was allowed for the total area of ellipses. Finally .dxf files were generated which were exported to Slide and RS2.

### 3.3.3 Model in Slide (version 9.0)

Slide is a two-dimensional (2D) limit equilibrium slope stability code for analysing the safety of a slope. It implies the method of slices for the stability analyses of slopes. It is possible to use the different methods of slices, for example, Ordinary/Fellenius (1936), Bishop simplified (1960), Janbu simplified (1954), Janbu corrected (1973), GLE/Morgenstern-Price (1965) and Spencer (1967) etc.

Slide 9.0 was used for fine matrix and coarse matrix analyses to validate the result of the Minuto and Morandi (2015), and also for the homogeneous models based on the criteria of Lindquist and Kalender et al. The geometry of the slope was imported from the AutoCAD which was tracked by Minuto and Morandi (2015), on the field. The material properties are defined in Table 3.1 and the Mohr-Coulomb criterion was used. For bedrock and concrete retaining walls, an infinite strength criterion was chosen.

A critical surface search was performed for circular surfaces of failure. The search was performed with the auto search grid option in Slide as shown in 3.4.

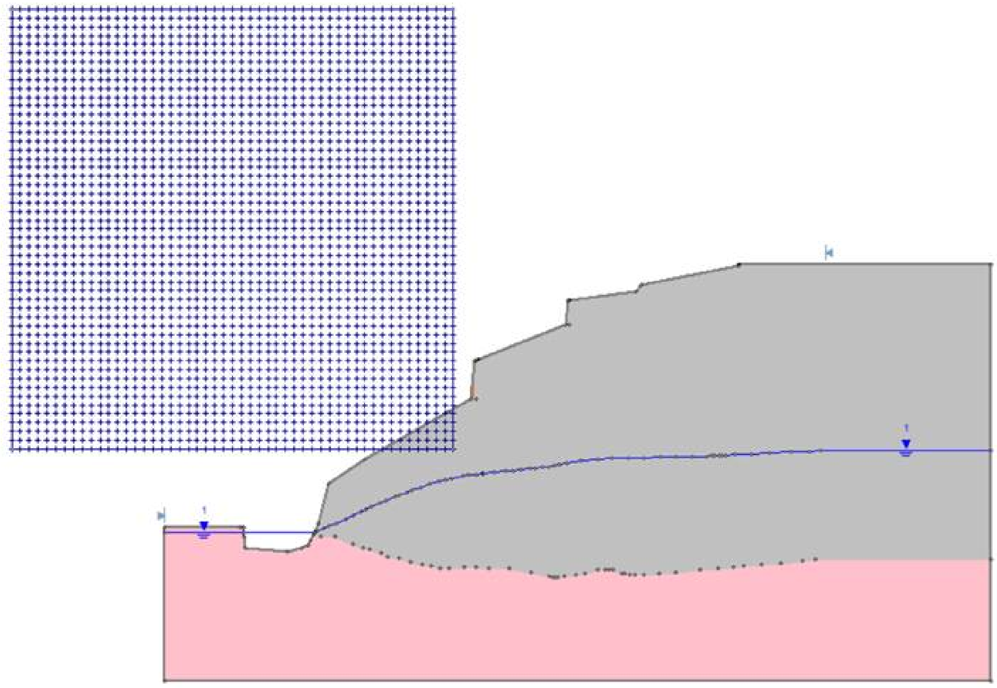

**Figure 3.4:** Geometry of the slope in Slide reconstructed to validate the results of Minuto & Morandi (2015). On the left top is the grid for critical surface search. The green colour at the bottom shows the bedrock.

### 3.3.4 Models in RS2 (version 11.0)

RS2 is a two-dimensional Finite element code, used to analyse a wide range of geotechnical and mining engineering problems. It allows using a range of materials with different constitutive laws. The response of materials to static and dynamic loads can also be studied. For the problems of slope stability, this type of analysis has the following advantages over LEM analyses.

- It is not mandatory to define the failure surface beforehand. RS2 uses strength reduction method for slope stability analysis.
- Both elastic and plastic constitutive laws can be used.
- It is possible to follow the strain process.

A finite element code divides a geometry into several discrete portions known as finite elements. These elements, in the simple shape of a triangle or rectangle, are connected by shared nodes. This whole set of nodes and elements is called mesh.

Stress analyses and slope stability analyses in RS2 are based on the methods and principles from literature e.g. Duncan et al. (1970); Pande et al (1990); Duncan et al. (2000); Hoek et al. (2002) etc. In RS2 different convergence criteria, constitutive laws and other conventions are used for stress analysis. The convergence criteria include absolute force and energy, absolute energy, and square root energy while some constitutive laws are Mohr-Coulomb, Hoek Brown and Cam-clay with some other dynamic constitutive laws. For slope stability analysis, FEM codes such as RS2 use the technique of shear strength reduction (SSR).

#### Shear Strength Reduction

Shear strength reduction (SSR) is a finite element slope stability analysis technique which allows calculating the critical strength reduction factor for a slope. Critical SSR is equivalent to the safety factor. According to Duncan (1996), the safety factor for a slope can be defined as *“the factor by which soil shear strength must be reduced to bring a slope to the verge of failure”*. The basic concept of the SSR is that the strength parameters of a slope are reduced by a certain factor, called “strength reduction factor” (SRF), and the finite element stress analysis is computed. This process is repeated for different values of SRF until the model becomes unstable i.e. the analysis does not converge. This SRF will be the critical SRF or safety factor of the slope.

In the SSR finite element technique, therefore, the material shear strength, assumed elastoplastic, is progressively reduced until collapse occurs

For Mohr-Coulomb material shear strength reduced by a factor F can be determined from the equation:

$$\frac{\tau}{F} = \frac{c'}{F} + \frac{\tan\phi'}{F} \tag{3.1}$$

It is possible to re-write the equation 3.1 as:

$$\frac{\tau}{F} = c^* + \tan\phi^* \tag{3.2}$$

In this case

$$c^* = \frac{c'}{F} \tag{3.3}$$

and

$$\tan\phi^* = arctan(\frac{\tan\phi^{'}}{F}) \tag{3.4}$$

Equations 3.3 and 3.4 are reduced Mohr-Coulomb shear strength parameters. These values can be put into a FE model and analysed

Following is described the process for systematically searching the critical factor of safety value, F, which brings a previously stable slope to the edge of failure. The steps for a Mohr-Coulomb material are as follows:

- Step 1: For a FE model of a slope the deformation and strength properties, established for the slope materials, are defined. The model is computed and the maximum total deformation in the slope is recorded.
- Step 2: The value of F is increased and the factored Mohr-Coulomb material parameters are computed as described above. The new strength properties are entered into the slope, the model is re-computed. The maximum total deformation is recorded.
- Step 3: Step 2 is repeated, systematically incrementing F, until the FE model does not converge to a solution, i.e. continue to reduce material strength until the slope fails. The critical F value just beyond which failure occurs is the slope factor of safety.

In the case of an unstable slope, safety factor values in steps 2 and 3 must be reduced until the FE model converges to a solution.

The elastoplastic SSR finite element approach eliminates the need for a priori assumptions on failure mechanisms which include the type, shape, and location of failure surfaces. Despite all the benefits, the limit-equilibrium approach has some important deficiencies. The failure surface is assumed a priori and it is not possible to follow the stress-strain behaviour of soils and rocks. It also makes arbitrary assumptions regarding inter-slice forces to ensure static determinacy. The critical failure mechanism is a result of the SSR technique. Another positive aspect of the SSR approach is its elimination of arbitrary assumptions regarding the inclinations and locations of inter-slice forces. Furthermore, the method can automatically monitor the development of failure zones, from localized areas to total slope failure. It can also predict expected deformations at the stress levels found in slopes.

### Characteristics of the RS2 models

To analyse the slope in RS2 it was necessary to define the geometrical and mechanical characteristics of the model. The geometry of the slope was provided by Minuto and Morandi (2015) and has a height of 40m at the highest level. Initially, the geometry was created in AutoCAD along with the block inclusions by the stochastic approach of Napoli et al. (2018) and then exported to RS2 as .dxf file. During the export of the geometry to RS2, it is important to assign the relevant function to the boundaries i.e. external boundary, material boundary, piezometer line etc. A geometry clean-up was run to delete any two vertices which are closer to each other according to user defined tolerance. Without geometry clean-up difficulties in meshing the model will arise. The geometry of the model was extended beyond its real limit after different parametrical analysis so that we do not have any influence from the boundary conditions. The geometry of the model is shown in Fig. 3.5.

A finite element mesh was created after defining all boundaries. Before generating the mesh the boundaries were first discretized. This process subdivides the boundary line segments into discretization. After discretizing the finite elements were meshed with three noded triangular elements. These elements are more practical in creating a high quality mesh as we also had the presence of rock block inclusions. Due to the presence of the (ellipses) rock blocks, the mesh quality varied a lot and it was guaranteed to have no “bad elements” in the model. This condition was checked by using the “show mesh quality” command under the window of “Mesh” in RS2. These ‘bad elements’ are peculiar elements with very high or very low interior angles (in case of triangular elements). An element can also be called “bad” if it has a very high ratio of the maximum side length to the minimum side length of the triangle.

Boundary conditions were set in terms of displacement. The ground surface was set free, vertical boundaries were restrained from displacement in the horizontal direction and horizontal boundaries were restrained from vertical displacement. The boundary conditions are shown in 3.5.

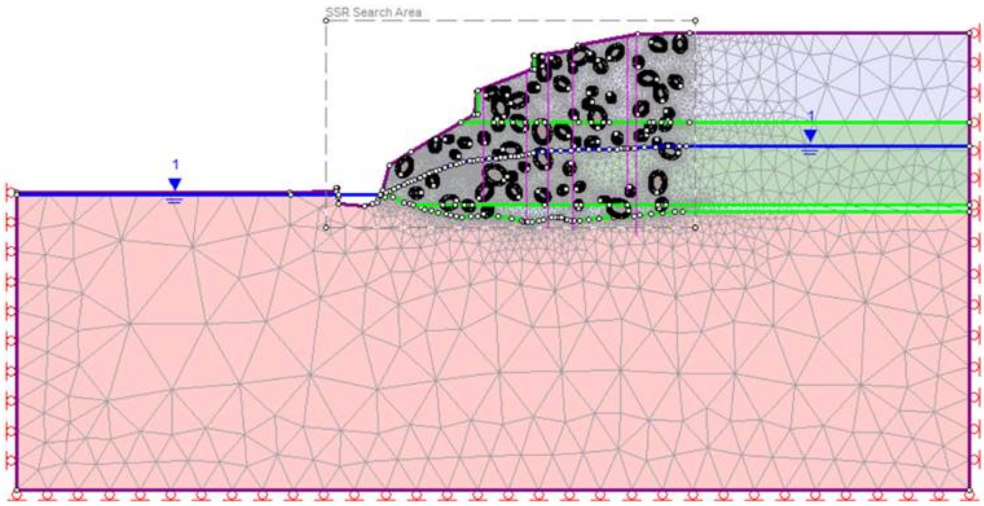


**Figure 3.5:** RS2 model for 15% VBP with boundary conditions. The different colour indicates different materials. The model is meshed with triangular elements and the meshed is finer in the SSR search area.

In order to define the behaviour of the materials in the model, a constitutive law was assigned to each element. The strength properties, for fine and coarse matrix models, were taken from the laboratory tests of Minuto and Morandi (2015) and are summarized in Table 3.1. The deformability coefficient of the materials was taken from the data of a down-hole test performed by Minuto and Morandi as shown in Fig. 3.6. By looking at the profile of down hole tests in the borehole No. 4, it was decided to divide the slope into three layers of materials with depths equal to 16m, 18m and 6m respectively.

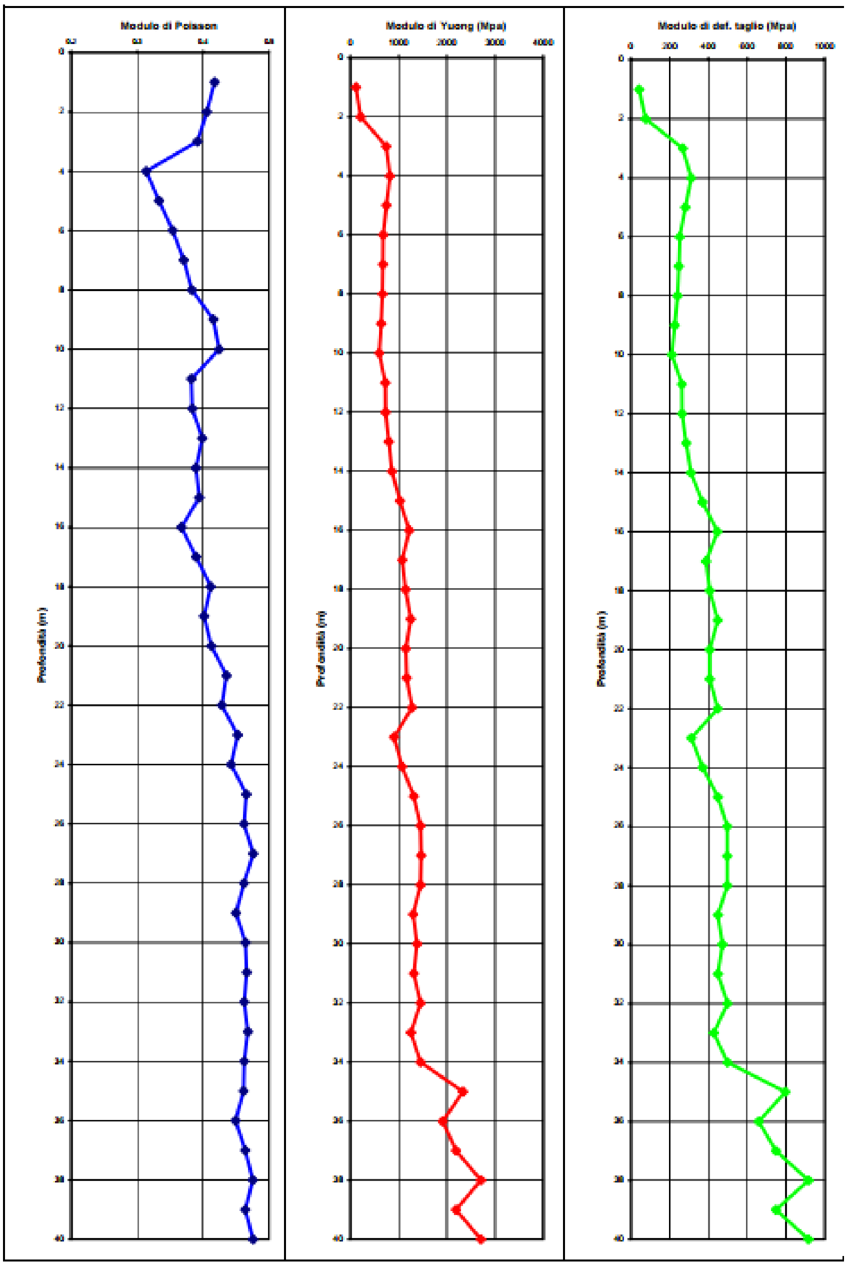


**Figure 3.6:** Result of downhole test performed in borehole-4. On left is the profile of the poison ratio, in middle the profile of the young modulus and on right is the profile of shear modulus are shown. (Minuto and Morandi 2015)

For the three layers of soil, the elastoplastic criterion of Mohr-coulomb was selected. The retaining walls were made of concrete and in the analysis they are considered as elastic because the aim of the study was to analyse the slope. The deformability properties used in the model for different materials are summarized in Table 3.2

| | Layers of material | | |
|---|---|---|---|
| Material Properties | 1-16 m | 16-34 m | 34-40 m |
| E (MPa) | 700 | 1300 | 2300 |
| $\nu$ (-) | 0.32 | 0.37 | 0.4 |
| $\gamma$ (kN/m$^3$) | 18 | 18 | 18 |

**Table 3.2:** Deformability properties for different layers of material

The bedrock was almost 40m from the ground surface. According to Minuto and Morandi (2015), the bedrock consists of flysch sediments related to a turbidite sequence of limestones, marls and mudstones. The GSI value for the intact rock ranged between 40-60, uniaxial compressive strength ranged between 50-60 MPa and the Elastic Modulus (E) was 45 GPa. The constitutive law used for the bedrock in the model was Hoek-Brown. The Hoek-Brown parameters $m_i$ and s for bedrock were calculated from the parameters of intact rock. Minuto and Morandi provided the parameters of intact rock and they were used for rock blocks. With the use of RocData (Rocscience Inc.), the parameters of the bedrock were obtained. The RocData program uses the equations of Hoek-Brown criterion for the calculation of these parameters. The parameters used for the bedrock and rock blocks in the models are summarized in Table 3.3

| | Bedrock | Rock Blocks |
|---|---|---|
| E (MPa) | 18 | 45 |
| $\nu$ (-) | 0.3 | 0.3 |
| $\gamma$ (kN/m$^3$) | 27 | 27 |
| UCS (MPa) | 60 | 60 |
| $m_i/m_b$ | 1.084 | 9 |
| s | 0.007 | 1 |

**Table 3.3:** Mechanical properties used for bedrock and rock blocks in the models.

For the field stress, a gravitational stress distribution was used, which is reasonable in slope stability analyses. The code automatically determines the ground surface above every finite element and defines the vertical stress in the elements based on the weight of material above it. The horizontal stress ratio is selected as 1, implying the hydrostatic initial stresses.

In RS2 from "project settings" the use of SSR was enabled and SSR search area was defined which was selected after a parametric study of slope stability analysis. The advantage of the definition of SSR search area is that it reduces the time of analysis. In Fig. 3.5 and Fig. 3.7 the meshed model of slope for 15% VBP with boundary conditions, block inclusions, and SSR search area is shown. The Pink lines in the figure show the location of boreholes conducted by Minuto and Morandi (2015)

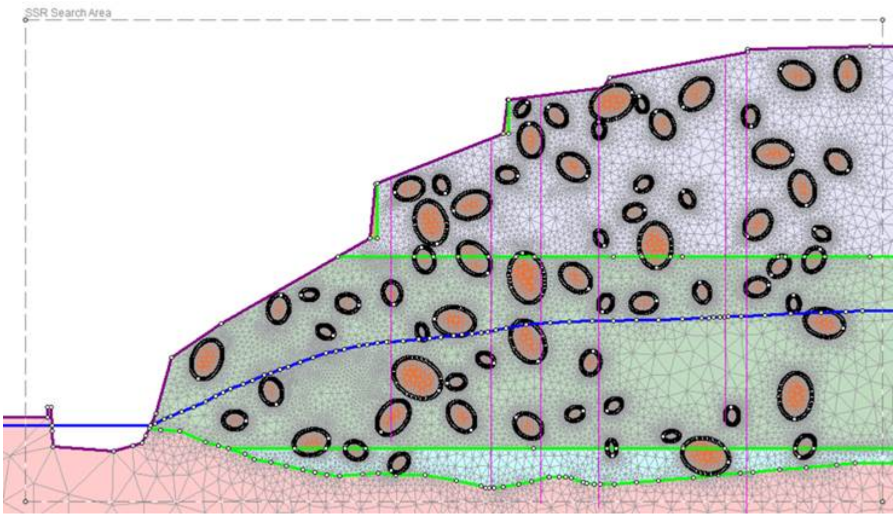


**Figure 3.7:** Zoomed-in snap of the RS2 model for 15% VBP. The different layers of material and rock blocks are visible also. The model is meshed finely with triangular elements.

### 3.3.5 Equivalent homogeneous approaches

Explained above were the models analysed with the heterogeneous approach in which the mechanical properties of the rock blocks were different from those of the matrix. For this thesis, the two homogenous approaches of Lindquist (1994) and Kalender et al. (2014) were used. These two strength criteria are discussed in section 1.3.1 of chapter 1.

The model implementation for the equivalent homogenous approaches is the same as discussed above. Here the adoption of these two strength criteria for analyses is explained. Lindquist (1994) found that the content of the blocks influences the mechanical properties of the material if the block content is more than 25%. In this study, we had two block contents of 15% and 30%, so the Lindquist's criterion was applicable only to the 30% VBP model. The Kalender's criterion was applied to both the models of 15% and 30% VBP. These models were analysed with both LEM and FEM codes.

Lindquist (1994), in his study of artificially created laboratory models, observed that the friction angle increases by 3° with every increment of 10% in block content after 25% VBP. Therefore, for 30% VBP model, the following mechanical properties were used.

$$c'_{30\%\,VBP} = c'_{matrix} \times (1 - VBP) = 10 \times (1 - 0.3) = 7kPa$$

$$\phi'_{30\%\,VBP} = \phi'_{matrix} + \Delta\phi_{matrix} = 35 + 4.5 = 39.5°$$

where $\Delta\phi_{matrix} = \Delta VBP/10 \times 3 = 4.5$

Kalender et al. (2014) based on their laboratory tests together with other studies of bimrocks in literature including Lindquist (1994), Altinsoy (2006), Coli et al., (2011) and Afifipour et al.,(2009) developed a preliminary approach to predict the strength parameters ($\phi_{bimrock}$, $c_{bimrock}$ and $UCS_{bimrock}$) of bimrocks. Kalender et al. (2014) presented the following equations for the strength parameters.

$$\phi_{bimrocks} = \phi_{matrix}\left[1 + \frac{1000[\frac{\tan\alpha}{\tan\phi_{matrix}} - 1]}{100 + 5(\frac{100-VBP}{15})}(\frac{VBP}{VBP+1})\right] \tag{3.5}$$

$$UCS_{bimrock} = \left[\frac{A - A^{\frac{VBP}{100}}}{A - 1}\right]UCS_{matrix} \qquad 0.1 \leq A \leq 500 \tag{3.6}$$

$$c_{bimrock} = \frac{UCS_{bimrock}[1 - \sin\phi_{bimrock}]}{[2\ \cos\phi_{bimrock}]} \tag{3.7}$$

Here $\alpha$ is the angle of repose of blocks, UCS is the material uniaxial compressive strength, and 'A' is a parameter that can be defined according to both the compressive strength of the matrix and parameter . The values of A can be extracted from the graph shown in Fig. 3.8.

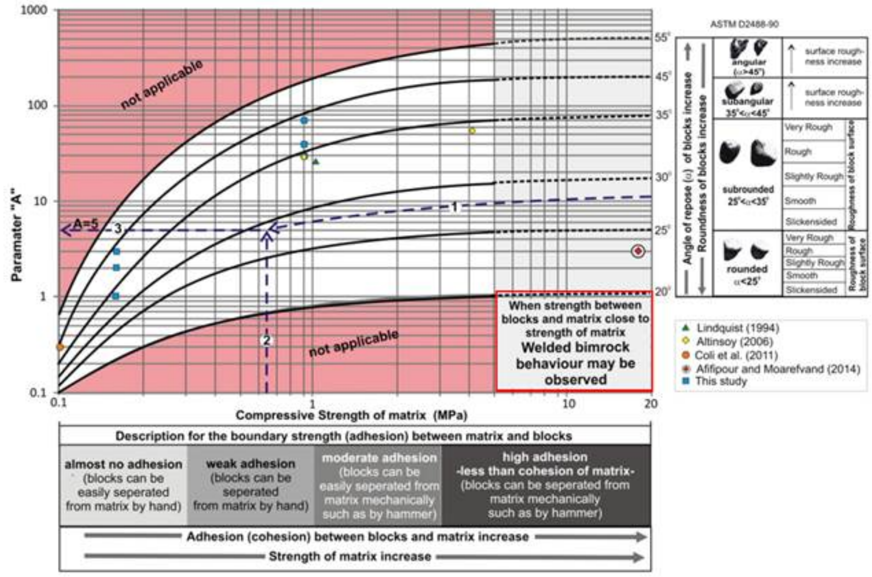


**Figure 3.8:** The graph used for the calculation of parameter ‘A’ used in Kalender strength criterion. The parameter ‘A’ can be obtained by using an angle of repose ($\alpha$) of blocks and compressive strength of the matrix. (Kalender et al. 2014)

For the calculation of parameter ‘A’, the value of $UCS_{matrix}$ was calculated using the Hoek-Brown criterion equations by inserting the values of c and $\phi$ of the matrix. For the angle of repose, a value of 45° was used as the blocks are tabular in shape. With these values of  and $UCS_{matrix}$ the value of A was calculated to be 0.3. By putting these values in equations 3.5, 3.6 and 3.7 the obtained strength parameters are summarized in Table 3.4

| | Lindquist Criterion | Kalender Criterion | |
|---|---|---|---|
| Strength Parameters | 30% VBP | 15% VBP | 30% VBP |
| $c_{bimrock}$ (kPa) | 7 | 19.5 | 13.7 |
| $\phi_{bimrock}$ (°) | 39.5 | 35.9 | 38.4 |
| $UCS_{bimrock}$ (kPa) | - | 76.4 | 56.69 |

**Table 3.4:** Mechanical properties of bimrocks material for Lindquist and Kalender criteria

# Chapter 4

# Slope stability analysis of a relict landslide in bimrocks: results

## 4.1 General introduction

The slope stability analysis of the relict landslide studied by Minuto and Morandi (2015) was based on a real case study in the downtown of Genova, Italy. The authors analyzed the slope with the LEM code and used both the homogenous and heterogenous approaches for the analyses. Minuto and Morandi (2015), from borehole logs and the Medley's (1997) chart of uncertainty for VBP calculation, found the block content to be in the range of 15% to 30%. So, two VBPs of 15% and 30% were used for the analyses.

In this thesis, the same slope was analyzed with both LEM and FEM methods. First, two different types of matrices were analyzed named 'fine matrix' and 'coarse matrix' with LEM to validate the results of Minuto and Morandi (2015). The fine matrix, as its name implies, has the properties of the fine material only. However, since the slope had a high content of gravel a "coarse matrix", with the properties of both the fine material and gravel, was also analyzed. In order to perform the FEM analyses, the FEM code RS2 was used. Since bimrocks have inherent spatial and dimensional variability in their nature a stochastic approach for the distribution of rock blocks in the slope was used. The rock blocks were randomly distributed in the slope using the stochastic approach of Napoli et al. (2018). To statistically validate the results, ten different analyses were done for each VBP considered (i.e. 15% and 30%) with different positions, dimensions and shapes of blocks. The equivalent homogenous approach of Lindquist (1994) and Kalender et al. (2014)

were also used. These two models were analyzed with both FEM and LEM codes.

In this chapter, the results of the analyses (in terms of safety factors) are described. To make the understanding of the results easy and clear, it was decided to nominate the cases of the various analyses with a code that distinguishes them. In total there are two matrices: fine matrix (FM) and coarse matrix (CM), ten models with a VBP of 15% and ten models with a VBP of 30%, one model for Lindquist (LIN) criterion and two models for Kalender (KAL) criterion. The code contains the model type (i.e. FM, CM, 15%, LIN etc) and for 15% and 30% of blocks the reference extraction, and at the end an acronym FEM or LEM which indicates the approach by which the results were obtained. For example, FM_LEM indicates the model of fine matrix analysed with Limit Equilibrium Method and 15%_4_FEM indicates the model relative to the 4th extraction of block distribution carried out for 15% of VBP and analysed with Finite Element Method. LIN_30%_LEM indicates the model of the homogeneous approach using Lindquist strength criterion for 30% VBP analysed with Limit Equilibrium Method. Similarly, KAL_15%_FEM is for the model of the homogeneous approach using Kalender et al. (2014) criterion for 15% VBP and analysed with Finite Element Method.

## 4.2 Validation of results of Minuto and Morandi (2015)

The results of Minuto and Morandi (2015) were validated by reanalysing the models of fine matrix and coarse matrix with the LEM approach. The two matrices were analysed using GLE/Morgenstern-Price method of slices. The procedure to set up the model in Slide® and the properties of the material used were explained in chapter 3.

The result of the fine matrix analysis showed a shallow failure surface with the lowest safety factor of 0.85. However, since the study of Minuto and Morandi (2015) was aimed at studying potential deep surfaces they ignored the shallow surfaces and found a safety factor of 0.99. Fig 4.1 shows a shallow failure surface which possibly was ignored by Minuto and Morandi (2015) and a deeper failure surface with a safety factor of 0.99 which corresponds to that found by the authors.

The coarse matrix was analysed and a safety factor of about 1.11 was obtained for a shallow surface. Another deep failure surface with a safety factor of 1.28 was searched to be in agreement with the result of Minuto and Morandi (2015) ignoring other shallow failure surfaces. Fig 4.2 shows both the shallow and deep failure surfaces for coarse matrix.

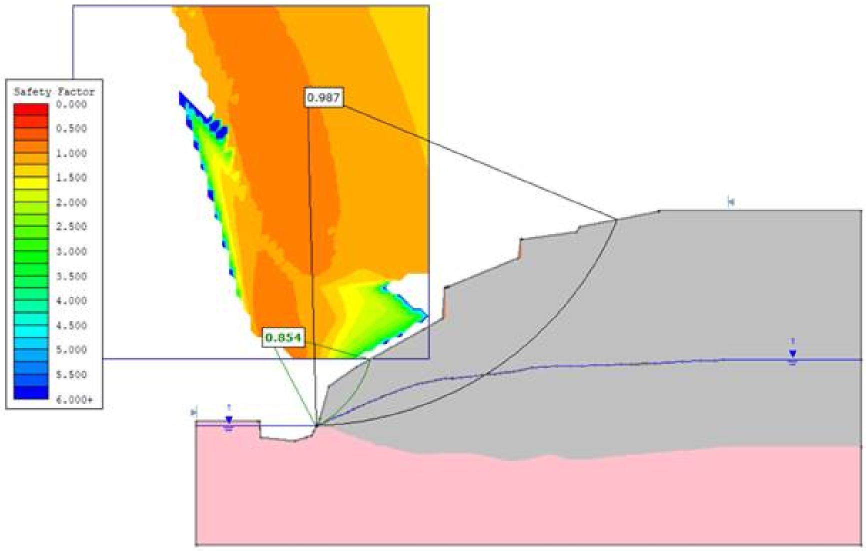


**Figure 4.1:** Safety factor and failure surface for fine matrix analysed with Slide. The software generated a shallow surface with SF of 0.85. The failure surface with a value of 0.99 corresponds to Minuto and Morandi (2015)

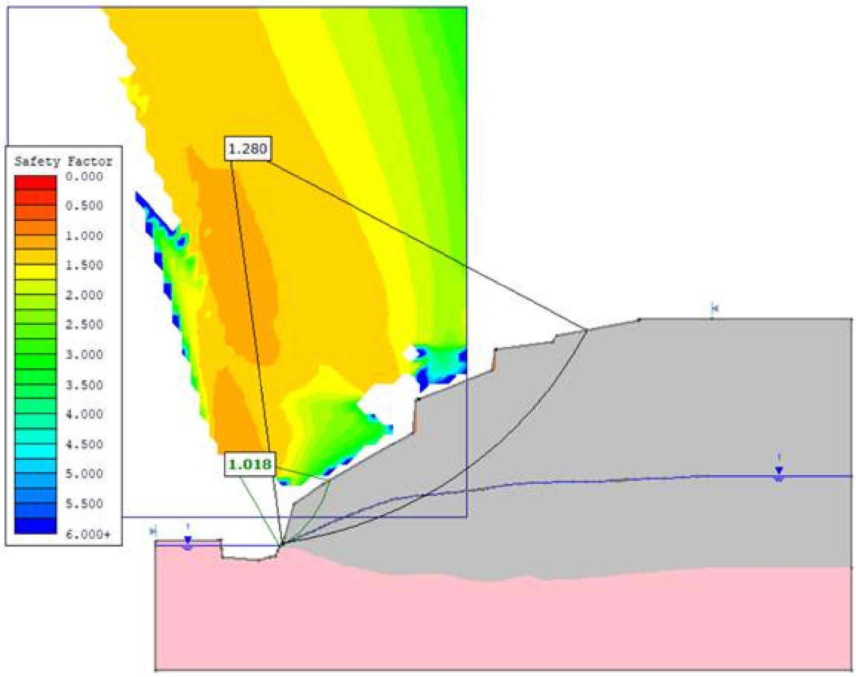


**Figure 4.2:** Values of safety factors for coarse matrix analysed with Slide. The shallow failure surface was ignored according to Minuto and Morandi (2015) opting, instead, the surface with SF of 1.28.

The analyses of fine matrix and coarse matrix with LEM are in agreement with the results of Minuto and Morandi (2015) and this result validates the model geometry and mechanical properties used in this study.

## 4.3 Numerical analyses

After validating the results of fine matrix and coarse matrix the models were analysed with RS2. The model implementation is explained in detail in chapter 3, as well as the strength properties used. In the first phase, parametric analyses were performed in order to study the influence of both the model size and mesh. Due to the presence of blocks of different sizes and positions in the various models, a specific mesh was created for each model. Generally, three nodes triangular elements were utilized but their number varied among models.

### 4.3.1 Fine matrix and coarse matrix models: FEM

After defining the mesh, boundary conditions and material properties the models were analysed. The fine matrix had a safety factor of 0.85 with a comparatively deeper failure surface. The critical failure surface is shown in Fig.4.3 along with the failure surface corresponding to Minuto and Morandi (2015) (shown in Fig.4.1) in white colour having safety factor of 0.99.

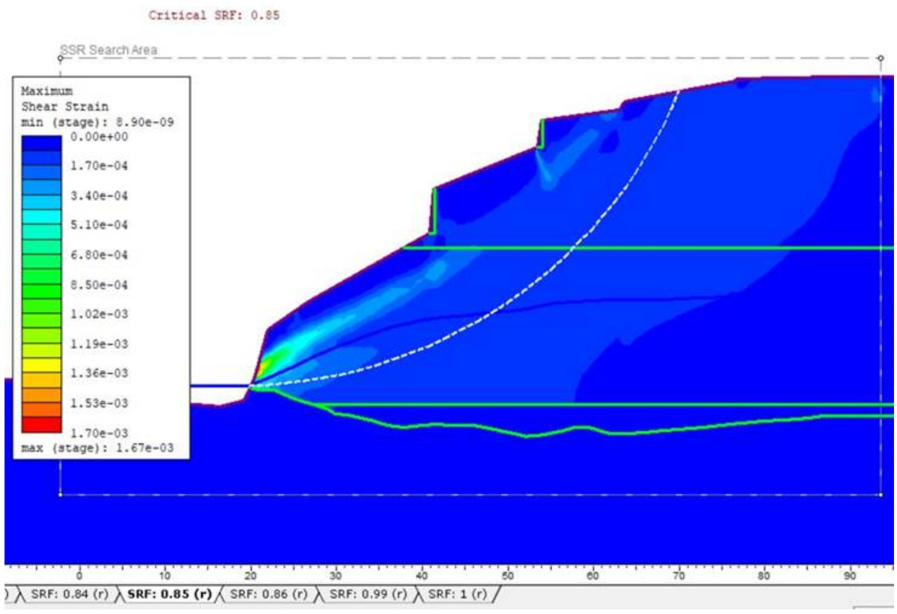


**Figure 4.3:** The maximum shear strains for fine matrix analysed with RS2. The dotted line shows the failure surface of Minuto and Morandi (2015)

Fig. 4.3 shows that the numerical analyses have different safety factor and failure surface position as compared to that corresponding to Minuto and Morandi (2015). It is because the authors ignored the shallow and other failure surfaces. After all, their study was aimed at analysing only deep failure surfaces. In numerical analyses, when observing the progressive failure by navigating through the tabs of different SRF values, the maximum shear strains increase as the SRF increases and show deep failure surfaces at higher values. Fig.4.4 shows a deeper failure surface at SRF value of 0.99 which is comparable to that obtained by Minuto and Morandi (2015).

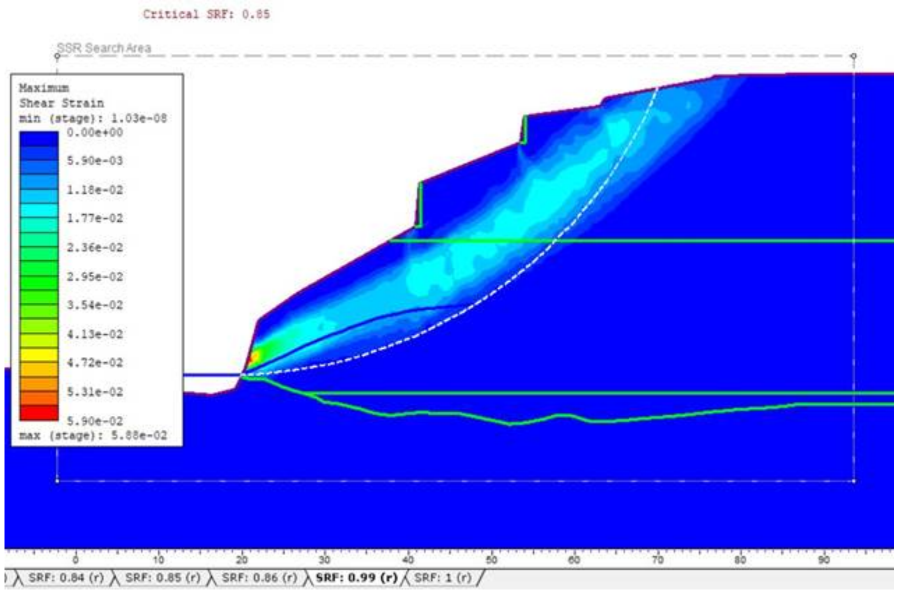


**Figure 4.4:** Maximum shear strains at SRF of 0.99 for the fine matrix model along with the failure surface of Minuto and Morandi (2015). At the bottom, the tabs to follow the progression of failure can be seen.

The coarse matrix had a surface with a safety factor of 1.11 which was also observed from the LEM analysis and is shown in Fig.4.5. In the figure, the red line shows the failure surface obtained by Minuto and Morandi (2015) for coarse matrix corresponding to the safety factor of 1.28 (shown in Fig.4.2).

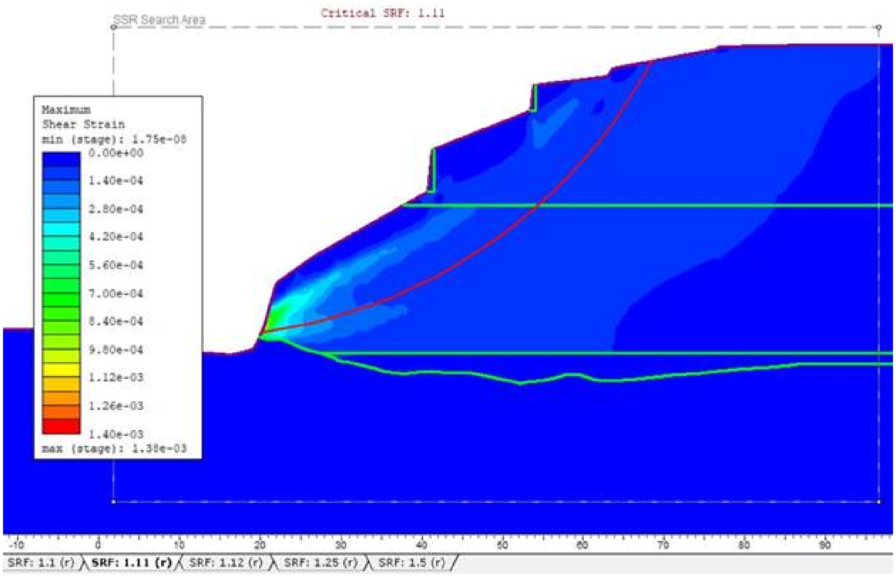


**Figure 4.5:** Maximum shear strains for the coarse matrix along with the failure surface of Minuto and Morandi (2015) in red. At the bottom, the tabs to follow the progressive failure are visible.

Fig.4.6 and 4.7 show the progression of failure surface for the coarse matrix model analysed with RS2. So, the SRF value of 1.11 corresponds to a shallow failure surface while a deeper failure surface had the value of the safety factor around 1.25 which is comparable with that obtained by Minuto and Morandi (2015) value of 1.28.

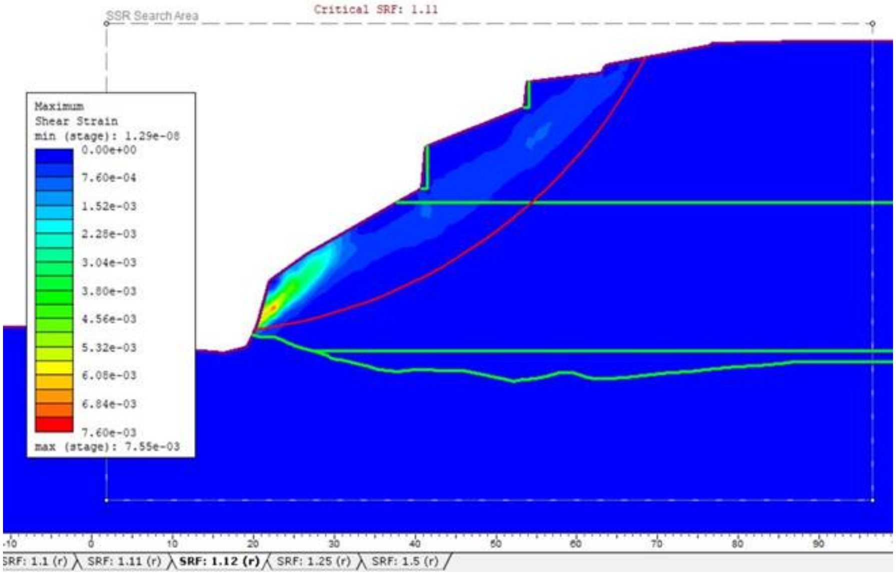


**Figure 4.6:** Maximum shear stains for coarse matrix. The SRF is 1.12 here and the failure surface is shallow.

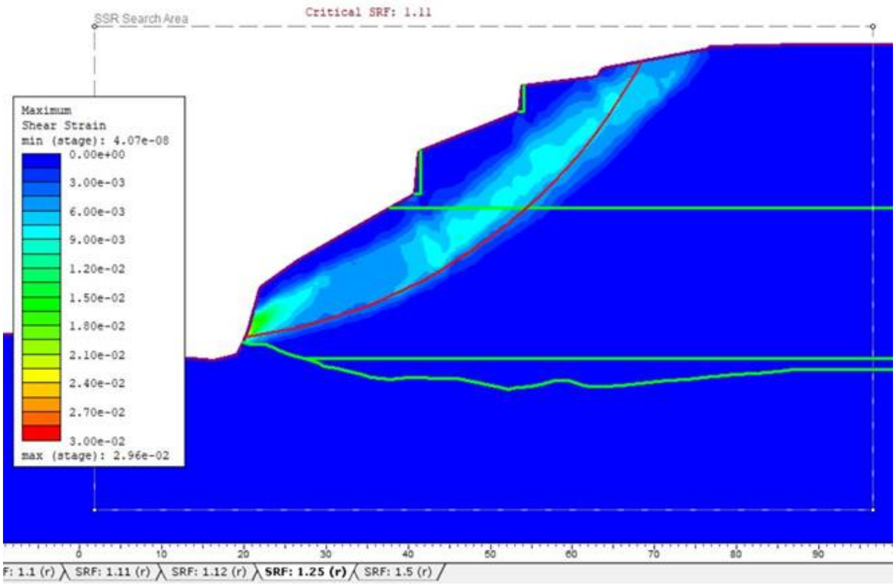


**Figure 4.7:** The progressive failure is very well animated. The SRF is 1.25 and the maximum shear strains have increased and resulted in a deep failure surface.

Table 4.1 summarizes the safety factors (SF) of both FEM and LEM for the homogeneous material (fine matrix and coarse matrix).

| | SF_LEM | | | SF_FEM | |
|---|---|---|---|---|---|
| Model Type | For shallow failure surfaces (lowest SF) | For deeper failure surfaces | For deep failure surfaces of Minuto and Morandi (2015) | Critical SRF | Progressive deeper failure surface |
| Fine matrix | 0.85 | 0.91 | 0.99 | 0.85 | 0.99 |
| Coarse matrix | 1.02 | 1.25 | 1.28 | 1.11 | 1.25 |

**Table 4.1:** The values of safety factors for the fine matrix and coarse matrix models analysed with both FEM and LEM

### 4.3.2 15% VBP models: finite element method

For 15% VBP ten models, with different block distributions, were prepared. The rock blocks in each configuration also had variation in eccentricities, varying between 0.4 and 0.9. Table 4.2 shows the average value of eccentricities for each configuration.

| Model | Average Eccentricity |
|---|---|
| 15%_1_FEM | 0.660 |
| 15%_2_FEM | 0.658 |
| 15%_3_FEM | 0.703 |
| 15%_4_FEM | 0.661 |
| 15%_5_FEM | 0.640 |
| 15%_6_FEM | 0.645 |
| 15%_7_FEM | 0.668 |
| 15%_8_FEM | 0.637 |
| 15%_9_FEM | 0.643 |
| 15%_10_FEM | 0.665 |

**Table 4.2:** Average eccentricities for all the ten configurations of the 15% VBP models

Models were analyzed with the RS2 code and the critical safety factors for each model are summarized in Table 4.3. The values ranged between 1.02 and 1.17.

| Model | SF |
|---|---|
| 15%_1_FEM | 1.08 |
| 15%_2_FEM | 1.04 |
| 15%_3_FEM | 1.05 |
| 15%_4_FEM | 1.12 |
| 15%_5_FEM | 1.07 |
| 15%_6_FEM | 1.10 |
| 15%_7_FEM | 1.14 |
| 15%_8_FEM | 1.11 |
| 15%_9_FEM | 1.03 |
| 15%_10_FEM | 1.10 |
| Mean SF | 1.08 |
| Standard Deviation | 0.034 |

**Table 4.3:** Safety factors for ten different block configurations having 15% VBP

The mean value for all the ten models was 1.08 which is almost the same as for coarse matrix model. The presence of blocks has not changed the safety factor much, but the failure surfaces have different paths depending on the distribution of the blocks. For example, as shown in Fig. 4.8 is the maximum shear strains of 15%_4_FEM model. The specific distributions of blocks in the slope has forced the failure surface to negotiate around the blocks.

In Fig. 4.9, model 15%_9_FEM shows a different block distribution, and a different failure surface which is very shallow and has a lower SF. This is maybe due to the absence of rock blocks between the two blocks at the toe and first concrete wall. The two blocks at the toe of the slope are carried away with failure surface. Complete results of the ten configurations are recorded in Appendix A.

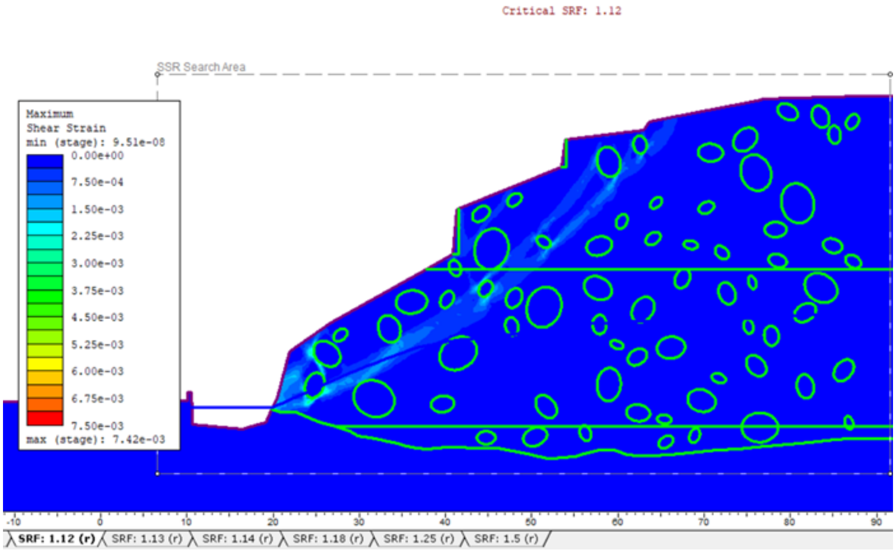


**Figure 4.8:** Maximum shear strains for15%_4_FEM. The failure surface is tortuous as compared to the fine or coarse matrix. The SF has not increased significantly relative to the coarse matrix.

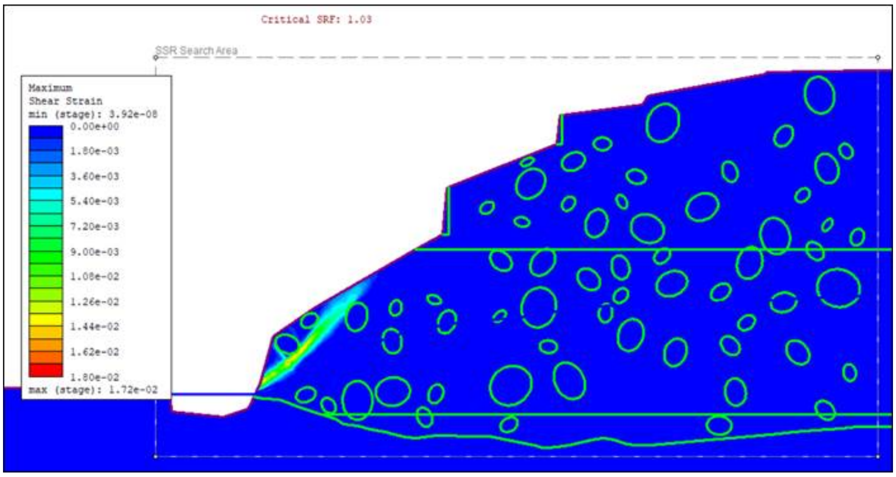


**Figure 4.9:** Maximum shear strains for model 15%_9_FEM. The failure surface is shallow despite the presence of some blocks. The position of the blocks influences the failure surfaces.

### 4.3.3 30% VBP models: finite element method

Ten models with VBP equal to 30% were prepared, which differ in terms of samples extracted from the block size distribution and position of the blocks inside the slope. The rock blocks in each configuration also had variation in eccentricities, varying between 0.4 and 0.9. Table 4.4 shows the average value of eccentricities for each configuration.

| Model | Average Eccentricity |
|---|---|
| 30%_1_FEM | 0.646 |
| 30%_2_FEM | 0.635 |
| 30%_3_FEM | 0.633 |
| 30%_4_FEM | 0.657 |
| 30%_5_FEM | 0.641 |
| 30%_6_FEM | 0.646 |
| 30%_7_FEM | 0.636 |
| 30%_8_FEM | 0.647 |
| 30%_9_FEM | 0.649 |
| 30%_10_FEM | 0.643 |

**Table 4.4:** Average eccentricities for all the ten configurations of the 30% VBP models

The models had the safety factors summarized in Table 4.5.

| Model | SF |
|---|---|
| 30%_1_FEM | 1.04 |
| 30%_2_FEM | 0.95 |
| 30%_3_FEM | 1.03 |
| 30%_4_FEM | 1.06 |
| 30%_5_FEM | 0.95 |
| 30%_6_FEM | 0.91 |
| 30%_7_FEM | 1.11 |
| 30%_8_FEM | 1.00 |
| 30%_9_FEM | 1.16 |
| 30%_10_FEM | 1.19 |
| Mean SF | 1.04 |
| Standard Deviation | 0.087 |

**Table 4.5:** Safety factors for ten different block configurations having 30% VBP

The values of SF ranges between 0.91 and 1.19 with a mean value of 1.04 but a significantly higher standard deviation. No significant increase was observed in the average SF value compared to the matrix only and 15% VBP models. Some of the models have SF values lower than one this could be due to the lower cohesion assigned to the matrix. As for 30% VBP models, the value of effective cohesion was reduced to 5 kPa for taking into account the increase in VBP by Minuto and Morandi (2015). It is important to note that in all cases the deformations develop in the matrix and never inside the blocks. The maximum shear strains for 30%_9_FEM is shown in Fig. 4.10. The results for all the configurations of 30% VBP are recorded in the Appendix B.

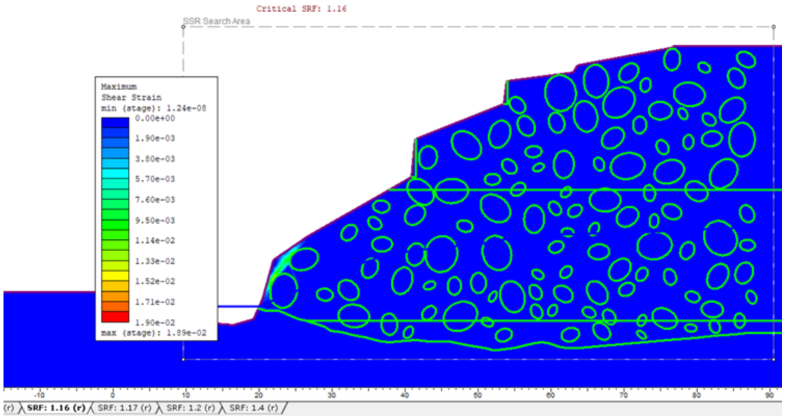

**Figure 4.10:** Maximum shear strains for model 30%_9_FEM.

The safety factors of all the configurations, for both VBPs of 15% and 30%, and their average values are compared in Fig. 4.11

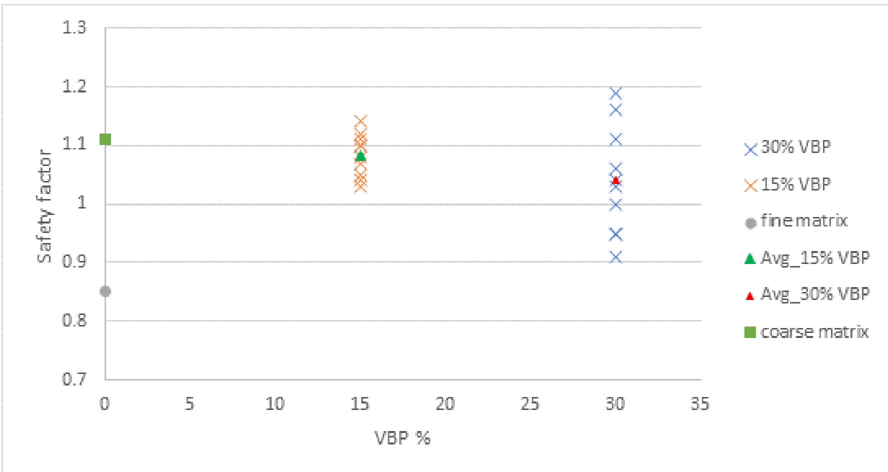


**Figure 4.11:** Comparison of safety factors of ten different model slopes for both 15% and 30% VBP.

The increase in VBP has not resulted in an increase in the safety factors although these values correspond to shallow failure surfaces. There is more scatter in the values of 30% VBP configuration. Some configurations have critical SF less than one which might be due to the specific shape of slope compounding with the lower cohesion value as compared to matrix only and 15% VBP. The presence of blocks at the toe and near the first retaining wall (Fig. 4.12) makes the difference in SF values. In all models of 30% VBP, the critical failure surface is local at one of these two specific locations as shown in Fig. 4.12 which is the model of configuration 30%_8_FEM.

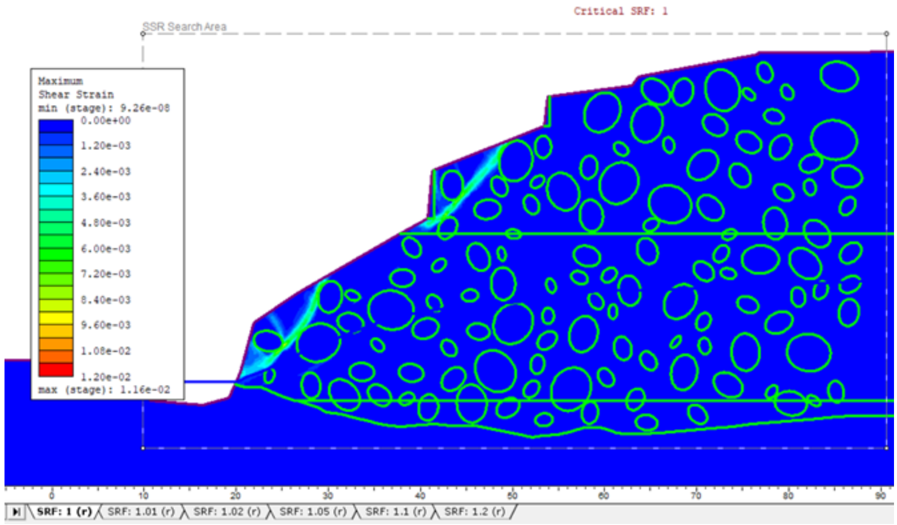


**Figure 4.12:** Maximum shear strains for 30%_8_LEM model. Two specific locations, where all the shallow failure surfaces occur, can be seen.

### 4.3.4 30% VBP models: higher cohesion

The analyses of 30% VBP models with the strength properties provided in Table 3.1 has resulted lower SF values and in some cases even less than 1. Due to lower value of cohesion the slope fails at the steeper parts of toe and first retaining wall in the absence of any rock block at these locations. This unrealistic results necessitated to re-analyze the slope using the strength properties of "coarse matrix" for the matrix material i.e. c=10 kPa and $\phi = 35°$.

The models had the safety factors summarized in Table 4.6.

| Model | SF |
|---|---|
| 30%_1_FEM | 1.21 |
| 30%_2_FEM | 1.17 |
| 30%_3_FEM | 1.16 |
| 30%_4_FEM | 1.21 |
| 30%_5_FEM | 1.13 |
| 30%_6_FEM | 1.16 |
| 30%_7_FEM | 1.25 |
| 30%_8_FEM | 1.12 |
| 30%_9_FEM | 1.23 |
| 30%_10_FEM | 1.28 |
| Mean SF | 1.19 |
| Standard Deviation | 0.0498 |

**Table 4.6:** Safety factors for re-analyzed ten different block configurations with c=10 kPa having 30% VBP

The values of SF ranges between 1.12 and 1.28 with a mean value of 1.19. An increase of 10% was observed in the average SF value compared to the average SF of 15% VBP models. The maximum shear strains for re-analyzed 30%_1_FEM is shown in Fig 4.13. The results for all the configurations of 30% VBP are recorded in the Appendix C.

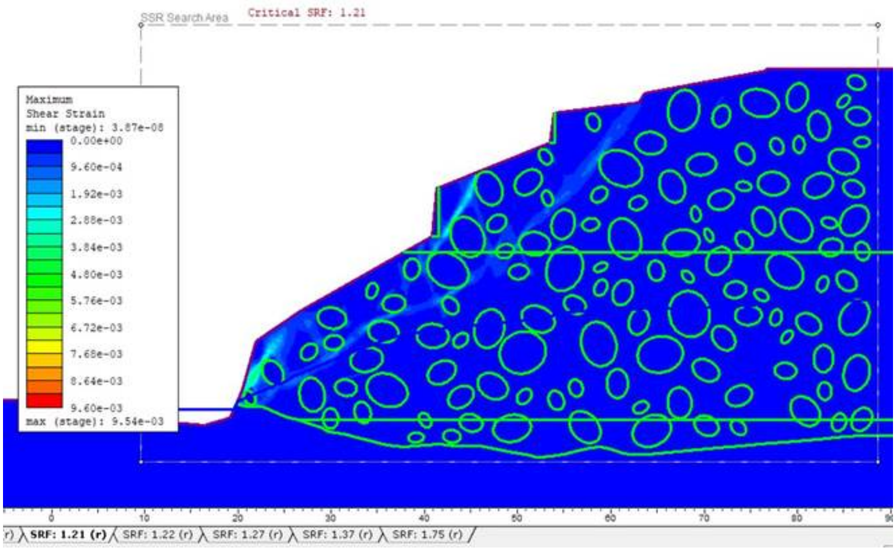


**Figure 4.13:** Maximum shear strains for model 30%_1_FEM.

When the progressive failure surfaces are observed, a deeper failure surface is encountered at SRF values of around 1.27 to 1.37. Fig 4.14 shows the maximum shear strains for re-analyzed 30%_1_FEM at SRF of 1.37. A deeper and tortuous failure surface is evident. The value of SF corresponding to the deep failure surface is lower than 1.49 obtained by Minuto and Morandi (2015) for the same VBP.

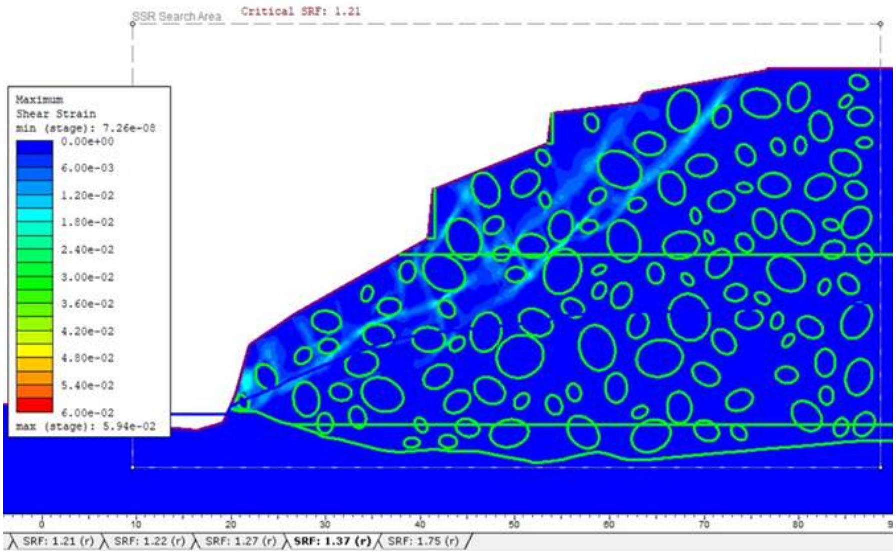


**Figure 4.14:** Maximum shear strains for re-analyzed 30%_1_FEM model. The progressive failure shows a deep failure surface around a safety factor of 1.37.

### 4.3.5 Equivalent homogeneous approach

The two strength criteria of Lindquist (1994) and Kalender et al. (2014) were used for the analysis. The material properties obtained for both criteria are discussed in chapter 3. The models were analysed with both the FEM and LEM approaches. The safety factors obtained from each approach are summarized in Table 4.7.

| Model | SF |
|---|---|
| LIN_30%_FEM | 1.08 |
| LIN_30%_LEM | 0.94 |
| KAL_15%_FEM | 1.37 |
| KAL_15%_LEM | 1.36 |
| KAL_30%_FEM | 1.33 |
| KAL_30%_LEM | 1.27 |

**Table 4.7:** Safety factors of models using the Lindquist (199) and Kalender et al. (2014) strength criteria.

The failure surfaces of Lindquist criterion models were shallow for both the FEM and LEM models and had lower safety factors than that of Minuto and Morandi (2015). The values of maximum shear strains for LIN_30%_FEM model are shown in Fig. 4.15. The progression of the failure surface shows a potential deep surface at SRF value of 1.5 which is comparable with 1.49, obtained by Minuto and Morandi (2015). However, the probability of occurrence of such deep failure surface is much lower relative to a shallow surface.

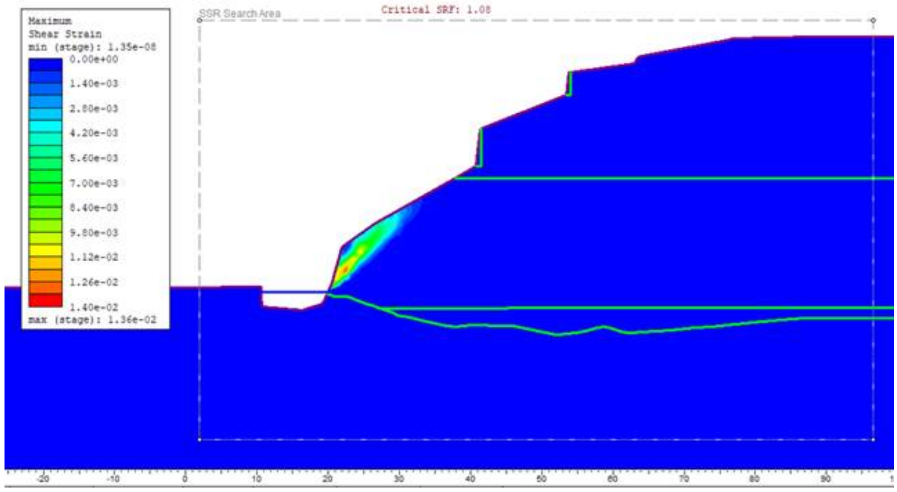


**Figure 4.15:** Maximum shear strains for model LIN_30%_FEM. The critical SRF is 1.08 and the failure surface is shallow.

SF values for Kalender et al. (2014) criterion are higher as compared to Lindquist (1994) and this is reflected in deeper failure surfaces. The SF values obtained by this criterion have a strong dependence on the parameters ‘A’ and Unconfined Compressive strength of the matrix ($UCS_{matrix}$). Fig. 4.16 shows the maximum shear strains for KAL_15%_FEM model. Complete results of the homogeneous approach are recorded in Appendix D.

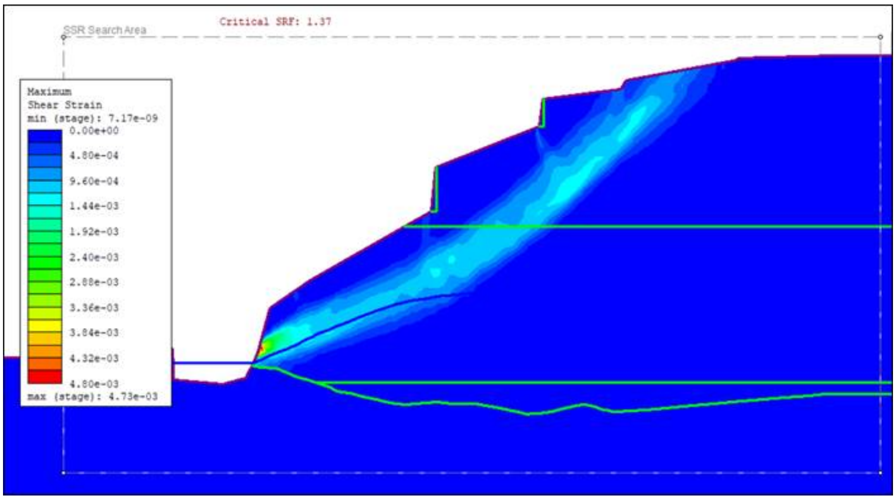


**Figure 4.16:** Maximum shear strains for model KAL_15%_FEM

Fig. 4.17 compares the results provided by the different approaches used. No significant increase was observed with an increase in VBP partly because most of the analyses, other than Kalender's models and some configurations in 30% VBP (re-analyzed), yielded a shallow failure surfaces. Minuto and Morandi (2015) ignored such shallow surfaces. According to Minuto and Morandi, there was no sign of cracks or any failure on the field which means that any type of failure can occur. Consequently, shallow surfaces were also considered in this thesis. The analyses showed that there is a high probability that a shallow failure might occur as compared to deep failure.

If deep failure surfaces for coarse matrix have to be considered, SF values of around 1.2 to 1.25 are obtained, which are almost similar to the result of Minuto and Morandi (2015). For 15% the safety factor had average values of 1.08 which correspond to shallow failure surfaces. The safety factor for coarse matrix and 15% VBP are almost the same. The deep failure surfaces for 15% VBP, observed with failure surface progression, have SF of 1.2 to 1.25 similar to the coarse matrix and to that obtained by Minuto and Morandi (2015).

The 30% VBP models, when analysed with the strength parameters of that used by Minuto and Morandi (2015) have lower average SF of 1.04. Some of the models had SF less than one. In the cases of SF less than one no potential deep failure surfaces were observed. The 30% VBP models with strength parameters of coarse matrix had an average SF value of 1.19. The progressive failure yielded potential deep failure surfaces around SF of 1.27 to 1.37 which is lower than 1.49, obtained by Minto and Morandi (2015).

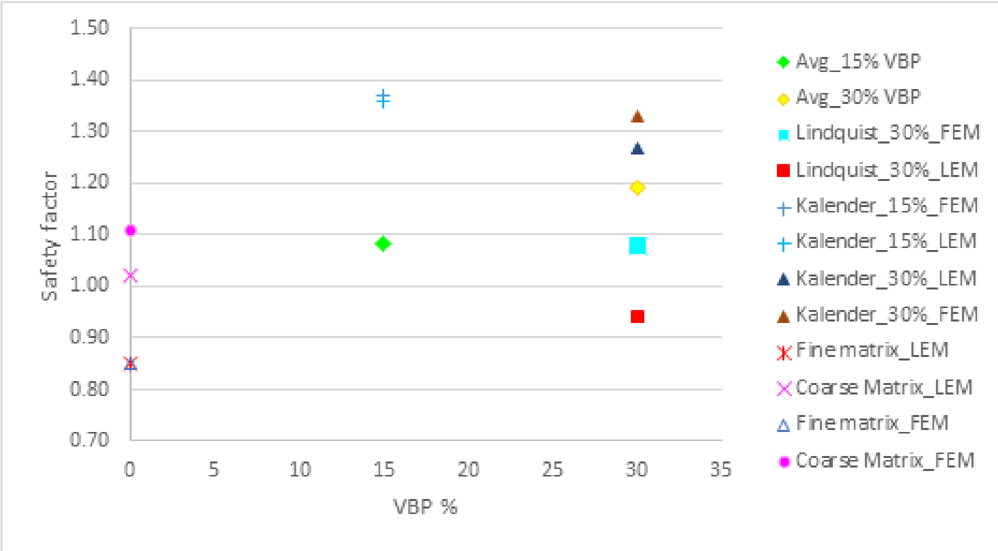


**Figure 4.17:** Comparison of different models analysed with different approaches and different methods. The occurrence of shallow failure surface is more likely in the case of low VBP.

The models with 15% and 30% VBP, when analysed with Kalender strength criterion, had safety factors of 1.37 and 1.33 respectively. By comparing the values of the safety factors for Kalender et al. and Lindquist's strength criteria, it can be concluded that the deep surfaces had almost the same values in both cases. For 30% VBP the safety factor values corresponding to deeper failure surfaces are comparable between homogeneous and heterogeneous approaches. For lower VBP i.e. 15% models the homogenous approaches have higher safety factors.

# Conclusions

The present dissertation reports a study carried out to analyse the stability of a relict landslide in bimrocks in the downtown of Genova, Italy. Previously, this slope was analysed by Minuto and Morandi (2015) using a deterministic approach and the Limit Equilibrium Method (LEM). According to Minuto and Morandi (2015), the slope consisted of colluvium soil with the inclusion of gravels and rock blocks. This was found after the investigation of the slope by drilling six boreholes of depth varying between 25m and 40m. Laboratory tests were performed on the samples of fine material. Initially, a matrix was analysed with the material properties of this fine material. However, since the real slope included also a considerable amount of gravel. Another matrix was analysed after increasing its mechanical properties according to Lindquist (1994) findings. This coarse matrix included the properties of both the fine and the coarse material. The authors estimated the volumetric block proportion using the chart developed by Medley (1997). This chart is used in the estimation of VBP from borehole logs and accounts for uncertainties in VBP estimates from LBP measurements and resulted in two VBPs of 15% and 30%. Minuto and Morandi (2015) used rectangular blocks in the slope.

This thesis focused on the 2D numerical analyses of this relict landslide using the Slide and RS2 codes (Rocscience Inc). In the first phase, the results of Minuto and Morandi were validated with LEM, for both the fine matrix and coarse matrix. Due to the high spatial and dimensional variability of bimrocks the use of a stochastic approach was proposed for the rock block distribution in the slope. The stochastic approach is based on a Matlab code performing numerical Monte Carlo simulations. The code can generate populations of 2D blocks with random sizes, eccentricities, positions and orientations within the slope, according to specific statistical rules and given block contents. The used rock blocks were elliptical, with eccentricity values between 0.4 and 0.9. For each VBP, ten different block configurations were used to statistically establish the results.

In this dissertation, the slope was also analysed with the two different strength criteria of Lindquist (1994) and Kalender et al. (2014). Such criteria consider bimrocks to be homogenous and isotropic materials. These models were analysed with both the FEM and LEM approaches. It can be concluded that:

- the numerical analyses have complemented the outcomes of Minuto and Morandi (2015) in case of matrix-only and 15% VBP, if deep failure surfaces are considered;
- the analysis of the fine matrix had a factor of safety (FS) less than 1, implying a failure of the slope. In reality, since the slope has not failed it is reasonable and necessary to consider the presence of rock blocks;
- in all the analyses it was found that the shallow failure surfaces are more likely to occur. The safety factors for deep failure surfaces are comparable with that of Minuto and Morandi (2015) but have a lower probability of occurrence as compared to shallow surfaces;
- the models of coarse matrix and 15% VBP has almost the same SF in both cases of shallow and deep failure surfaces;
- the similar values of SF for coarse matrix and 15% VBP might be suggesting that the mechanical behaviour of bimrocks are not affected by lower VBP but the path of failure surface is affected by the position of the blocks and are deeper if rock blocks are located at the toe of the slope;
- the 30% VBP models when analysed with the strength parameters of Minuto and Morandi (2015) yields lower SF and in some cases less than 1. This unrealistic result can be due to lower cohesion value;
- when 30% VBP models are analysed with the strength properties of coarse matrix, an increase of 10% is observed as compared to 15% VBP. In case of deep failure surfaces this increase is 16%;
- for 30% VBP models when deep failure surfaces are considered the SF values are 8% less than that obtained by Minuto and Morandi (2015).
- the use of a stochastic approach in distributing the blocks in the slope is more practical than the deterministic approach used by Minuto and Morandi (2015);

The analysis of the homogeneous approaches revealed that:

- Lindquist criterion yields lower safety factors as compared to Kalender et al. criterion partly because Lindquist criterion yielded shallow failure surfaces;

- Kalender et al., criterion has almost the same values of SF for both 15% and 30% VBP models;
- for 15% VBP, the approach of Kalender et al. (2014) provides higher values of safety factor as compared to the heterogeneous approach if deep failure surfaces are considered. The safety factors for Kalender et al. are largely affected by the value of parameter 'A' and UCS of the matrix;

# Bibliography

Afifipour, M., Moarefvand, P., 2013. Mechanical behavior of bimrocks having high rock block proportion. Int. J. Rock Mech. Min. Sci. 65, 40–48.

Altinsoy, H., 2006 Matriks içinde blok içeren kayaların makaslama dayanımın belirlenmesi için fiziksel model esaslı bir araştırma [M.Sc.Thesis] Ankara: Hacettepe Univ.

Barbero, M., Bonini, M., Borri-Brunetto, M., 2006. Analisi numeriche della stabilità di un versante in bimrock. Proceedings of Incontro annuale dei ricercatori di Geotecnica– IARG 2006, Pisa, 2006.

Barbero, M., Bonini, M., Borri-Brunetto, M., 2008. Three-Dimensional Finite Element Simulations of Compression Tests on Bimrock. In: Proceedings of the 12th Int. Conference of International Association for Computer Methods and Advances in Geomechanics (IACMAG), Goa, India, 631-637

Barton, N., Choubey, V., 1977. The shear strength of rock joints in theory and practice. Rock Mechanics Vol.10, 1-54

Bishop, A.W. and Morgenstern, N., 1960. Stability coefficients for earth slopes. Geotechnique, 10(4), pp.129-153.

Button, G., Riedmuller, W., Schubert, K., Klima, E., Medley, E., 2001. Tunnelling in Tectonic Melanges – Accommodating the Impacts of Geomechanical Complexities and Anisotropic Rock Mass Fabrics. Bulletin of Engineering Geology and the Environment

Coli, N., Berry, P., Boldini, D., 2011. In situ non-conventional shear tests for the mechanical characterisation of a bimrock. Int J Rock Mech Min Sci 48(1):95–102

Cowan, D., 1985. Structural styles in Mesozoic and Cenozoic melanges in the western Cordillera of North America. Geological Society of America Bulletin, v.96, April 1985

Duncan, J.M. and Chang, C.Y., 1970. Nonlinear analysis of stress and strain in soils. Journal of Soil Mechanics  Foundations Div.

Duncan, J.M., 1996. State of the art: limit equilibrium and finite-element analysis of slopes, Journal of Geotechnical Engineering, vol. 122, no. 7, pp. 577-596

Duncan, J.M., 2000. Factors of safety and reliability in geotechnical engineering. Journal of geotechnical and geoenvironmental engineering, 126(4), pp.307-316.

Fellenius W 1936 Calculations of the Stability of Earth Dams. In Proceedings of Second Congress of Large Dams, Washington DC, pp. 445-463.

Gokceoglu, C., 2002. A fuzzy triangular chart to predict the uniaxial compressive strength of the Ankara Agglomerates from their petrographic composition. Engineering Geology 66, 39-51

Guerra, C.I., Pinzón, J.J., Prada, L.F. and Ramos, A.M., 2016. Multiscale modelling of the slope stability of block-in-matrix materials. In Geo-Chicago 2016 (pp. 658-667).

Haneberg, W.C., 2004. Simulation of 3D block populations to characterize outcrop sampling bias in bimrocks. Felsbau Rock and Soil Engineering-Journal for Engineering Geology, Geomechanics and Tunneling 22(5), 19-26

Hoek, E., Carranza-Torres, C. and Corkum, B., 2002. Hoek-Brown failure criterion-2002 edition. Proceedings of NARMS-Tac, 1(1), pp.267-273.

Irfan, T.Y., Tang, K.Y., 1993. Effect of the Coarse Fractions on the Shear Strength of Colluvium. GEO report No.22 – Hong Kong Geotechnical Engineering Office, Reprinted, 1995, 223

Janbu, N., 1954. Application of composite slip surface for stability analysis. In Proceedings of European Conference on Stability of Earth Slopes, Sweden, 1954 (Vol. 3, pp. 43-49).

Janbu, N., 1973. Slope stability computations. Publication of: Wiley

(John) and Sons, Incorporated.

Kahraman, S., Alber, M. 2008. Triaxial strength of fault breccias of weak rocks in a strong matrix. Bull of Eng Geo and Env 67(3):435–441.

Kalender, A., Sonmez, H., Medley, E., Tunusluoglu, C. and Kasapoglu, K.E., 2014. An approach to predicting the overall strengths of unwelded bimrocks and bimsoils. Engineering geology, 183, pp.65-79.

Ke, T Chih., 1995. Application of DDA to block-in-matrix materials. In 35th U.S. Symposium on Rock Mechanics (USRMS), A. A. Balkema, Rotterdam, PN 95–0033

Li, X., Liao Q. L., He, J. M., 2004. In-situ tests and a stochastic structural model of rock and soil aggregate in the three Gorges Reservoir area, China. Int. J. Rock Mech. Min. Sci., 41, No. 3, 702-707

Li, Y.Y., Jin, X.G., Wang, L. and Lv, Z.T., 2014. Shear strength and failure characteristics identification of soil-rock mixture. Electron J Geotech Eng (EJGE), 19, pp.6827-6838

Lindquist, E.S., 1991. Fractals-Fracture and Franciscan Melange, Term Paper for CE 280, Rock Mechanics instructor: Prof. R.E Goodman, Dept Civil Engineering, University of California, Berkeley.

Lindquist, E., 1994. The Strength and Deformation Properties of Melange. Ph.D. dissertation, Department of Civil Engineering, University of California, Berkeley.

Lindquist, E.S., Goodman, R.E., 1994. Strength deformation properties of a physical model melange. Proceedings 1st North American Rock Mech. Symp., Austin, Texas, 843-850

Mandelbrot, B.B., 1983. The fractal geometry of nature. W.H. Freeman and Co, New York, 468 pp.

Medley, E., 1994. The engineering characterization of melanges and similar block-in-matrix rocks (bimrocks). Dept of Civil Engineering, University of California, Berkley, California, PhD diss., UMI Diss. Svc., Ann Arbor, NI.

Medely, E., 1997. Uncertainty in estimates volumetric proportions in melange bimrocks. Proceedings of International Symposium on Engineering

Geology and the Environment, Athens, 23-27 June 1997, eds P.G Marinos et al., 267-272.

Medley E., 1999. Systematic characterization of melange bimrocks and other chaotic soil/rock mixtures. Felsbau 17 (1999), No.3.

Medley, E., 2001. Orderly Characterization of Chaotic Franciscan Melanges. Felsbau Rock and Soil Engineering-Journal for Engineering Geology, Geomechanics and Tunneling 19, 4,20-4,21.

Medley, E., 2002. Estimating Block Size Distributions of Melanges and Similar Block-in Matrix Rocks (Bimrocks). Proceedings of 5th North American Rock Mechanics Symposium (NARMS), Toronto, July 2002, 509-606.

Medley, E., 2004. Observations on tortuous failure surface in bimrocks. Felsbau Vol.22 (2004), No. 5, 35-43.

Medley, E., 2007a. Bimrocks Article Part 1: Introduction. Newsletter of HSSMGE, No. 7, February 2007.

Medley E., 2007b. Bimrocks Article Part 2: Case Histories and Practical Guidelines. Newsletter of HSSMGE, No. 8, April 2007.

Medley, E., Lindquist., E.S., 1995. The engineering significance of the scale independence of some Franciscan melanges in California, USA. Proceedings of the 35th US Rock Mechanics Symposium, Reno, 907-914.

Medley, E., Sanz Rehermann, P.F., 2003. Increases in slope stability of rock/soil mixtures due to tortuosity of failure surfaces around rock blocks. Annual Meeting Geol. Soc. America, Seattle, WA

Medley, E., Sanz Rehermann, P.F., 2004. Characterization of Bimrocks (Rock/Soil Mixtures) with Application to Slope Stability Problems. Proceedings Eurock 2004 53rd Geomechanics Colloquium Salzburg, Austria October 2004.

Medley, E., Wakabayashi, J., 2004. Geological Characterization of Melanges for Practitioners. Felsbau Rock and Soil Engineering-Journal for Engineering Geology, Geomechanics and Tunneling 22(5), 10-18.

Minuto, D. and Morandi, L., 2015. Geotechnical Characterization and Slope Stability of a Relict Landslide in Bimsoils (Blocks in Matrix Soils) in

Dowtown Genoa, Italy. In Engineering Geology for Society and Territory-Volume 2 (pp. 1083-1088). Springer, Cham.

Morgenstern, N.R., Price, V.E., 1965. The analysis of the stability of general slip surfaces. Geotechnique, v.15, 79-93.

Napoli, M.L., Barbero, M., Ravera, E. and Scavia, C., 2018. A stochastic approach to slope stability analysis in bimrocks. International Journal of Rock Mechanics and Mining Sciences, 101, pp.41-49.

Pan, Y.W., M.H. Hsieh, M.H., Liao, J.J., 2008. Mechanical Properties of virtual block-inmatrix colluvium. In: Proceedings of ARMA 2008, American Rock Mechanics Association, 42nd U.S. Rock Mechanics Symposium, San Francisco, USA, ARMA08-51, 8.

Pande, G.N., Beer, G., Williams, J.R., 1990. Numerical Methods in Rock Mechanics, John Wiley and Sons, Ltd.

Peitgen, H.-O., Jurgens, H., Saupe, D., 1992. Chaos and Fractals: New Frontiers of Sciences. Springer-Verlag, New York.

Raymond, L.A,. 1984. Classification of melanges. In Raymond L.A., ed, Melanges: Their nature, origin and significance. Geological Society of America Special Paper, 198, 7-20

Rocscience, 2004. Rocscience software products: RS2 version 11.0

Rocscience, 2004. Rocscience software products: Slide version 9.0

Rocscience, 2004. A new era in slope stability analysis: Shear strength reduction Finite Element Technique. RocNews, Summer 2004, 2-9.

Sammis, C.G., Biegel, R.L., 1989. Fractals, fault gouge, and friction. Pure and Appl. Geophysics 131, 255-271.

Sonmez, H., Gokceoglu, C., Tuncany, E., Medley, E., Nefeslioglu, H.A., 2004a. Relationships Between Volumetric Block Proportions and Overall UCS of a Volcanic Bimrock. Felsbau Rock and Soil Engineering- Journal for Engineering Geology, Geomechanics and Tunneling 22(5), 27-32.

Sonmez„ H., Tuncay, E., Gokceoglu, C., 2004b. Models to predict the uniaxial compressive strength and the modulus of elasticity for Ankara Agglomerate. Int. Jour. Rock Mech. Min. Sci. 41, 717–729.

Sonmez, H., Altinsoy, H., Gokgeoglu, C., Medley, E., 2006a. Considerations in Developing an Empirical Strength Criterion for Bimrocks. Proceedings 4th Asian Rock Mechanics Symposium (ARMS 2006), November 6-10, Singapore.

Sonmez, H., Gokceoglu, C., Medley, E., Tuncay, E., Nefeslioglu, H.A., 2006b. Estimating the Uniaxial Compressive Strength of a Volcanic Bimrock. Int. Jour. Rock Mech. Min. Sci. 43, 554-561.

Sonmez, H., Kasapoglu, K.E., Coskun, A., Tunusluglu, C., Medley, E.W., Zimmerman, R.W., 2009. A conceptual empirical approach for the overall strength of unwelded bimrocks. In ISRM Regional Symposium, Rock Engineering in Difficult Ground Condition, Soft Rock and Karst, Dubrovnik, Croatia.

Sonmez, H., Tunusluoglu, C., 2010.Development of a unified geomechanical classification system and a generalized empirical approach for jointed rock masses and bimrocks. TUBITAK Project no:108Y002.

Sonmez, H., Ercanoglu, M., Kalender, A., Dagdelenler, G., Tunusluoglu, C., 2016. Predicting uniaxial compressive strength and deformation modulus of volcanic bimrock considering engineering dimension. Int. Jour. Rock Mech. Min. Sci. 86, 91-103.

Spencer, E., 1967. A method of analysis of the stability of embankments assuming parallel inter-slice forces. Geotechnique, 17(1), pp.11-26.

Xu, W., Yueb, Z., Hu, R., 2008. Study on the mesostructure and mesomechanical characteristics of the soil–rock mixture using digital image processing based finite element method. Int. J. Rock Mech. Min. Sci., 45,749–62.

Xu, W.J., Wang, S., Zhang, H.Y. and Zhang, Z.L., 2016. Discrete element modelling of a soil-rock mixture used in an embankment dam. International Journal of Rock Mechanics and Mining Sciences, 86, pp.141-156.

Zhang, Z.L., Xu, W.J., Xia, W. and Zhang, H.Y., 2016. Large-scale insitu test for mechanical characterization of soil–rock mixture used in an embankment dam. International Journal of Rock Mechanics and Mining Sciences, 86, pp.317-322.

# Appendix A

## Maximum shear strains and progressive failure for 15% VBP: FEM

### 15%_1_FEM

Crtical SRF=1.08

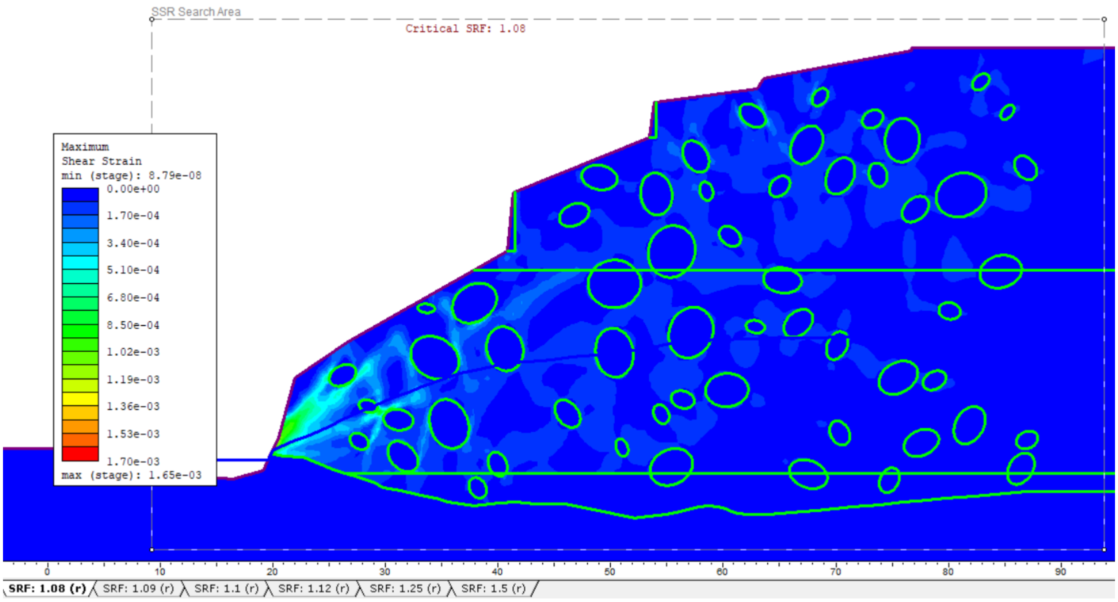

SRF=1.09

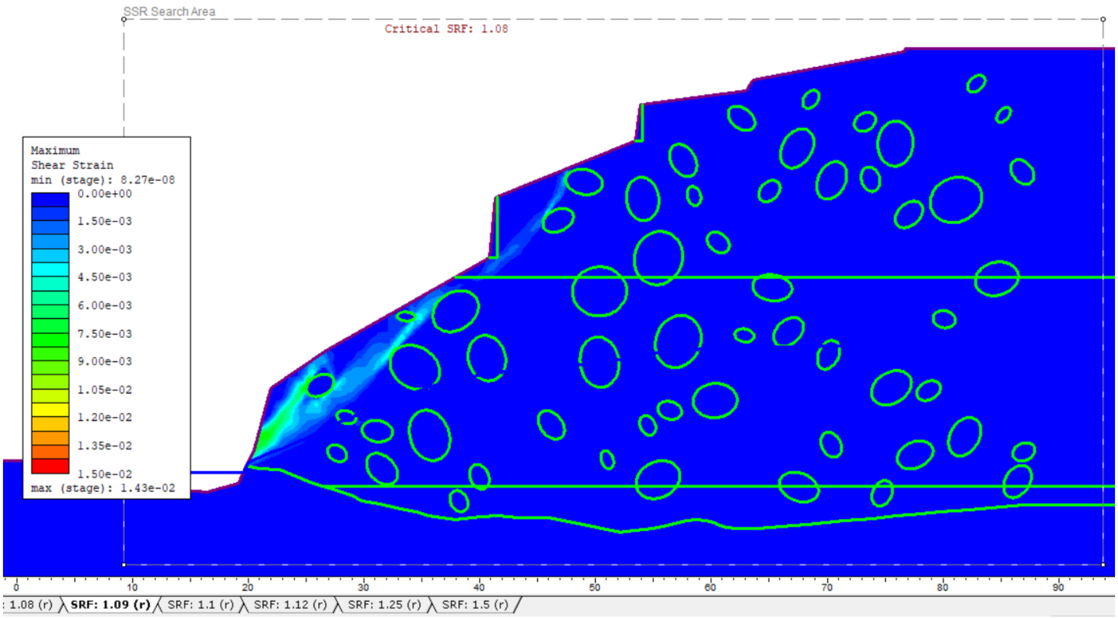


SRF=1.10

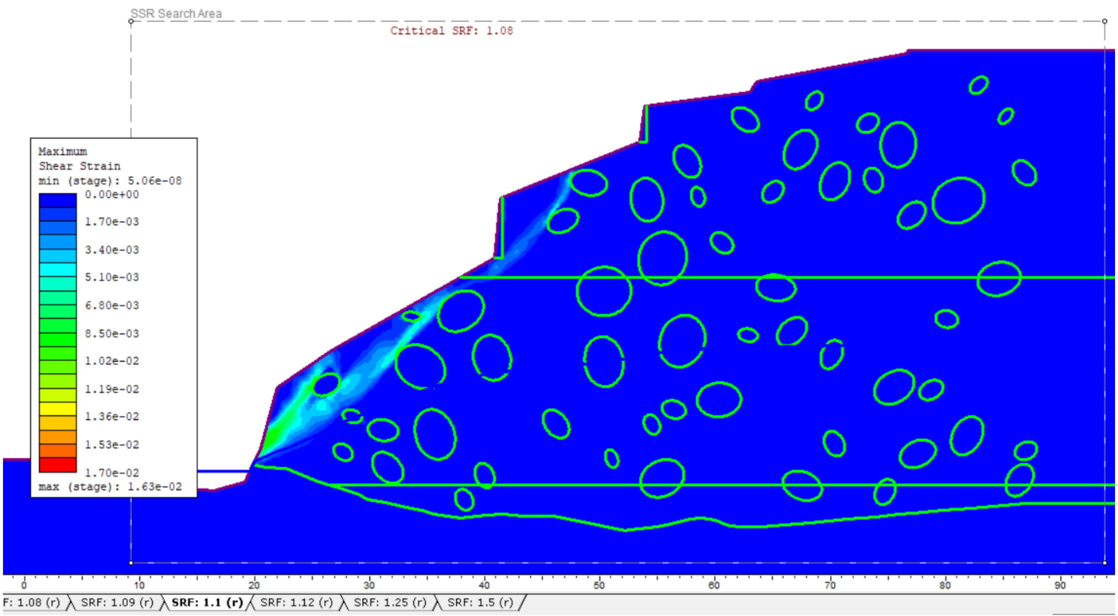

SRF=1.12

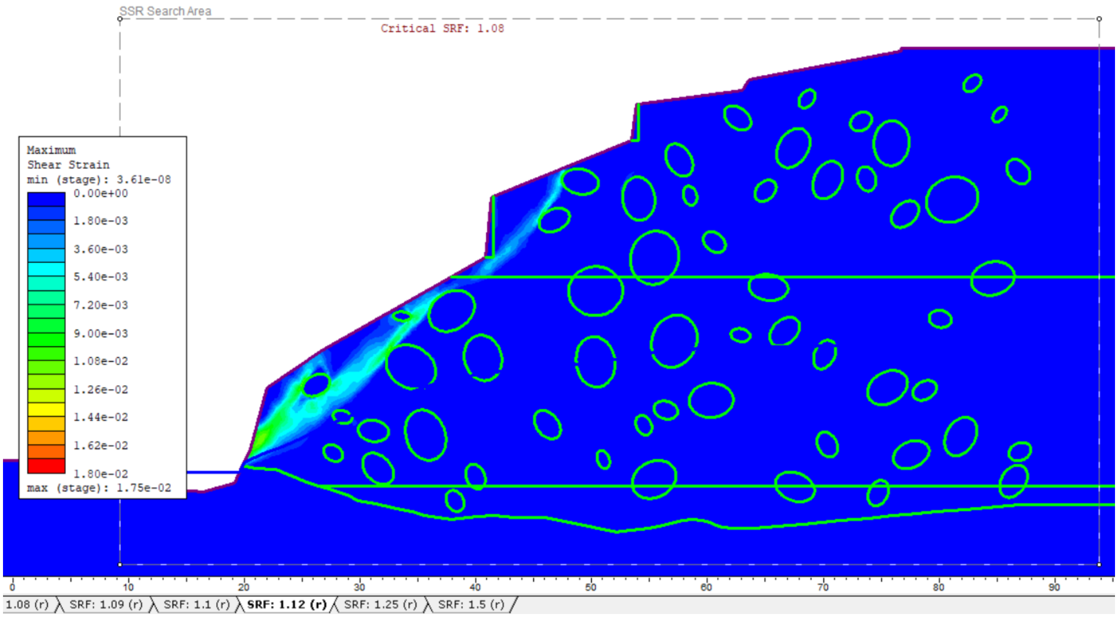


SRF=1.25

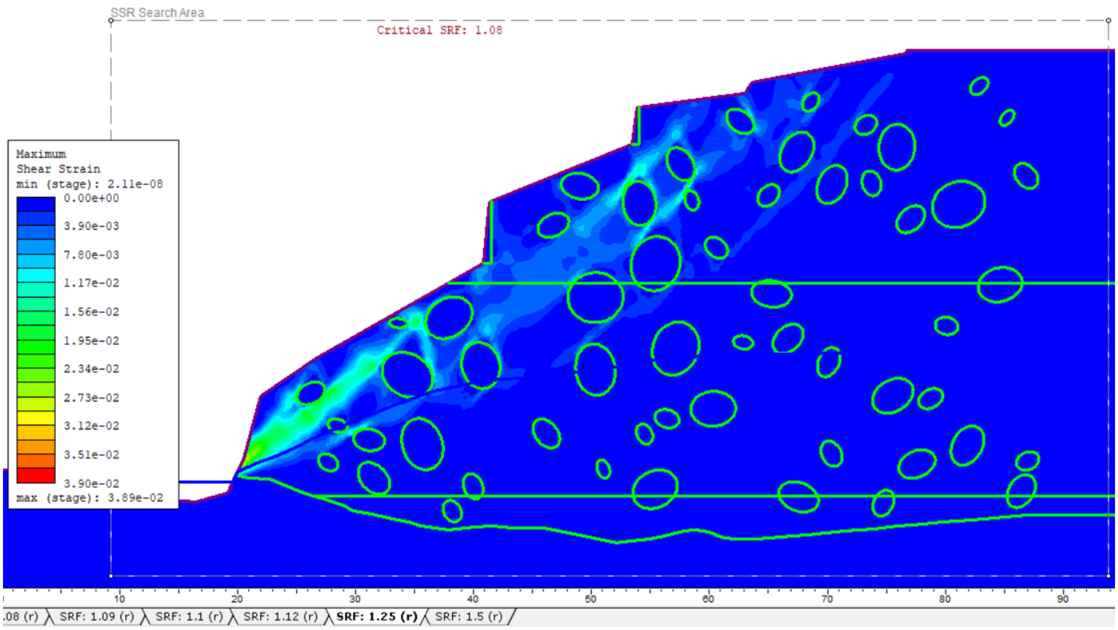

SRF=1.5

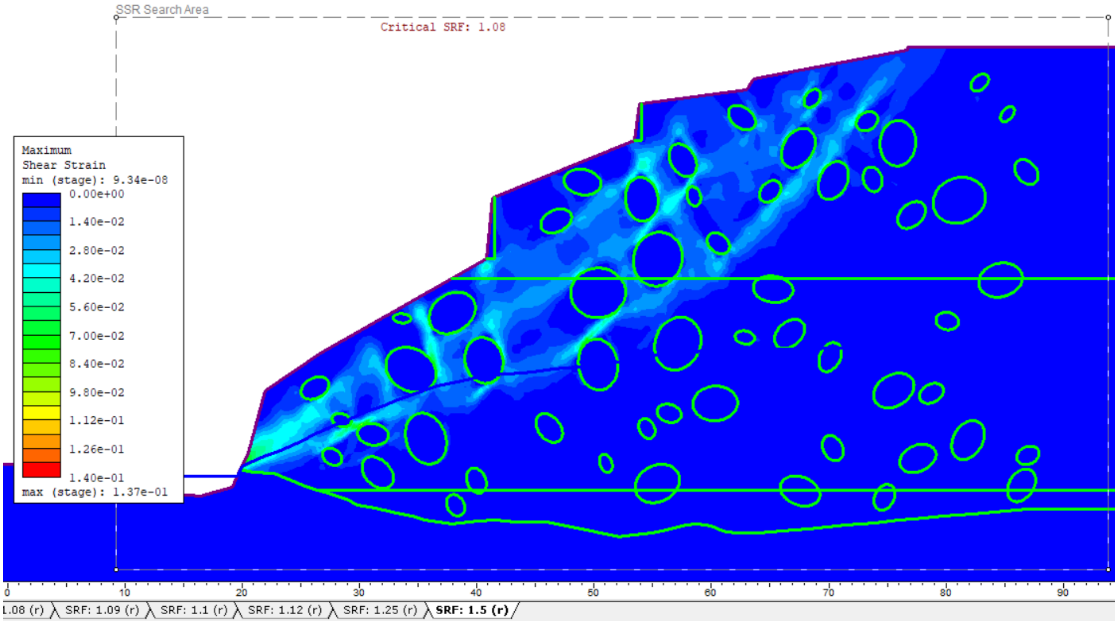

SSR Search Area
Critical SRF: 1.08
Maximum
Shear Strain
min (stage): 9.34e-08
0.00e+00
1.40e-02
2.80e-02
4.20e-02
5.60e-02
7.00e-02
8.40e-02
9.80e-02
1.12e-01
1.26e-01
1.40e-01
max (stage): 1.37e-01
0
10
20
30
40
50
60
70
80
90
1.08 (r)
SRF: 1.09 (r)
SRF: 1.1 (r)
SRF: 1.12 (r)
SRF: 1.25 (r)
SRF: 1.5 (r)

**15%_2_FEM**

Critical SRF= 1.04

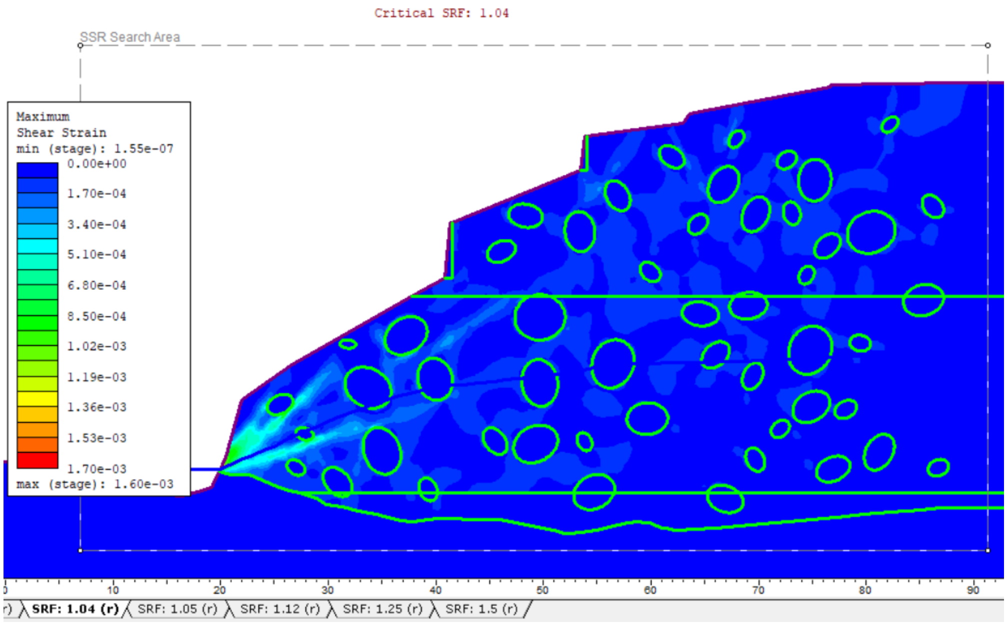


SRF= 1.05

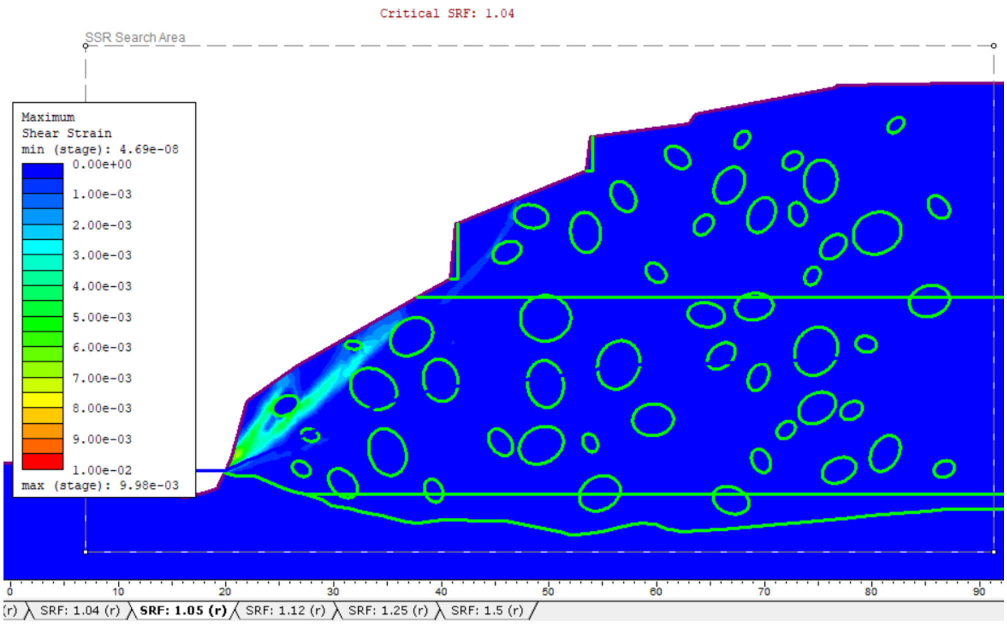

SRF= 1.12

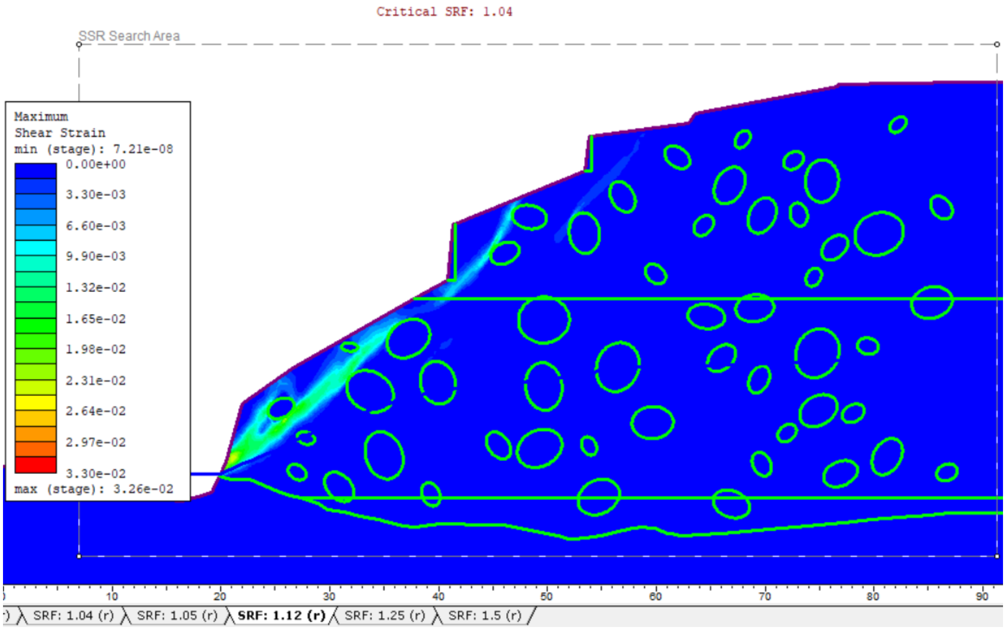


SRF= 1.25

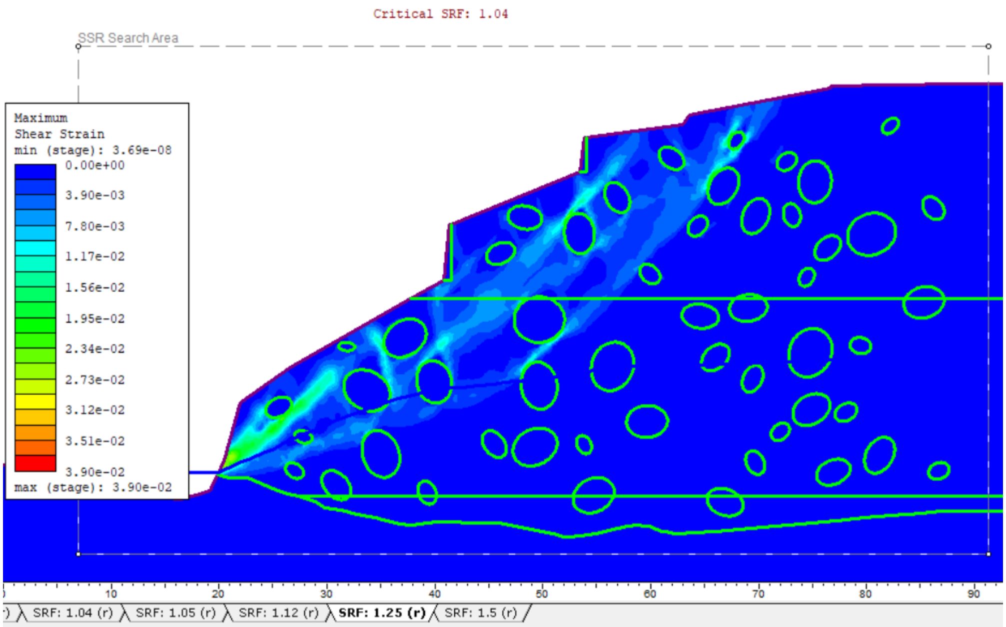

SRF= 1.50

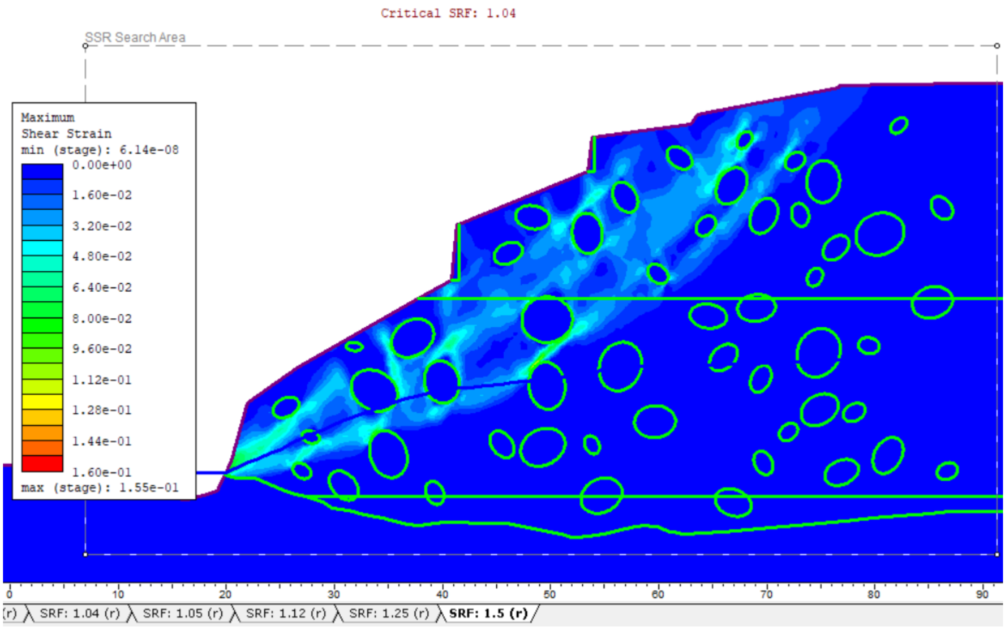
Critical SRF: 1.04
SSR Search Area
Maximum
Shear Strain
min (stage): 6.14e-08
0.00e+00
1.60e-02
3.20e-02
4.80e-02
6.40e-02
8.00e-02
9.60e-02
1.12e-01
1.28e-01
1.44e-01
1.60e-01
max (stage): 1.55e-01
0
10
20
30
40
50
60
70
80
90
SRF: 1.04 (r)
SRF: 1.05 (r)
SRF: 1.12 (r)
SRF: 1.25 (r)
SRF: 1.5 (r)

**15%_3_FEM**

Critical SRF= 1.05

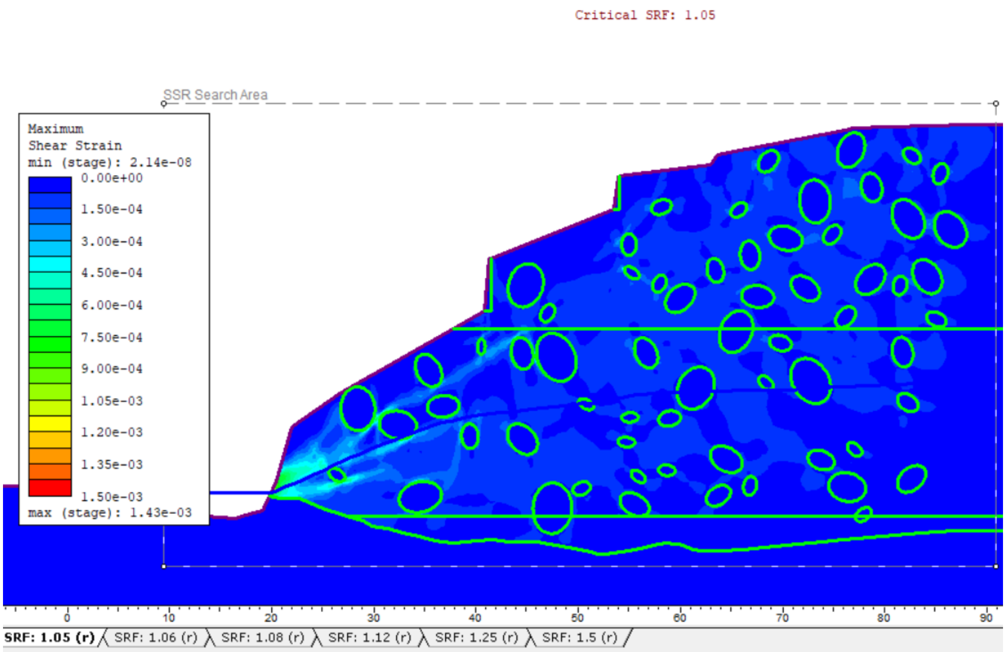


SRF= 1.06

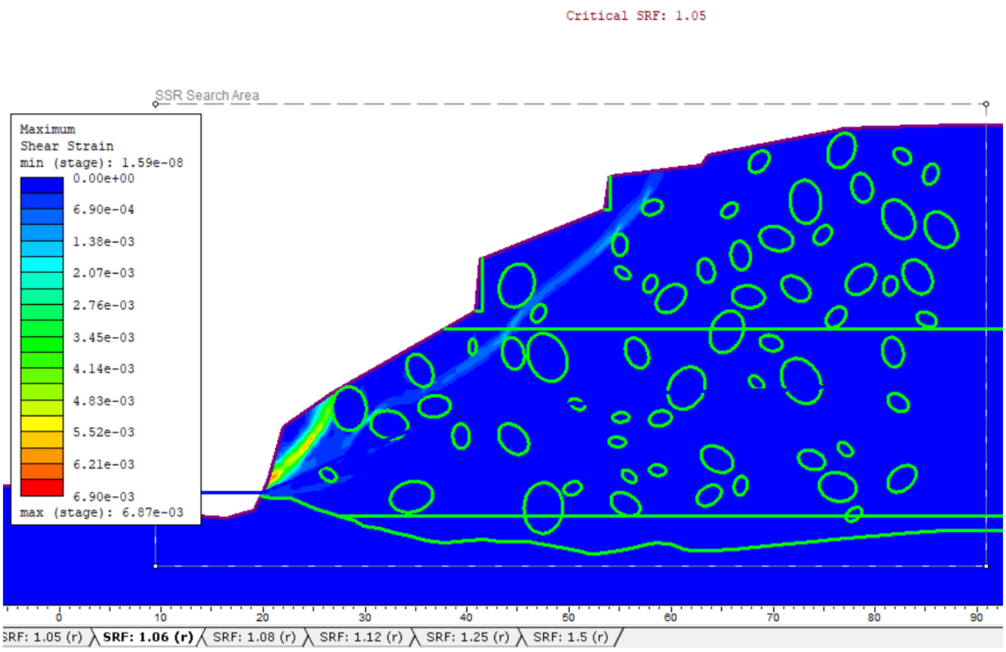

SRF= 1.08

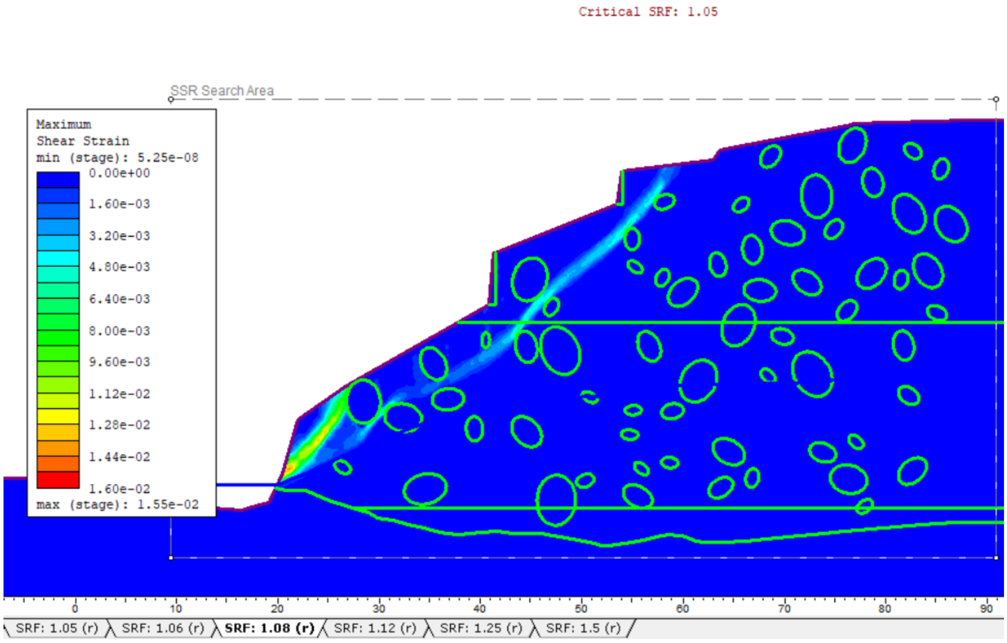


SRF= 1.12

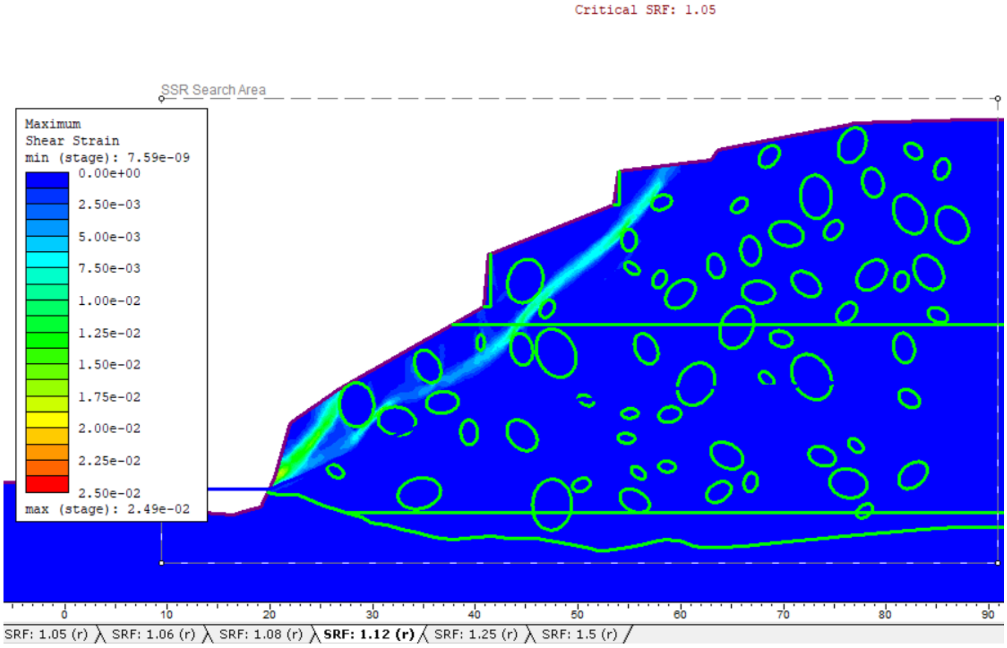

SRF= 1.25

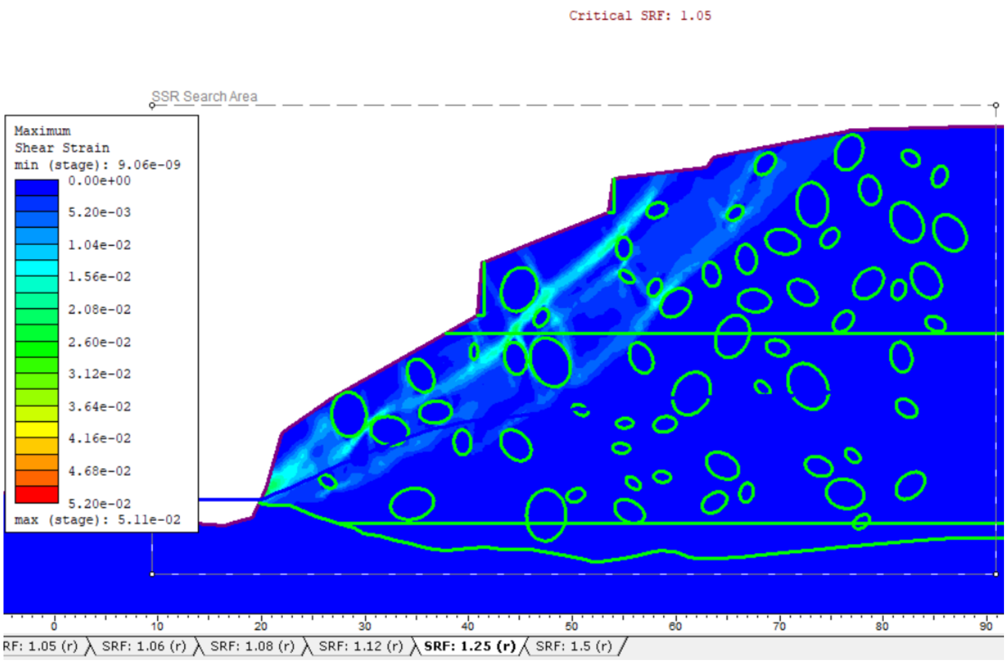


SRF= 1.50

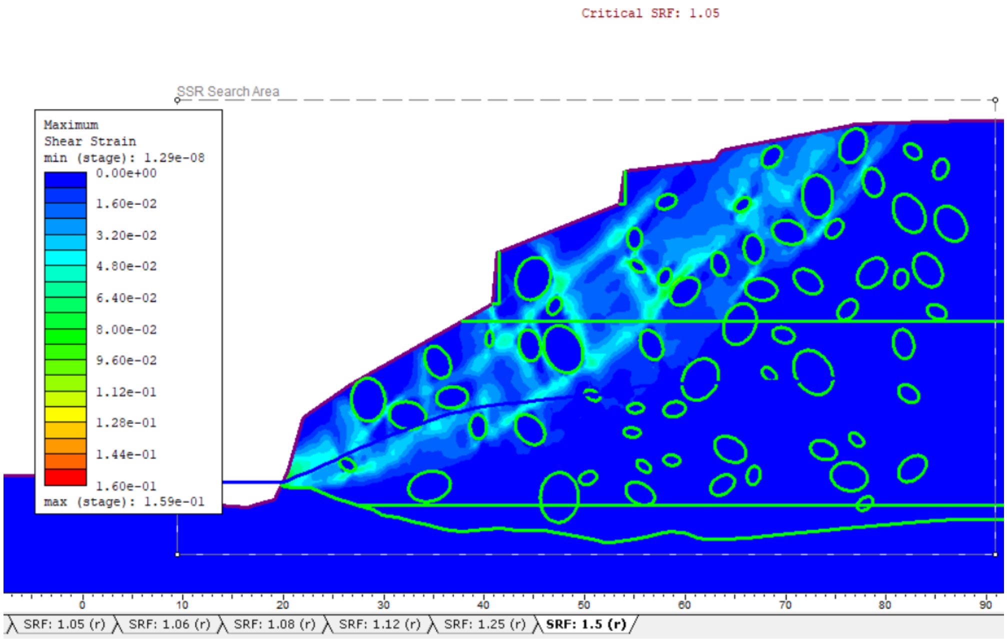

**15%_4_FEM**

Critical SRF= 1.12

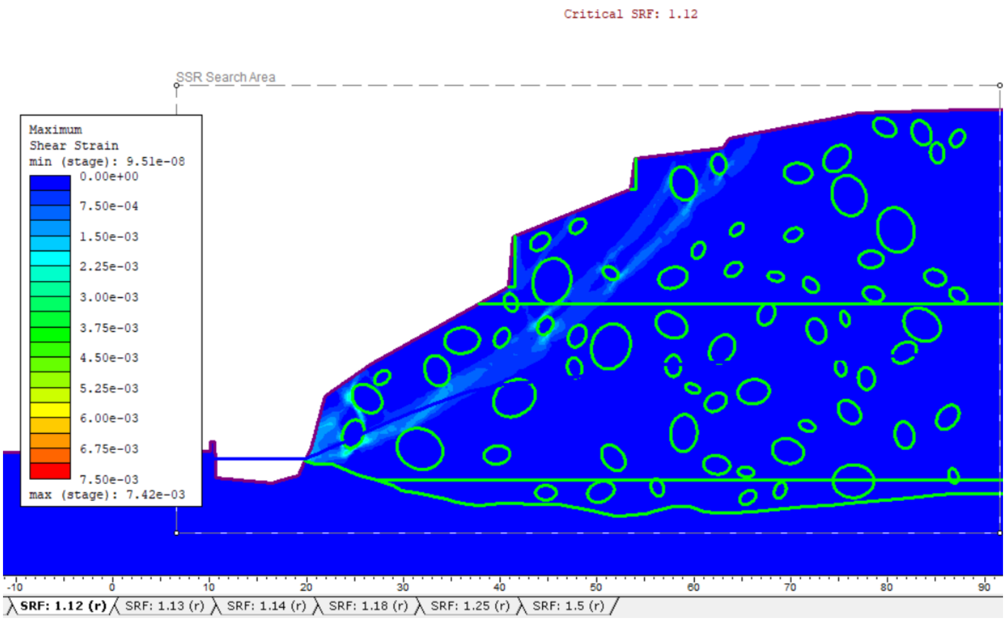


SRF= 1.13

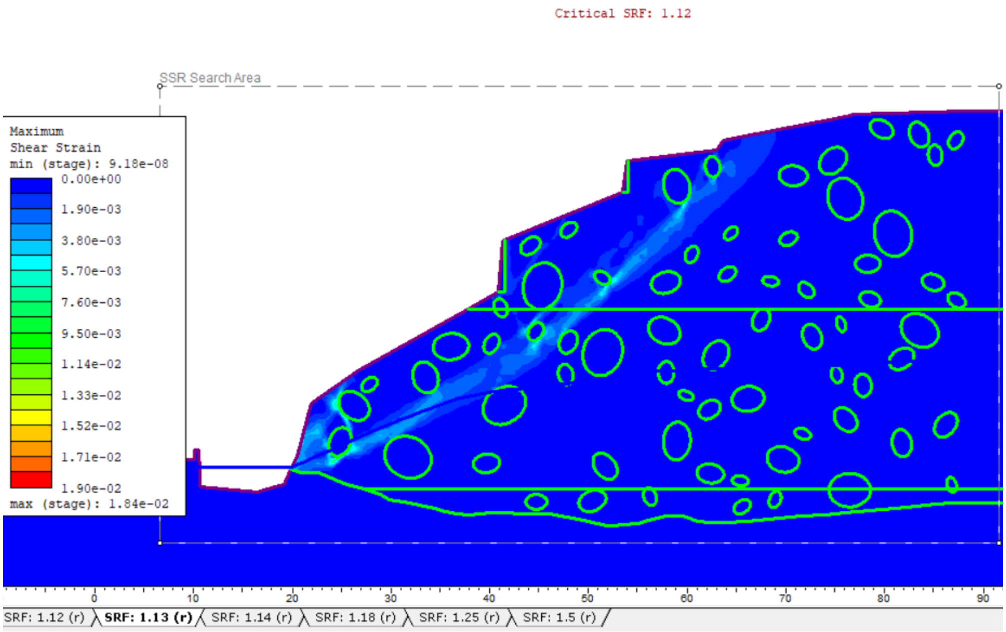

SRF= 1.14

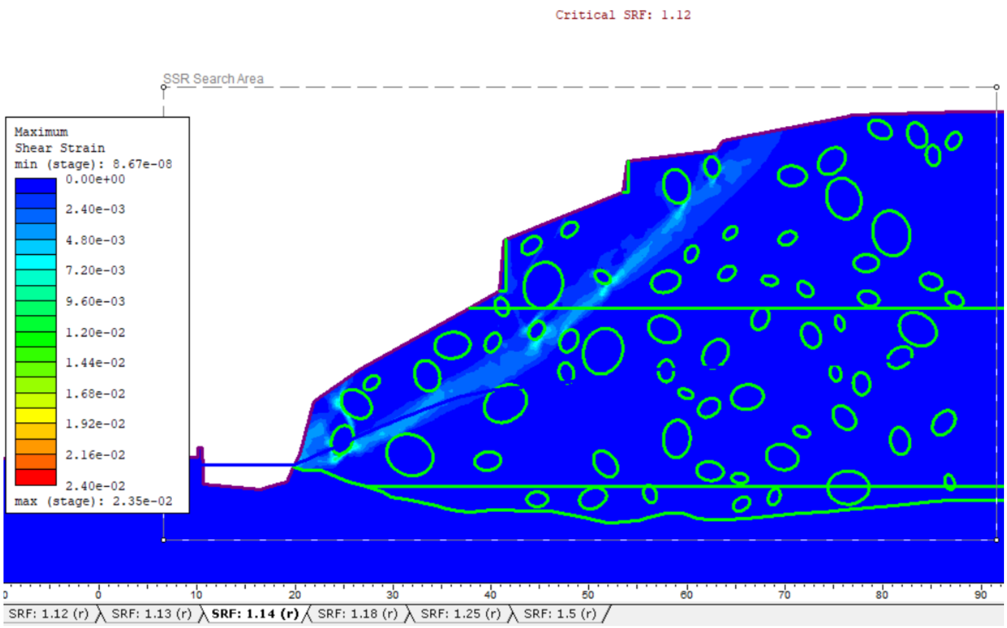


SRF= 1.18

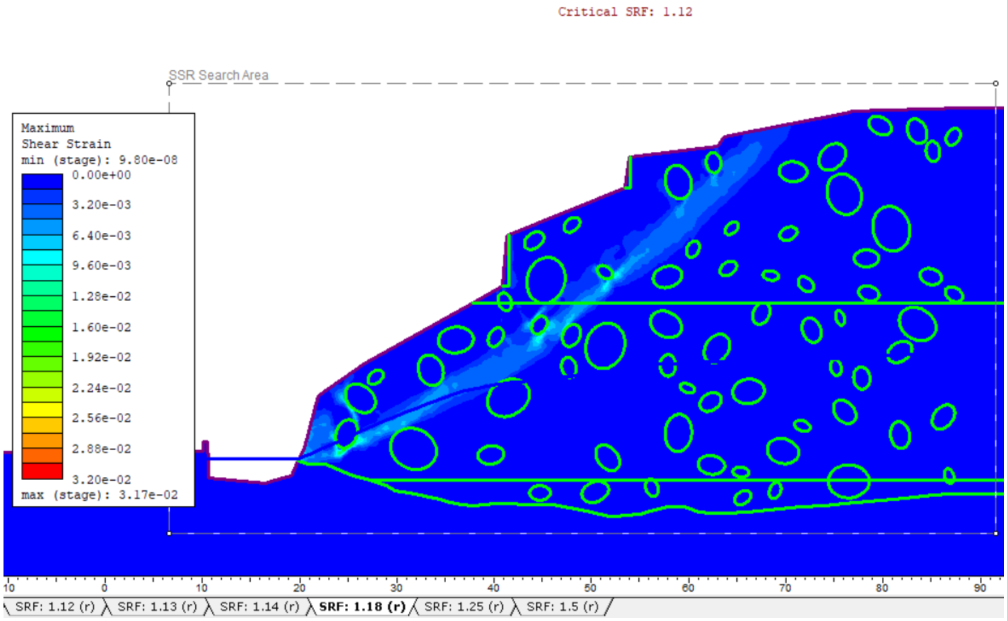

SRF= 1.25

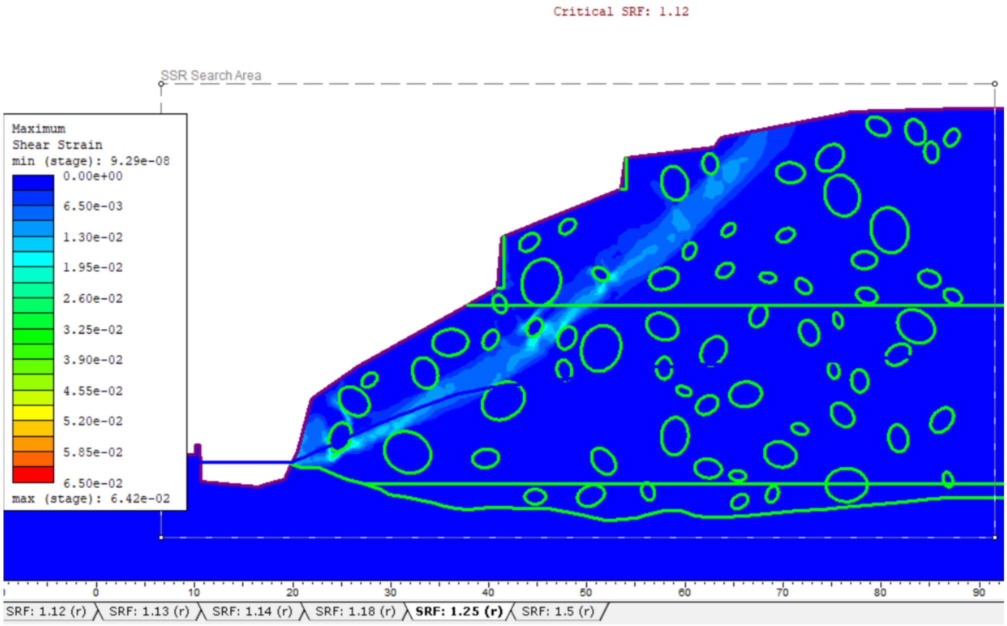


SRF= 1.50

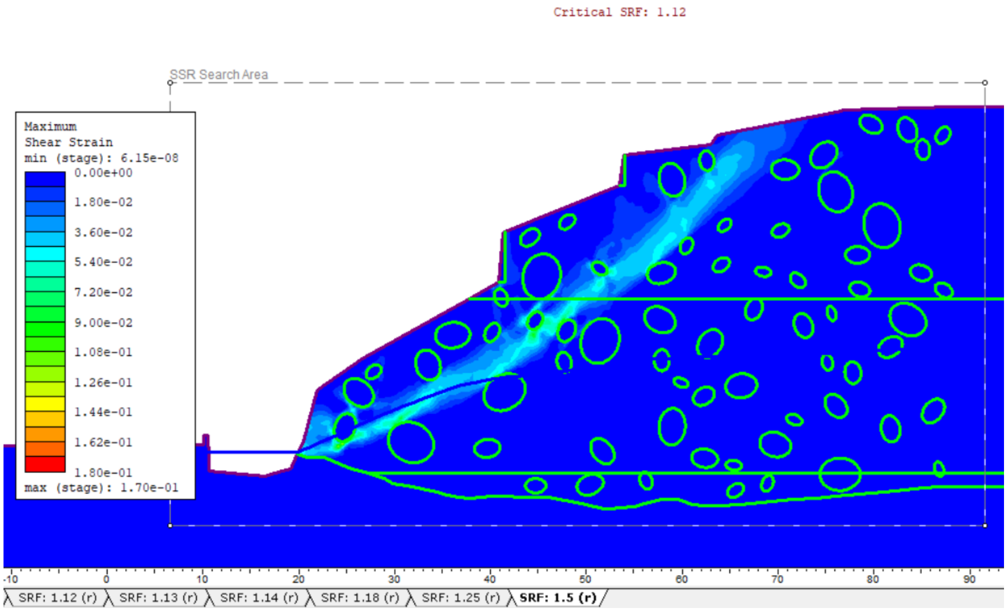

**15%_5_FEM**

Critical SRF= 1.07

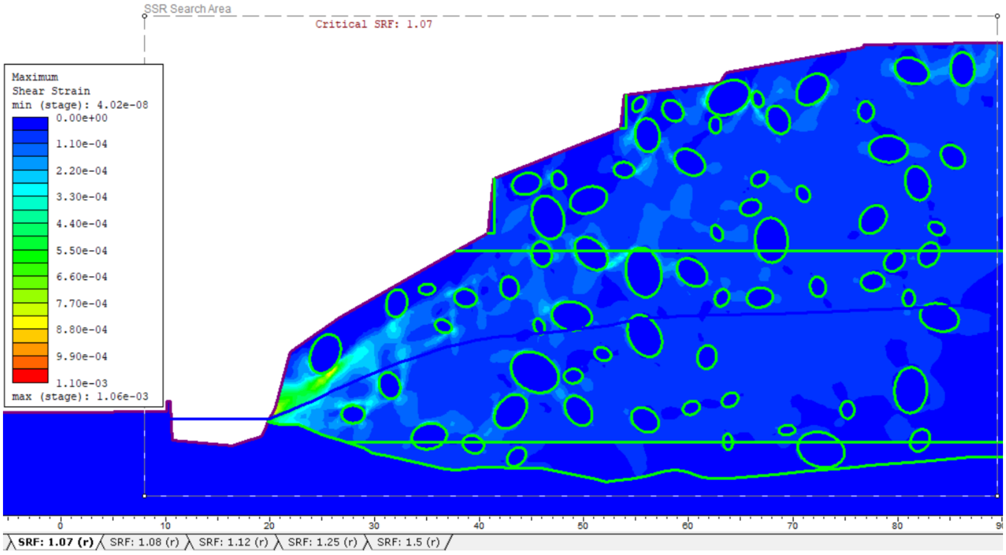


SRF= 1.08

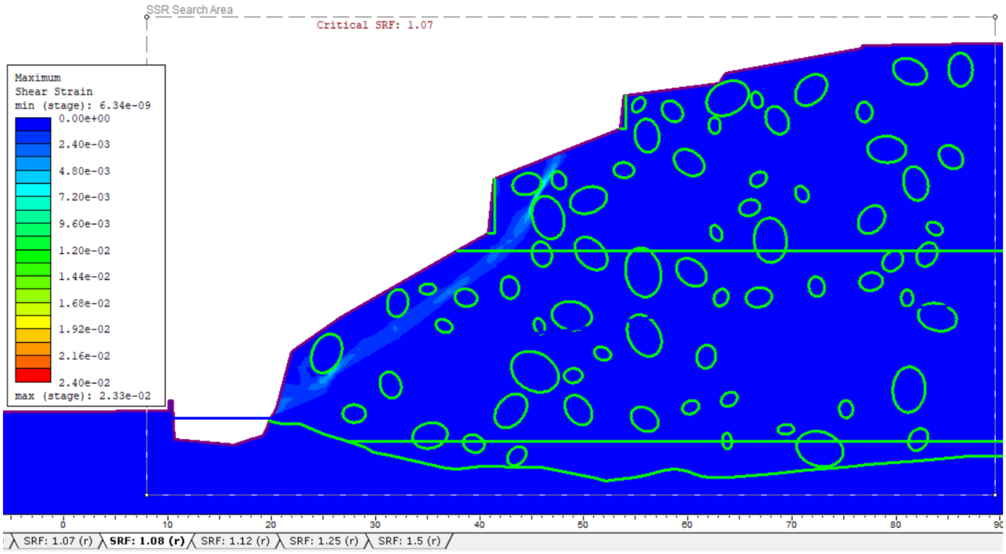

SRF= 1.12

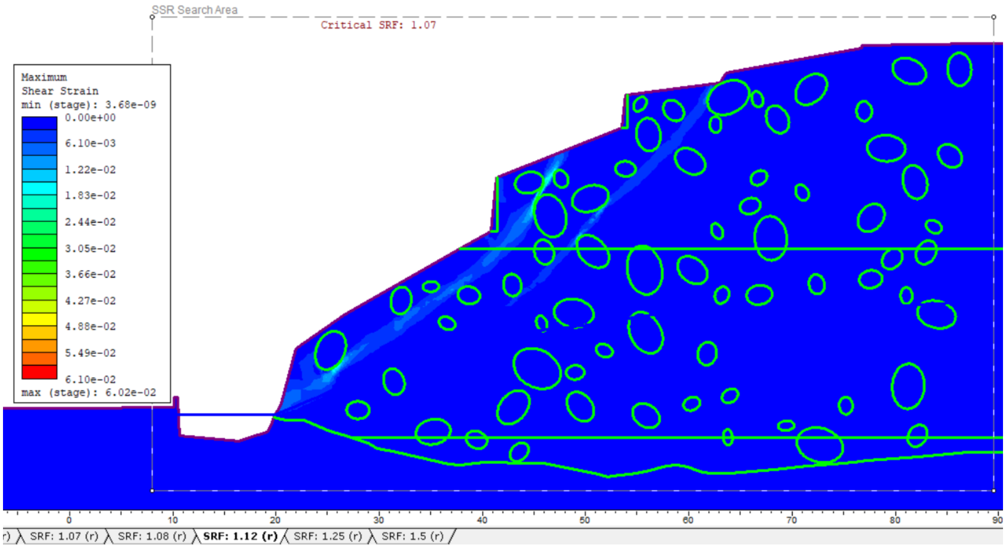


SRF= 1.25

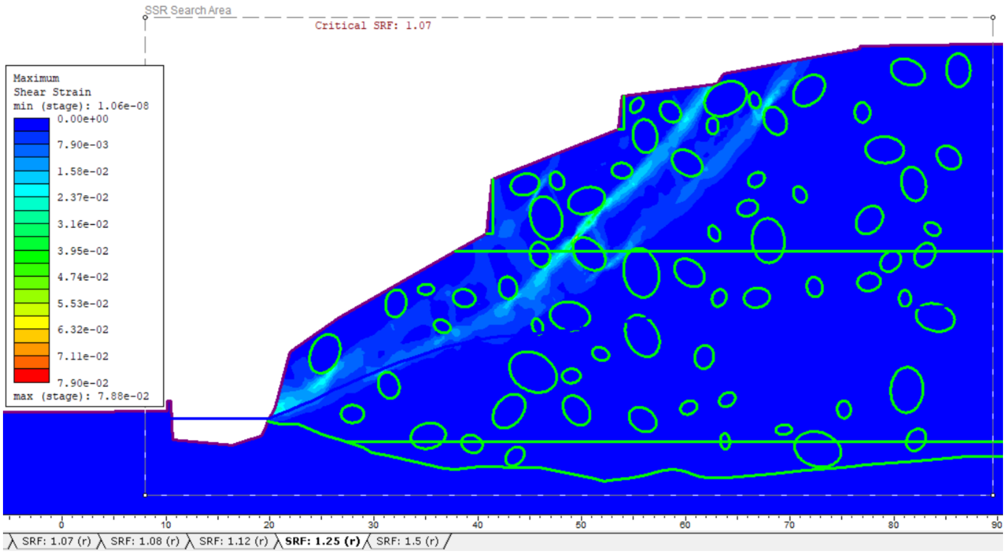

SRF= 1.50

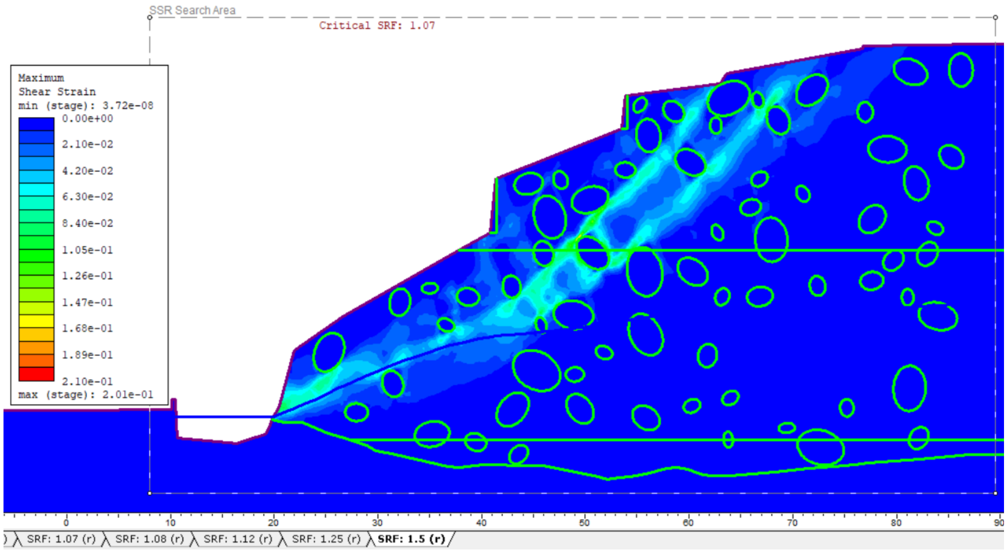
SSR Search Area
Critical SRF: 1.07
Maximum
Shear Strain
min (stage): 3.72e-08
0.00e+00
2.10e-02
4.20e-02
6.30e-02
8.40e-02
1.05e-01
1.26e-01
1.47e-01
1.68e-01
1.89e-01
2.10e-01
max (stage): 2.01e-01
0
10
20
30
40
50
60
70
80
90
SRF: 1.07 (r)
SRF: 1.08 (r)
SRF: 1.12 (r)
SRF: 1.25 (r)
SRF: 1.5 (r)

**15%_6_FEM**

Critical SRF= 1.10

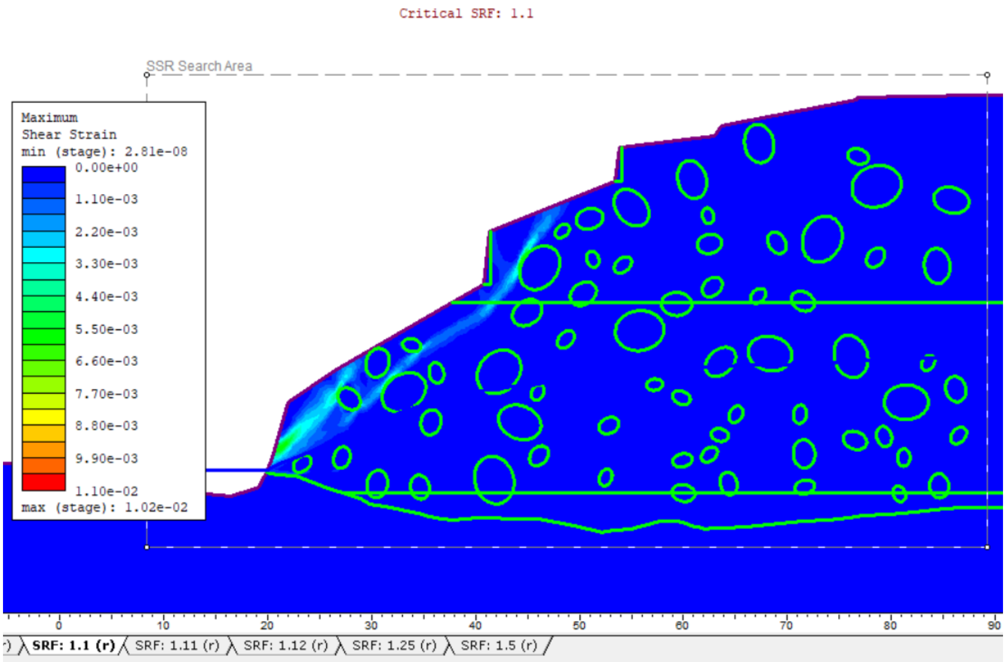


SRF= 1.11

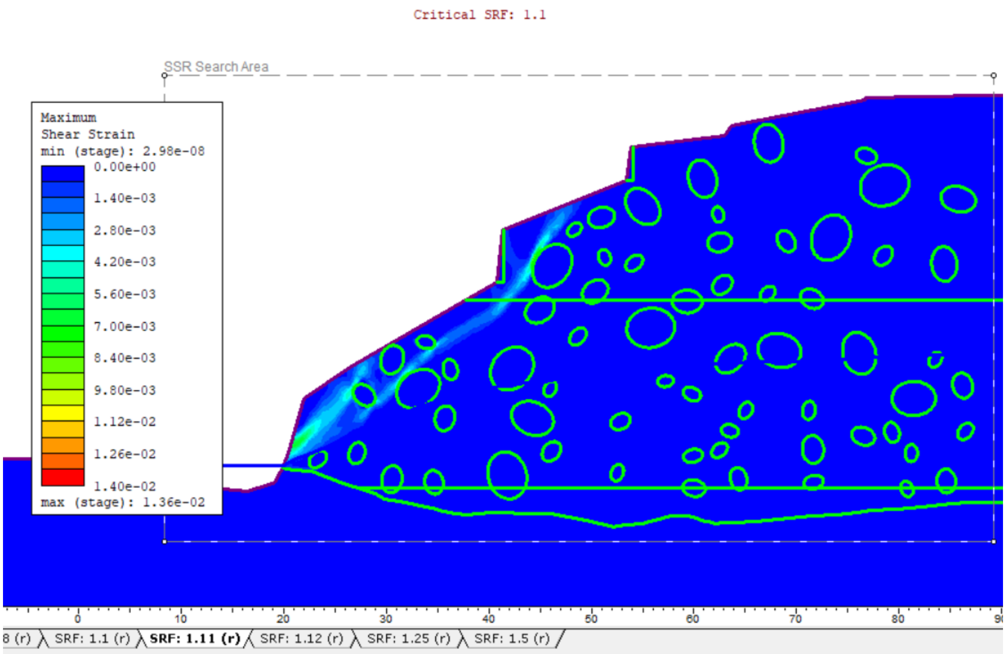

SRF= 1.12

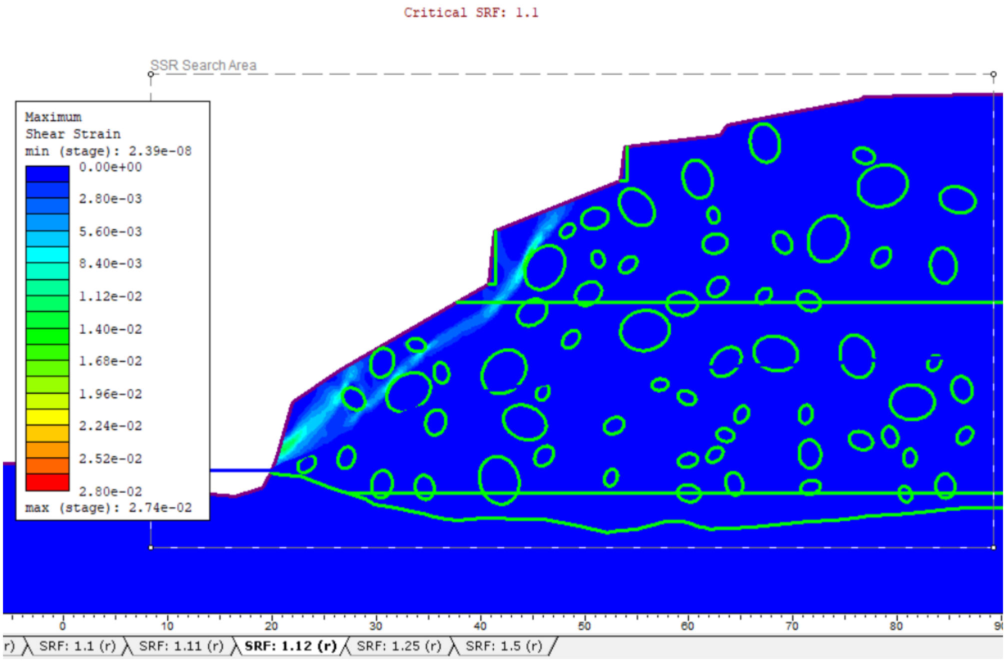


SRF= 1.25

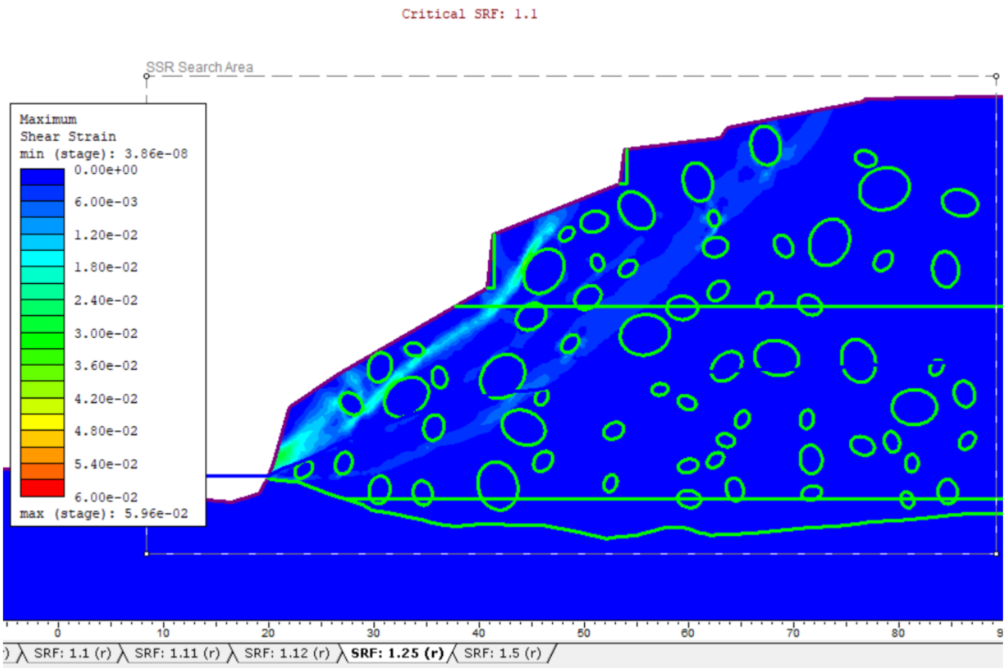

SRF= 1.50

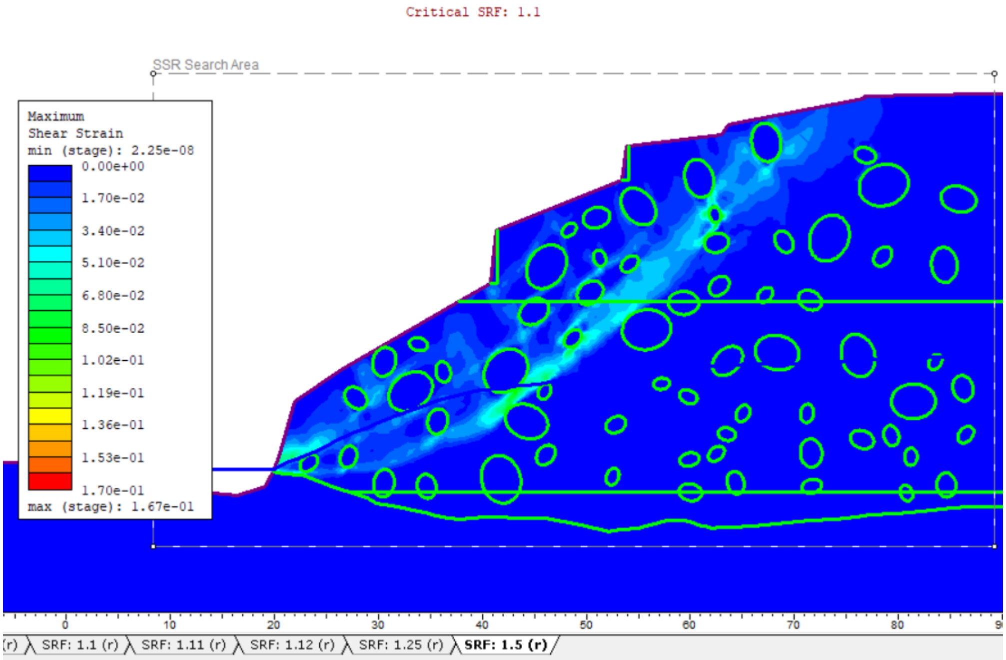

Critical SRF: 1.1
SSR Search Area
Maximum
Shear Strain
min (stage): 2.25e-08
0.00e+00
1.70e-02
3.40e-02
5.10e-02
6.80e-02
8.50e-02
1.02e-01
1.19e-01
1.36e-01
1.53e-01
1.70e-01
max (stage): 1.67e-01
0
10
20
30
40
50
60
70
80
SRF: 1.1 (r)
SRF: 1.11 (r)
SRF: 1.12 (r)
SRF: 1.25 (r)
SRF: 1.5 (r)

**15%_7_FEM**

Critical SRF= 1.14

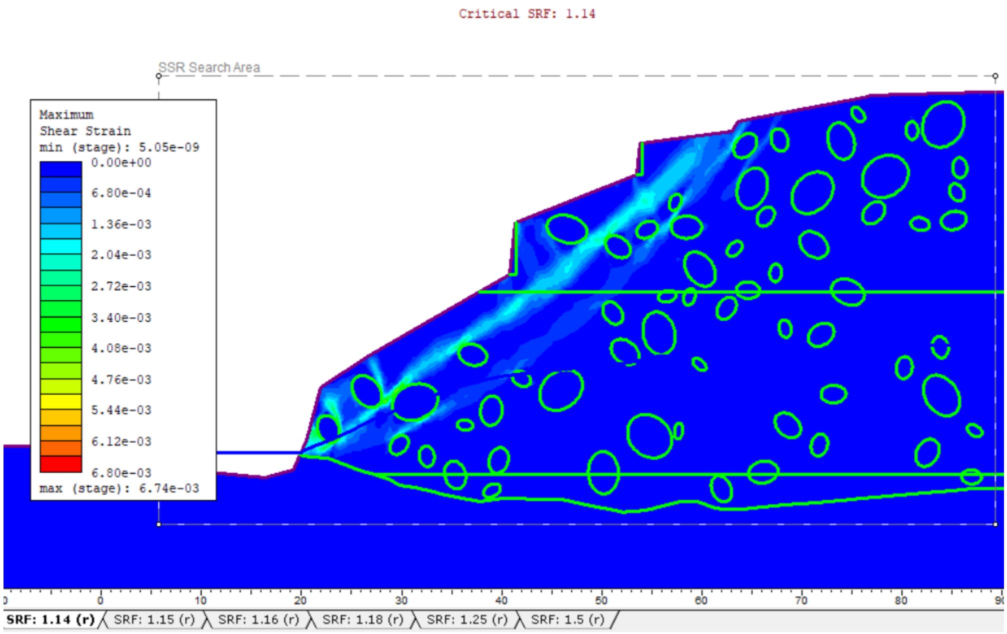


SRF= 1.15

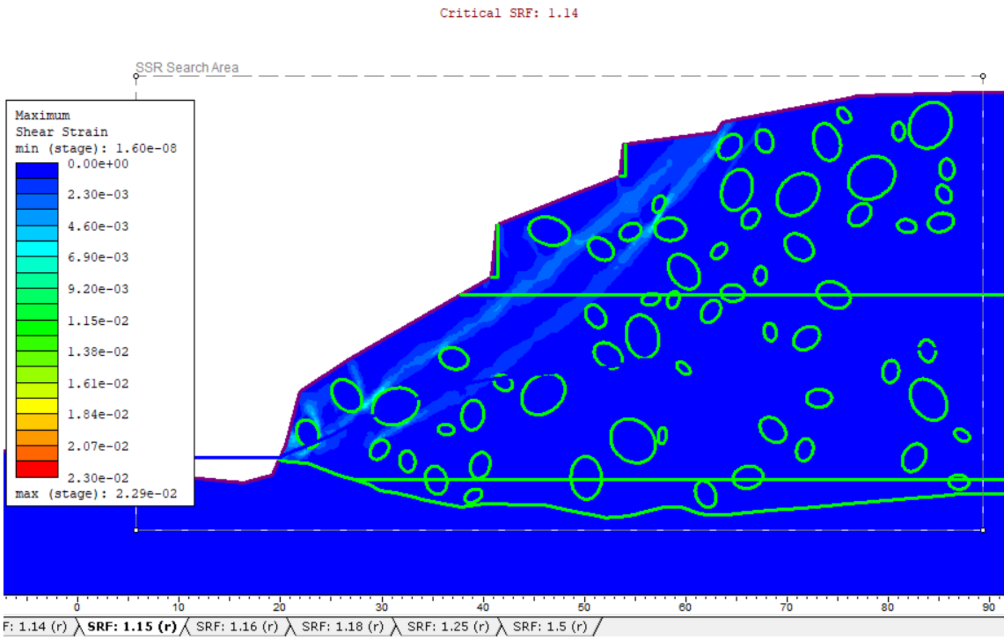

SRF= 1.16

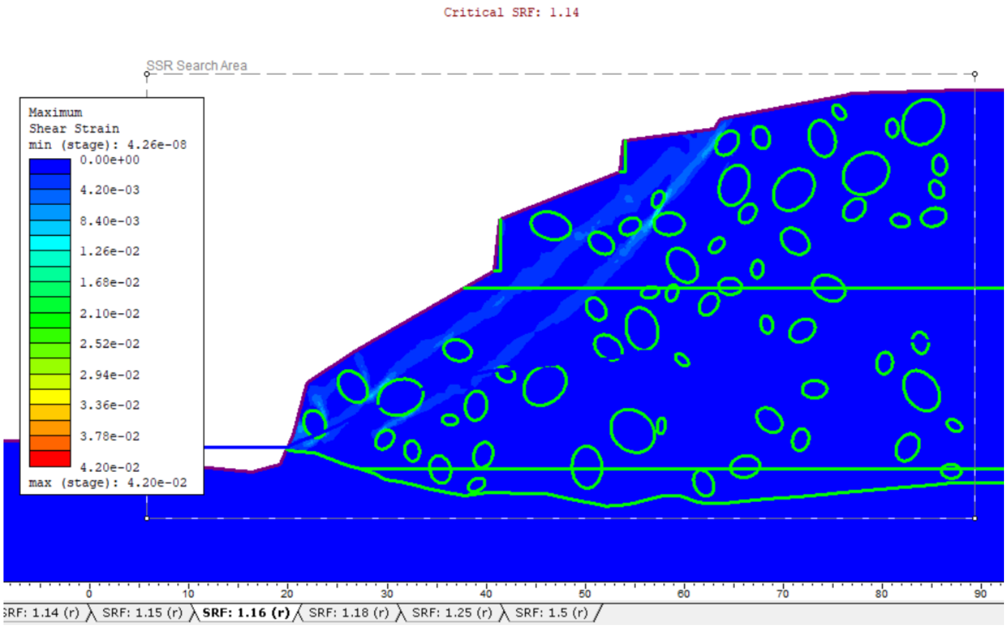


SRF= 1.18

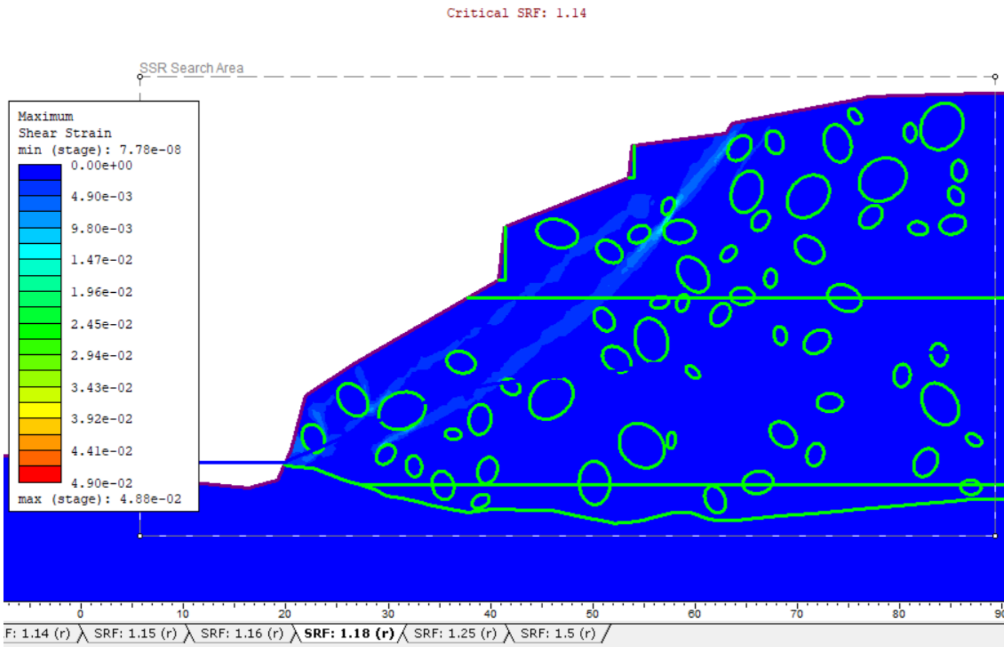

SRF= 1.25

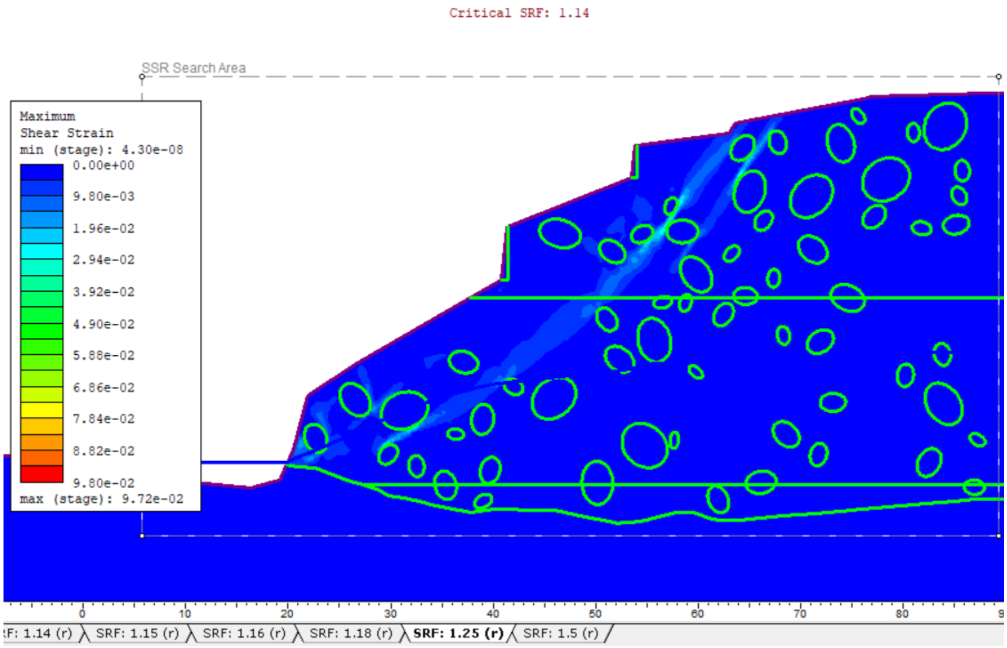


SRF= 1.50

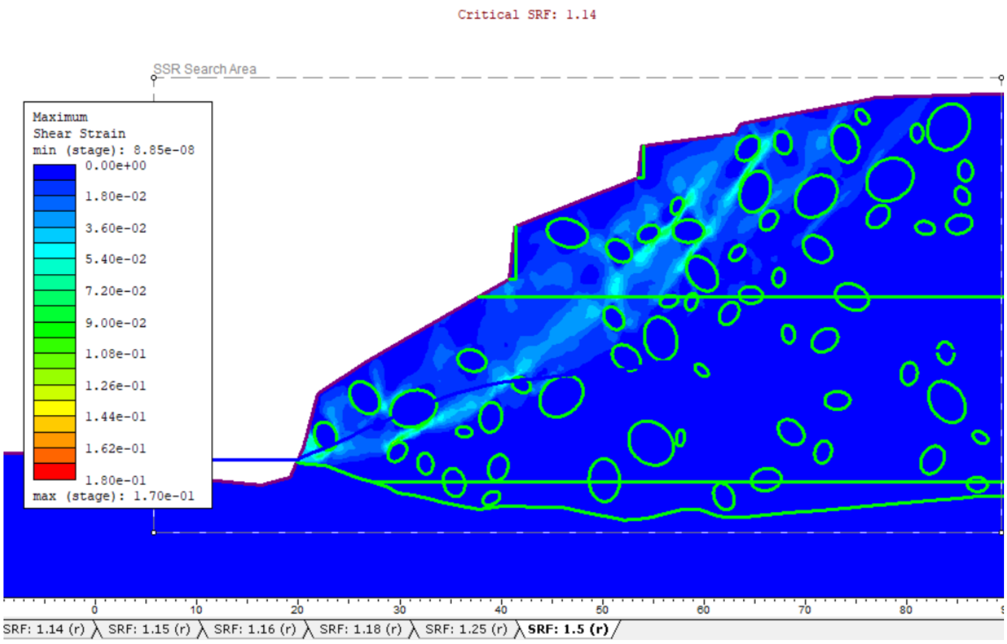

## 15%_8_FEM

Critical SRF=1.11

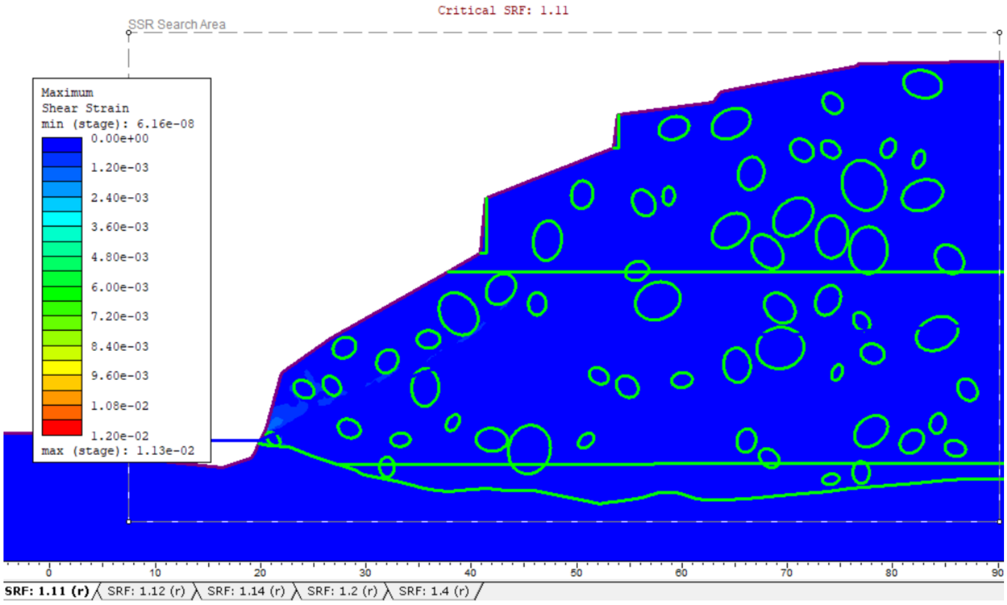


SRF=1.12

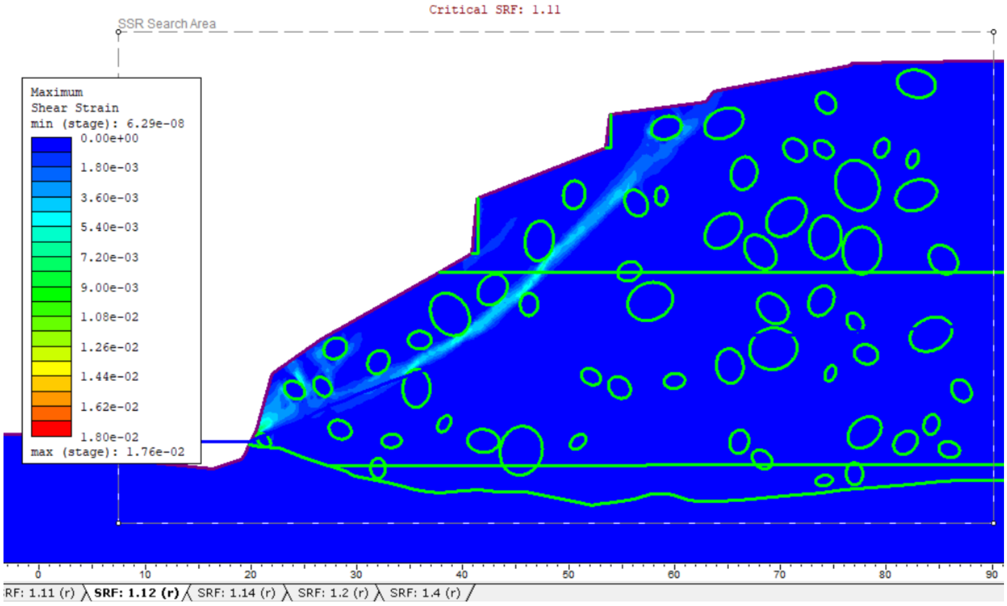

SRF=1.14

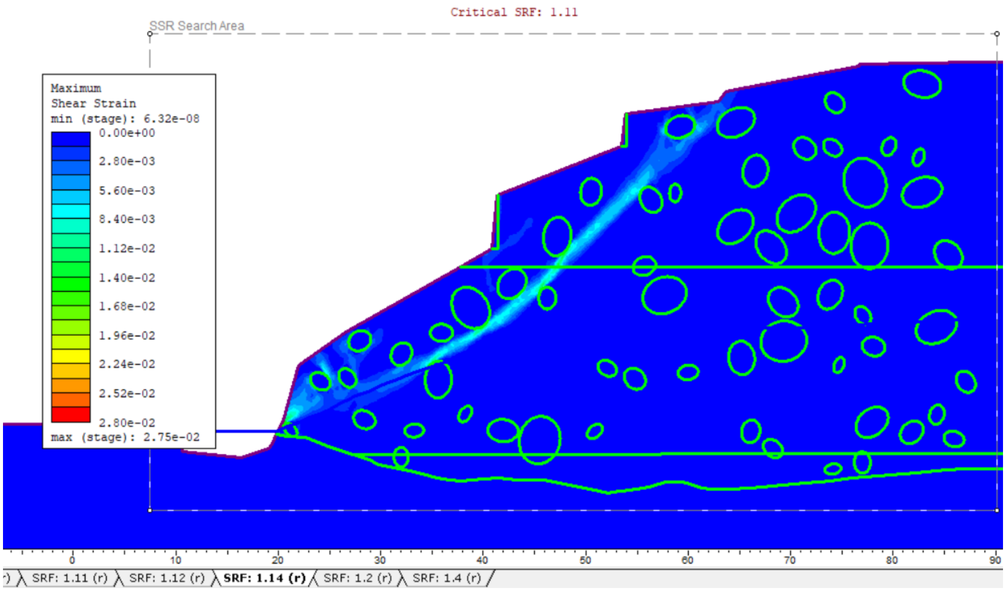


SRF=1.20

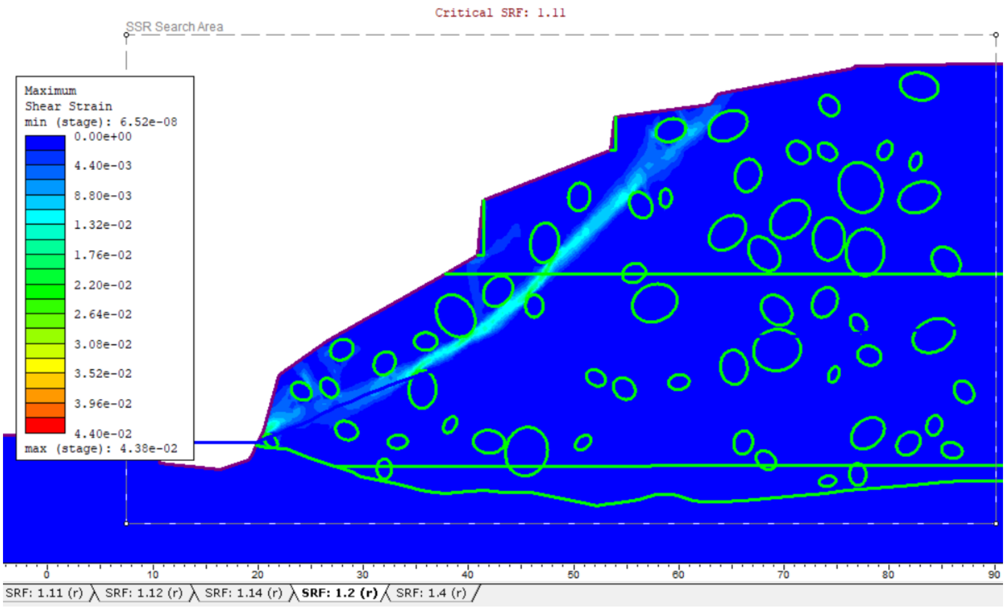

SRF=1.40

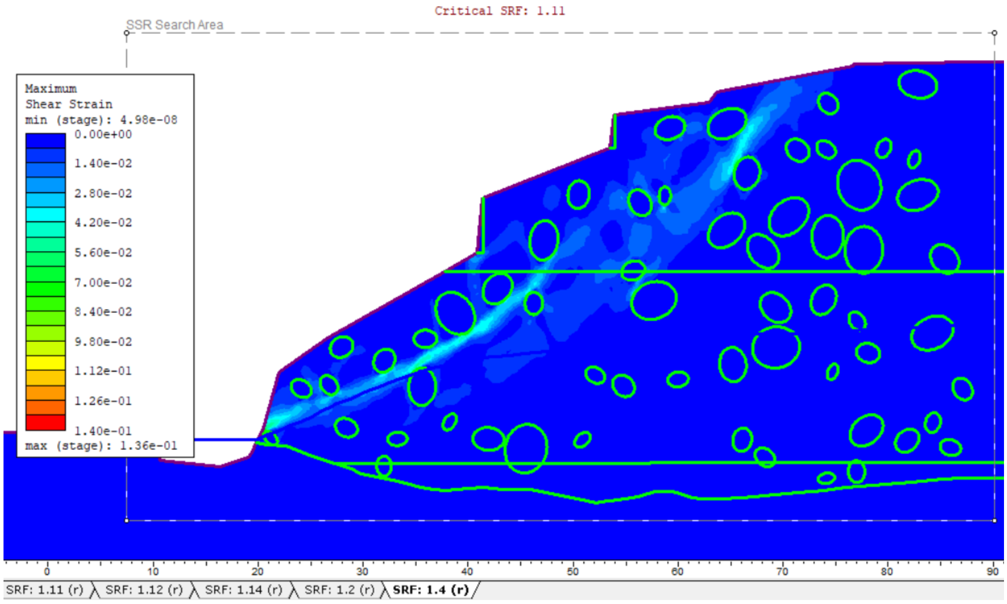

Critical SRF: 1.11
SSR Search Area
Maximum
Shear Strain
min (stage): 4.98e-08
0.00e+00
1.40e-02
2.80e-02
4.20e-02
5.60e-02
7.00e-02
8.40e-02
9.80e-02
1.12e-01
1.26e-01
1.40e-01
max (stage): 1.36e-01
0
10
20
30
40
50
60
70
80
90
SRF: 1.11 (r)
SRF: 1.12 (r)
SRF: 1.14 (r)
SRF: 1.2 (r)
SRF: 1.4 (r)

## 15%_9_FEM

Critical SRF= 1.03

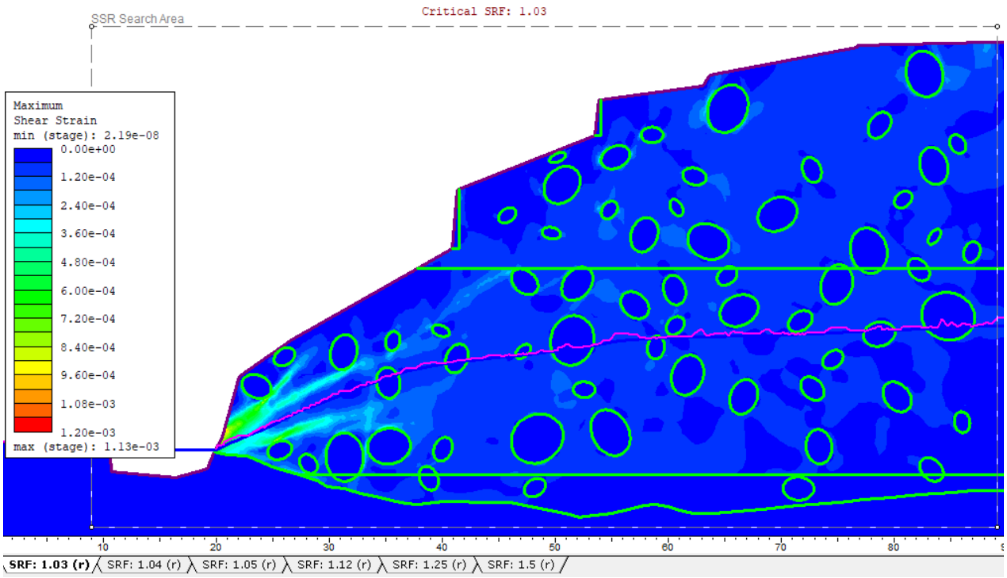


SRF= 1.04

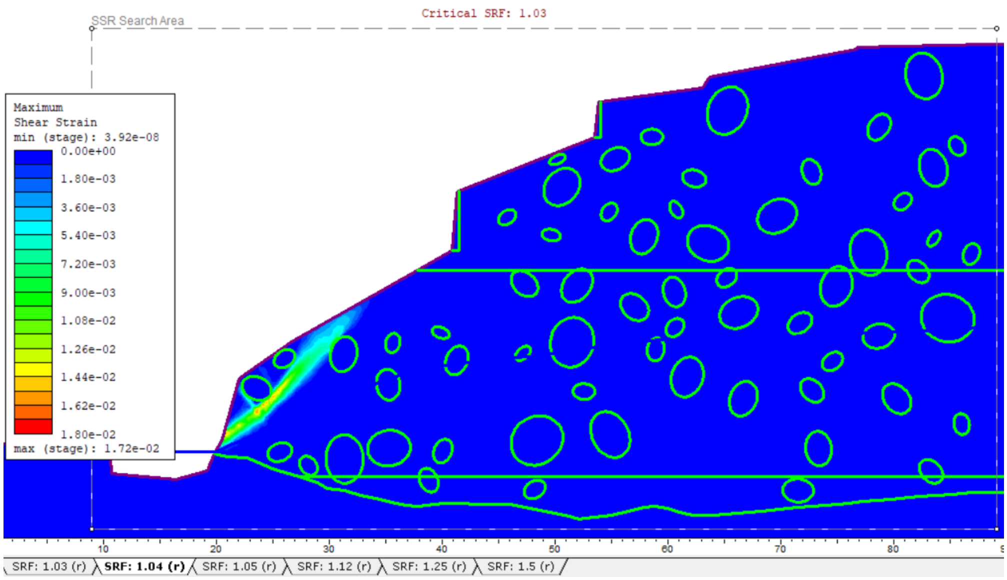

SRF= 1.05

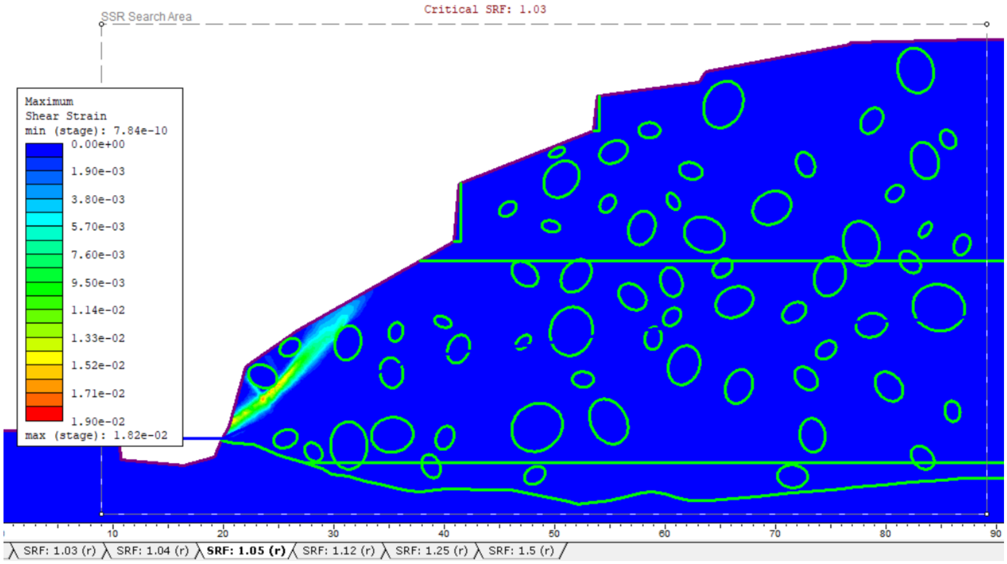


SRF= 1.12

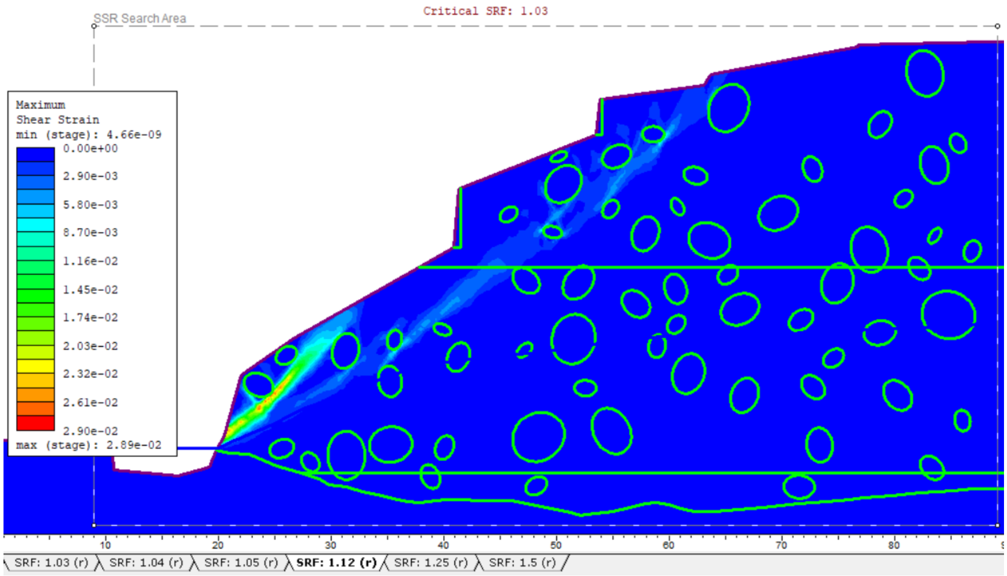

SRF= 1.25

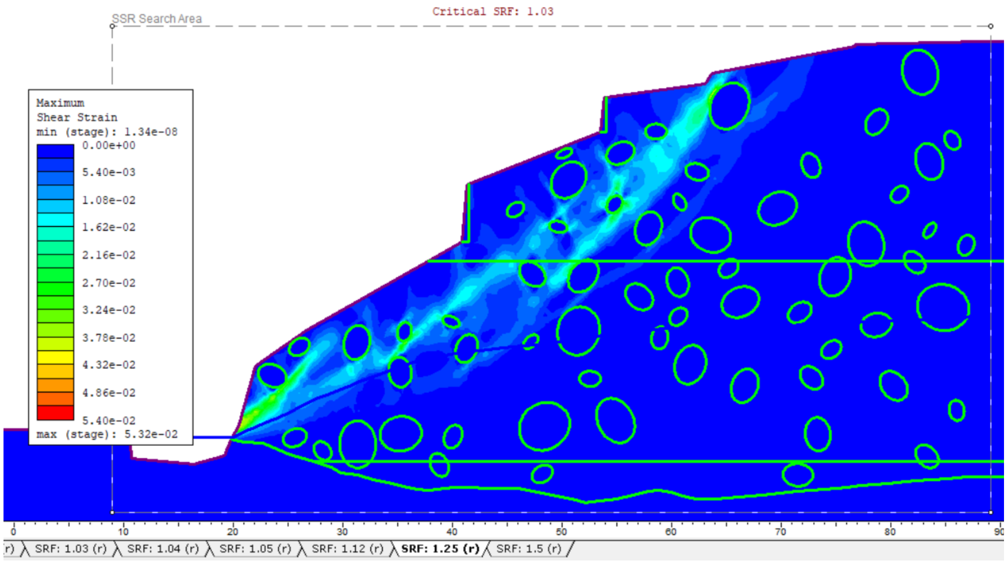


SRF= 1.50

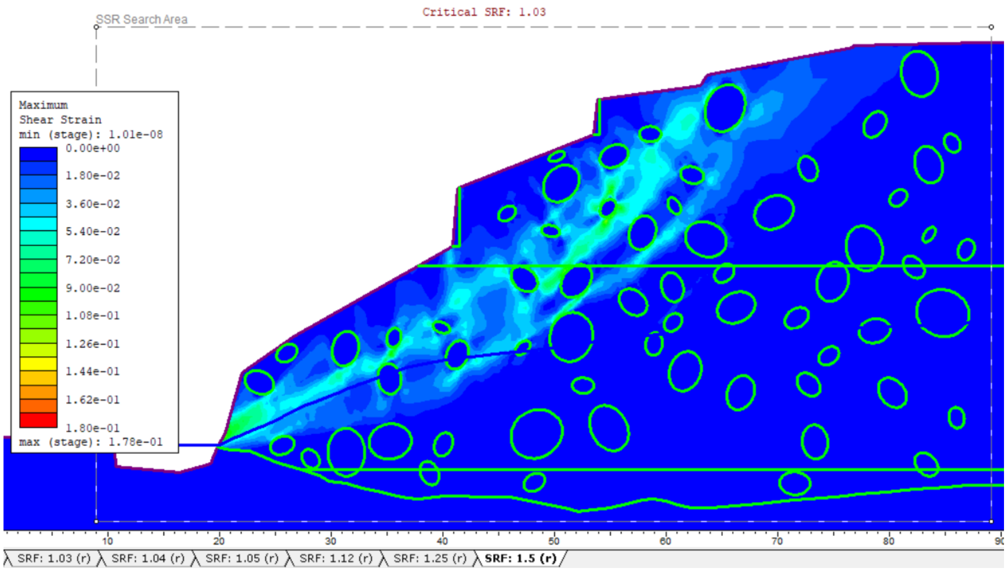

**15%_10_FEM**

Critical SRF= 1.10

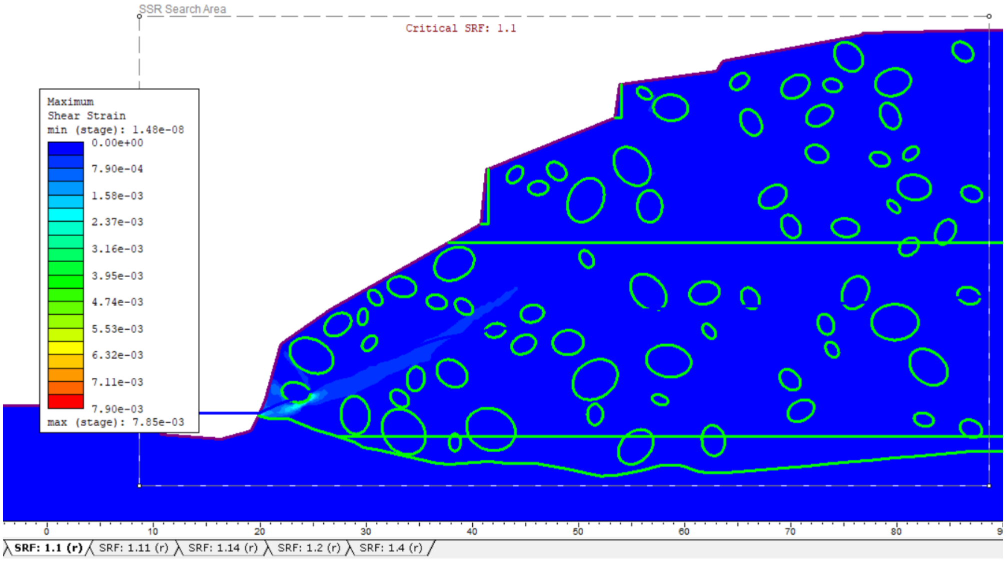


SRF= 1.11

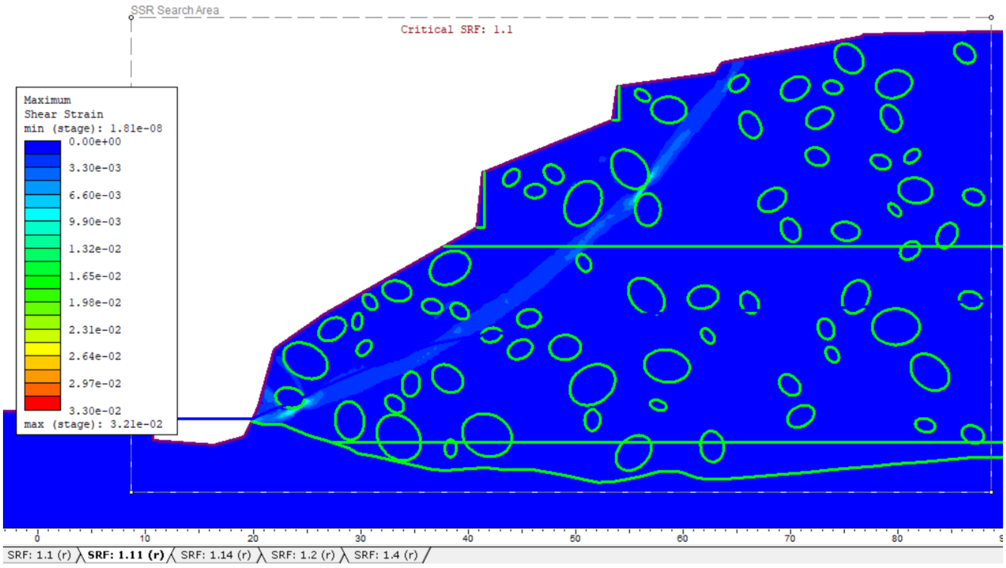

SRF= 1.14

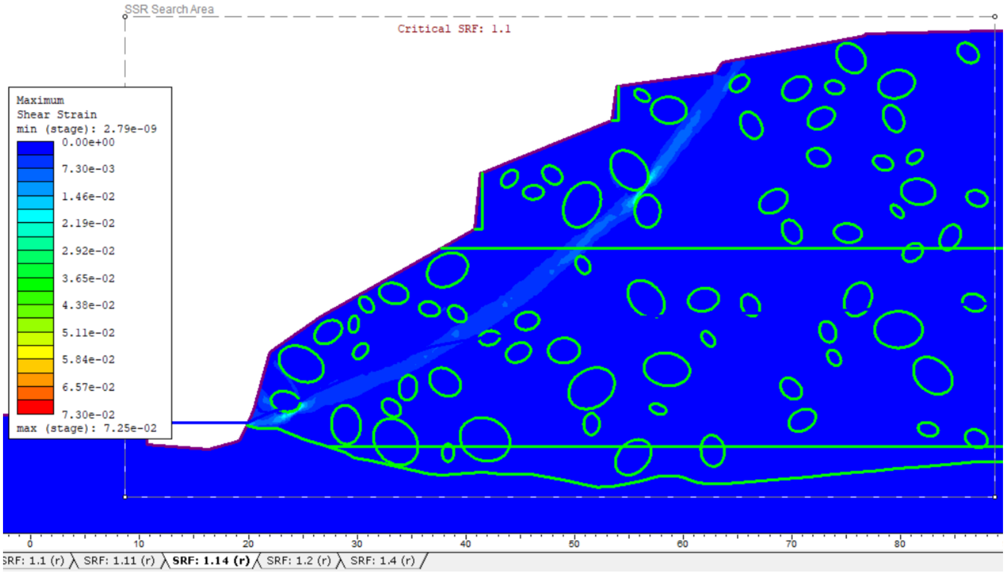


SRF= 1.20

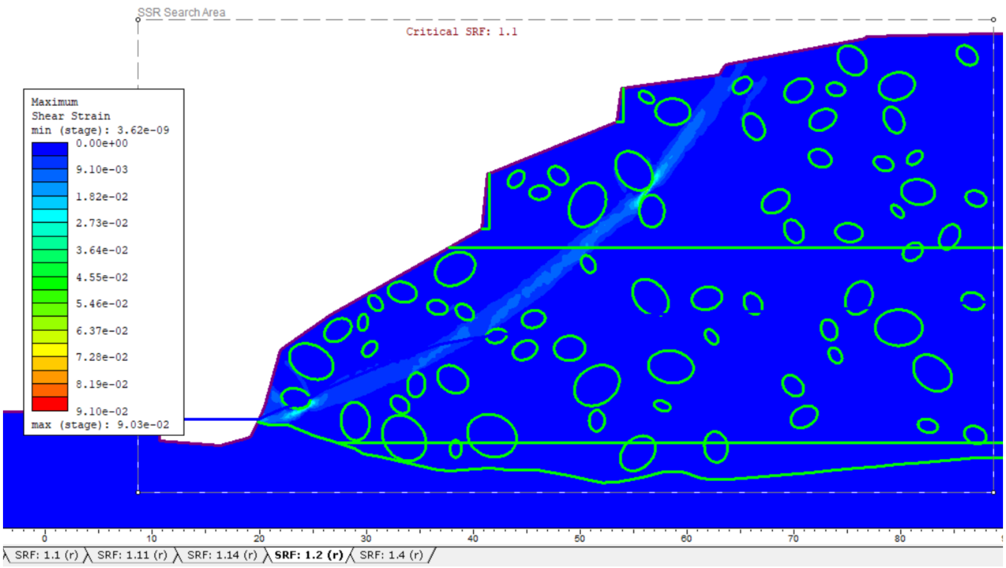

SRF= 1.40

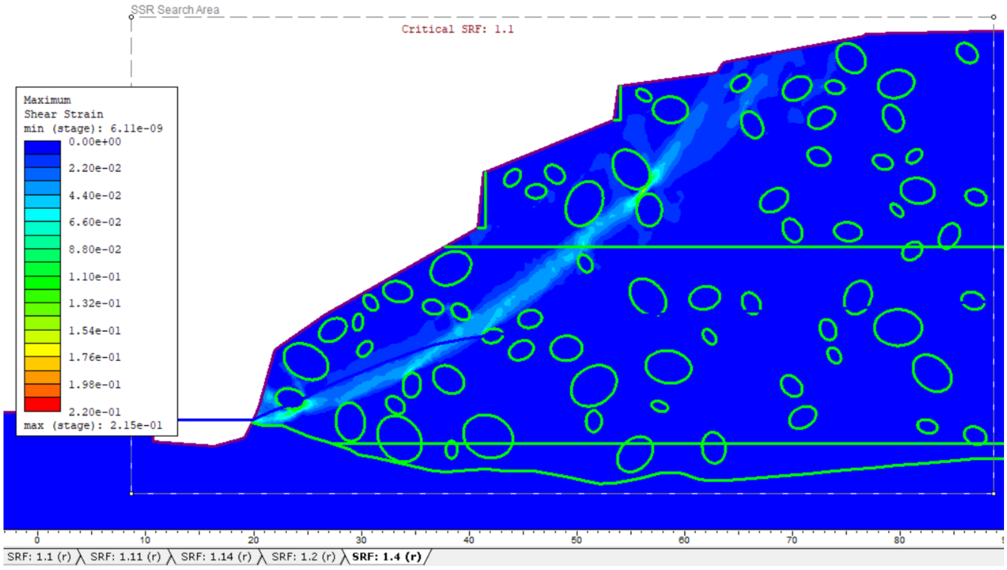
SSR Search Area
Critical SRF: 1.1
Maximum
Shear Strain
min (stage): 6.11e-09
0.00e+00
2.20e-02
4.40e-02
6.60e-02
8.80e-02
1.10e-01
1.32e-01
1.54e-01
1.76e-01
1.98e-01
2.20e-01
max (stage): 2.15e-01
0
10
20
30
40
50
60
70
80
SRF: 1.1 (r)
SRF: 1.11 (r)
SRF: 1.14 (r)
SRF: 1.2 (r)
SRF: 1.4 (r)

# Appendix B

## Maximum shear strains and progressive failure for 30% VBP with c=5 kPa & $\phi = 37°$

### 30%_1_FEM

Critical SRF=1.04

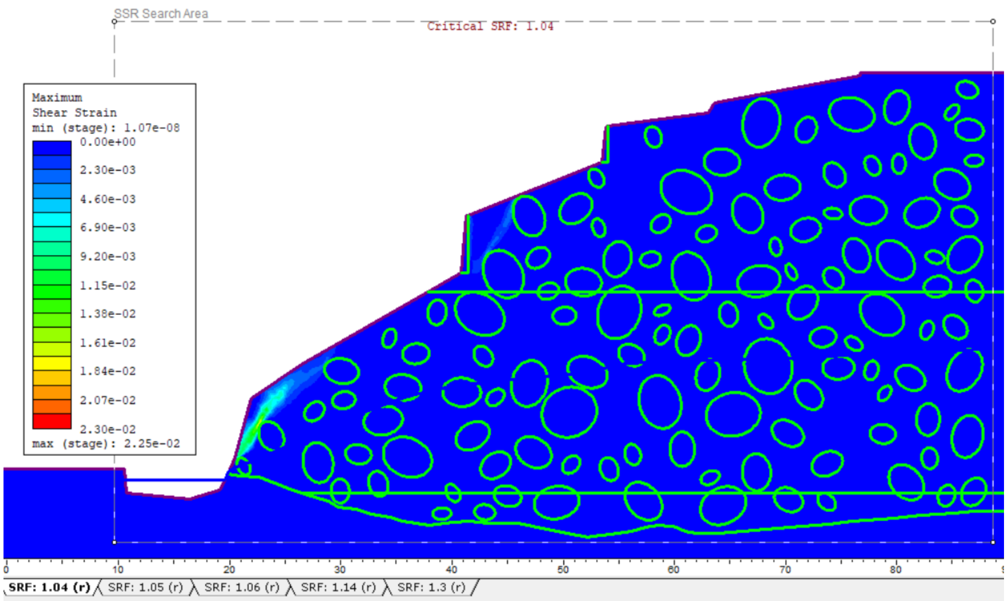

SRF=1.05

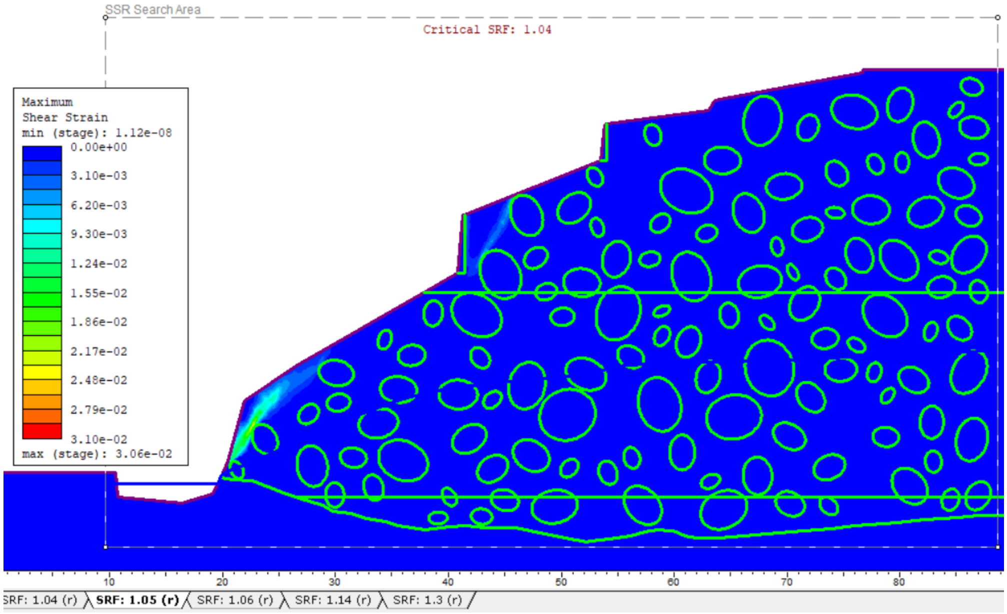


SRF=1.06

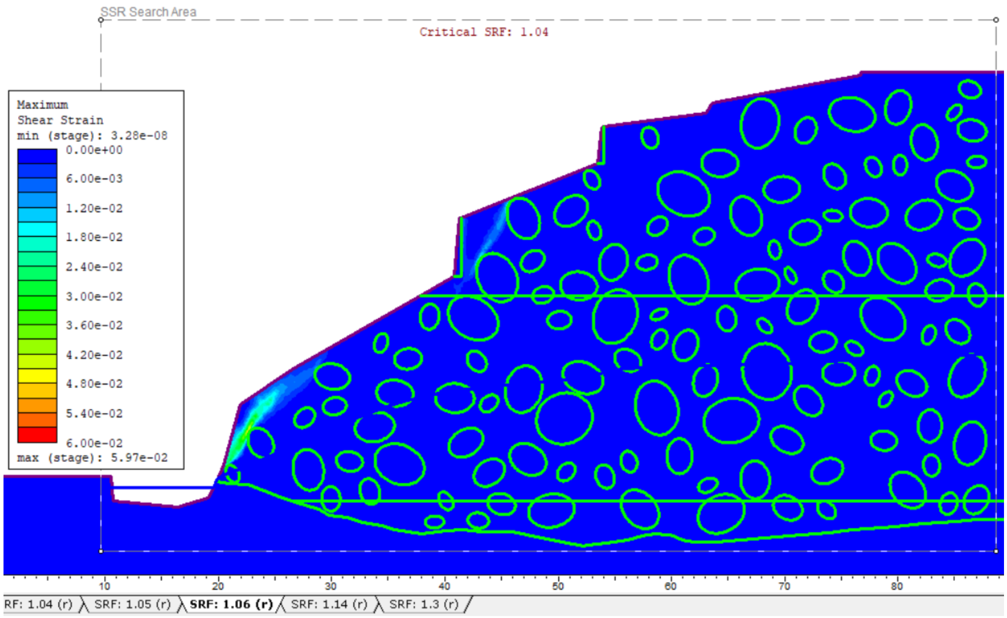

SRF=1.14

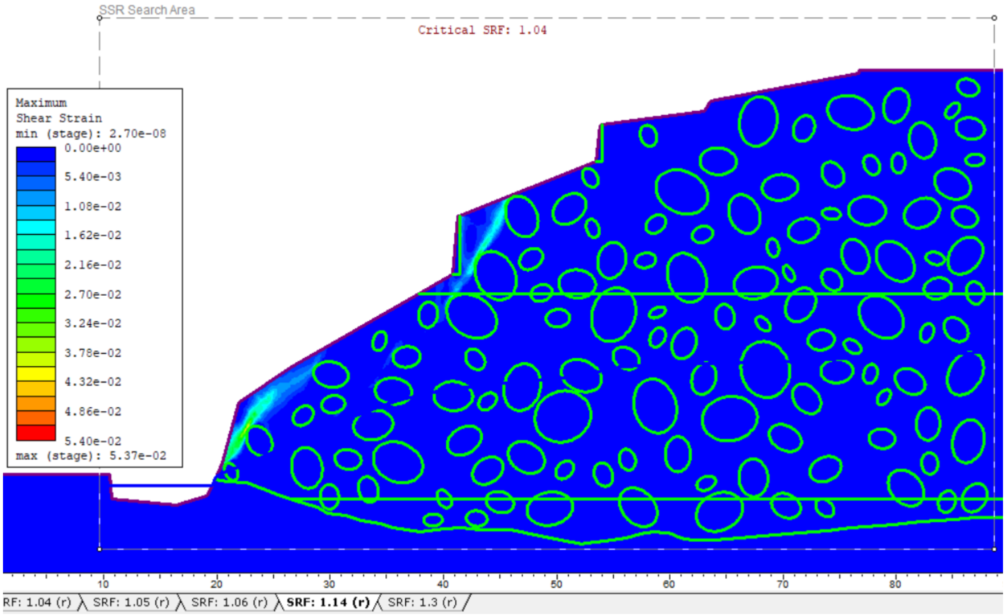


SRF=1.30

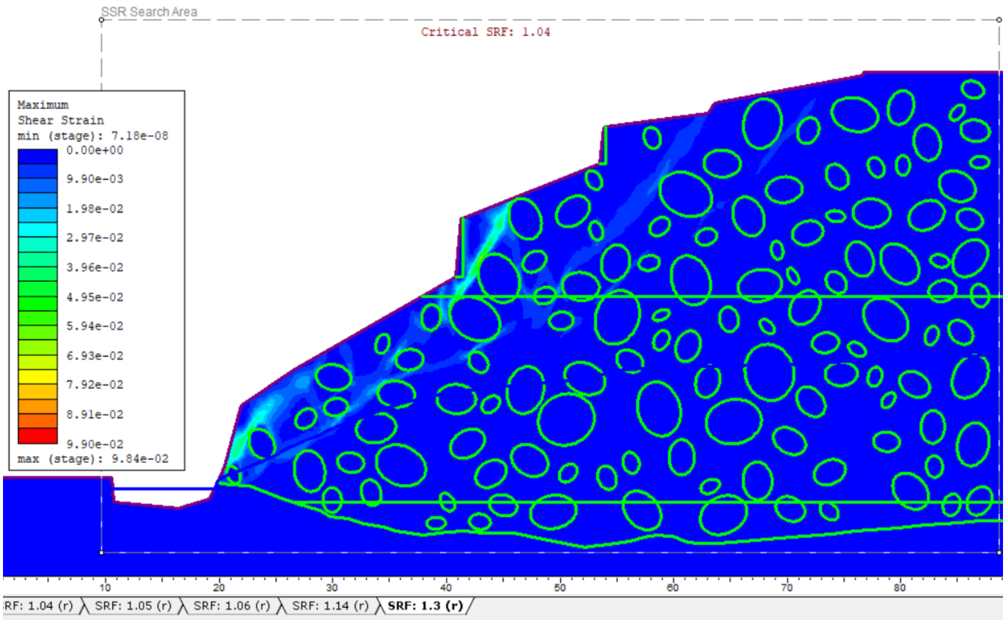

**30%__2__FEM**

Critical SRF=0.95

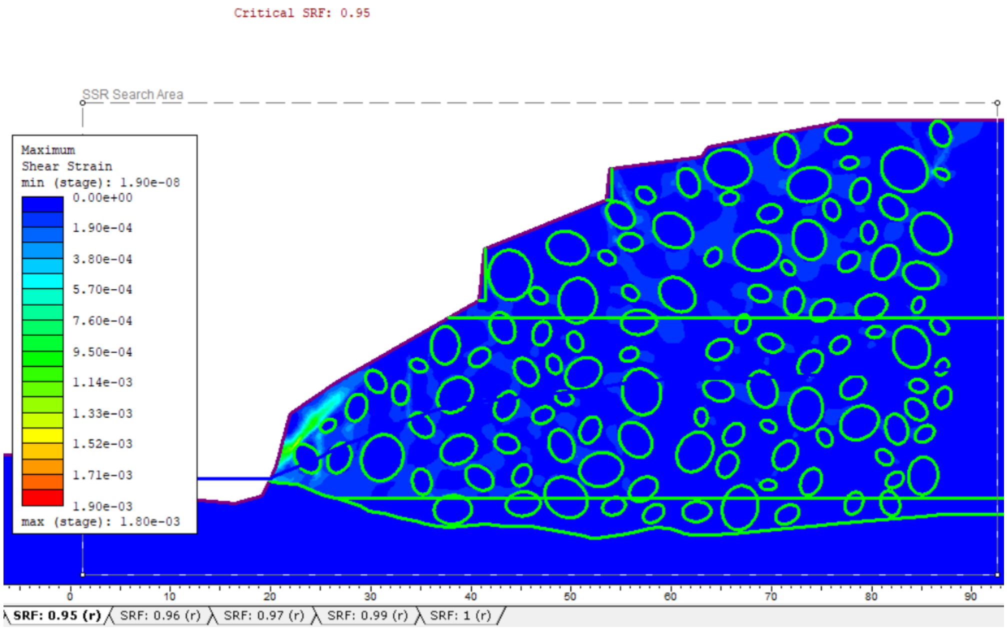


SRF=0.96

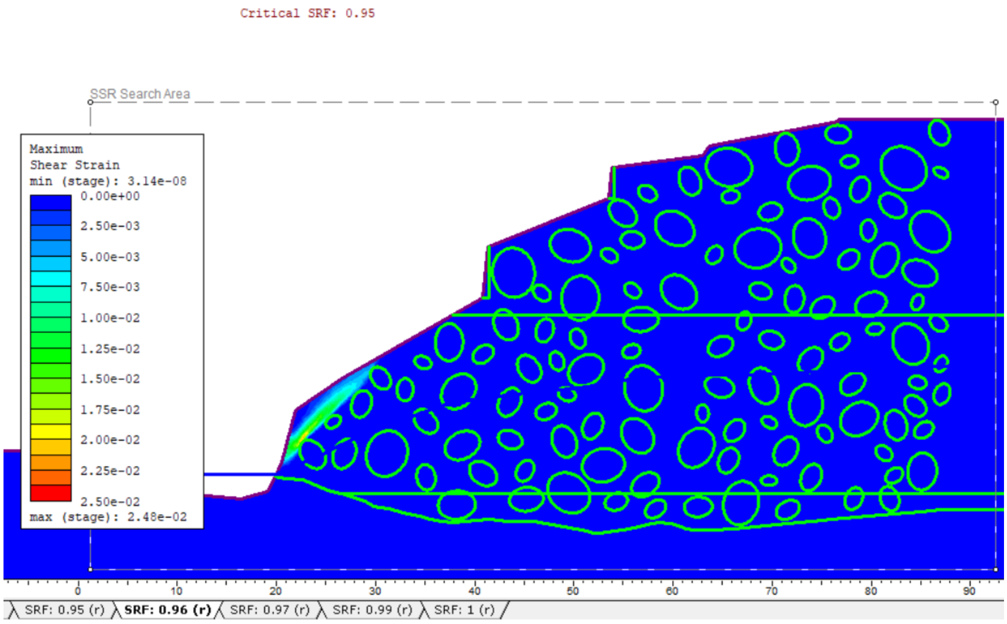

SRF=0.97

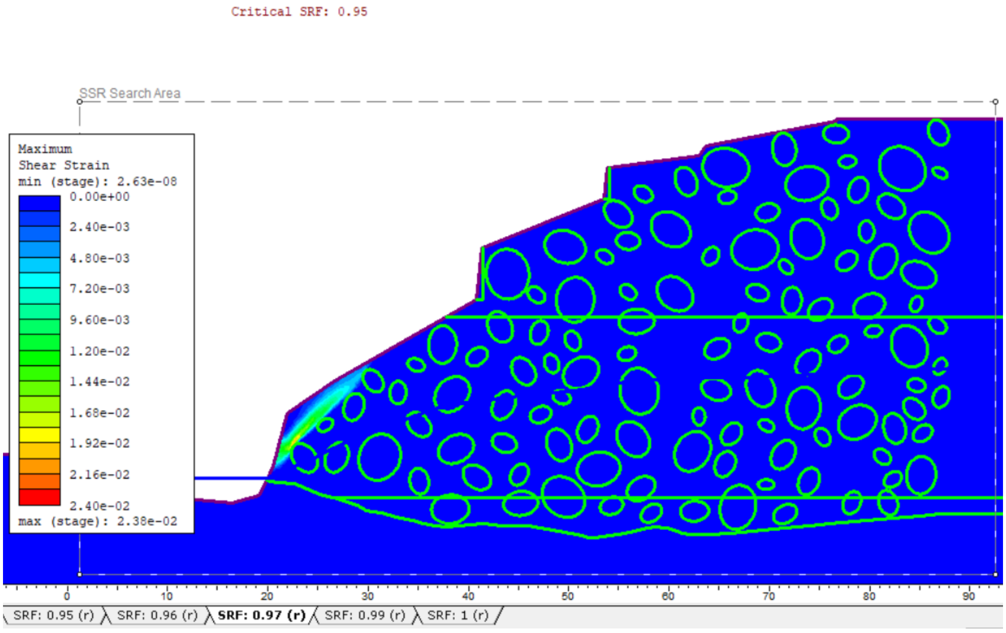


SRF=0.99

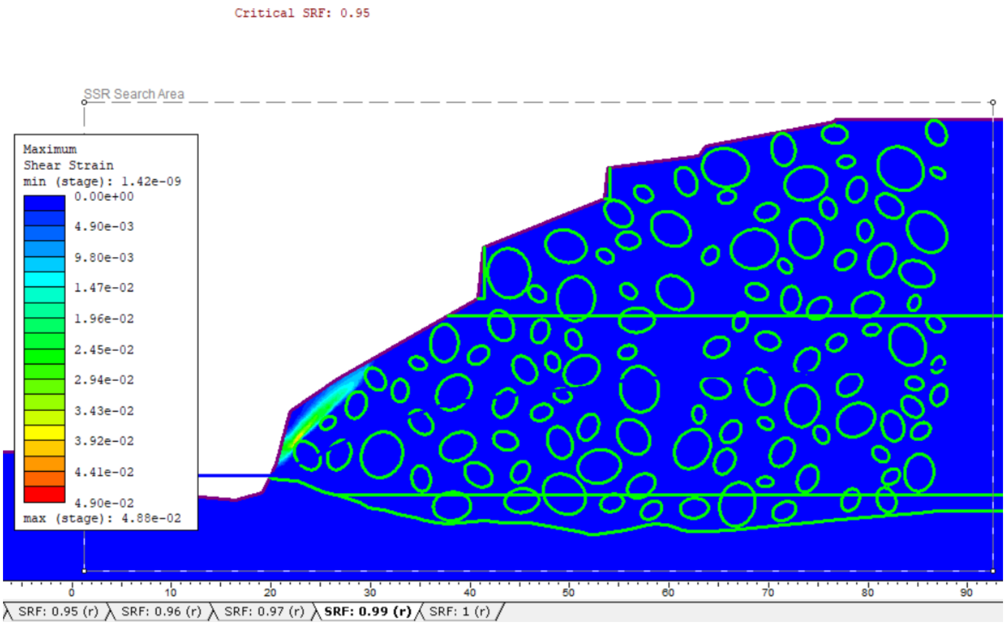

SRF=1.00

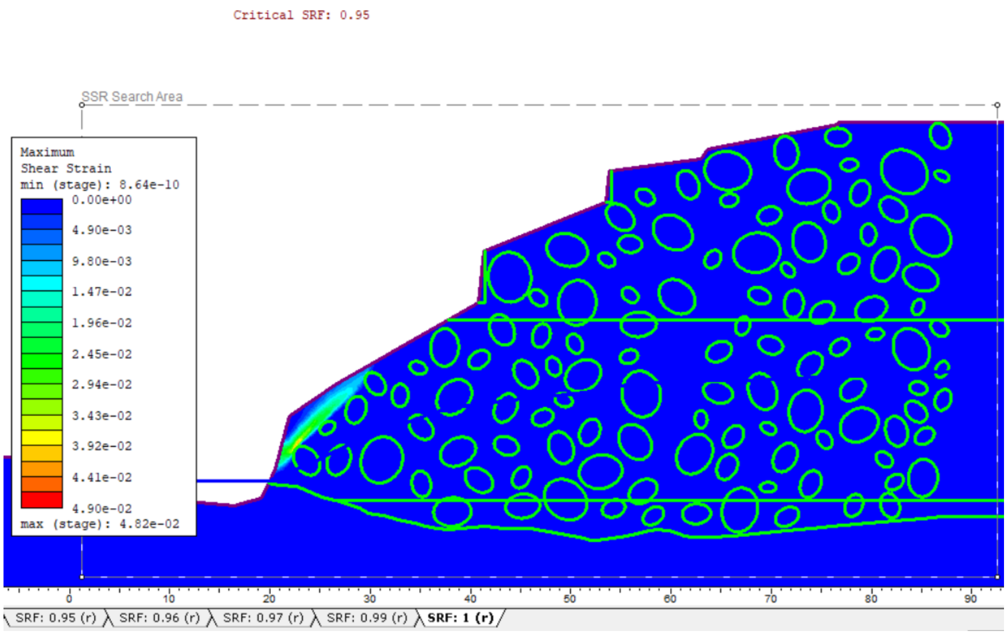

Critical SRF: 0.95
SSR Search Area
Maximum
Shear Strain
min (stage): 8.64e-10
0.00e+00
4.90e-03
9.80e-03
1.47e-02
1.96e-02
2.45e-02
2.94e-02
3.43e-02
3.92e-02
4.41e-02
4.90e-02
max (stage): 4.82e-02
0
10
20
30
40
50
60
70
80
90
SRF: 0.95 (r)
SRF: 0.96 (r)
SRF: 0.97 (r)
SRF: 0.99 (r)
SRF: 1 (r)

**30%_3_FEM**

Critical SRF=1.03

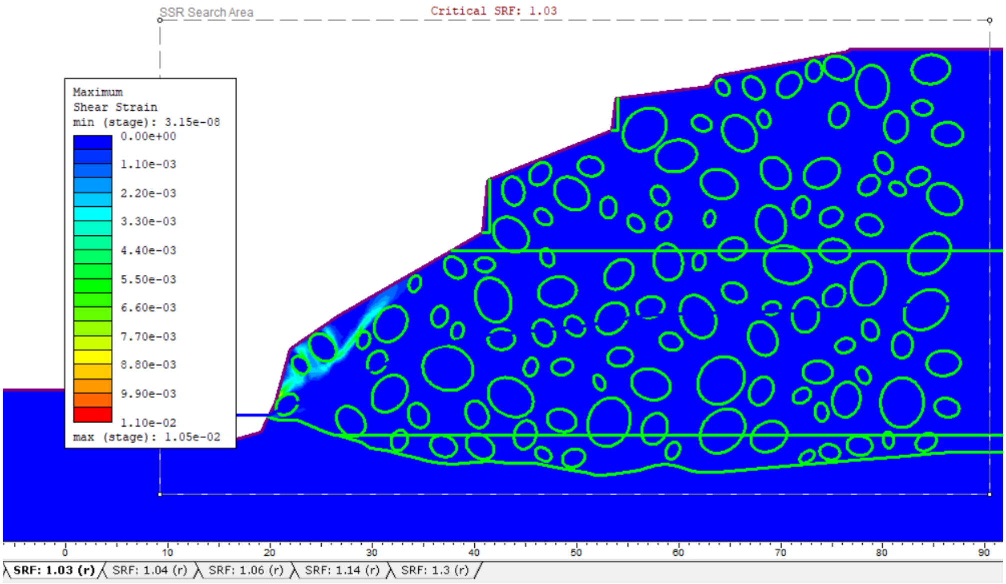


SRF=1.04

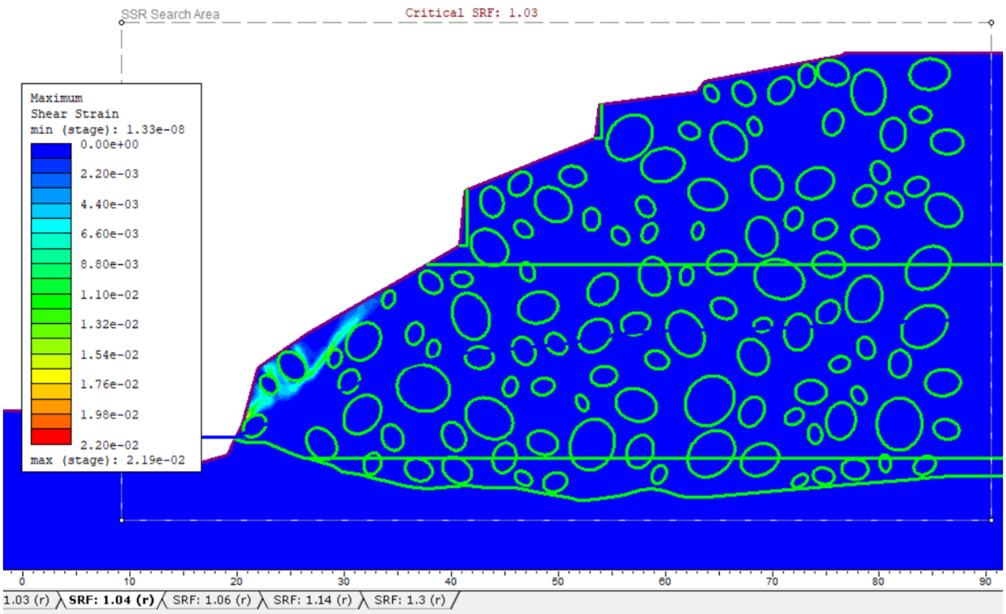

SRF=1.06

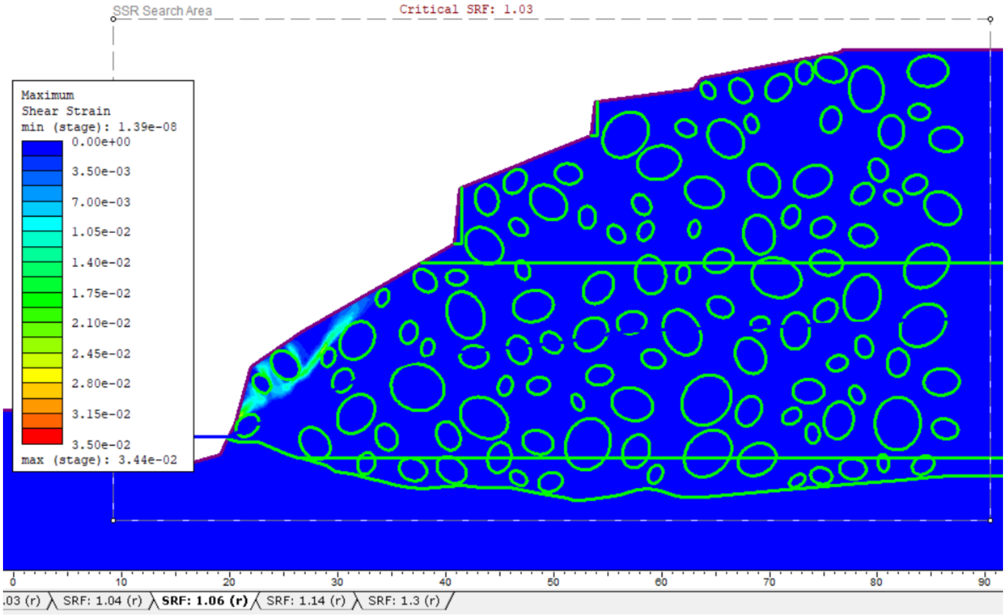


SRF=1.14

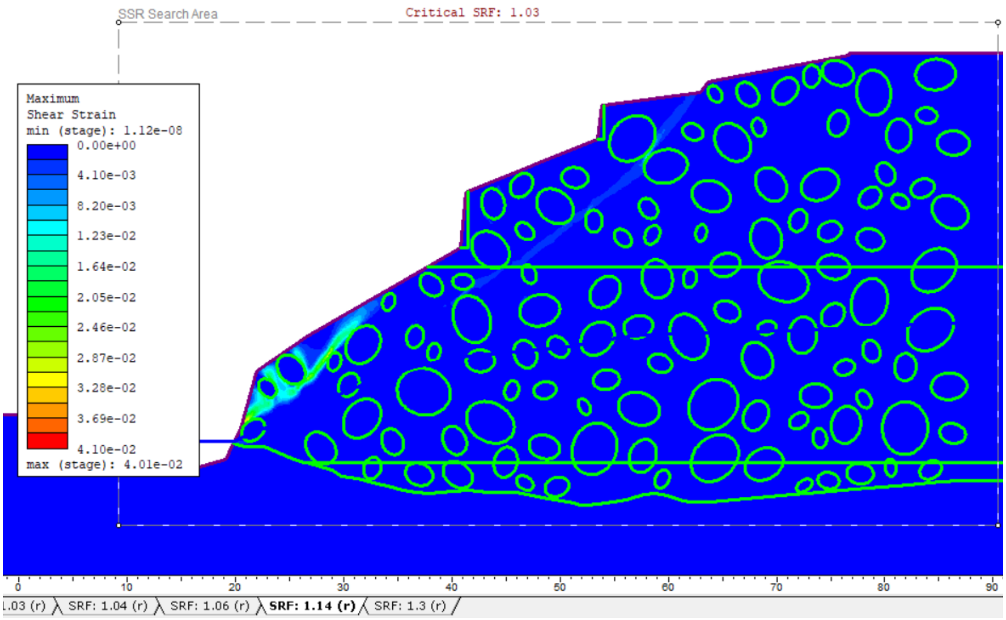

SRF=1.30

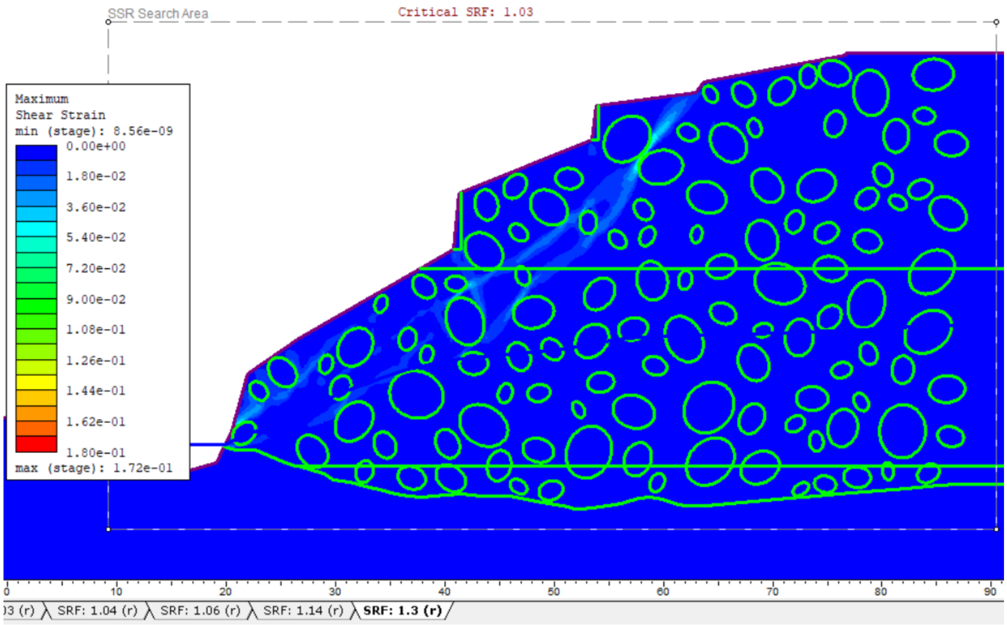
SSR Search Area
Critical SRF: 1.03
Maximum
Shear Strain
min (stage): 8.56e-09
0.00e+00
1.80e-02
3.60e-02
5.40e-02
7.20e-02
9.00e-02
1.08e-01
1.26e-01
1.44e-01
1.62e-01
1.80e-01
max (stage): 1.72e-01
0
10
20
30
40
50
60
70
80
90
SRF: 1.04 (r)
SRF: 1.06 (r)
SRF: 1.14 (r)
SRF: 1.3 (r)

**30%_4_FEM**

Critical SRF=1.06

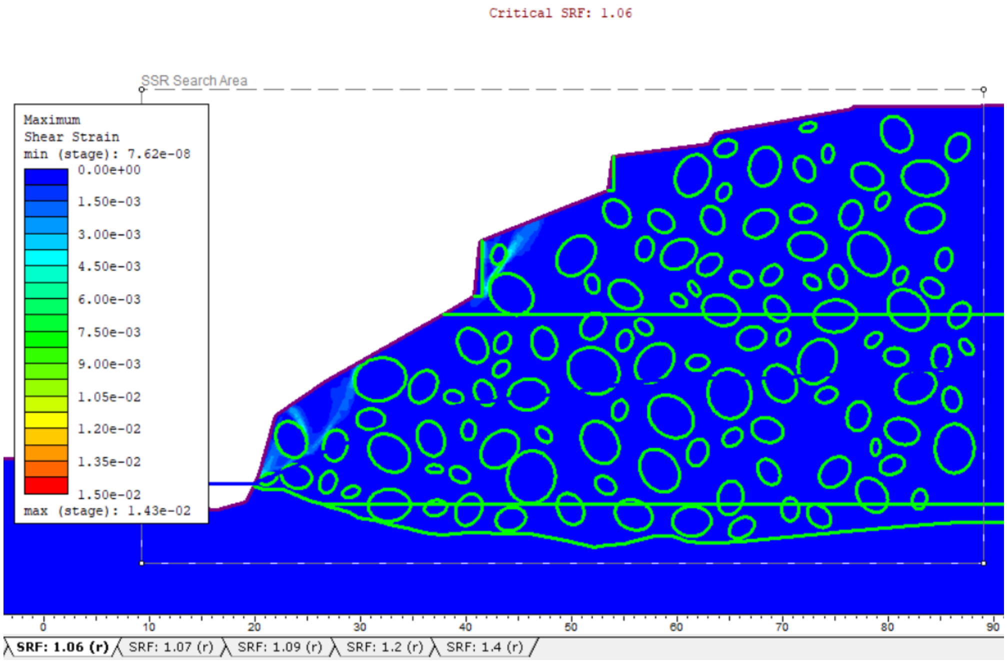


SRF=1.07

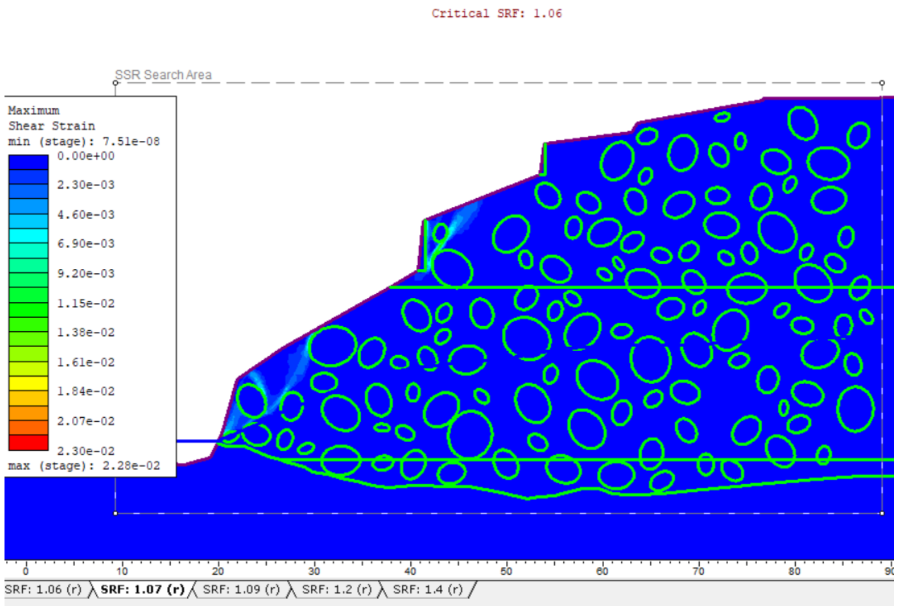

SRF=1.09

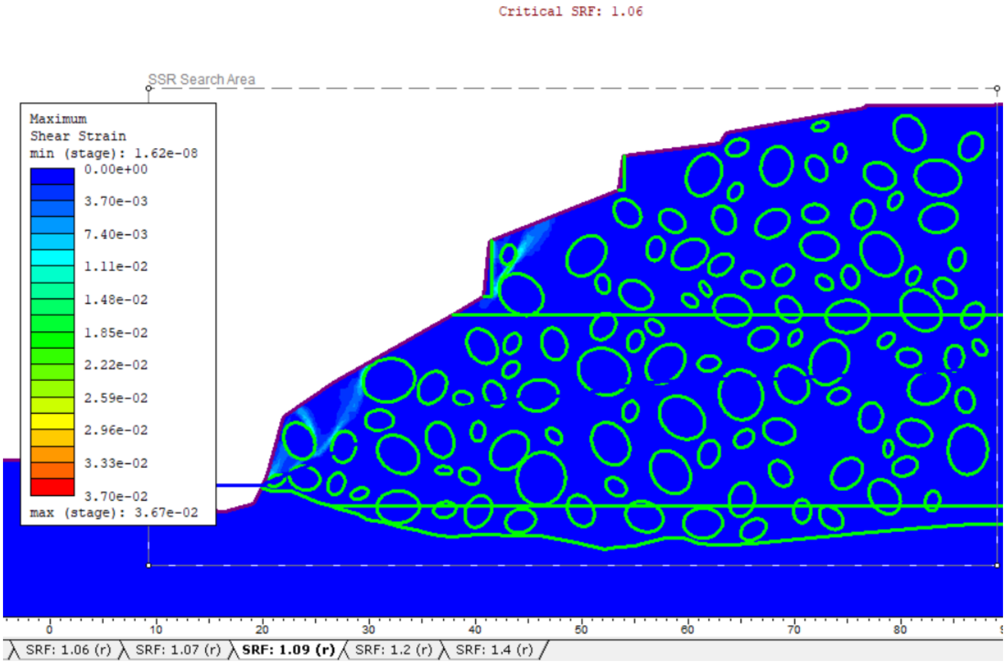


SRF=1.20

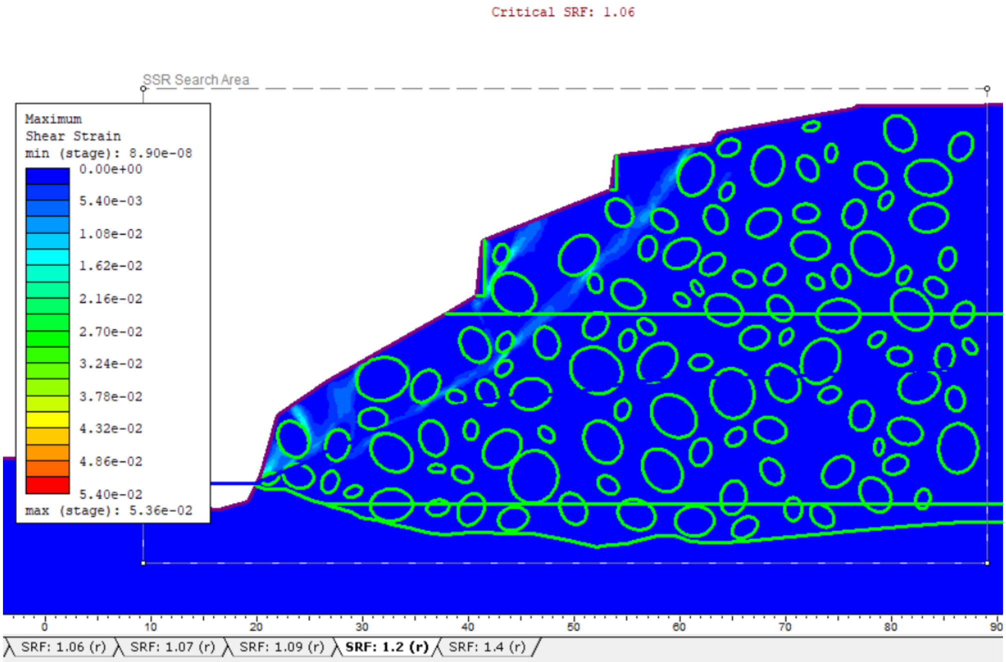

SRF=1.40

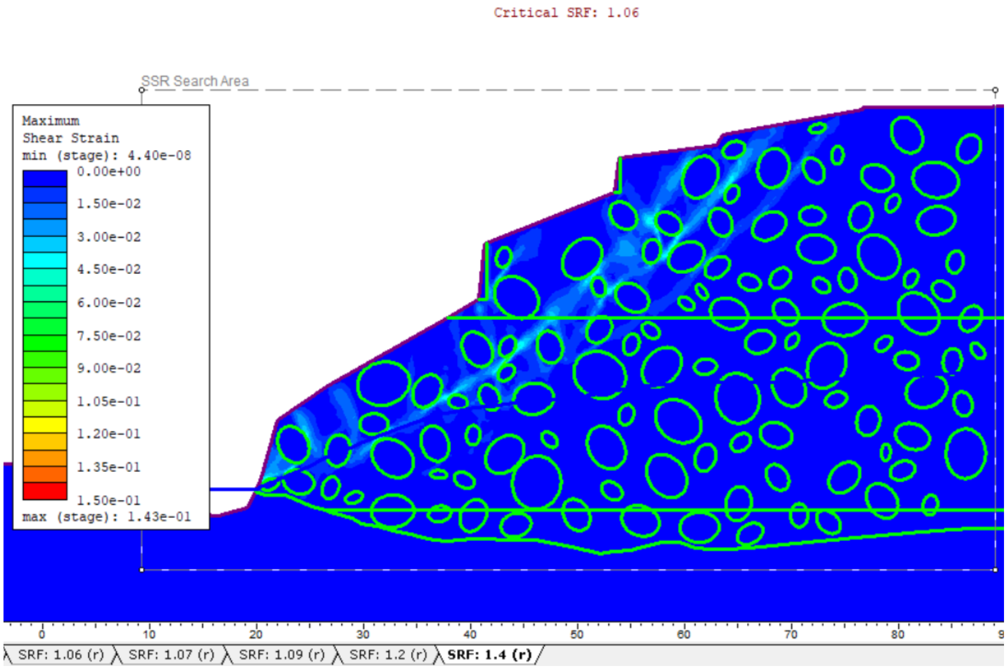

Critical SRF: 1.06
SSR Search Area
Maximum
Shear Strain
min (stage): 4.40e-08
0.00e+00
1.50e-02
3.00e-02
4.50e-02
6.00e-02
7.50e-02
9.00e-02
1.05e-01
1.20e-01
1.35e-01
1.50e-01
max (stage): 1.43e-01
0
10
20
30
40
50
60
70
80
SRF: 1.06 (r)
SRF: 1.07 (r)
SRF: 1.09 (r)
SRF: 1.2 (r)
SRF: 1.4 (r)

**30%_5_FEM**

Critical SRF=0.95

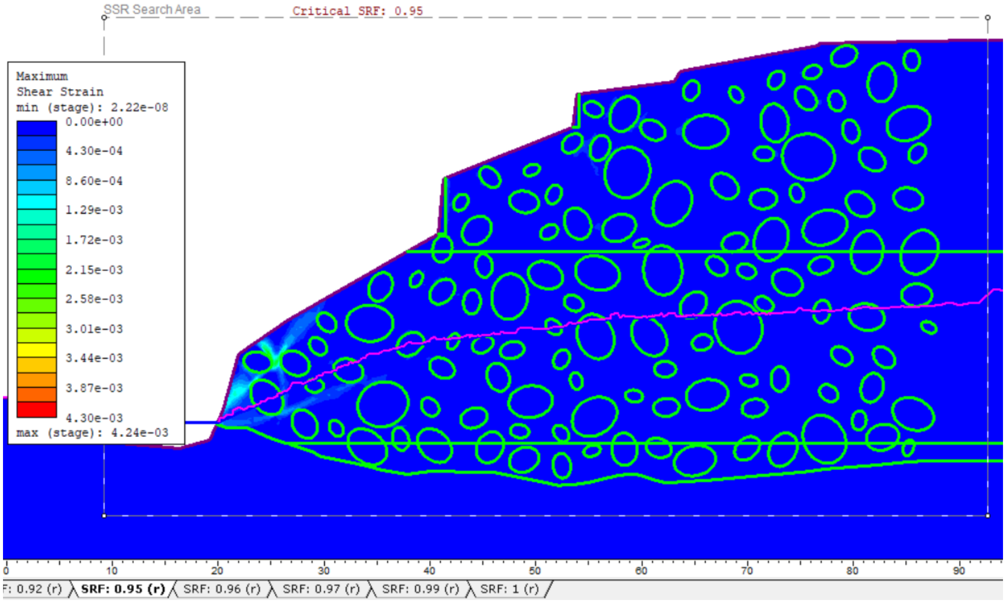


SRF=0.96

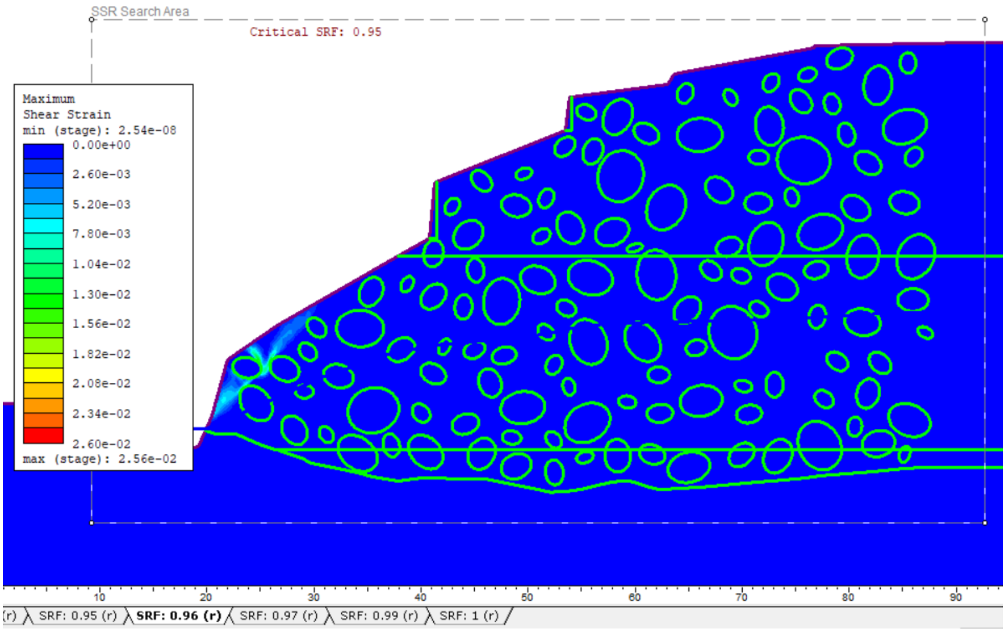

SRF=0.97

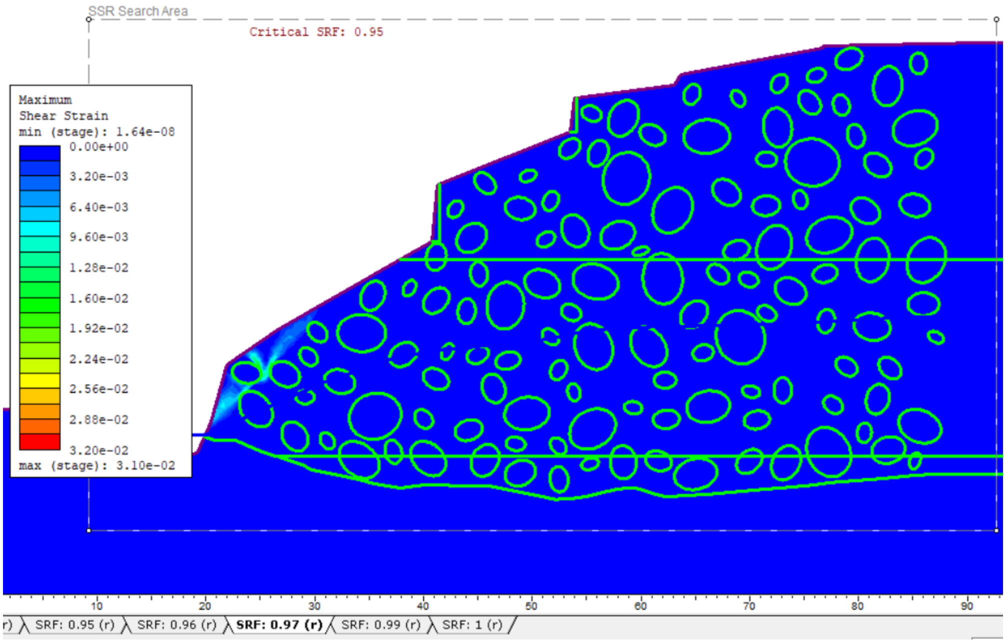


SRF=0.99

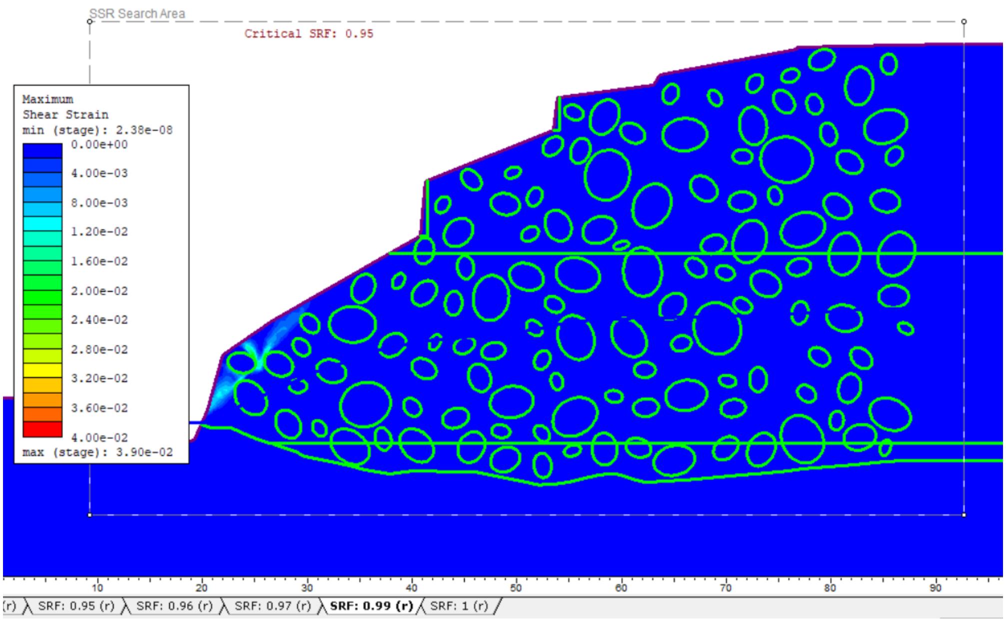

SRF=1.00

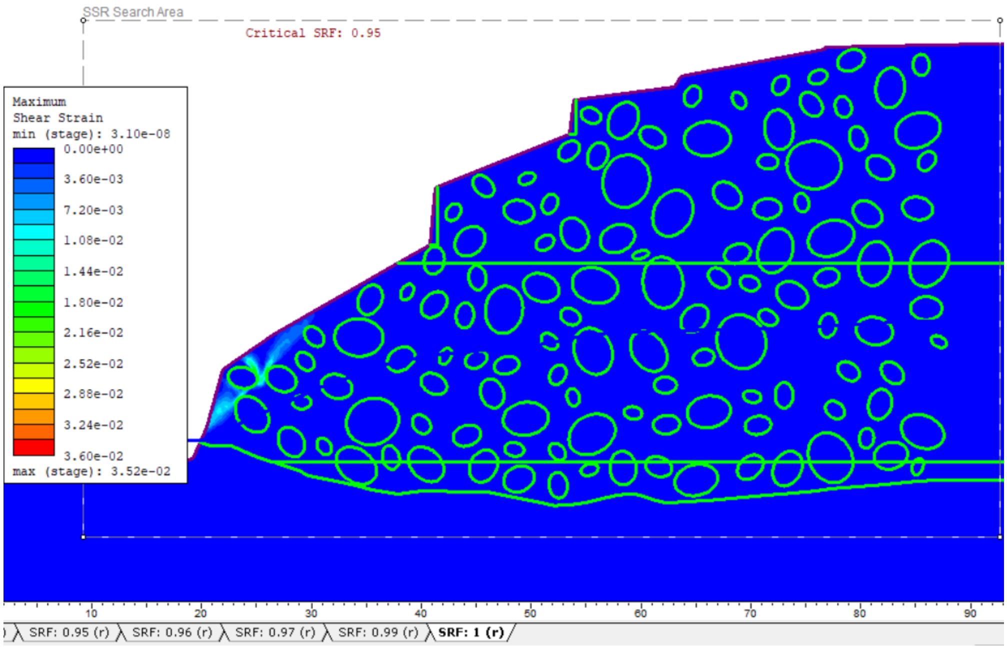

SSR Search Area
Critical SRF: 0.95
Maximum
Shear Strain
min (stage): 3.10e-08
0.00e+00
3.60e-03
7.20e-03
1.08e-02
1.44e-02
1.80e-02
2.16e-02
2.52e-02
2.88e-02
3.24e-02
3.60e-02
max (stage): 3.52e-02
10
20
30
40
50
60
70
80
90
SRF: 0.95 (r)
SRF: 0.96 (r)
SRF: 0.97 (r)
SRF: 0.99 (r)
SRF: 1 (r)

**30%_6_FEM**

Critical SRF=0.91

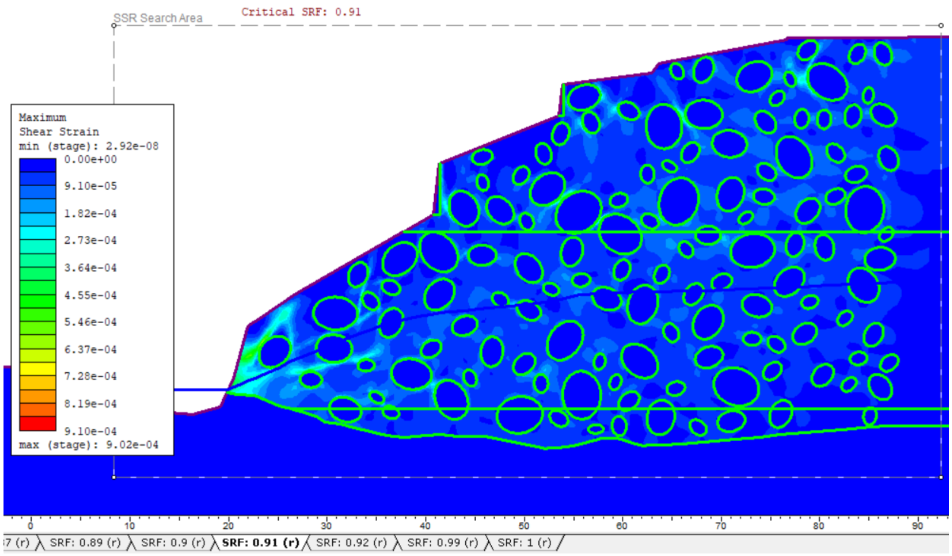


SRF=0.92

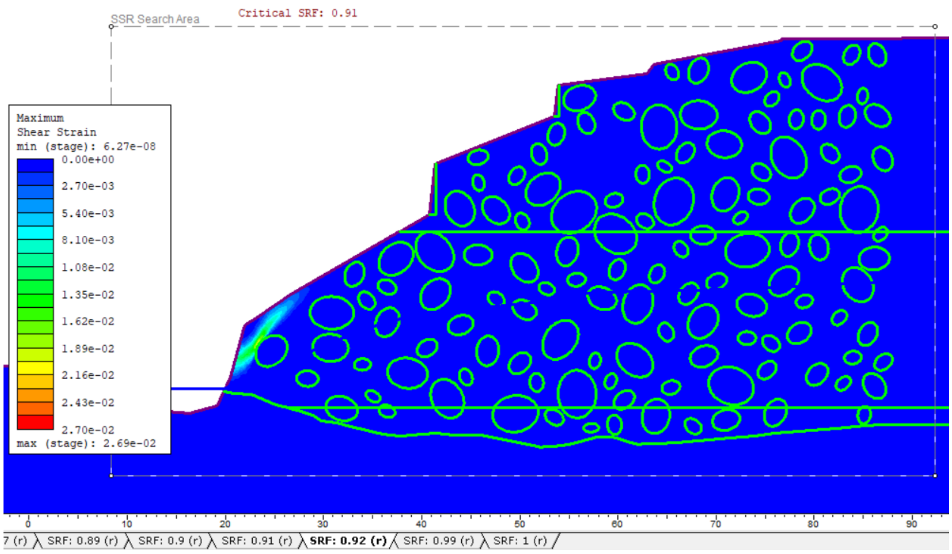

SRF=0.99

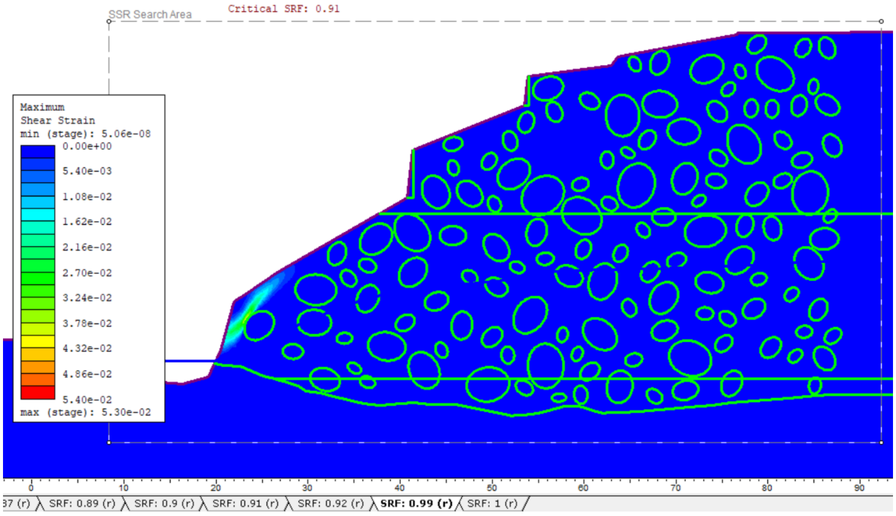


SRF=1.00

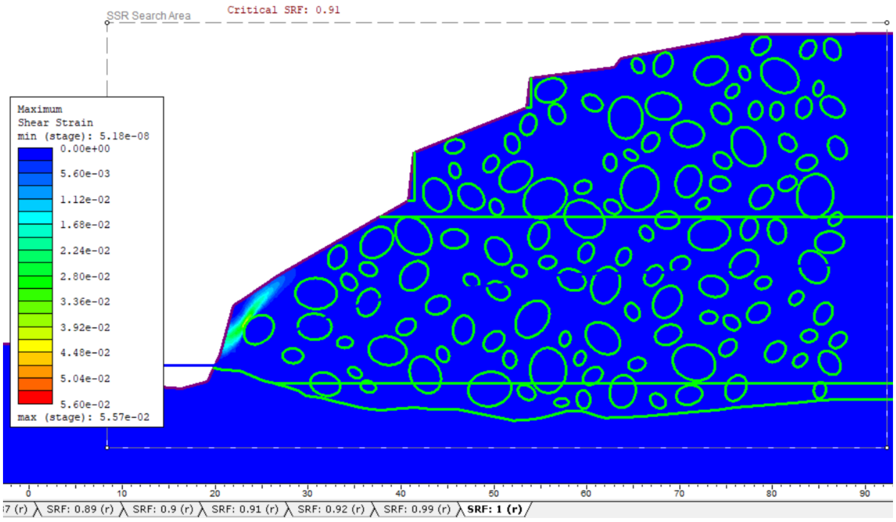

**30%_7_FEM**

Critical SRF=1.11

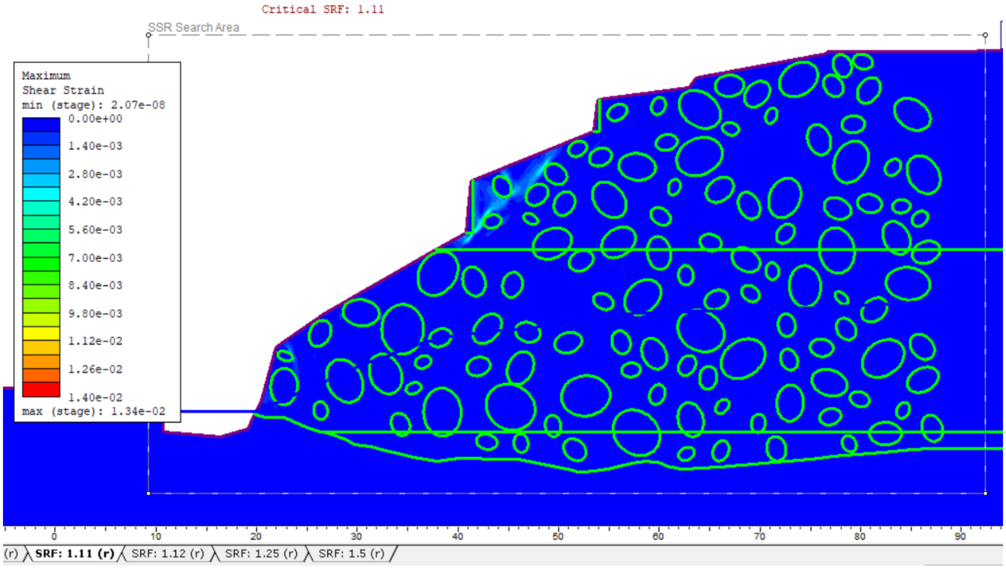


SRF=1.12

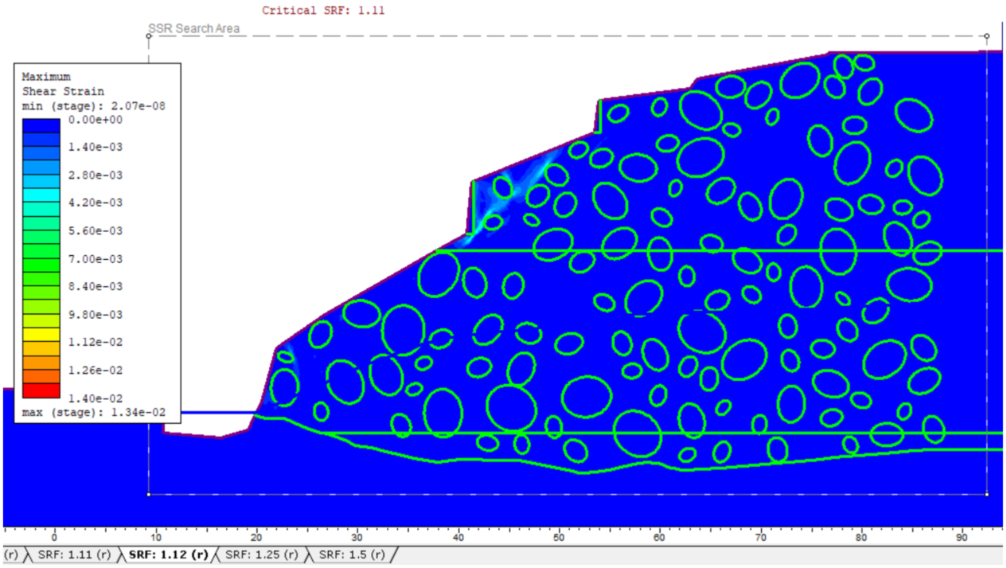

SRF=1.25

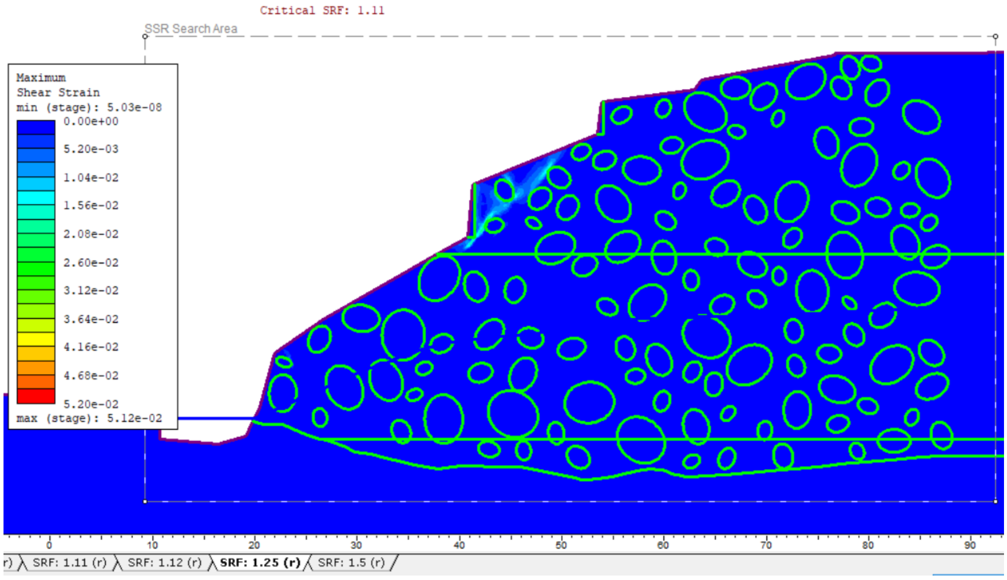


SRF=1.50

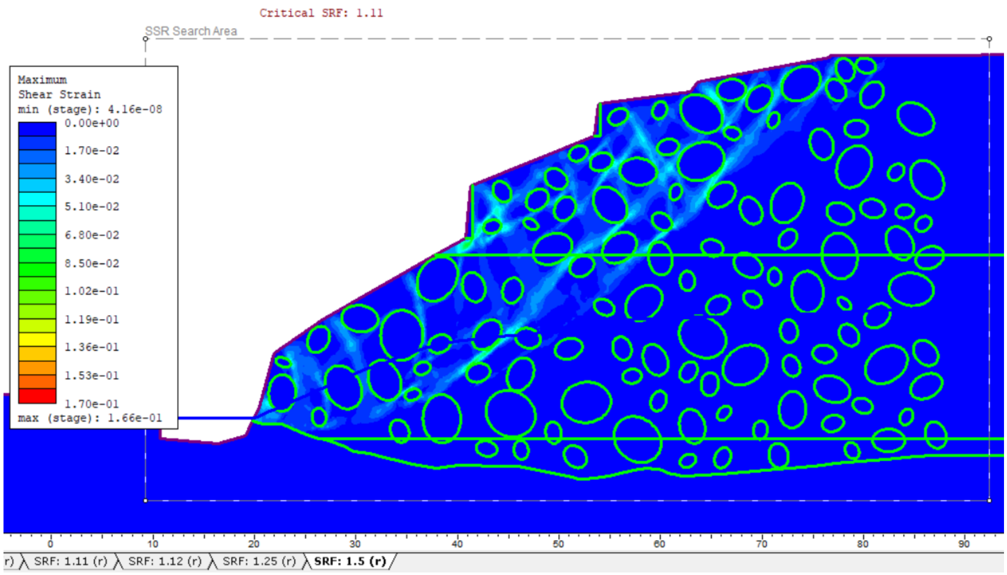

**30%_8_FEM**

Critical SRF=1.01

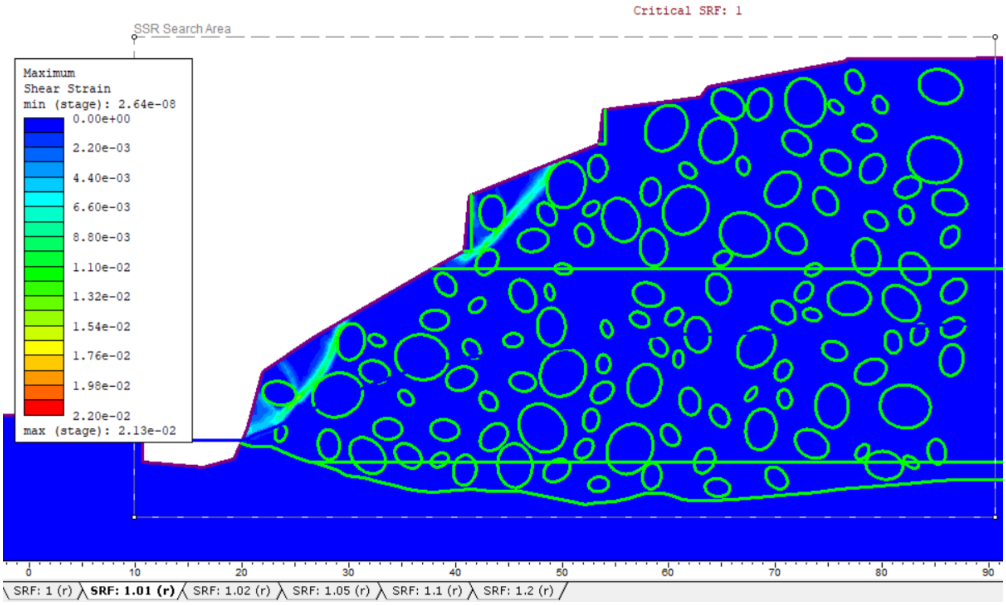


SRF=1.02

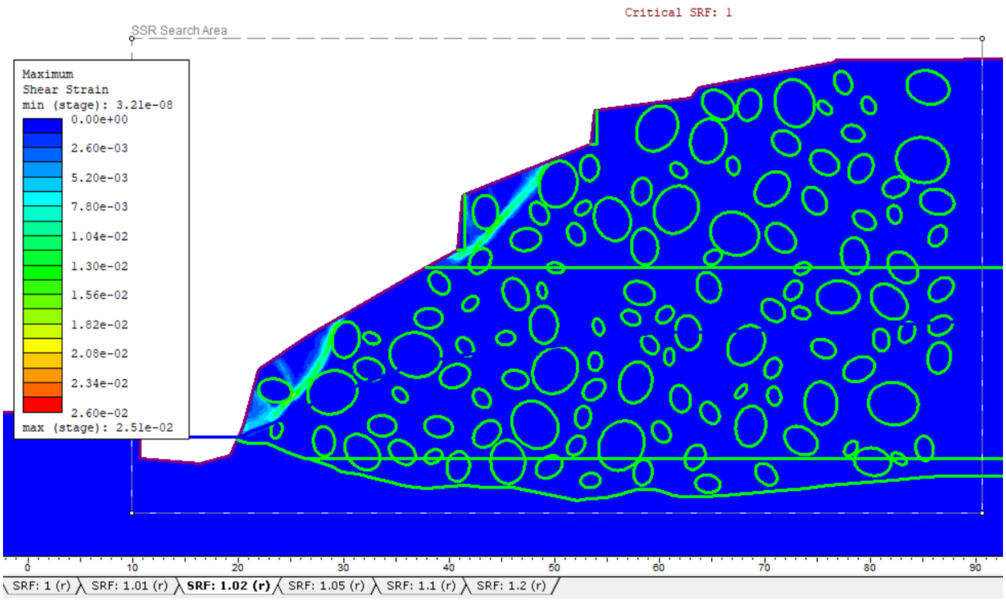

SRF=1.05

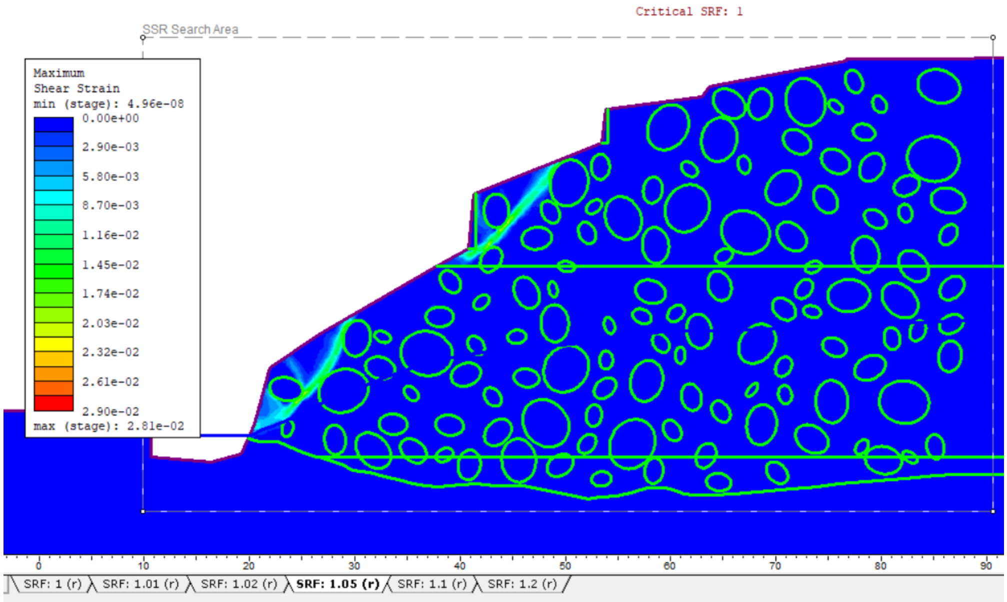


SRF=1.11

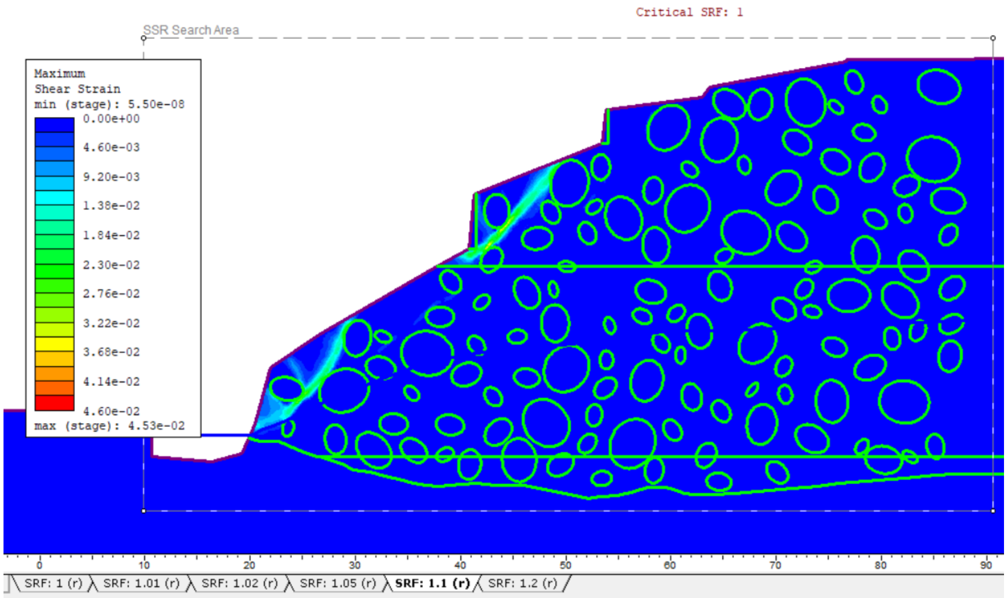

SRF=1.20

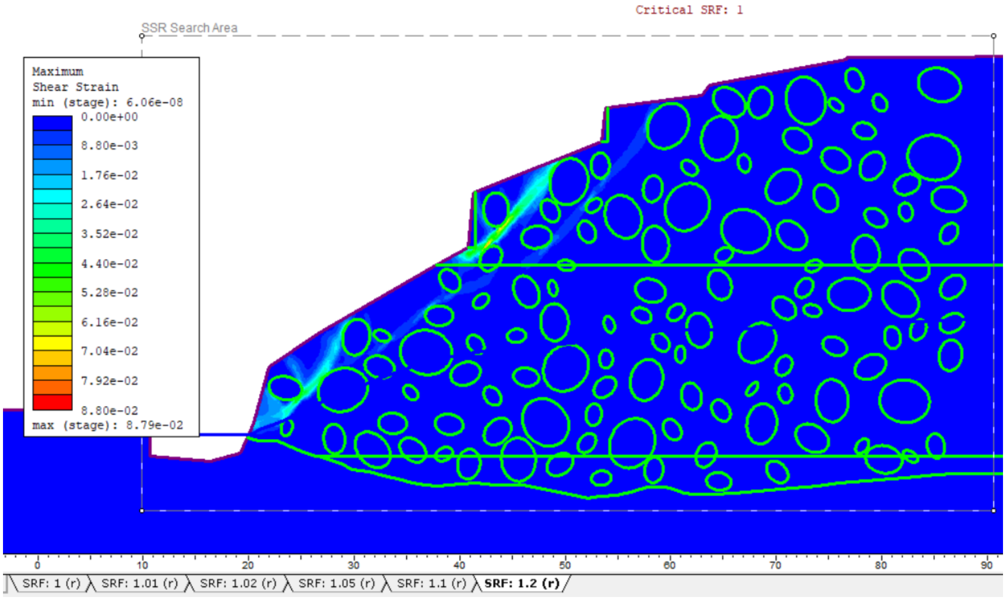
Critical SRF: 1
SSR Search Area
Maximum
Shear Strain
min (stage): 6.06e-08
0.00e+00
8.80e-03
1.76e-02
2.64e-02
3.52e-02
4.40e-02
5.28e-02
6.16e-02
7.04e-02
7.92e-02
8.80e-02
max (stage): 8.79e-02
0
10
20
30
40
50
60
70
80
90
SRF: 1 (r)
SRF: 1.01 (r)
SRF: 1.02 (r)
SRF: 1.05 (r)
SRF: 1.1 (r)
SRF: 1.2 (r)

**30%_9_FEM**

Critical SRF=1.16

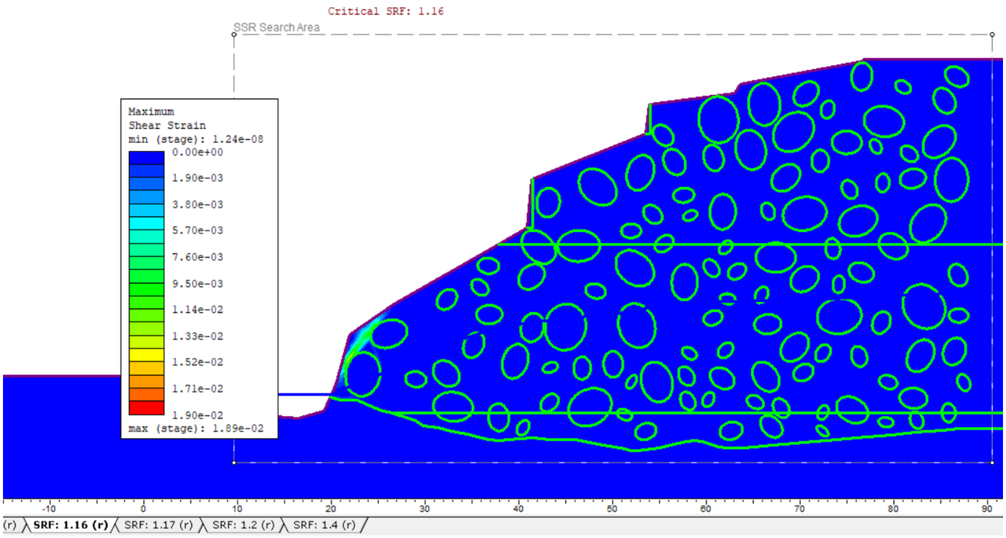


SRF=1.17

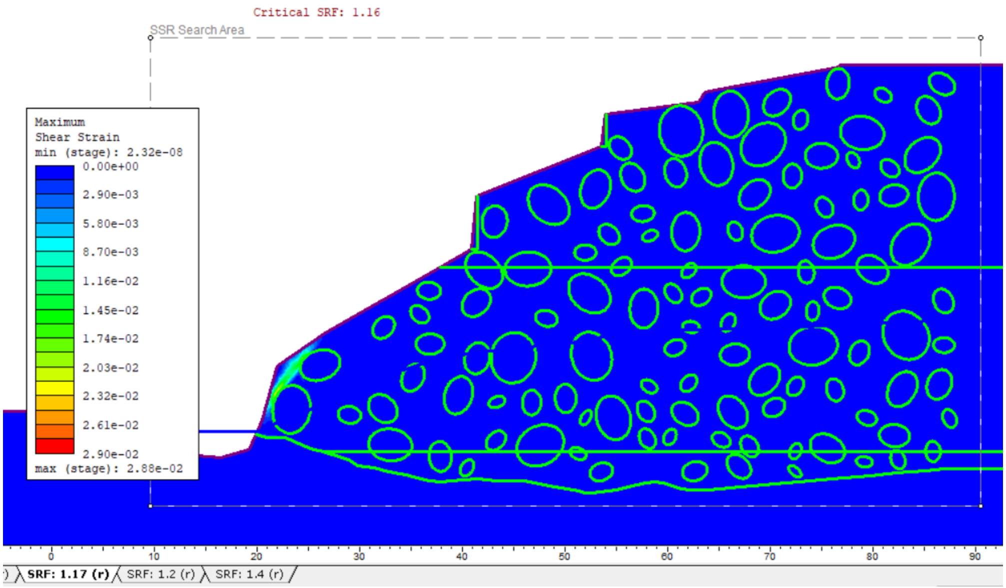

SRF=1.20

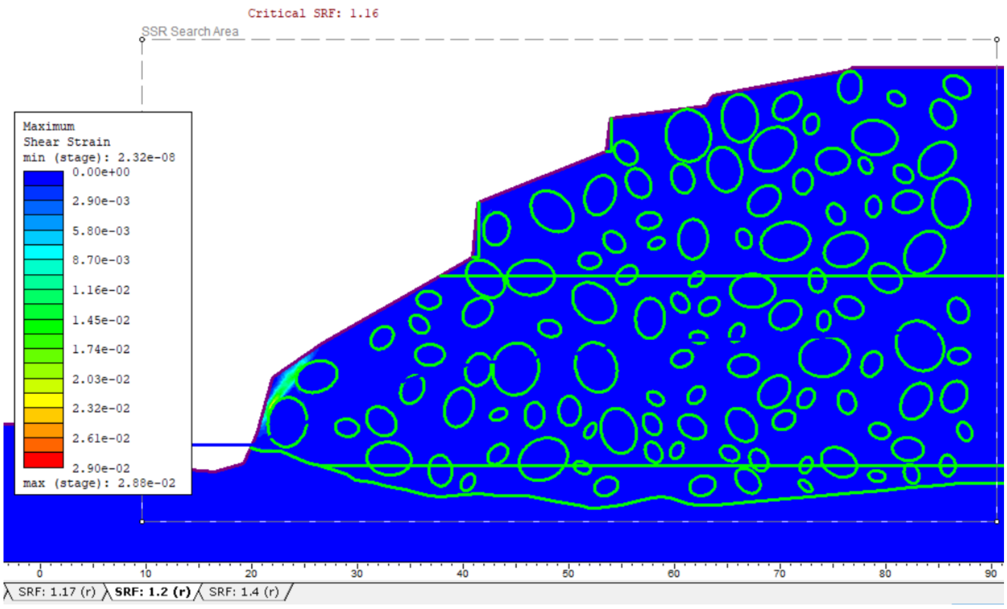


SRF=1.40

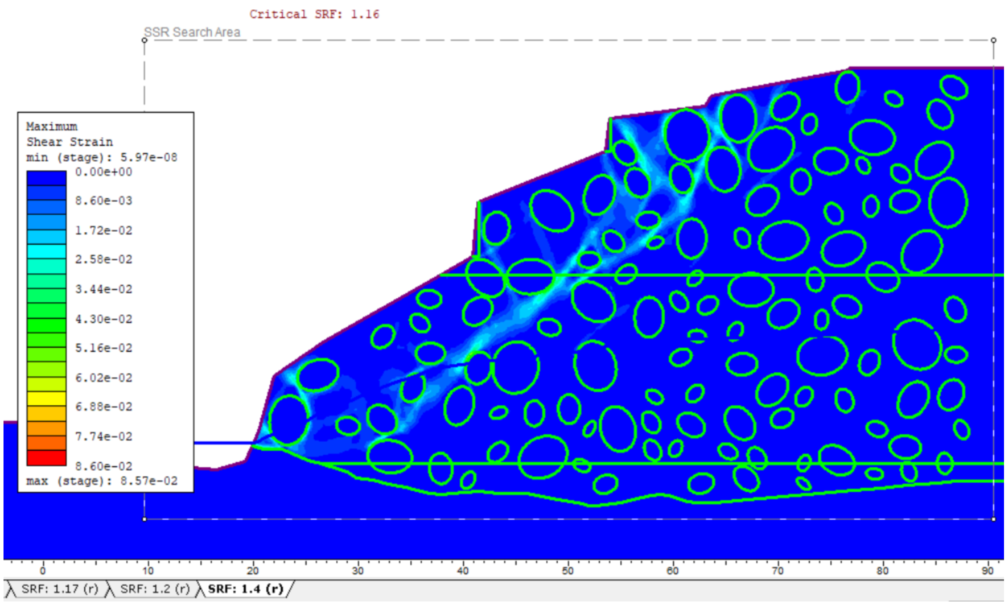

**30%_10_FEM**

Critical SRF=1.19

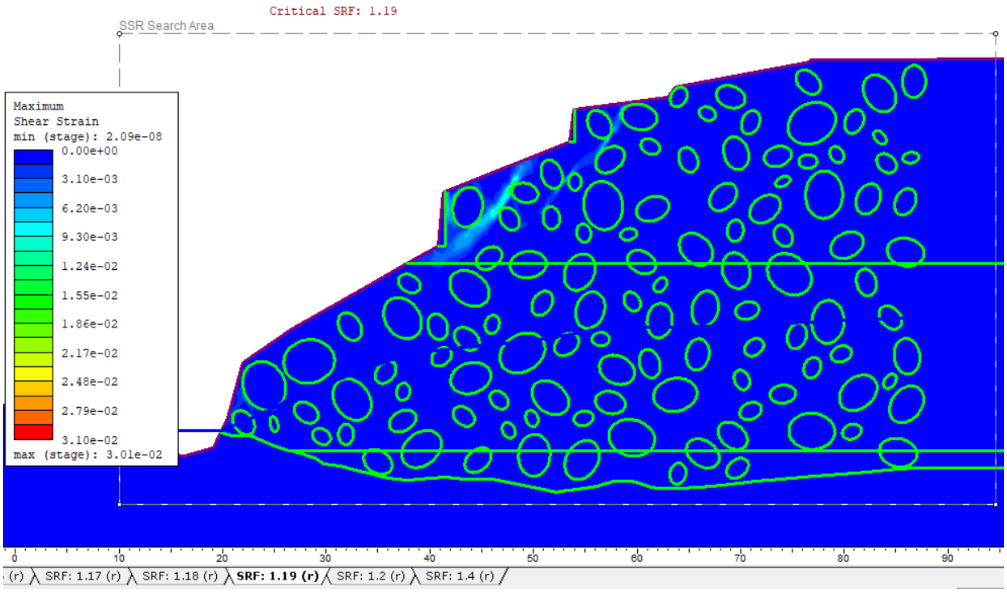


SRF=1.20

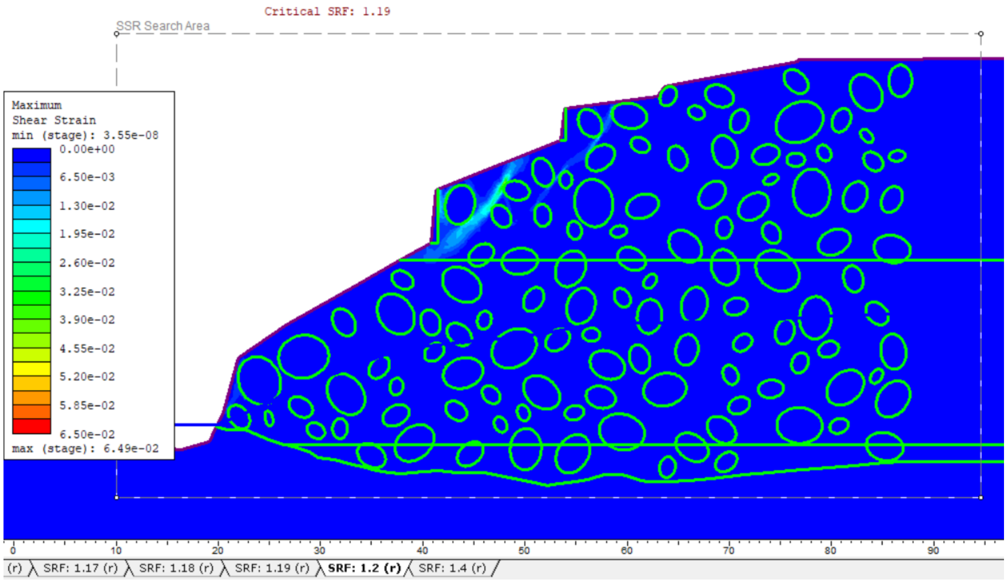

SRF=1.40

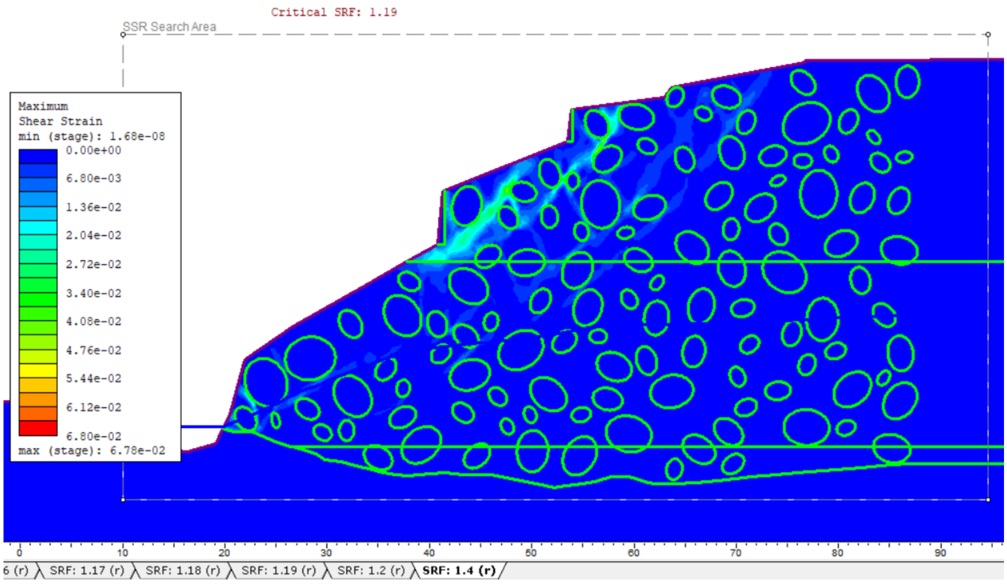
Critical SRF: 1.19
SSR Search Area
Maximum
Shear Strain
min (stage): 1.68e-08
0.00e+00
6.80e-03
1.36e-02
2.04e-02
2.72e-02
3.40e-02
4.08e-02
4.76e-02
5.44e-02
6.12e-02
6.80e-02
max (stage): 6.78e-02
0
10
20
30
40
50
60
70
80
90
6 (r)
SRF: 1.17 (r)
SRF: 1.18 (r)
SRF: 1.19 (r)
SRF: 1.2 (r)
SRF: 1.4 (r)

# Appendix C

## Maximum shear strains and progressive failure for 30% VBP with c=10 kPa & $\phi = 35°$

**30%_1_FEM**

Critical SRF=1.21

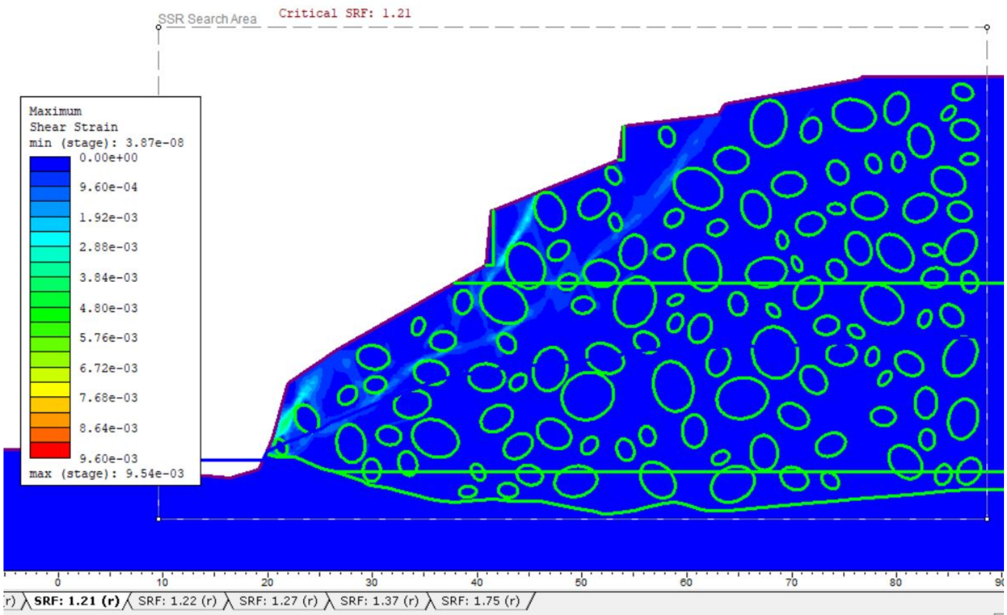

SRF=1.22

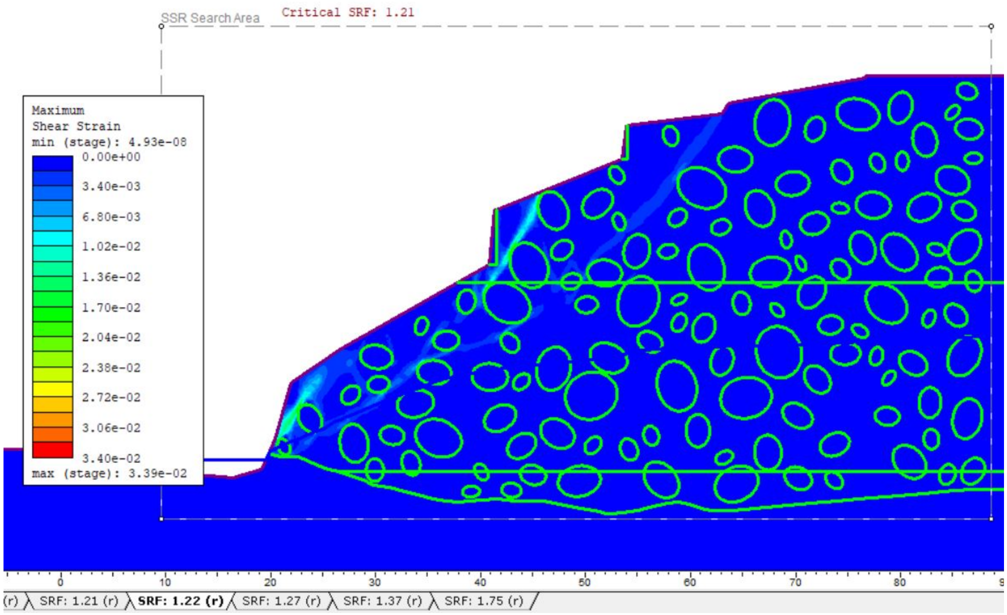


SRF=1.27

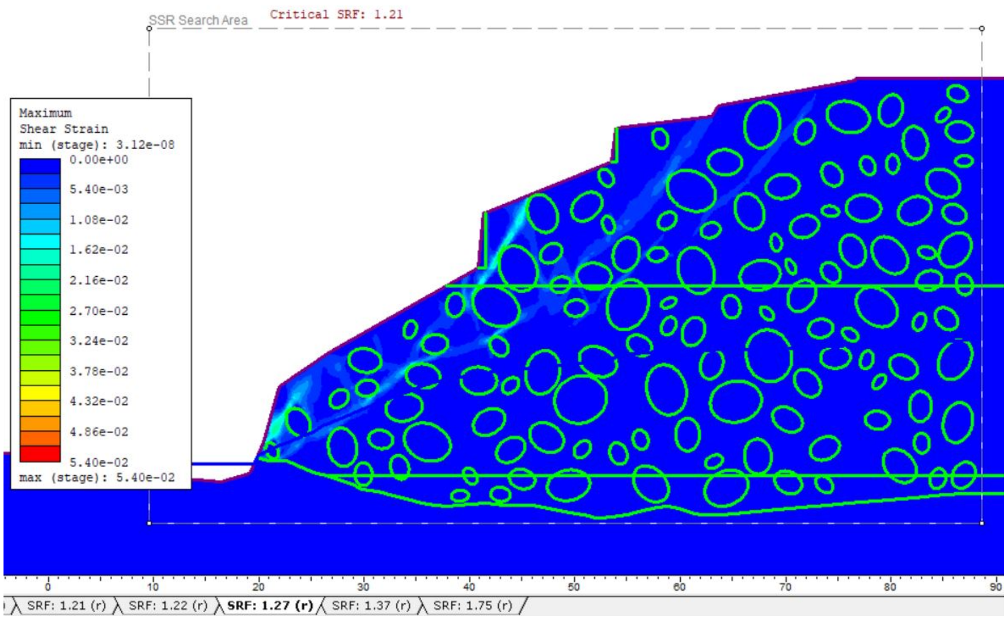

SRF=1.37

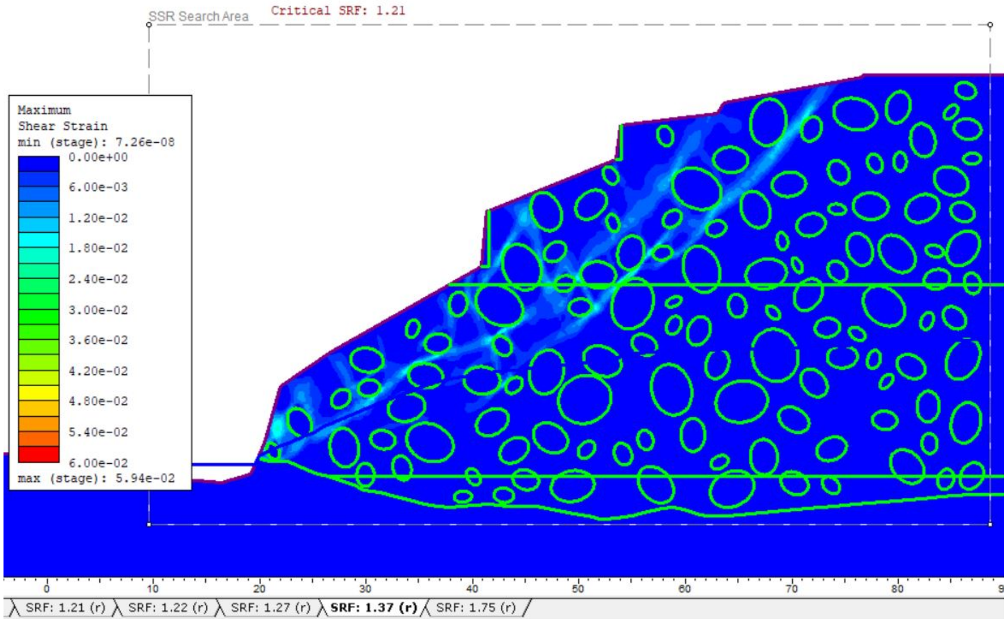


SRF=1.75

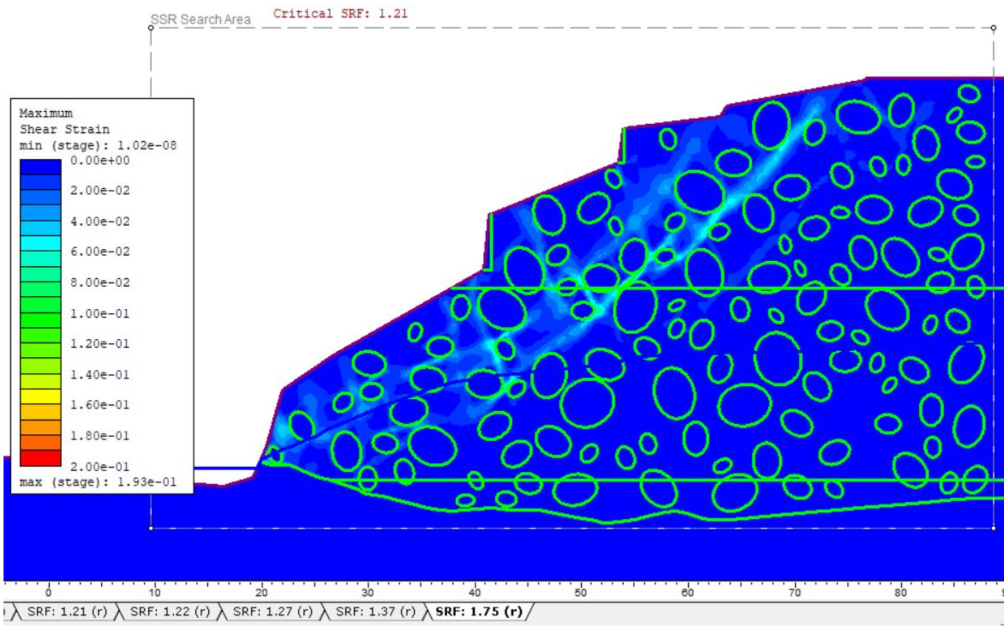

**30%_2_FEM**

Critical SRF=1.17

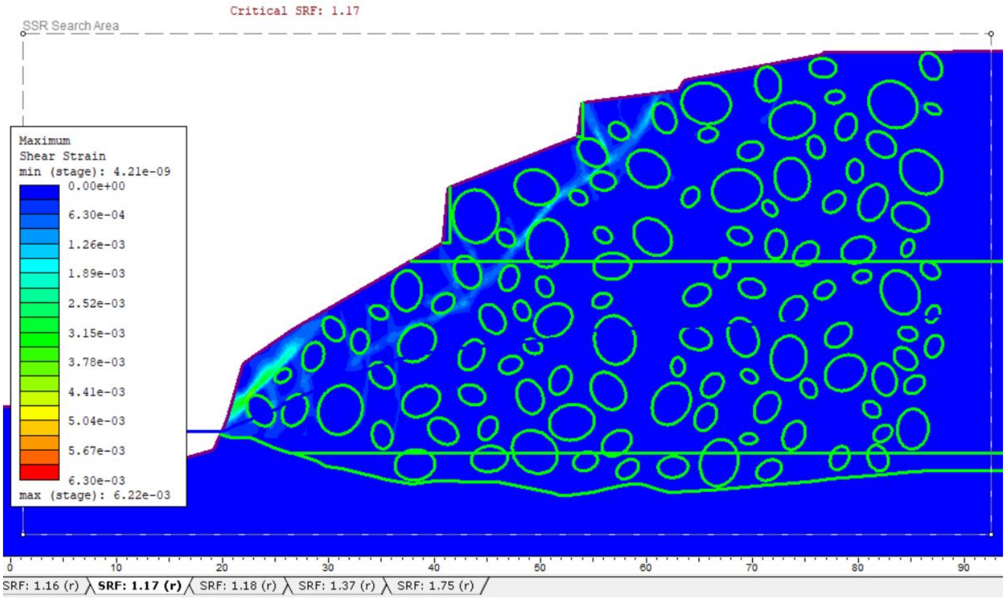


SRF=1.18

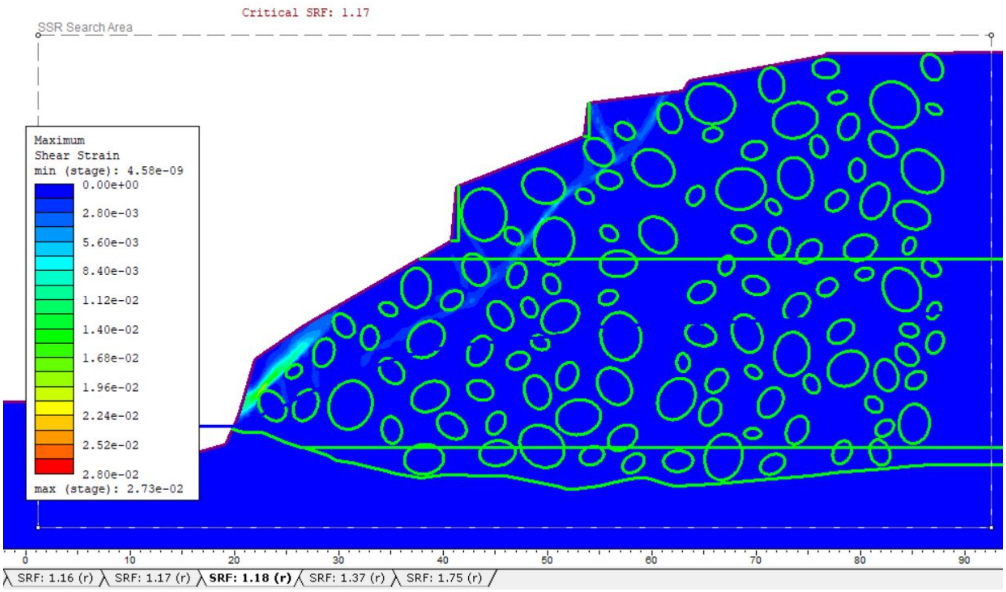

SRF=1.37

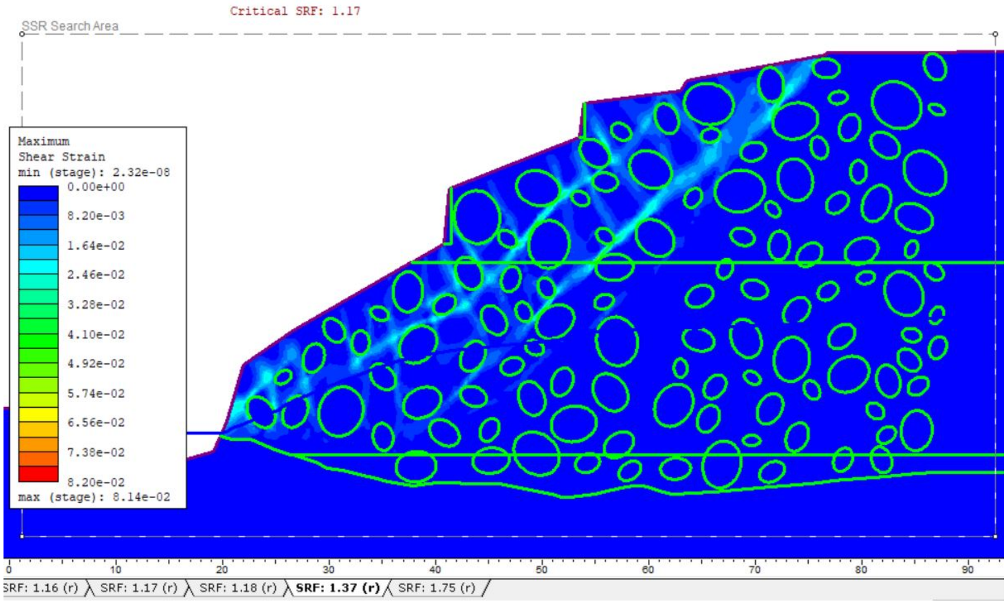


SRF=1.75

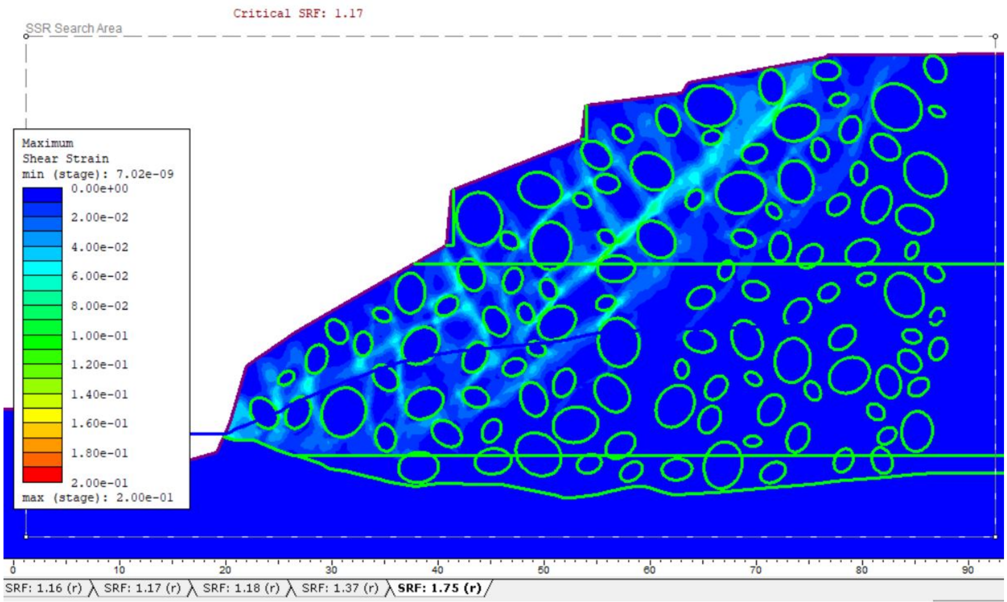

**30%_3_FEM**

Critical SRF=1.16

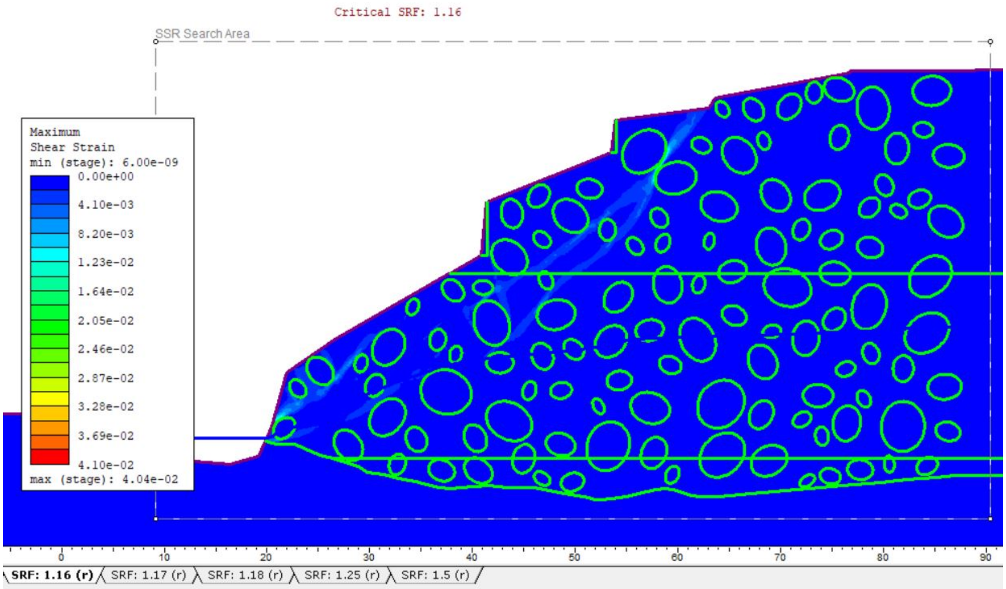


SRF=1.17

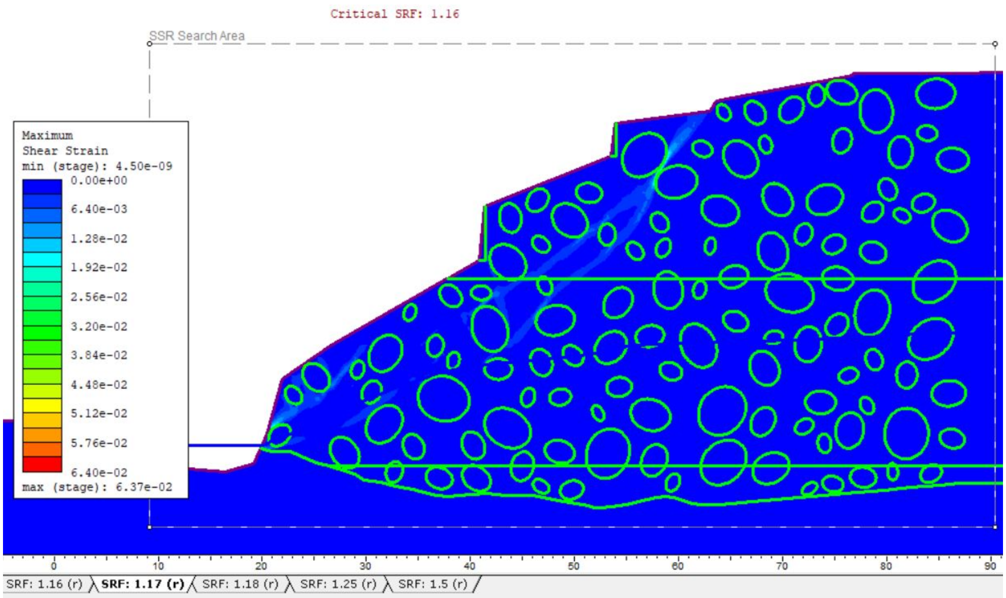

SRF=1.18

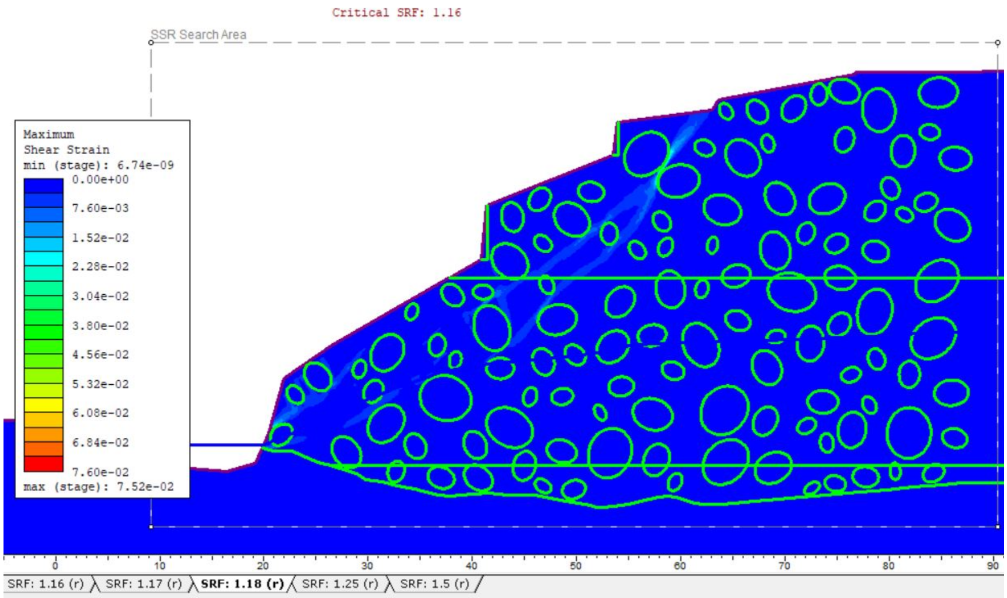


SRF=1.25

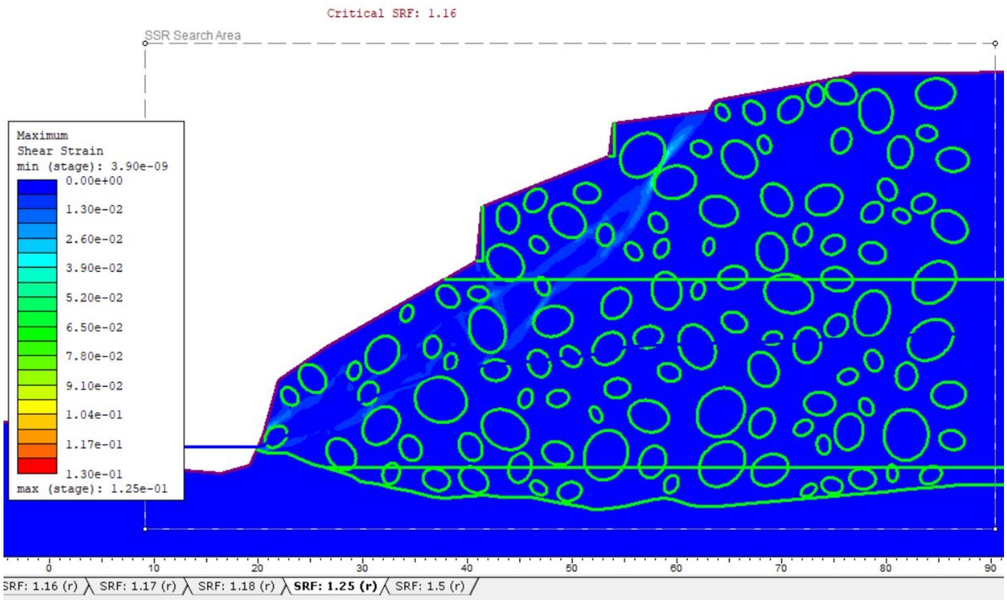

SRF=1.50

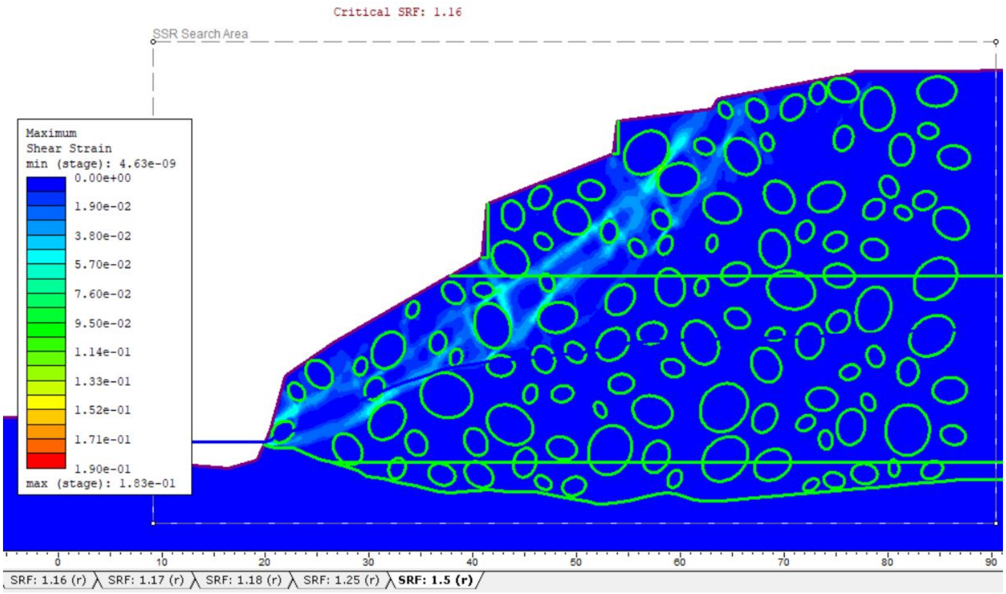
Critical SRF: 1.16
SSR Search Area
Maximum
Shear Strain
min (stage): 4.63e-09
0.00e+00
1.90e-02
3.80e-02
5.70e-02
7.60e-02
9.50e-02
1.14e-01
1.33e-01
1.52e-01
1.71e-01
1.90e-01
max (stage): 1.83e-01
0
10
20
30
40
50
60
70
80
90
SRF: 1.16 (r)
SRF: 1.17 (r)
SRF: 1.18 (r)
SRF: 1.25 (r)
SRF: 1.5 (r)

**30%_4_FEM**

Critical SRF=1.21

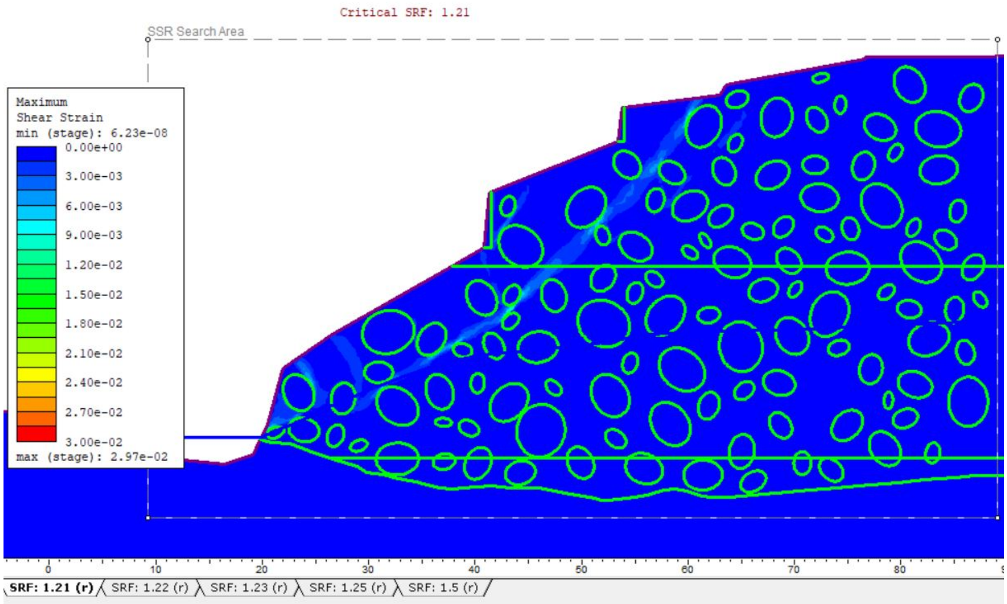


SRF=1.22

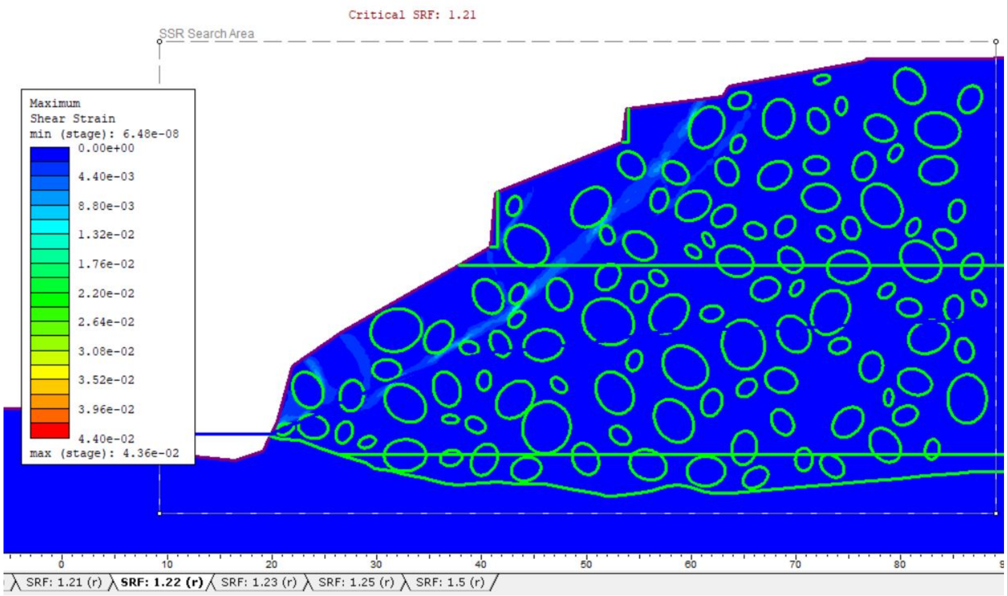

SRF=1.23

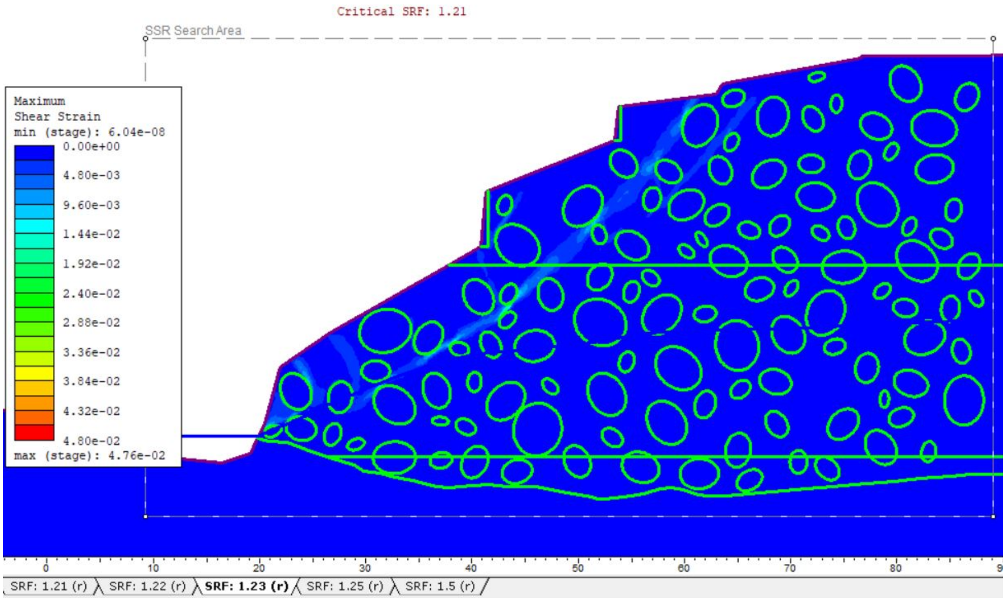


SRF=1.25

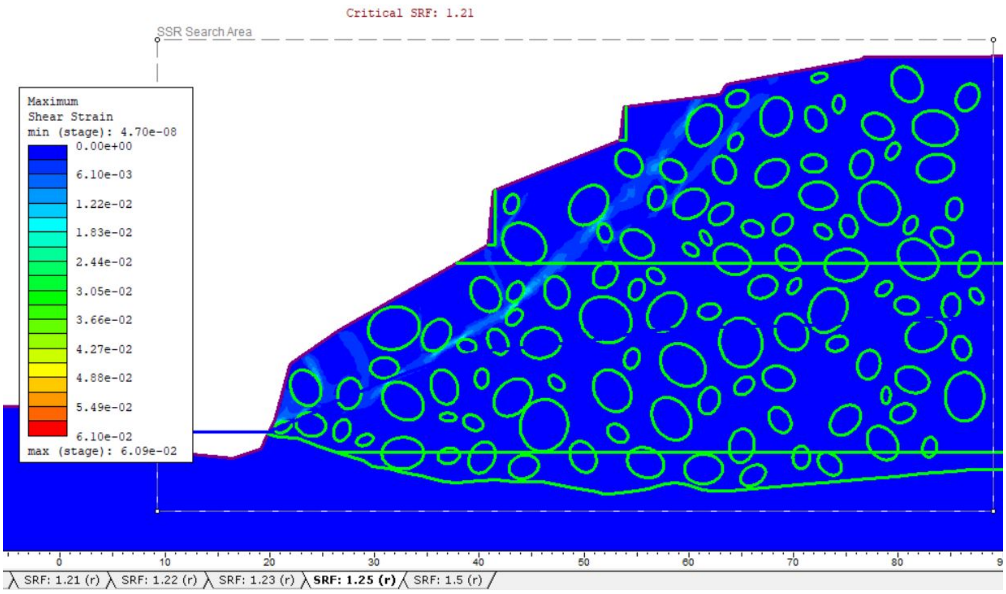

SRF=1.50

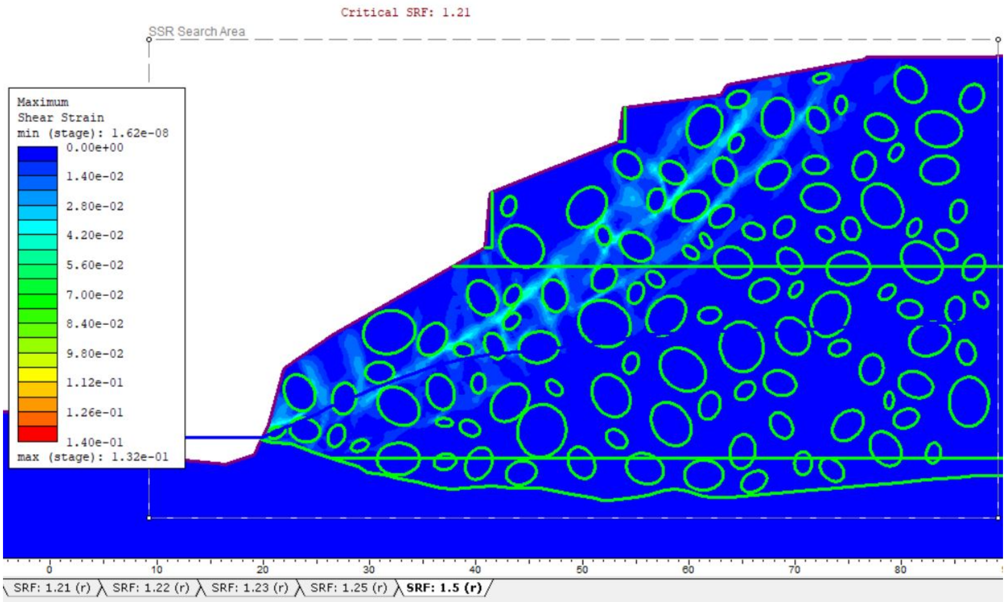
Critical SRF: 1.21
SSR Search Area
Maximum
Shear Strain
min (stage): 1.62e-08
0.00e+00
1.40e-02
2.80e-02
4.20e-02
5.60e-02
7.00e-02
8.40e-02
9.80e-02
1.12e-01
1.26e-01
1.40e-01
max (stage): 1.32e-01
0
10
20
30
40
50
60
70
80
SRF: 1.21 (r)
SRF: 1.22 (r)
SRF: 1.23 (r)
SRF: 1.25 (r)
SRF: 1.5 (r)

**30%_5_FEM**

Critical SRF=1.13

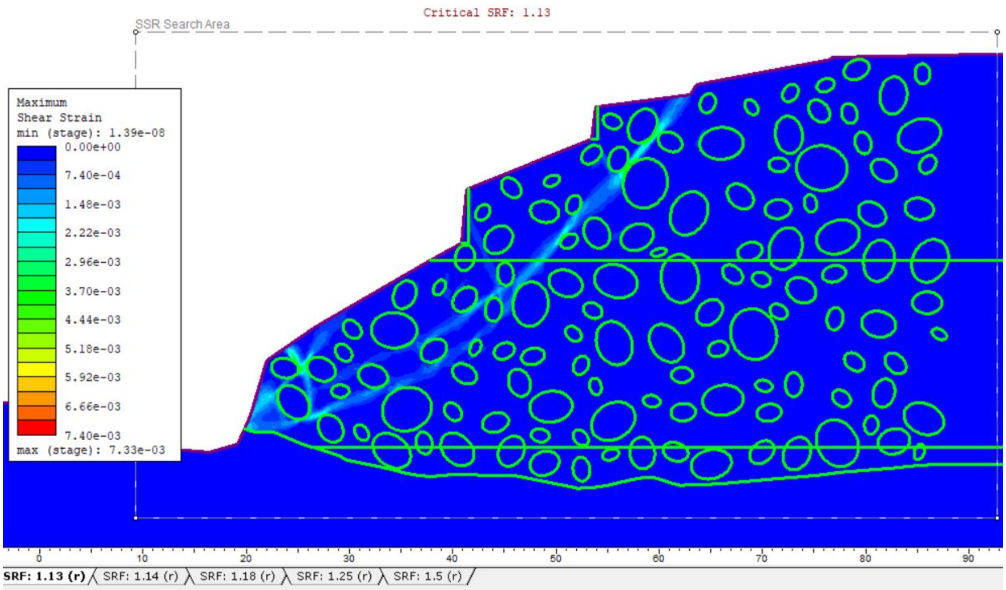


SRF=1.14

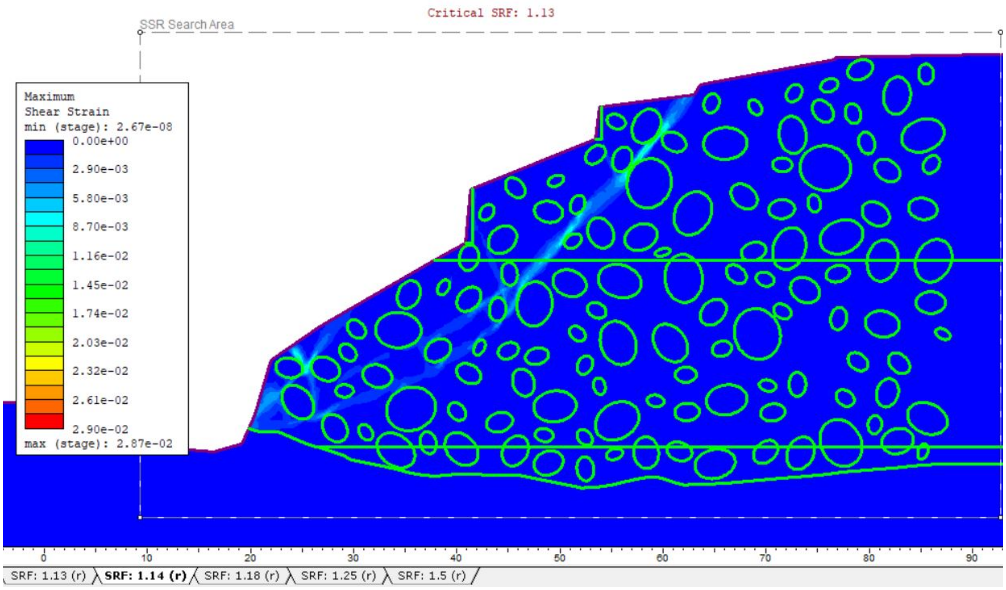

SRF=1.18

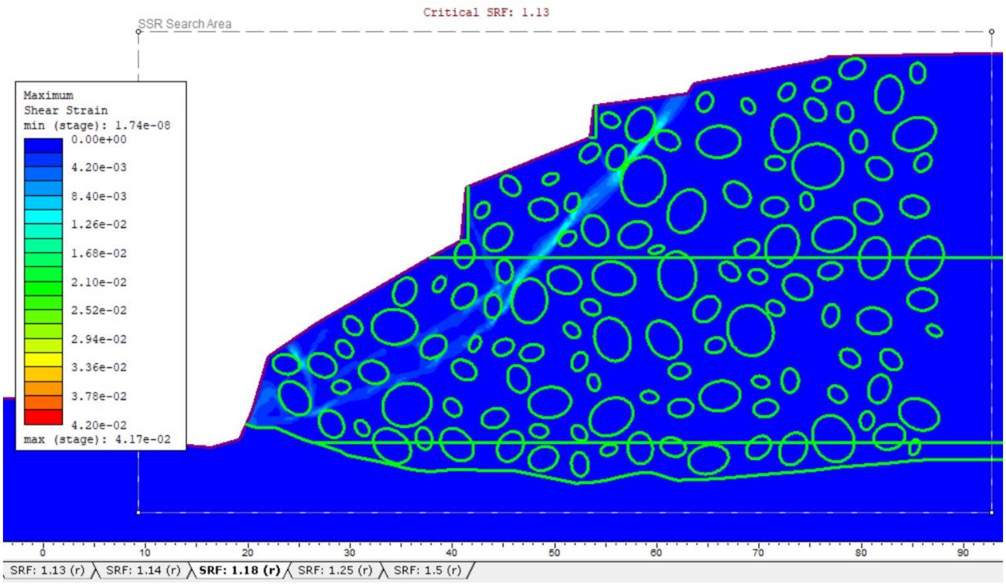


SRF=1.25

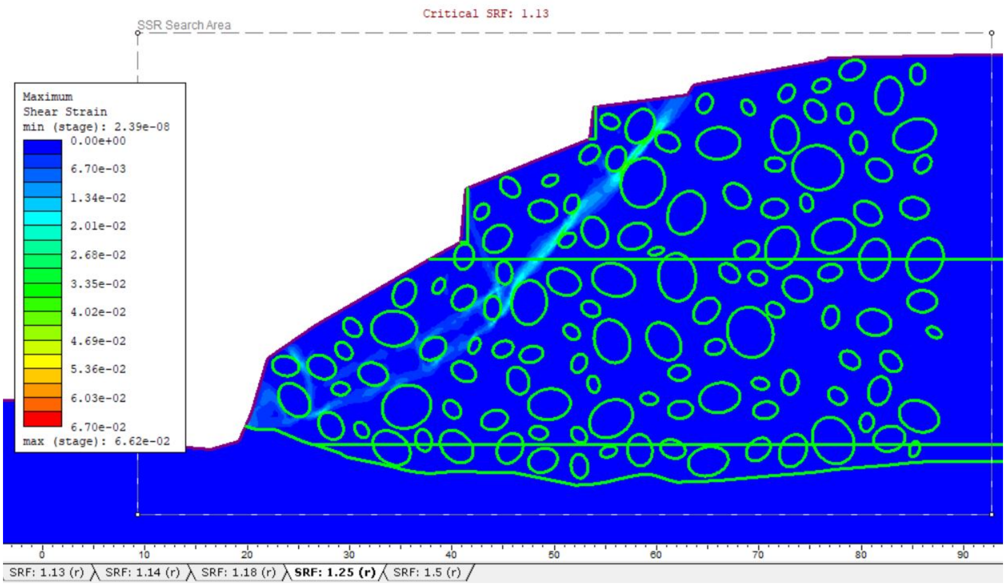

SRF=1.50

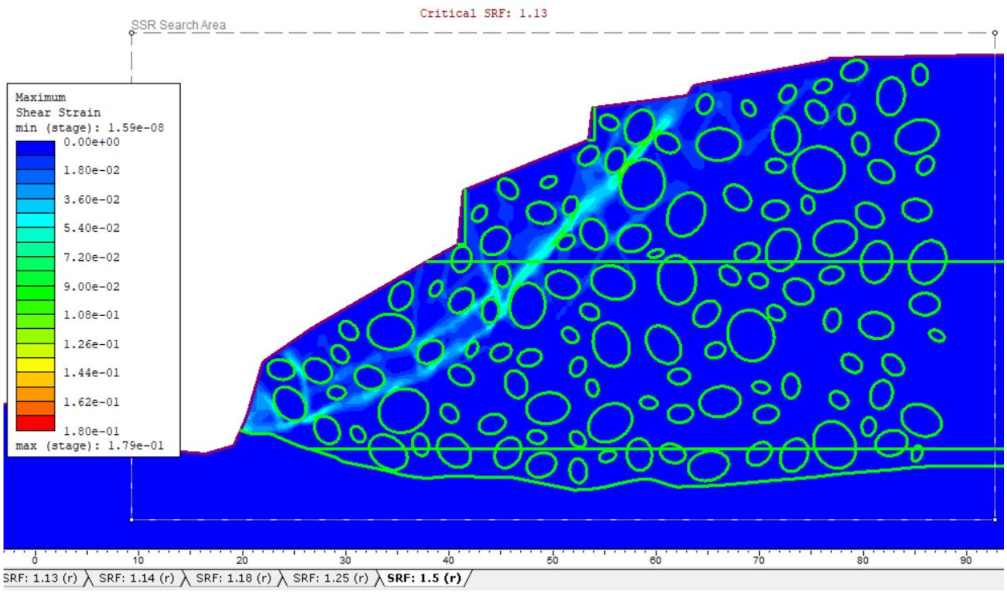

Critical SRF: 1.13
SSR Search Area
Maximum
Shear Strain
min (stage): 1.59e-08
0.00e+00
1.80e-02
3.60e-02
5.40e-02
7.20e-02
9.00e-02
1.08e-01
1.26e-01
1.44e-01
1.62e-01
1.80e-01
max (stage): 1.79e-01
0
10
20
30
40
50
60
70
80
90
SRF: 1.13 (r)
SRF: 1.14 (r)
SRF: 1.18 (r)
SRF: 1.25 (r)
SRF: 1.5 (r)

**30%_6_FEM**

Critical SRF=1.16

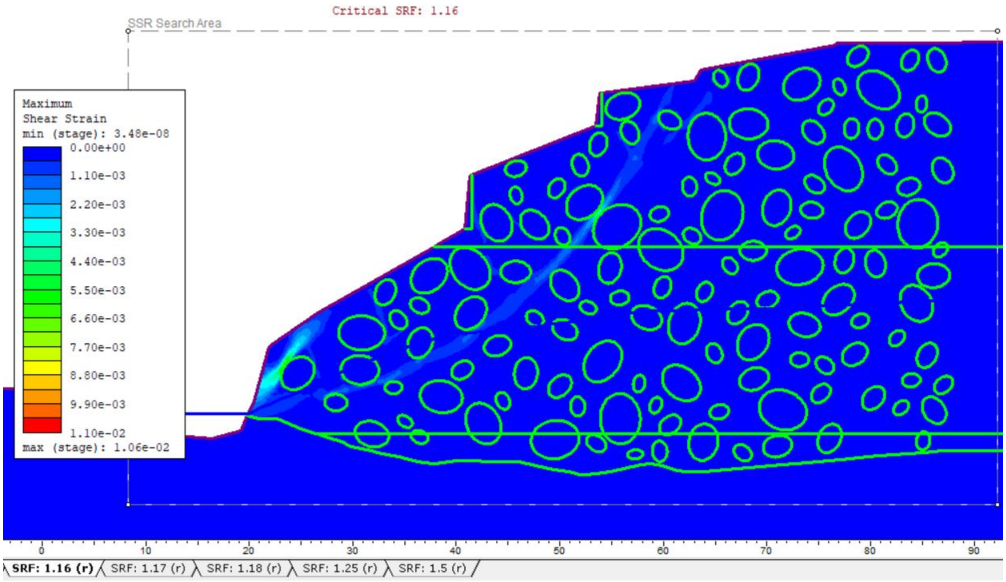


SRF=1.17

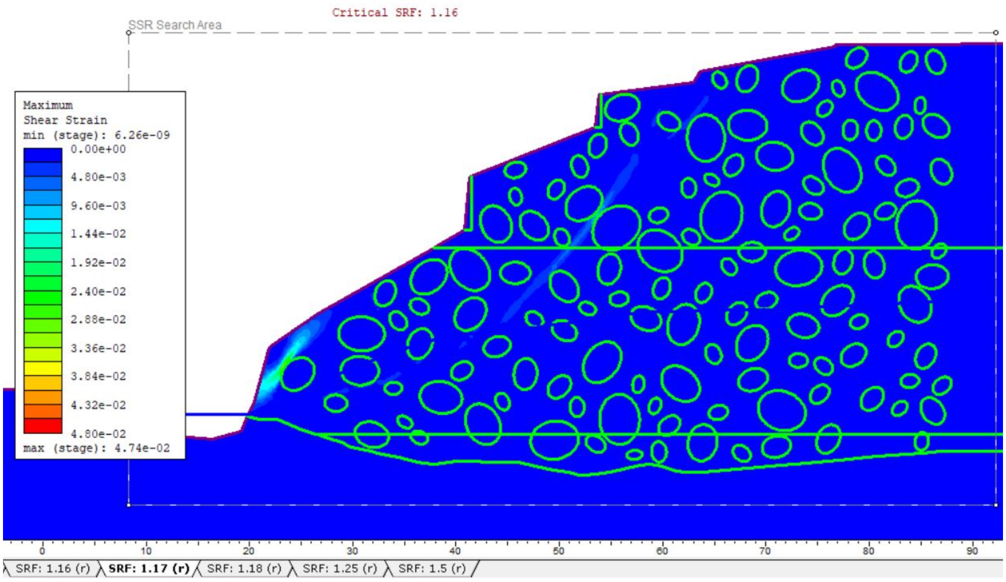

SRF=1.18

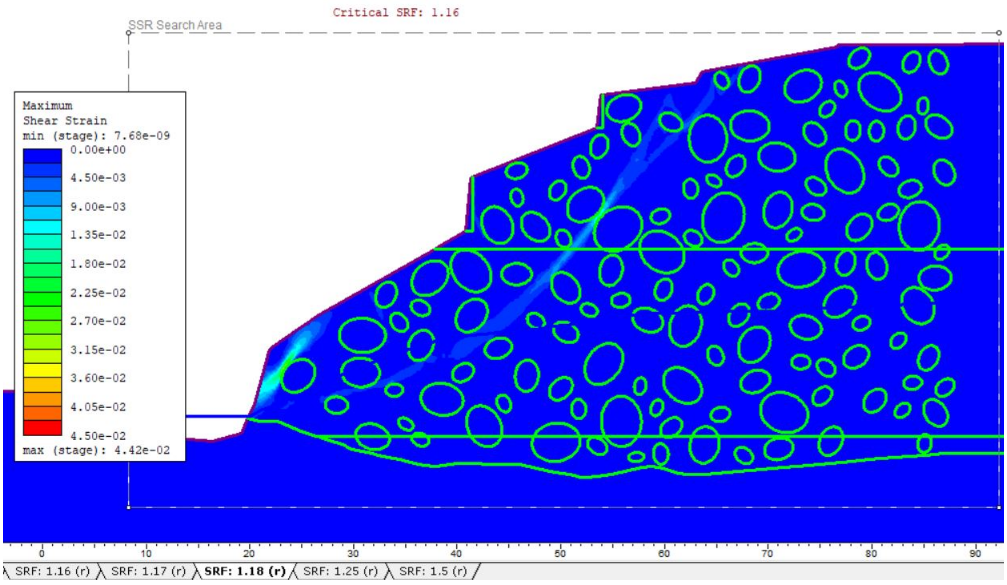


SRF=1.25

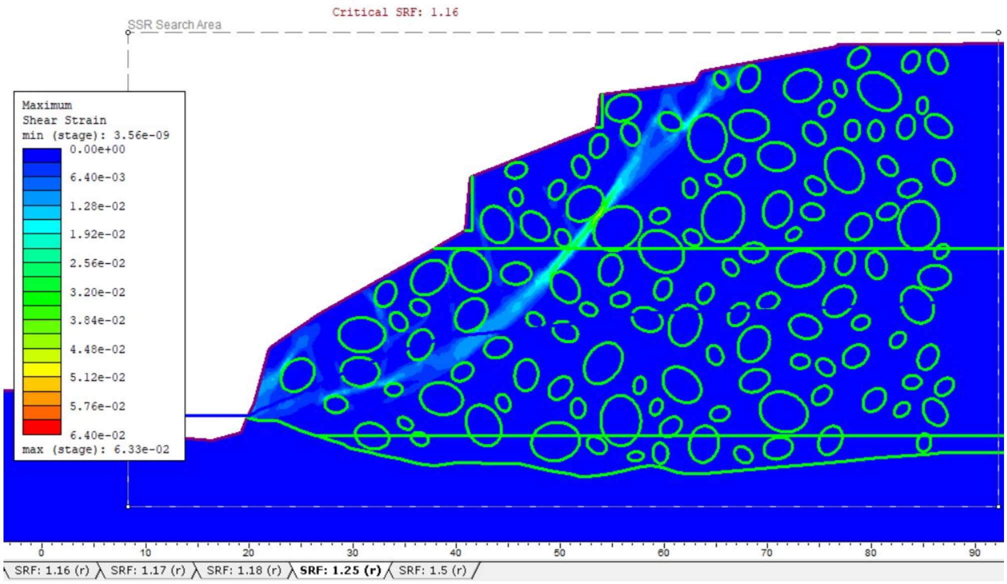

SRF=1.50

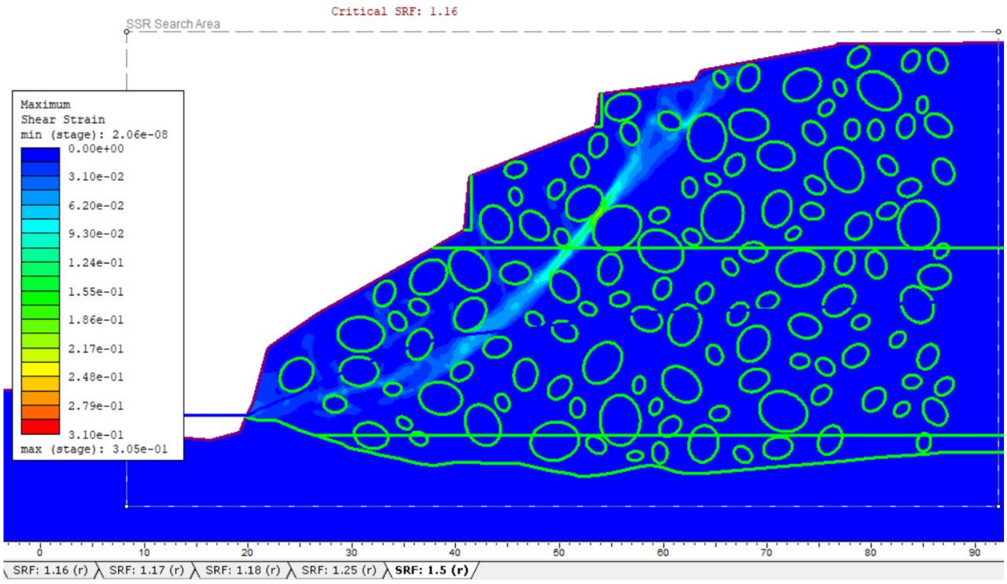

Critical SRF: 1.16
SSR Search Area
Maximum
Shear Strain
min (stage): 2.06e-08
0.00e+00
3.10e-02
6.20e-02
9.30e-02
1.24e-01
1.55e-01
1.86e-01
2.17e-01
2.48e-01
2.79e-01
3.10e-01
max (stage): 3.05e-01
0
10
20
30
40
50
60
70
80
90
SRF: 1.16 (r)
SRF: 1.17 (r)
SRF: 1.18 (r)
SRF: 1.25 (r)
SRF: 1.5 (r)

**30%_7_FEM**

Critical SRF=1.25

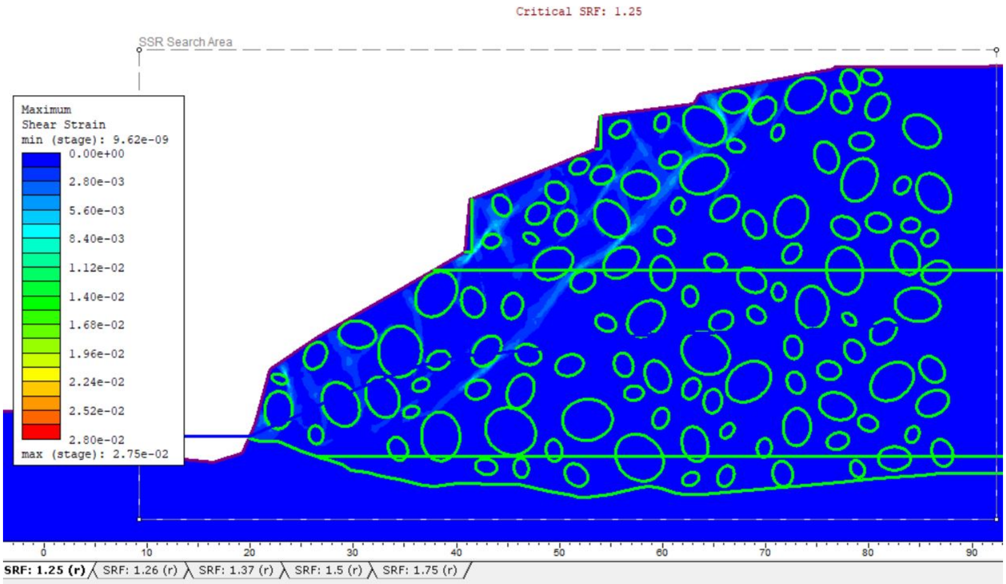


SRF=1.26

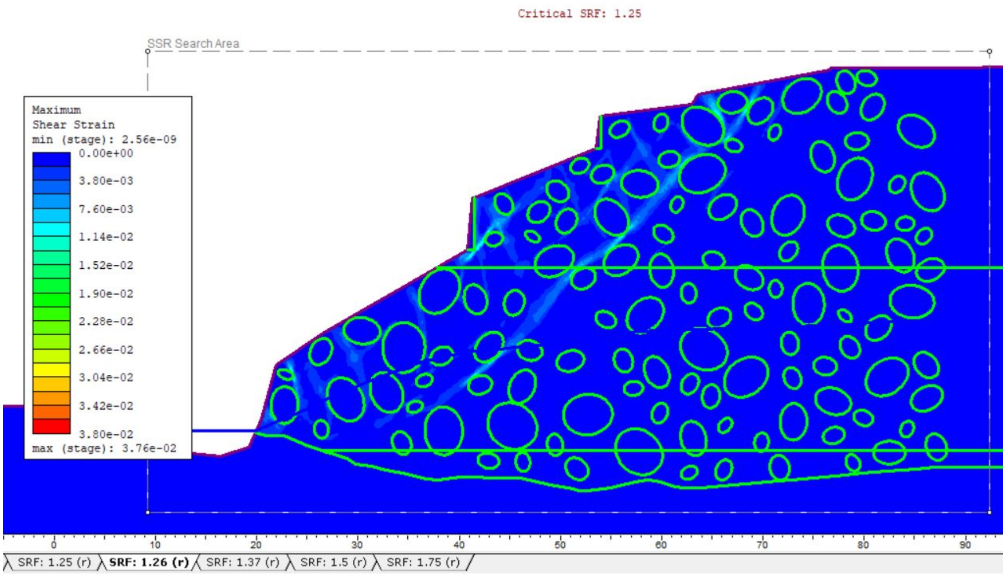

SRF=1.37

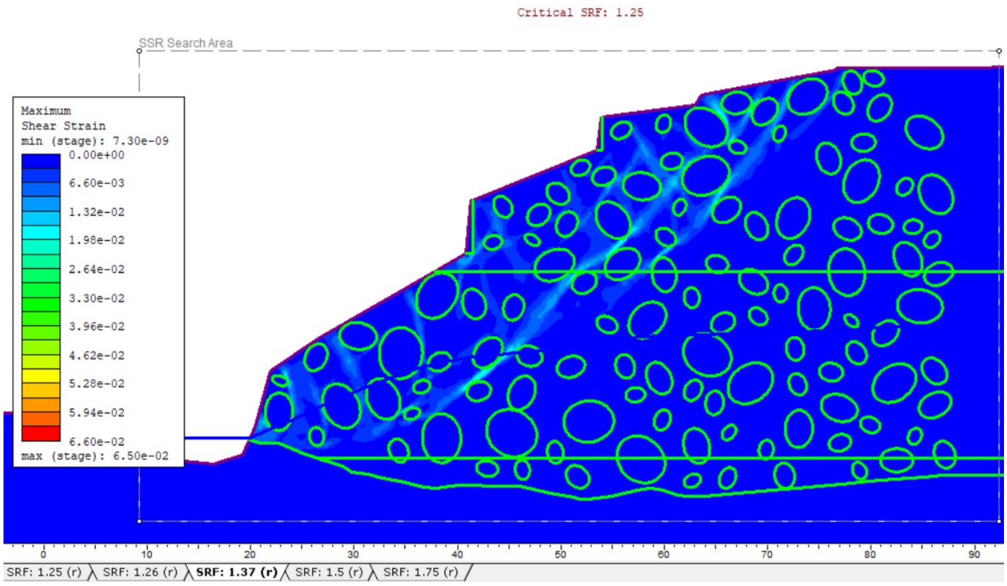


SRF=1.50

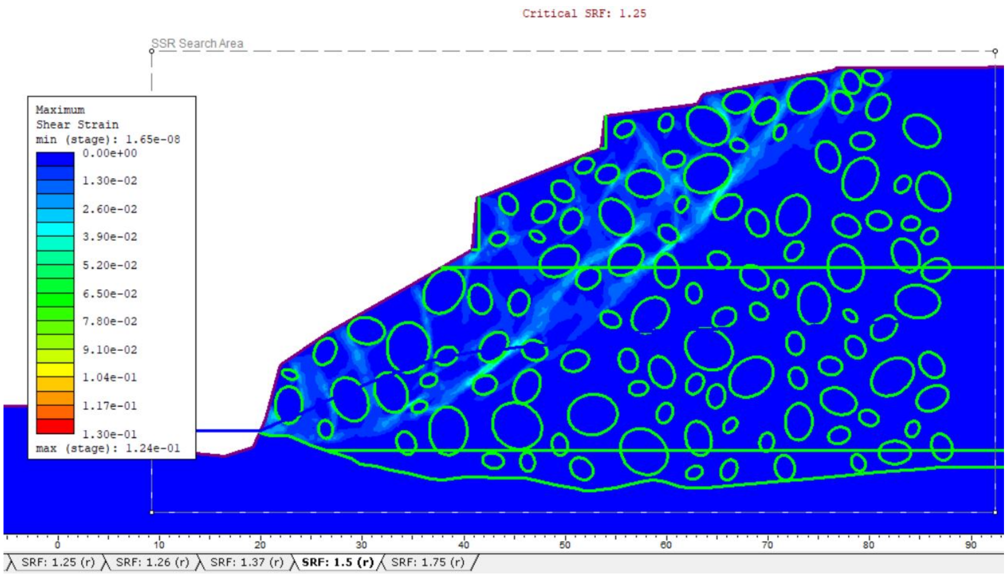

SRF=1.75

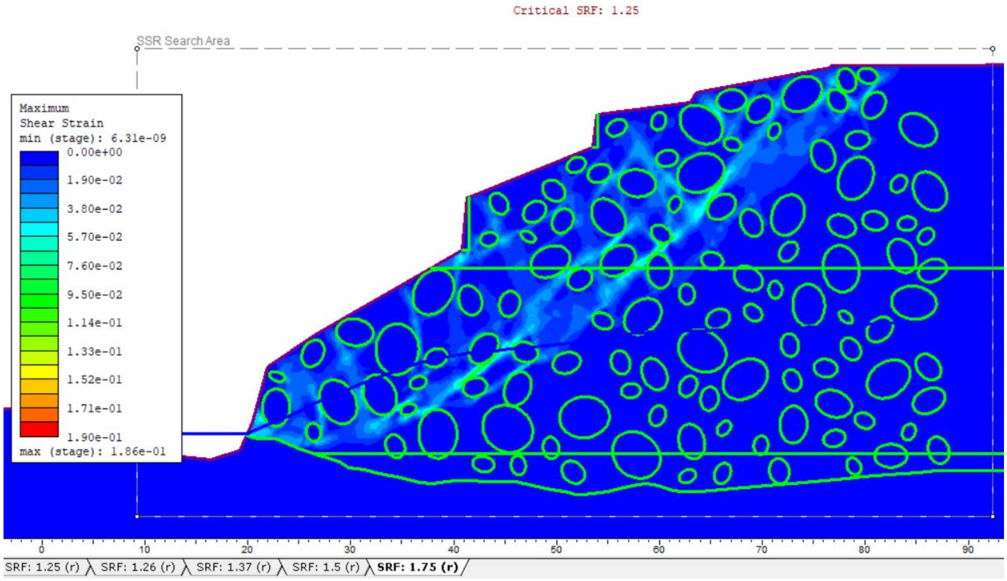

Critical SRF: 1.25
SSR Search Area
Maximum
Shear Strain
min (stage): 6.31e-09
0.00e+00
1.90e-02
3.80e-02
5.70e-02
7.60e-02
9.50e-02
1.14e-01
1.33e-01
1.52e-01
1.71e-01
1.90e-01
max (stage): 1.86e-01
0
10
20
30
40
50
60
70
80
90
SRF: 1.25 (r)
SRF: 1.26 (r)
SRF: 1.37 (r)
SRF: 1.5 (r)
SRF: 1.75 (r)

**30%_8_FEM**

Critical SRF=1.12

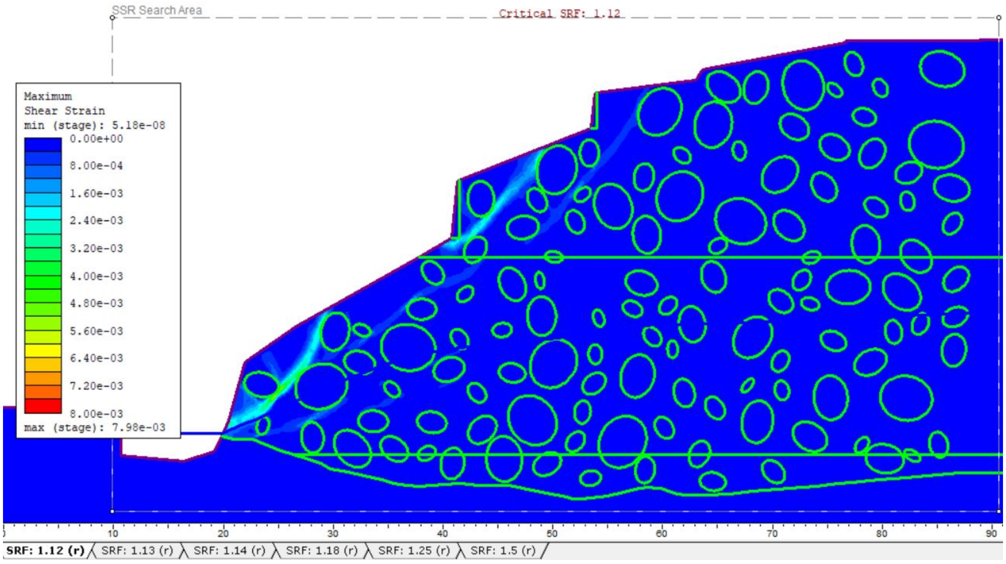


SRF=1.13

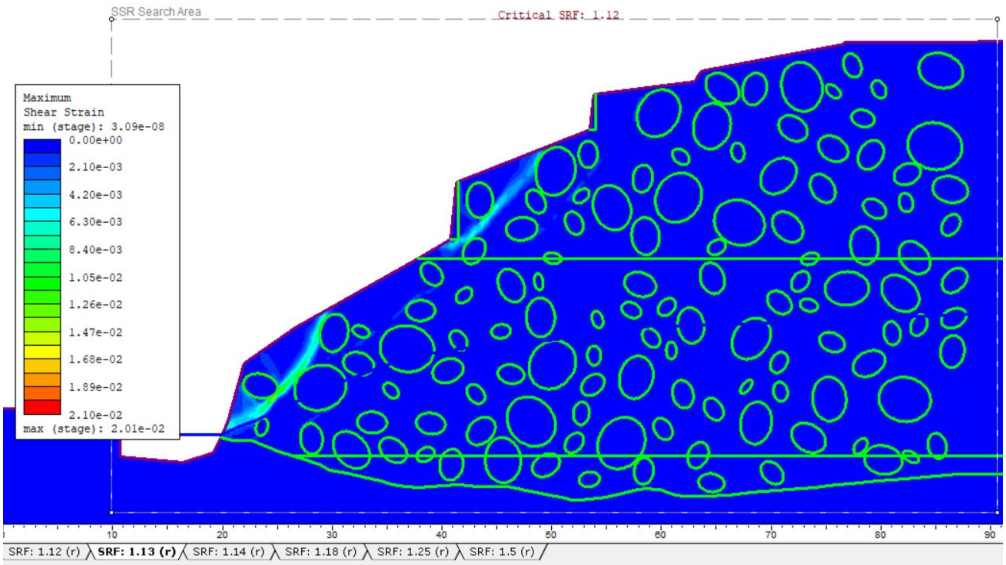

SRF=1.14

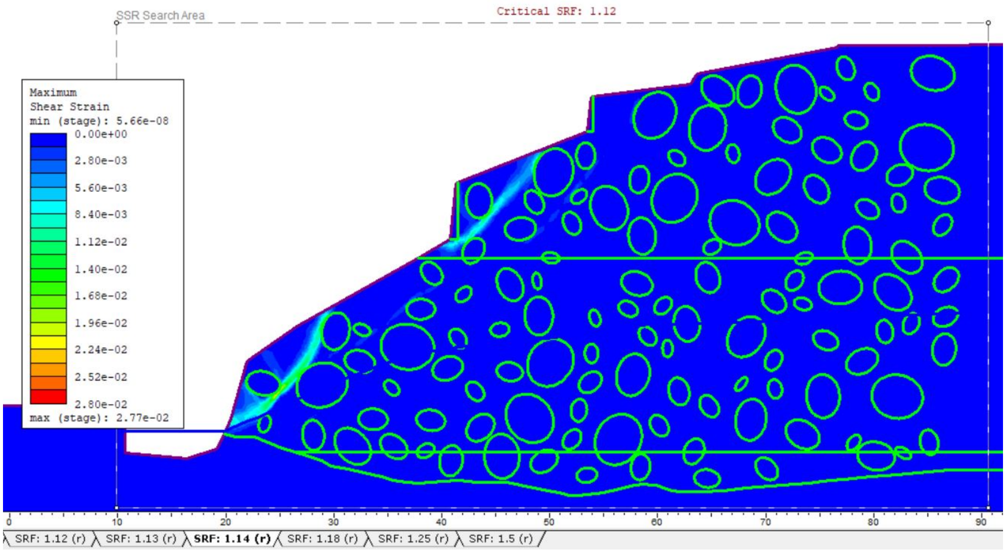


SRF=1.18

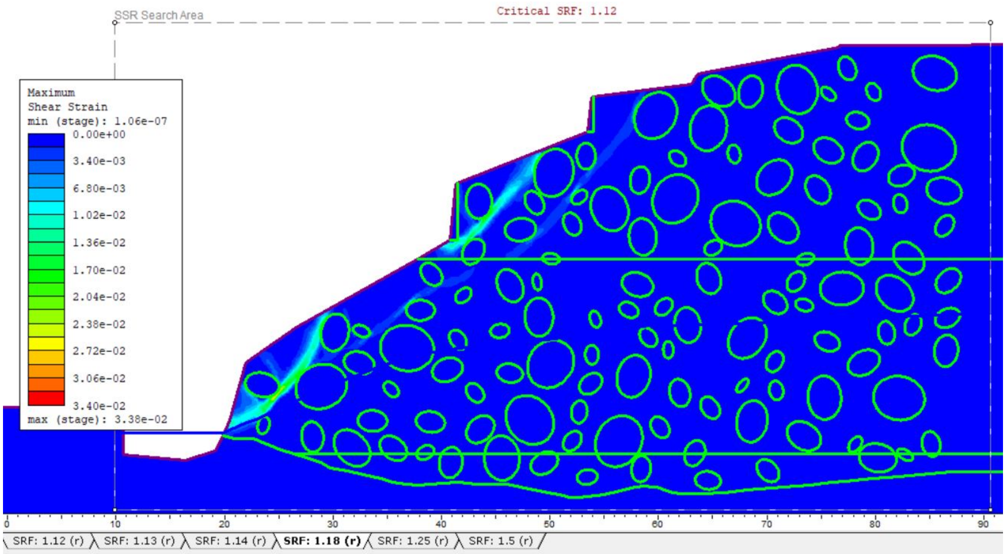

SRF=1.25

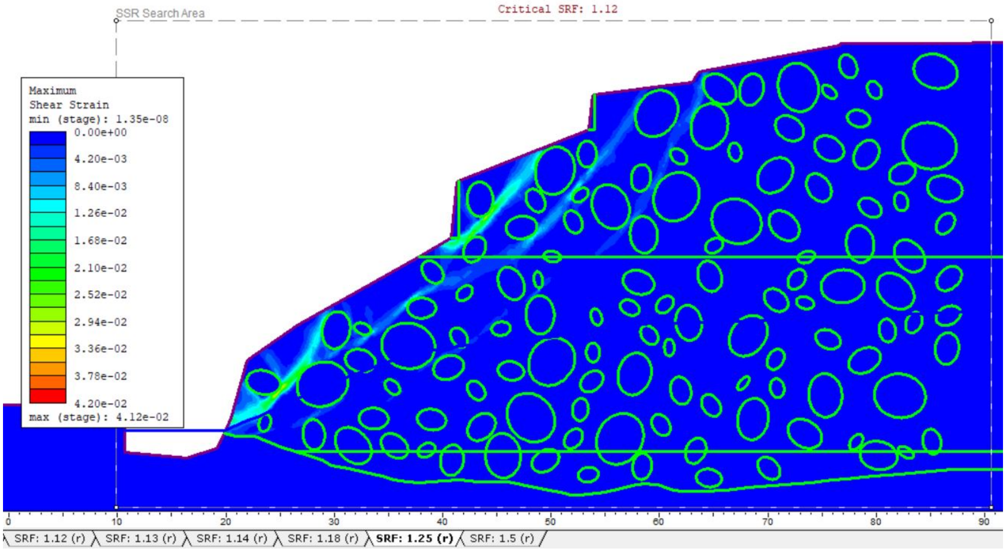


SRF=1.50

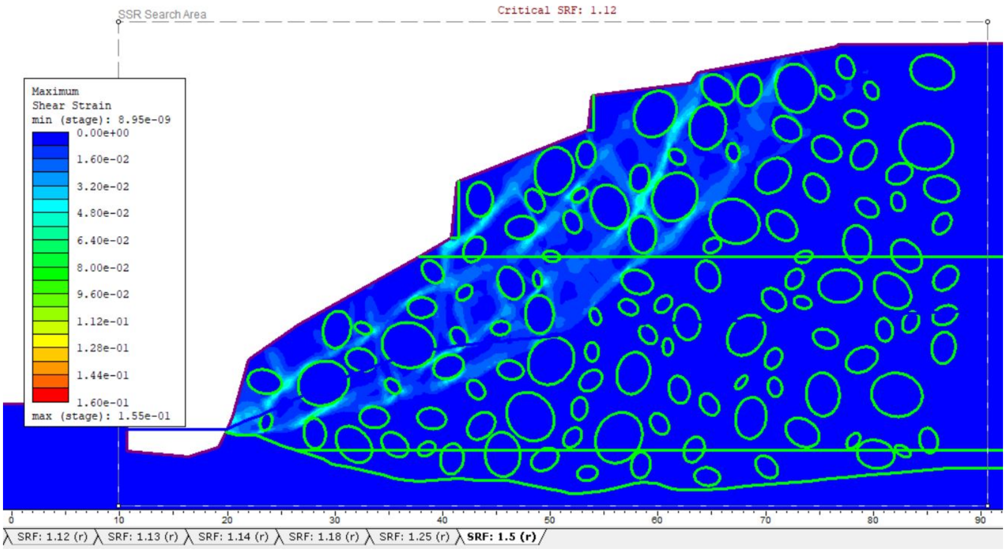

**30%_9_FEM**

Critical SRF=1.23

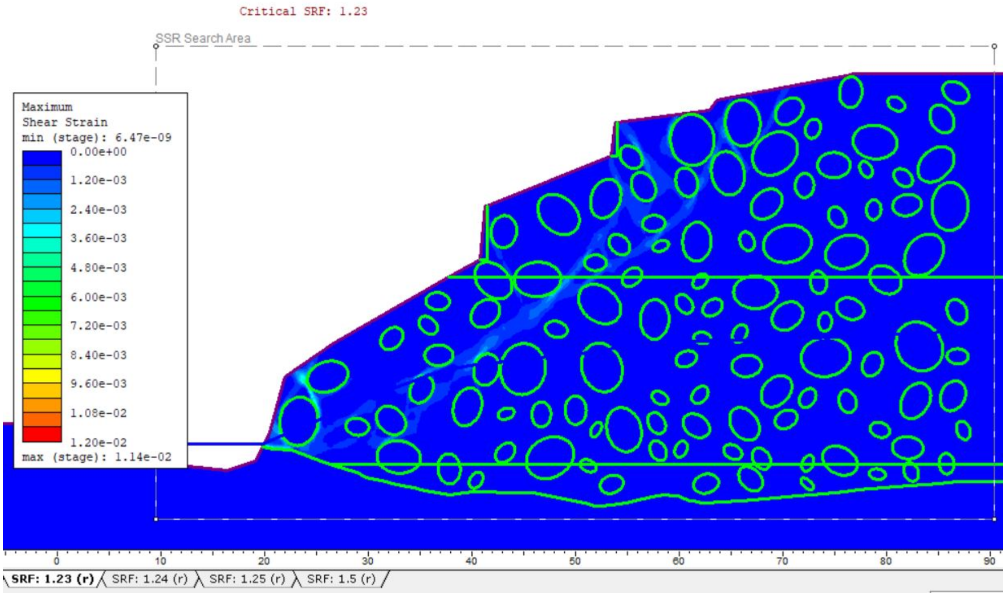


SRF=1.24

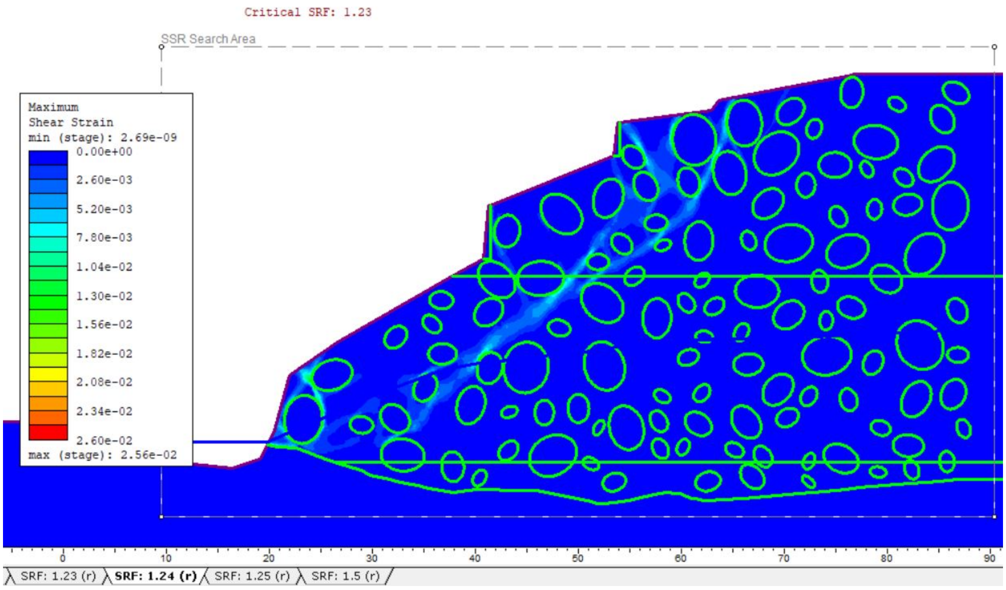

SRF=1.25

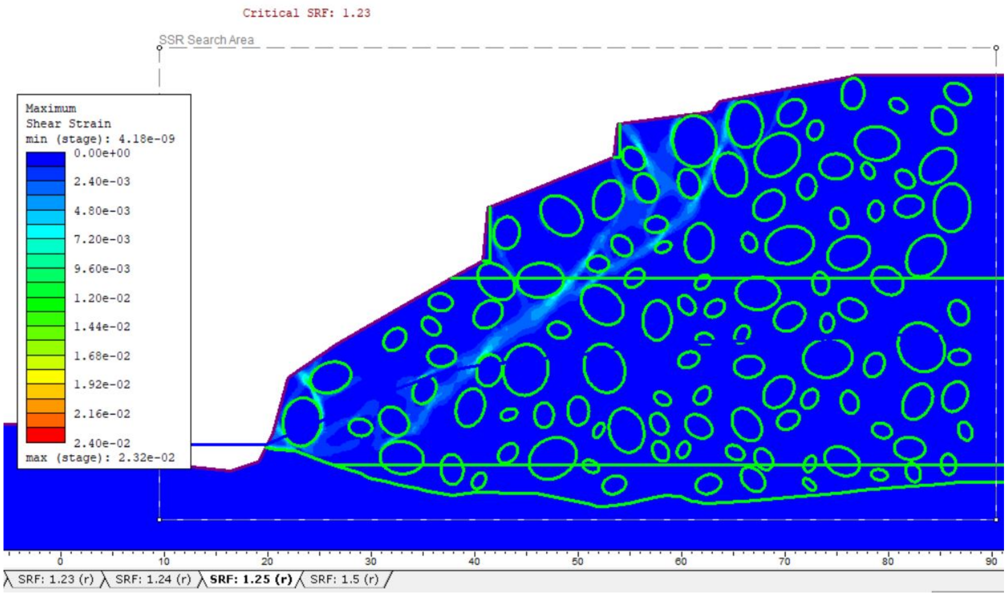


SRF=1.50

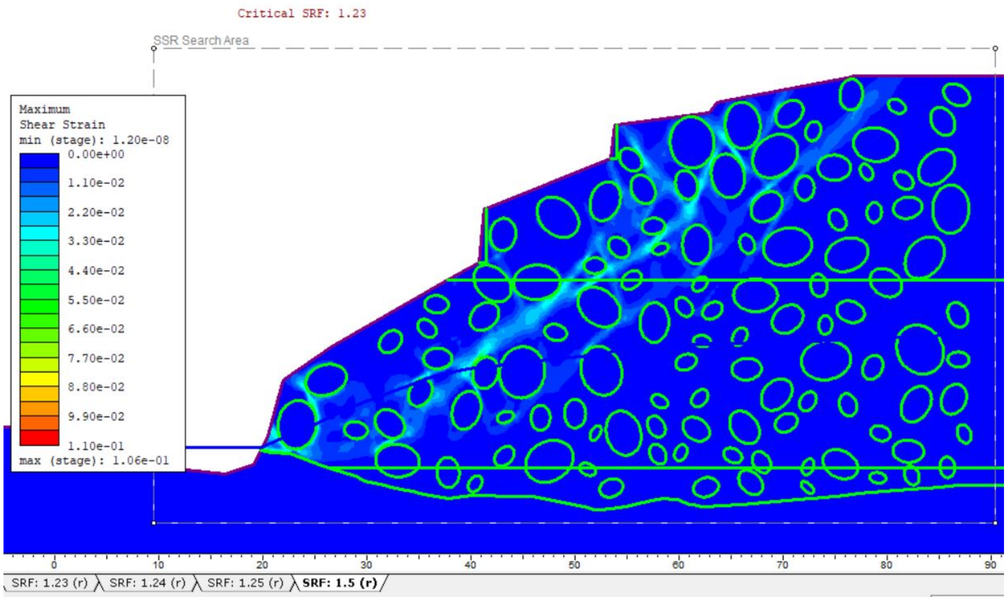

**30%_10_FEM**

Critical SRF=1.28

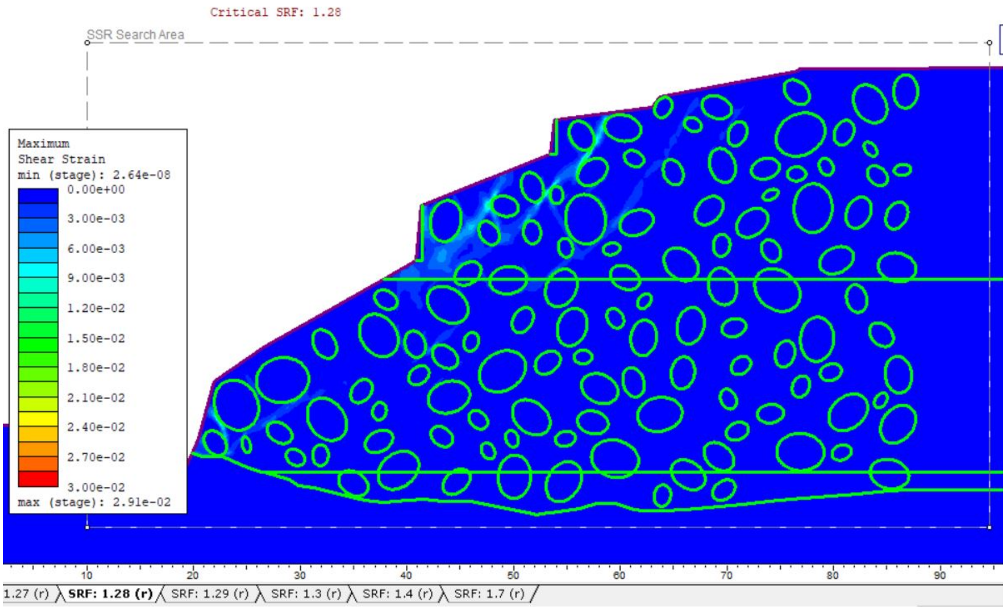


SRF=1.29

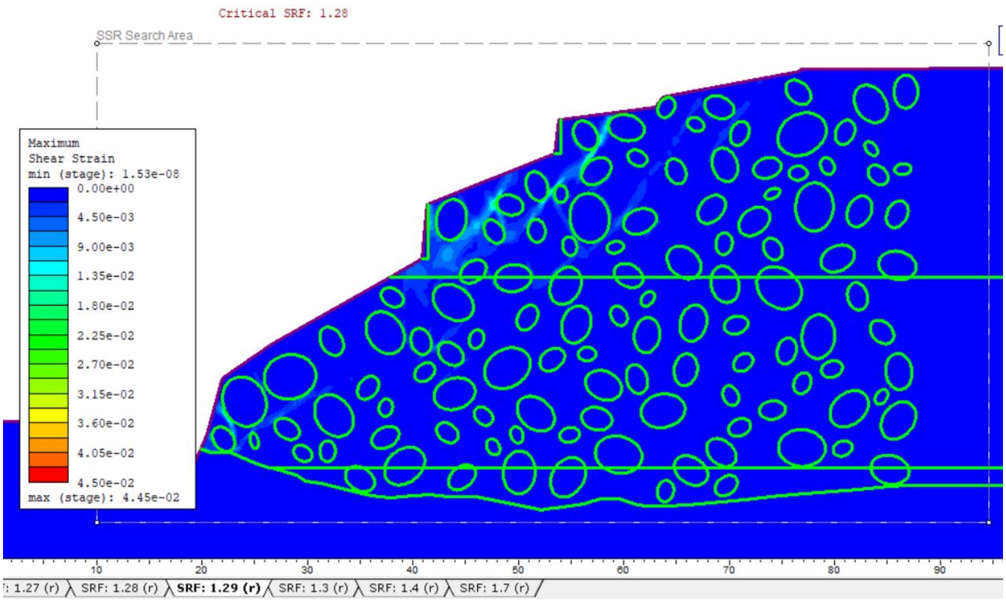

SRF=1.30

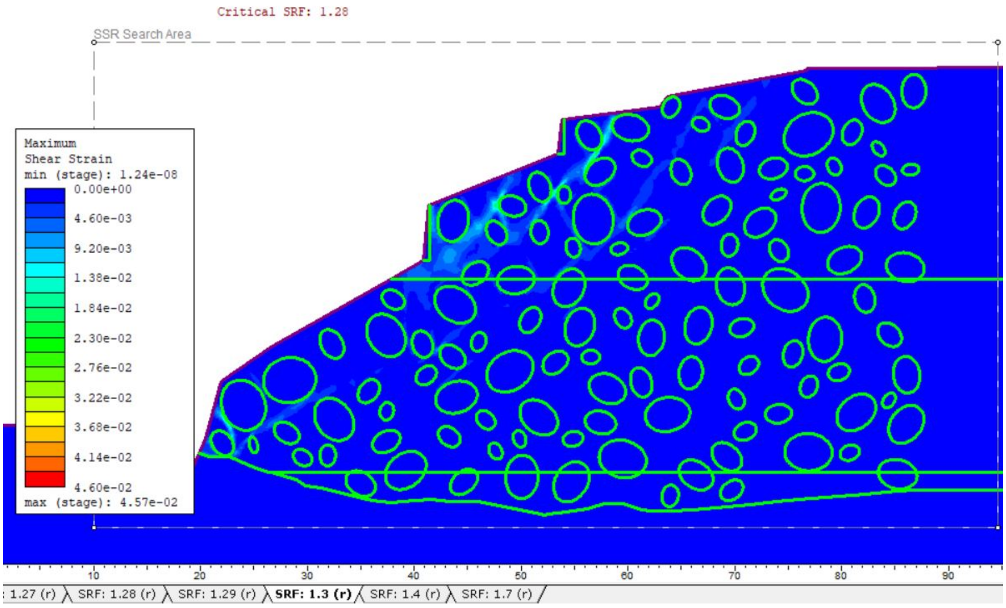


SRF=1.40

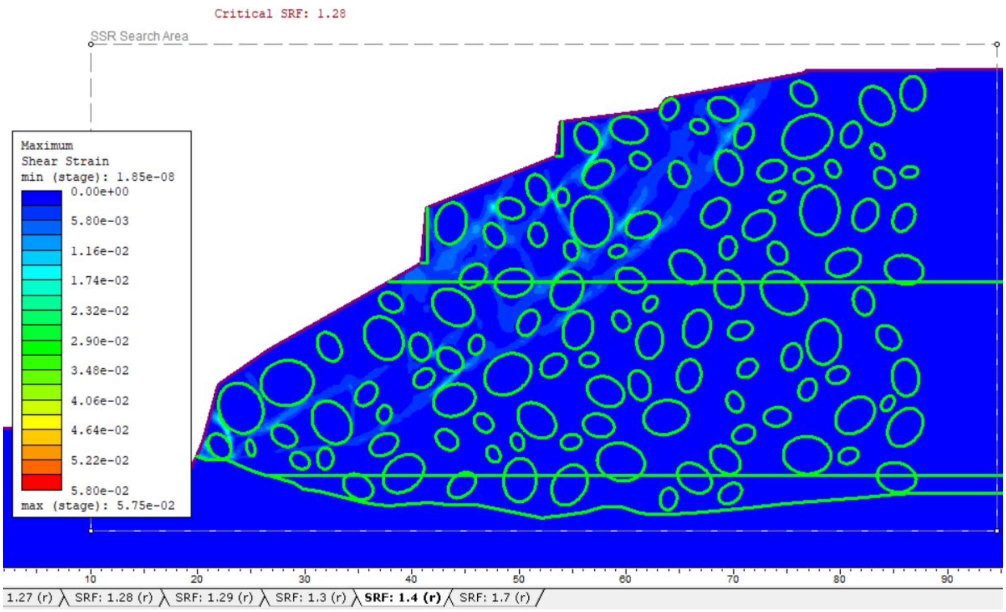

SRF=1.70

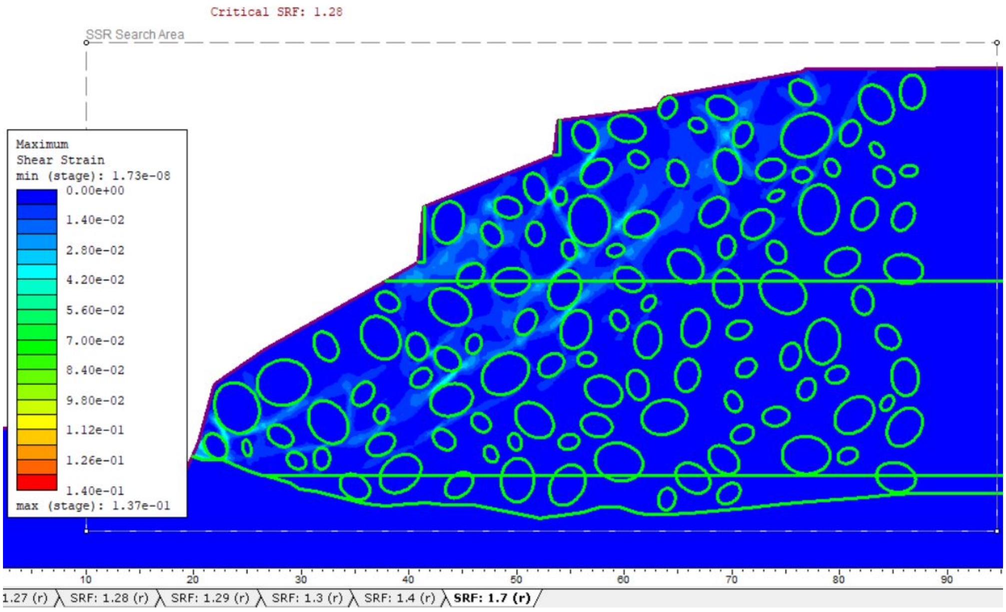

Critical SRF: 1.28
SSR Search Area
Maximum
Shear Strain
min (stage): 1.73e-08
0.00e+00
1.40e-02
2.80e-02
4.20e-02
5.60e-02
7.00e-02
8.40e-02
9.80e-02
1.12e-01
1.26e-01
1.40e-01
max (stage): 1.37e-01
10
20
30
40
50
60
70
80
90
1.27 (r)
SRF: 1.28 (r)
SRF: 1.29 (r)
SRF: 1.3 (r)
SRF: 1.4 (r)
SRF: 1.7 (r)

# Appendix D

## Homogeneous approaches

**LIN_30%_FEM**

critical SRF=1.08

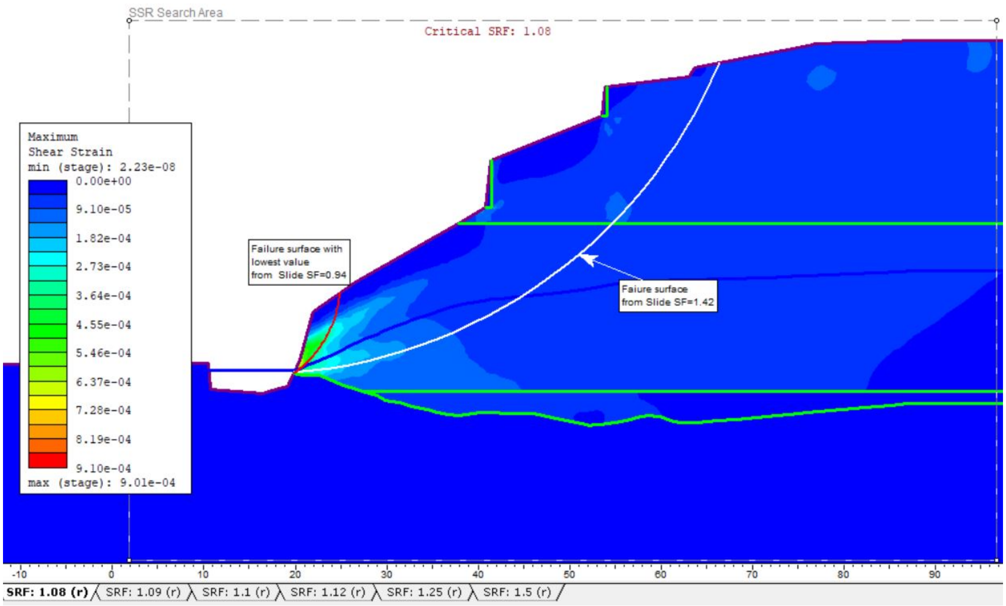

SRF=1.09

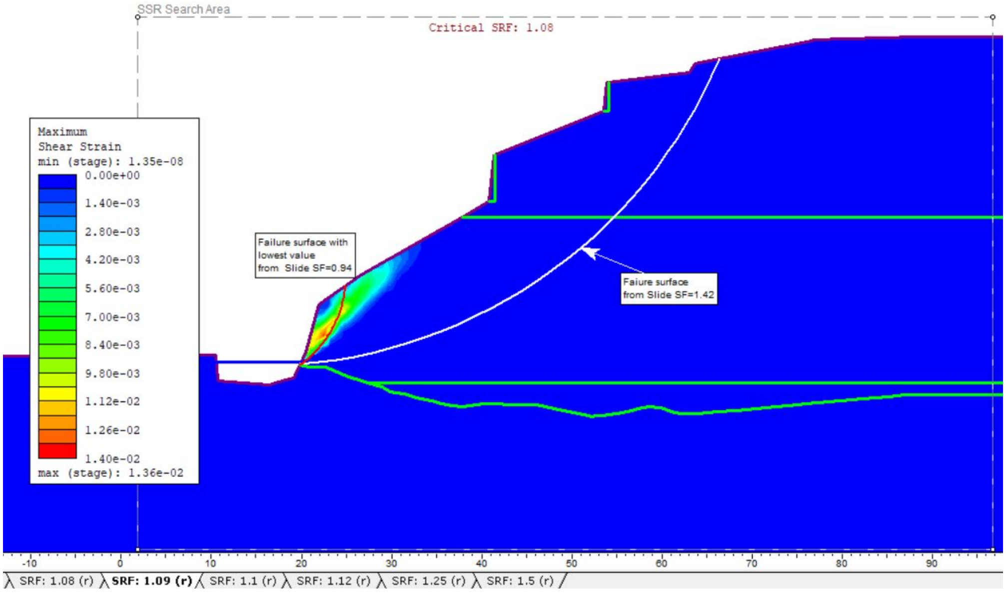


SRF=1.10

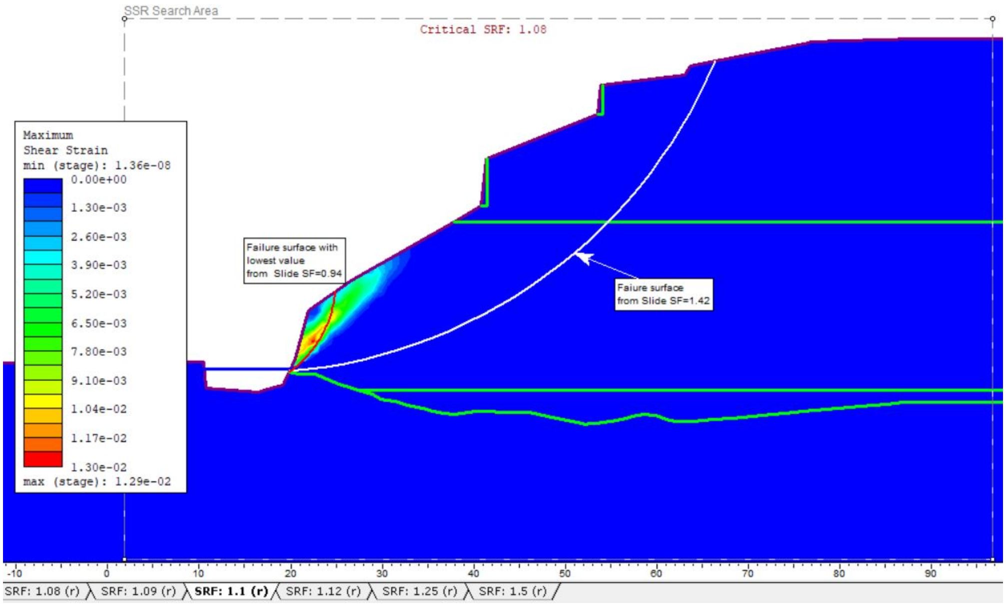

SRF=1.12

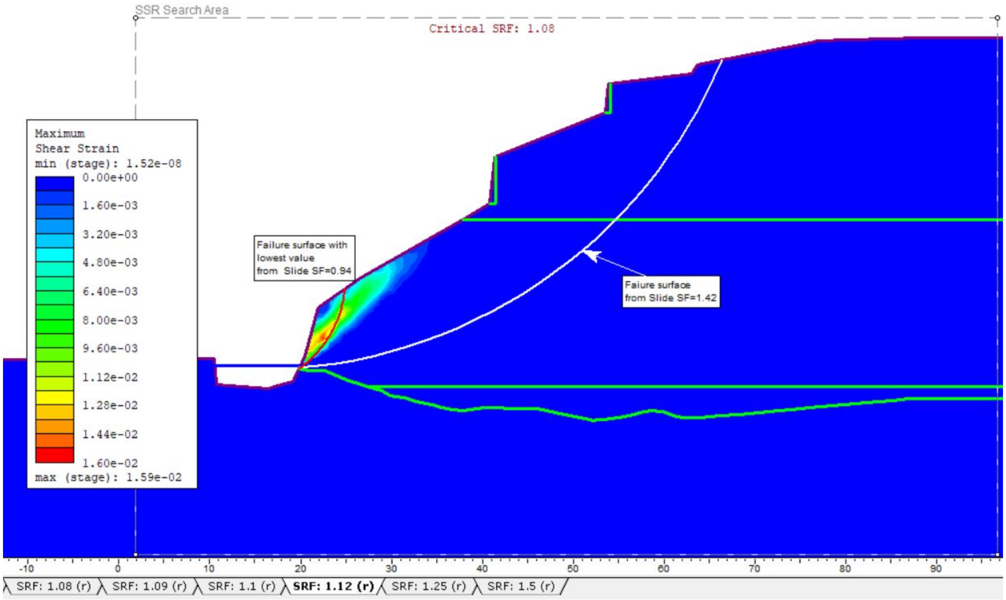


SRF=1.25

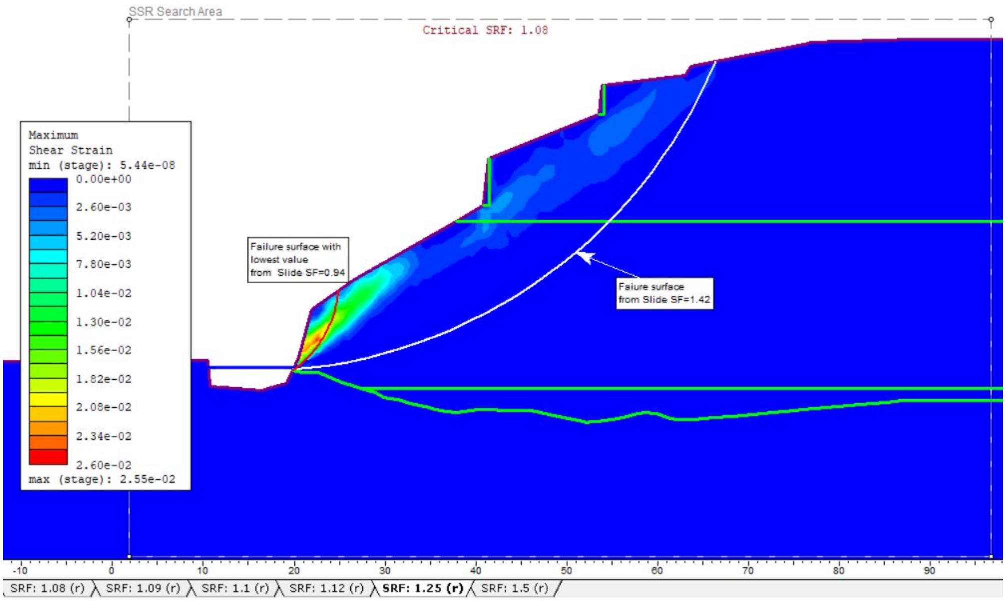

SRF=1.50

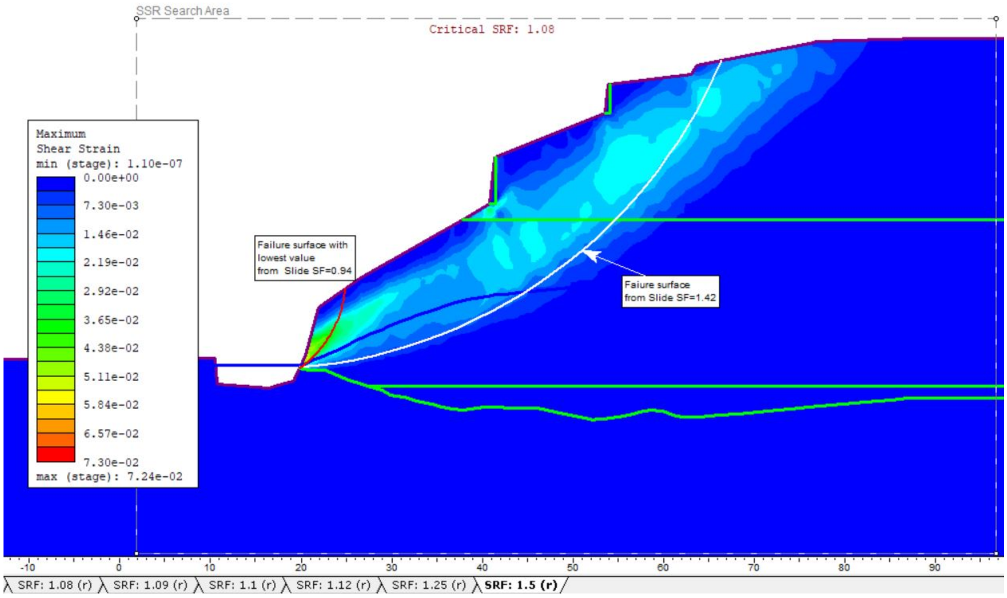


**LIN_30%_LEM**

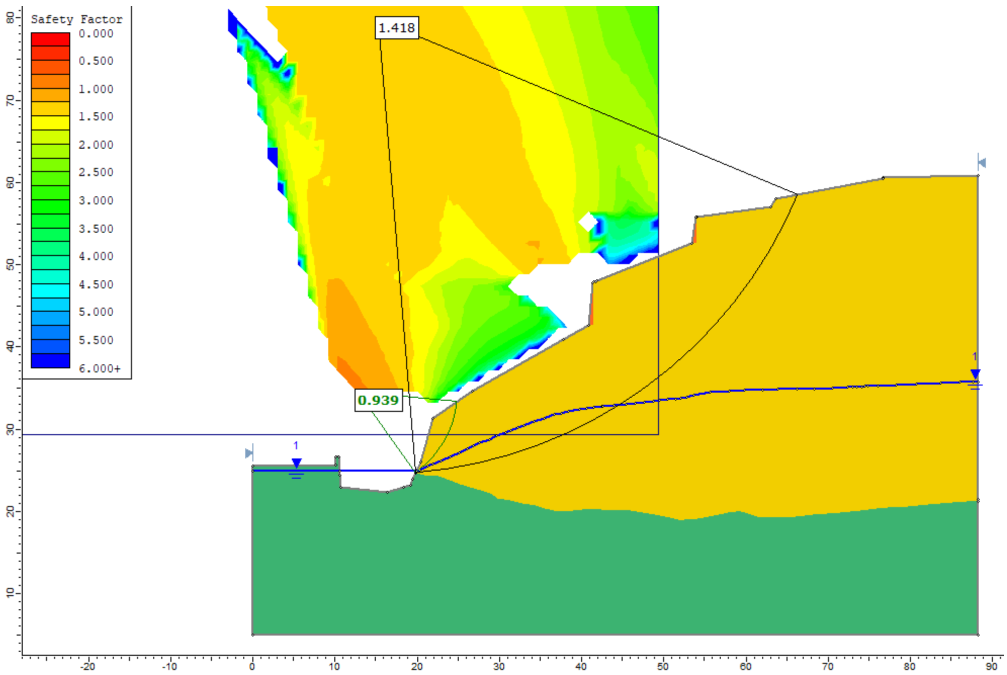

Maximum shear strains and progression of failure surface for Kalender's approach. Results of Slide are also included.

**KAL_15%_FEM**
Critical SRF=1.37

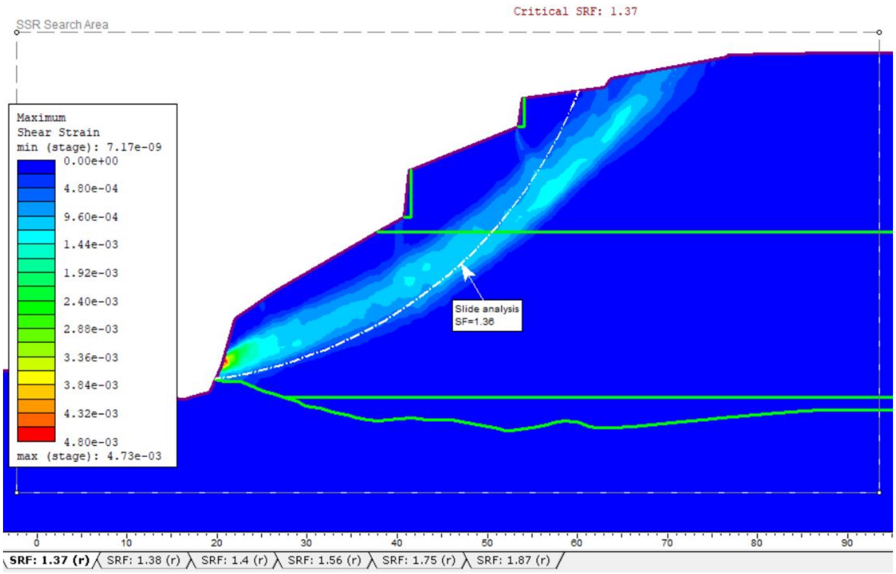


**KAL_15%_LEM**

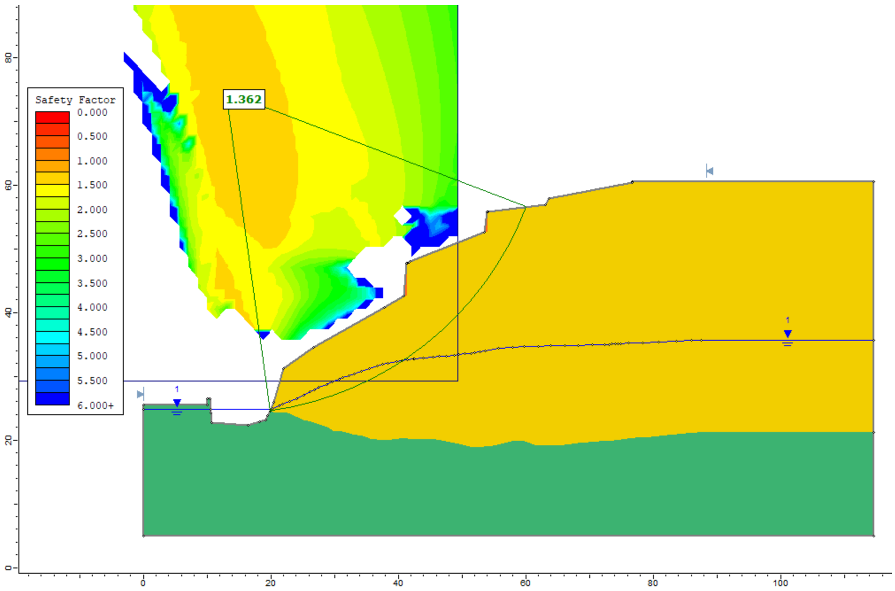

**KAL_30%_FEM**
Critical SRF=1.33

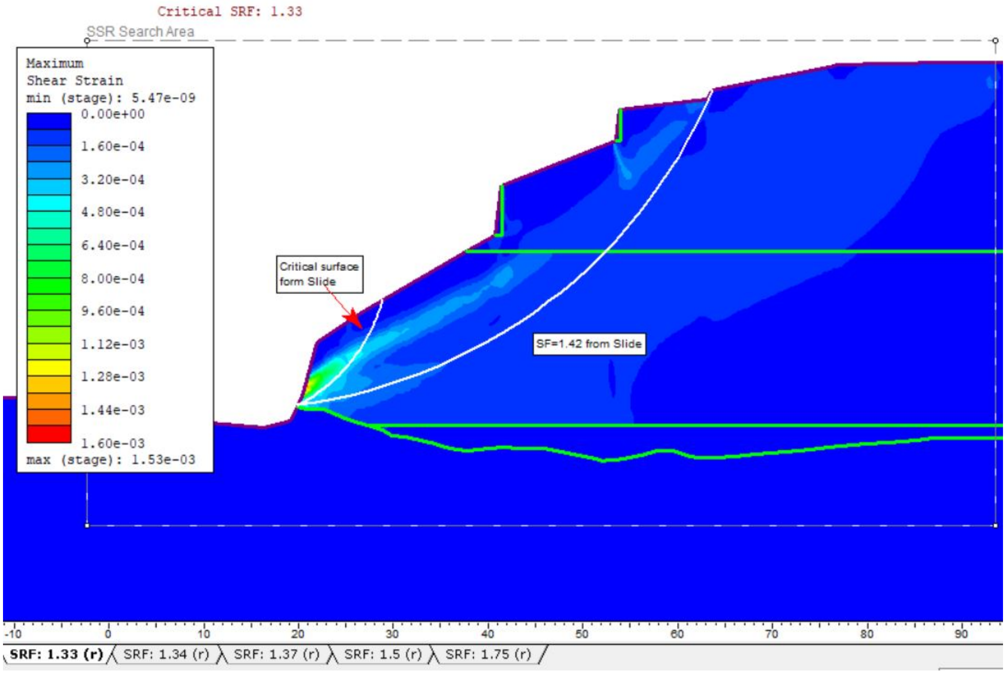


SRF=1.34

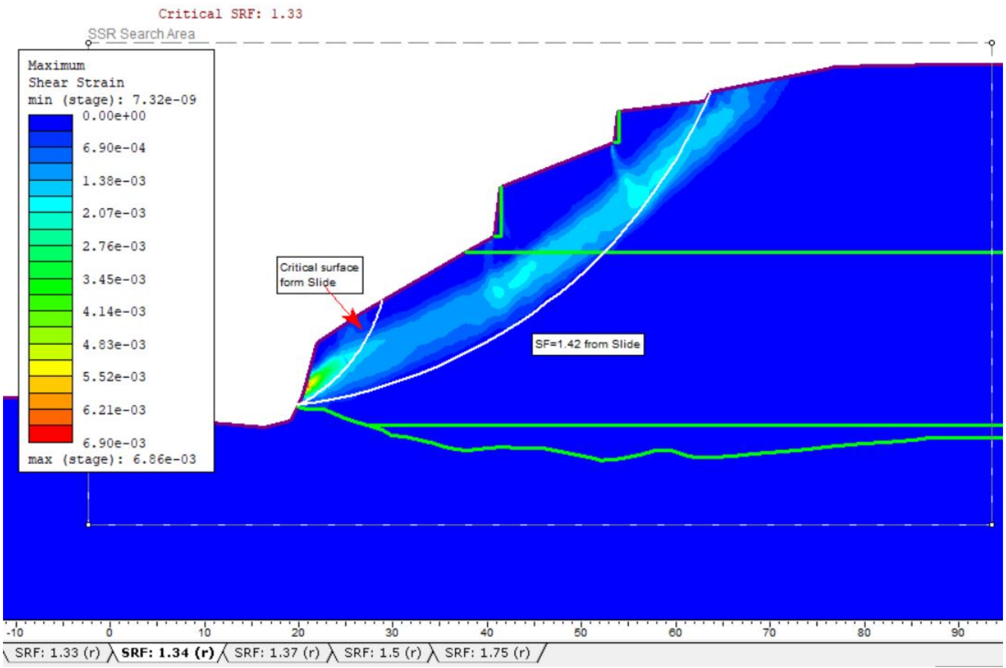

SRF=1.37

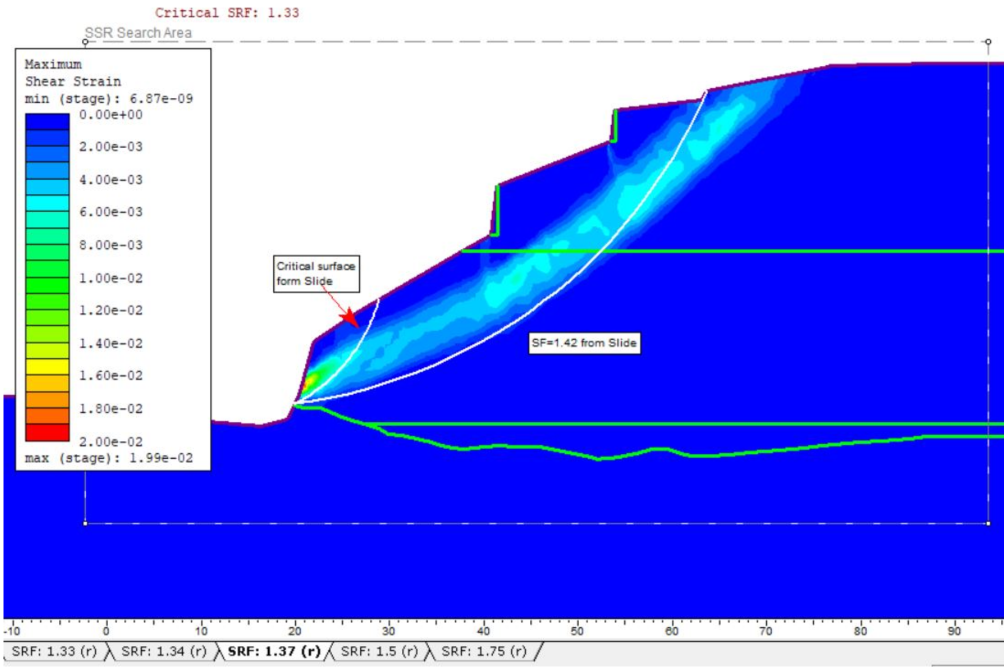


SRF=1.50

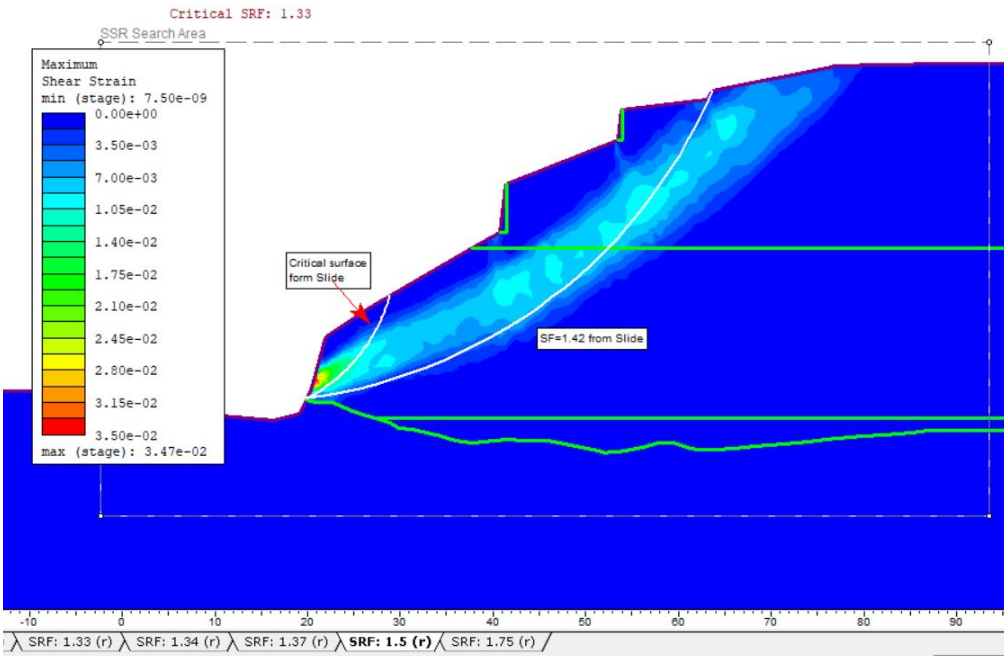

## KAL_30%_LEM

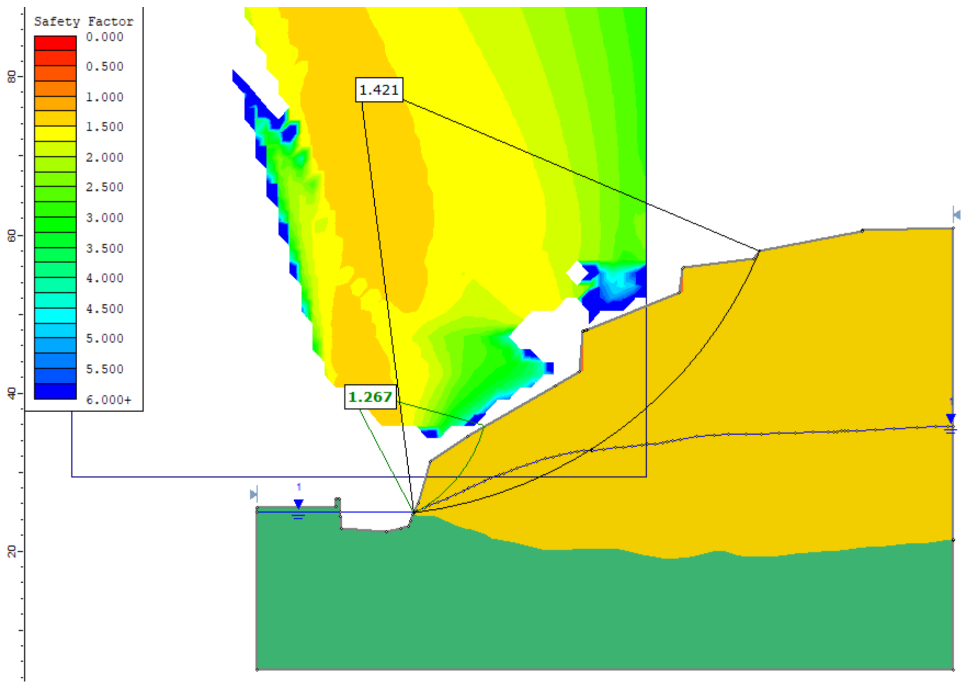
Safety Factor
0.000
0.500
1.000
1.500
2.000
2.500
3.000
3.500
4.000
4.500
5.000
5.500
6.000+
80
60
40
20
1.421
1.267